

NONITERATIVE DIGITAL BEAMFORMING IN CDMA
CELLULAR COMMUNICATIONS SYSTEMS

by

Wan Yi SHIU

A thesis submitted to the
Department of Electrical and Computer Engineering
in conformity with the requirements
for the degree of Master of Science (Engineering)

Queen's University
Kingston, Ontario, Canada
November 1998

Copyright © Wan Yi SHIU, 1998

Abstract

A novel application of a noniterative spherical subspace method to a beamforming network in a CDMA cellular communication system is introduced. This algorithm reduces the computational expense as compared to both batch and iterative weight-vector-update methods based on batch processing pre- and post-correlation covariance matrices.

A constraint for applying the spherical subspace methods as a Noniterative Rank-1 Signal Subspace eigenstructure Update (NR1SSU) algorithm for tracking the array response of a desired mobile's transmitting signals received at the base station in a CDMA communication system has also been analytically derived. It has also been shown analytically that such an algorithm can be applied to a CDMA beamforming networks with both zero time delay spread (flat fading or frequency non-selective) and non-zero time delay spread (frequency selective) fading propagation models.

To evaluate the NR1SSU algorithm, a generic CDMA system model has been used. In addition, different receiver structures are examined including beamforming, beamsteered-RAKE and diversity combining in both frequency-non-selective and frequency-selective fading channels. In particular, a PN chip-level IS-95 CDMA reference model [8] has also been used to evaluate the noniterative subspace beamforming algorithm via simulations in a flat fading channel.

Simulation results show that the NR1SSU algorithm accurately tracks the array response vector as long as the processing power gain is larger than the total interference-plus-noise power of the despread signal.

Acknowledgements

First of all, I would like to sincerely thank my supervisor, Dr. Steven D. Blostein, for his supervision, constructive and inspiring intelligent guidance. This thesis would not have been completed without his excellent supervision and advice.

Secondly, I would like to thank the CITR for their funding which supported this research. Also, I appreciate the availability of publications generated by dedicated researchers who have shared their innovations publically for exploration, further development, and new applications.

I would also like to thank Mark Earnshaw for allowing me to use his IS-95 chip-level CDMA simulator for part of the NR1SSU algorithm performance evaluation in this thesis. Also, I would like to thank him for taking his time to proof read of my thesis.

I would also like to thank Kathy Williams, the Electrical and Computer Engineering graduate student secretary, for her help during my graduate studies at Queen's.

I would also like to thank my labmates, friends at Queen's, and friends from McGill who constantly shared their wisdom and intellectual, joyful, and tearful moments with me during my studies at Queen's.

At last but definitely not the least, I would like to take this opportunity to express my thankfulness and gratefulness to my family and my best friends (especially Stanley K.C. Fung) for their unconditional love and support through every step of my life, especially during the final stage of finishing the writing of my thesis.

Contents

List of Tables	vii
List of Figures	viii
1 Introduction	1
1.1 Motivation	2
1.2 Summary of Contributions	3
1.3 Thesis Organization	4
2 Antenna Arrays and Digital Beamforming	5
2.1 Introduction	5
2.2 Antenna Arrays	5
2.2.1 Antenna Array Signal Model	7
2.2.2 Array Response Vector	8
2.2.3 Spatial Resolution	11
2.3 Antenna Array Spatial Filtering Capability	11
2.3.1 Effect of antenna time-delay weight	12
2.3.2 Effect of number of antenna elements	15
2.3.3 Effect of shading	15
2.3.4 Effect of antenna element spacing	18
2.3.5 Summary of effects of antenna array variables	20
2.4 Statistically Adaptive Optimum Beamforming Weight Vectors	21
2.4.1 Minimum mean square error (MMSE)	22

2.4.2	Maximization of signal-to-interference-plus-noise ratio (SINR)	24
2.4.3	Maximum likelihood (ML)	26
2.4.4	Linearly constrained minimum variance (LCMV)	27
2.4.5	Summary – Unifying optimum weight solution	31
2.5	Adaptive Algorithm for Beamforming	32
2.5.1	Least mean square (LMS) adaptive algorithm	33
2.5.2	Recursive least squares (RLS) adaptive algorithm	36
2.6	Summary	39
3	CDMA Cellular Communication Systems	40
3.1	Introduction	40
3.2	Spread Spectrum Signals	40
3.2.1	Bit-energy-to-total-noise ratio of a spread spectrum modulated signal	42
3.2.2	Code division multiple access (CDMA)	43
3.3	Multipath Fading Channel Models	46
3.4	Linear Diversity Combining	51
3.4.1	Selection Combining	52
3.4.2	Maximal-ratio Combining	52
3.4.3	Equal-gain Combining	53
3.5	The IS-95 reverse link	54
3.5.1	The reverse link/uplink channel waveform	54
3.6	State-of-the-Art Array Signal Processing applications to CDMA Cellular Communication Systems	56
3.6.1	2D-RAKE Receiver for Frequency-selective fading	58
3.7	Summary	59
4	Noniterative Rank-1 Signal Subspace Update Algorithm	61
4.1	Motivation of using NR1SSU	62
4.1.1	Rank-one update for time-varying statistics	63

4.2	Noniterative spherical subspace rank-one eigenstructure update . . .	64
4.3	Application of Noniterative subspace tracking to the CDMA System Model	73
4.4	DS-BPSK CDMA system model	74
4.4.1	Case of zero multipath time delay spread propagation model .	74
4.4.2	Case of non-zero multipath time delay spread propagation model	78
4.4.3	Interference-plus-noise matrix inverse estimation	81
4.5	DS-QPSK CDMA system model	82
4.5.1	NR1SSU for IS-95	86
4.6	Computational complexity of the NR1SSU algorithm	91
4.7	Summary	91
5	Performance of the NR1SSU Algorithm in CDMA	93
5.1	Introduction	93
5.2	NR1SSU Application to a IS-95 CDMA System	95
5.2.1	Monte-Carlo array response tracking simulation results	95
5.2.2	Perfect power control vs. imperfect power control	101
5.2.3	Different number of array antenna elements vs. performance .	104
5.3	NR1SSU application to a generic CDMA system	110
5.3.1	Beamformer with optimum SINR versus optimum SNR	110
5.3.2	NR1SSU compared to true array response vector	115
5.3.3	SNR vs. 2D-RAKE receiver	122
5.3.4	Diversity combining	126
5.3.5	Beamforming against Diversity combining	126
5.4	Summary	131
6	Conclusions	132
6.1	Thesis Conclusions	132
6.2	Summary of the Thesis Contributions	133
6.3	Future work	134

A Zero time delay spread propagation model autocovariance matrix	
derivations	135
A.1 Pre-correlation and Post-correlation vectors	135
A.1.1 The PN code pre-correlation matrix of the received stochastic signal vector	136
A.1.2 The PN code post-correlation covariance matrix of the received stochastic signal vector	138
A.2 The SINR of the weighted post-correlation vector	140
B Non-zero time delay spread autocovariance derivations	141
B.1 Pre-correlation and Post-correlation vectors	141
B.1.1 The PN code pre-correlation covariance matrix	142
B.1.2 The PN code post-correlation covariance matrix	144
B.2 The weighted post-correlation signal SINR	146
C First and second order statistics for a binary square pulse stochastic	
process	147
C.1 Autocovariance of pulse	147
C.2 Mean and autocorrelation of the PN chip and the information bit se- quences	150
Bibliography	152

List of Tables

2.1	Summary of the statistically optimum weight vector estimates	31
3.1	Criteria for frequency-nonselective and frequency-selective channel . .	49
3.2	Criteria for fast fading and slow fading channel	50

List of Figures

2.1	A beamformer	6
2.2	An eight-element circular array	10
2.3	A six-element uniform linear array	10
2.4	A 5-element UCA beam steering at different DOAs	14
2.5	A 5-element ULA beam steering at different DOAs	14
2.6	UCA 3, 4, 5, and 10 antenna elements	16
2.7	ULA 3, 4, 5, and 10 antenna elements	16
2.8	Using shading weights to shape the beampattern of a UCA	17
2.9	Using shading weights to shape the beampattern of a ULA	17
2.10	A 5-element ULA	19
2.11	A 5-element UCA	19
2.12	Reference signal adaptive antenna	23
2.13	Functional diagram of a M-element adaptive array	33
3.1	Model of spread spectrum digital communication system	41
3.2	DS-BPSK digital spread spectrum system model	44
3.3	2D-RAKE receiver	59
4.1	IS-95 reverse link mobile modulated signal	83
4.2	IS-95 CDMA base-station M-antenna array i^{th} mobile receiver model	84
4.3	An IS-95 CDMA NR1SSU beamforming block diagram	88
5.1	NR1SSU using FWFPC Monte-Carlo evaluation of a tracked moving mobile with 9 moving interferers	96

5.2	NR1SSU using post-correlation Monte-Carlo evaluation of a tracked moving mobile with 9 moving interferers	97
5.3	NR1SSU using FWFPC Monte-Carlo evaluation of a tracked faster moving mobile with 2 faster moving interferers	98
5.4	NR1SSU using post-correlation Monte-Carlo evaluation of a tracked faster moving mobile with 2 faster moving interferers	99
5.5	A tracked mobile using NR1SSU FWFPC of imperfect power control with 40 in-band mobiles	102
5.6	Another tracked mobile using NR1SSU FWFPC of imperfect power control with 40 in-band mobiles	103
5.7	A tracked mobile using NR1SSU FWFPC of perfect power control with 40 in-band mobiles	105
5.8	Another tracked mobile using NR1SSU FWFPC of perfect power control with 40 in-band mobiles	106
5.9	A tracked mobile using 4-element array NR1SSU FWFPC of perfect power control with 10 in-band mobiles	107
5.10	A tracked mobile using 6-element array NR1SSU FWFPC of perfect power control with 10 in-band mobiles	108
5.11	A tracked mobile using 8-element array NR1SSU FWFPC of perfect power control with 10 in-band mobiles	109
5.12	SINR vs SNR optimum (using perfect array response vector) vs NR1SSU with 10 mobiles in total	113
5.13	SINR vs SNR optimum (using perfect array response vector) vs NR1SSU with 25 mobiles in total	114
5.14	Exploiting delay spread with NR1SSU first multipath array response vector estimate in cellular channel, 10 mobiles in total	116
5.15	Exploiting delay spread with NR1SSU second multipath array response vector estimate in cellular channel, 10 mobiles in total	117

5.16	Exploiting delay spread with NR1SSU third multipath array response vector estimate in cellular channel, 10 mobiles in total	118
5.17	Exploiting delay spread with NR1SSU first multipath array response vector estimate in cellular channel, 25 mobiles in total	119
5.18	Exploiting delay spread with NR1SSU second multipath array response vector estimate in cellular channel, 25 mobiles in total	120
5.19	Exploiting delay spread with NR1SSU third multipath array response vector estimate in cellular channel, 25 mobiles in total	121
5.20	Exploiting delay spread with true array response and NR1SSU array response estimate in cellular channel, 10 mobiles in total with beamforming weight as true array response vector	123
5.21	Exploiting delay spread with true array response and NR1SSU array response estimate in cellular channel, 25 mobiles in total with beamforming weight as true array response vector	124
5.22	Diversity combining of a CDMA system with a single path propagation channel and 50 mobiles	127
5.23	Diversity combining of a CDMA system with a single path propagation channel with 25 mobiles	128
5.24	Artificial Diversity vs. SINR optimum Beamforming using perfect array response vectors with 10 mobiles in total	129
5.25	Artificial diversity vs. SINR optimum beamforming using perfect array response vector with 25 mobiles in total	130

List of Abbreviations

AWGN	Additive White Gaussian Noise
BPSK	Binary Phase Shift Keying
DS-BPSK	Direct Sequence Binary Phase Shift Keying
DS-QPSK	Direct Sequence Quadrature Phase Shift Keying
bpf	bits per frame
bps	bits per second
CDMA	Code Division Multiple Access
cps	chips per second
DPP	Delay power profile
DOA	Direction-Of-Arrival
DSMA	Direct Sequence Multiple Access
FSK	Frequency Shift Keying
FWFPC	Feedback Walsh function post-correlation
ISR	Interference-to-signal ratio
LCMV	Linearly Constrained Minimum Variance Beamforming
LMS	Least mean square
LOS	Line of sight
MAI	Multiple-access interference
MIP	Multipath intensity profile
MSC	Multiple Sidelobe Canceller
MSE	Mean Square Error
MMSE	Minimum Mean Square Error
PCS	Personal Communication Services
PN	Pseudo Noise
PSD	Power spectral density
PSK	Phase Shift Keying

RLS	Recursive least square
RMSE	Root mean square error
SINR	Signal-to-Interference-plus-Noise Ratio
SNR	Signal-to-Noise Ratio
sps	symbols per second
UCA	Uniform Circular Array
ULA	Uniform Linear Array
W	Watts
WSS	Wide-Sense-Stationary
w.r.t.	With respect to

List of Symbols

λ_c	Carrier wavelength
f_c	Carrier frequency
ω_c	Carrier angular frequency
$\mathbf{w}(t)$	Complex weight vector of an antenna array receiver at time t
\mathbf{w}	Discrete complex weight vector of the antenna array for combining
w_m	Discrete complex weight vector of the m^{th} antenna element branch
$\mathbf{w}(k+1)$	Weight vector after adaptation for beamforming at time index $k+1$
$\mathbf{w}(k)$	Weight vector after adaptation for beamforming at time index k
$\mathbf{w}(0)$	Initial weight vector for beamforming at time index 0
M	Number of total antenna array elements
$\mathbf{x}(t)$	Received baseband signal vector at antenna array
$x_{ik}(t)$	The received baseband signal of the i^{th} mobile's k^{th} diversity path
$\mathbf{x}(k)$	The received baseband signal vector received at time index k
$\mathbf{r}(t)$	Received RF signal vector at antenna array
$x_m(t)$	Received baseband signal of the m^{th} antenna branch
$y(t)$	Beamformed signal at time t where $y(t) = \mathbf{w}^\dagger(t)\mathbf{x}(t)$
$\mathbf{n}(t)$	Gaussian white noise vector received at antenna array
$s_i(t)$	Transmitted RF signal of the i^{th} transmitting mobile
$u_i(t)$	Transmitted baseband signal of the i^{th} transmitting mobile
\mathbf{s}	Received signal envelope vector
$u_s(t)$	Binary information-bearing signal
$\hat{u}_s(t)$	Binary information-bearing signal estimate
y_s	Beamformed signal of the received signal \mathbf{x} , i.e. $y_s = \mathbf{w}^\dagger \mathbf{x}$
\mathbf{i}	Received interference signal envelope vector
y_{IN}	Beamformed interference-plus-noise signal, i.e. $y_{IN} = \mathbf{w}^\dagger (\mathbf{i} + \mathbf{n})$
\mathbf{n}	Received noise vector

\mathbf{z}	Temporary substitution vector where $\mathbf{z} = \mathbf{R}_{\text{IN}}^{1/2} \mathbf{w}$
$i(t)$	Received interference envelope
J_i	Total number of resolvable multipath received of the i^{th} mobile
K_i	Total number of resolvable multipath received of the i^{th} mobile
J	Resolvable multipath
$\varrho_{i,k}(t)$	The channel amplitude attenuation/gain of the i^{th} mobile's k^{th} multipath
$\varrho_i(t)$	The channel amplitude gain experienced by the i^{th} mobile
τ	Time delay variable of a received signal
τ_m	Time delay of a received signal at the m^{th} antenna branch
$\hat{\tau}_m$	Estimated weight delay at the m^{th} antenna branch
τ_{ik}	Time delay of a received signal of the i^{th} mobile's k^{th} multipath
$\tau_{ik,jp}$	Relative time delay of the j^{th} mobile's p^{th} multipath reference to the i^{th} mobile's k^{th} multipath
$\tau_{i,j}$	Relative time delay of the j^{th} mobile reference to the i^{th} mobile
ϕ_{il}	Channel phase shift of the i^{th} mobile's l^{th} multipath
β	The phase shift of a received signal
$h(\tau; t)$	Time variant channel impulse response function
$G_m(\omega_c, \theta, \Omega_m)$	The m^{th} antenna's amplitude response
$\tau_m(\theta, \Omega)$	The m^{th} element's time delay response
$\theta(t)$	The time-varying direction-of-arrival (DOA)
θ	The simplified form of the time-varying direction-of-arrival (DOA)
Ω_m	Antenna inter-element mutual coupling resistance of the m^{th} antenna
ψ_m	Angle of the m^{th} antenna element measured w.r.t. center of a UCA
$\hat{\theta}$	The estimated DOA
R	The radius of a circular array
c	Speed of light
v	Speed of a mobile
d	Inter-element antenna spacing
$A(t)$	Signal amplitude

$A_i(t)$	Signal amplitude of the i^{th}
$A(\Theta)$	The directional/beam pattern function in terms of $\mathbf{a}(\Theta)$
$G(\Theta)$	The normalized directional pattern or the normalized gain
\mathbf{L}	Lower triangular matrix
\mathcal{D}	Diagonal matrix
\mathbf{D}	Diagonal eigenvalues matrix
\mathbf{Q}	Eigenvectors matrix corresponding to eigenvalues matrix \mathbf{D}
\mathbf{R}_{xx}	Autocorrelation matrix of \mathbf{x}
\mathbf{R}_{xx}^{-1}	Inverse of the autocorrelation matrix \mathbf{R}_{xx}
\mathbf{R}_{ss}	Correlation matrix of the desired signal envelope $s(t)$
\mathbf{R}_{IN}	Autocorrelation of interference-plus-noise
\mathbf{R}_{IN}^{-1}	Inverse of the autocorrelation of interference-plus-noise
$\mathbf{R}_{IN}^{-1/2}$	Inverse of the square root of the interference-plus-noise autocorrelation
$\mathbf{R}_{IN}^{-\dagger/2}$	Inverse of the conjugate of $\mathbf{R}_{IN}^{-1/2}$
\mathbf{Y}	Temporary matrix where $\mathbf{R}_{IN}^{-\dagger/2}\mathbf{R}_{ss}\mathbf{R}_{IN}^{-1/2}$
y_d	Training signal or reference signal
$y_d(t)$	Training signal or reference signal
\mathbf{r}_{xd}	Cross-correlation matrix of \mathbf{x} and y_d
λ	Eigenvalue
λ_{max}	Principal eigenvalue
\mathbf{v}	Eigenvector
\mathbf{u}	Eigenvector
$b(t)$	Binary information bit
$c(t)$	Binary chip
$p(t)$	Pulse function of time t
$\delta(t)$	Impulse function of time t
$\Phi(\tau_1, \tau_2; \Delta t)$	Autocorrelation function of the channel impulse response $h(\tau, t)$
B_D	Maximum Doppler spread
T_D	Coherence time

B_m	Channel coherence bandwidth
T_m	Coherence time
B	Information Bandwidth
B_e	Bandwidth expansion factor or processing gain
W_{ss}	Spread Spectrum Channel Bandwidth
$g(t)$	Channel attenuated signal amplitude
L	PN chip despread processing gain
r_m	The shading amplitude factor for beamforming of the m^{th} branch
\mathbf{I}	Identity matrix
σ_n^2	Gaussian noise power
σ_s^2	Signal power
$\hat{\sigma}_s$	Signal amplitude estimate
$\mathcal{U}(0, T_c)$	Uniformly distributed function over 0 to T_c
$\hat{\mathbf{R}}_{\text{IN}}^{-1}$	Inverse of the interference-plus-noise correlation matrix estimate
$\hat{\mathbf{R}}_{\text{IN}}$	The interference-plus-noise correlation matrix
$\mathbf{a}(\Theta)$	Array response vector in terms of its parameters Θ
$\hat{\mathbf{a}}(\Theta)$	Array response vector of its parameters Θ
$\mathbf{a}(t)$	Time varying array response vector equivalent to $\mathbf{a}(\Theta)$
$\hat{\mathbf{a}}(t)$	Array response vector estimate
$\mathbf{a}_{i,k}(\Theta)$	Array response vector of the i^{th} mobile's k^{th} multipath of parameters Θ
$\mathbf{a}_{i,k}$	Array response vector of the i^{th} mobile's k^{th} multipath, i.e. $\mathbf{a}_{i,k}(\Theta)$
$\mathbf{a}_i(t)$	Array response vector of the i^{th} mobile in terms of time
$\mathbf{a}(\theta, \omega_c)$	Array response vector with DOA θ and carrier frequency ω_c
ε	Difference of the referenced signal y_d and the beamformed signal $y = \mathbf{w}^\dagger \mathbf{x}$
$\varepsilon(k)$	Error function at index time k
\mathbf{w}_{MSE}	The minimum mean square error weight vector estimate
\mathbf{w}_{SINR}	The maximum signal-to-interference-noise ratio weight vector estimate
\mathbf{w}_{ML}	The maximum likelihood weight vector estimate
\mathbf{w}_{opt}	The optimum weight vector estimate

$\mathbf{w}_{opt_{i,l}}$	The optimum weight vector for the i^{th} mobile's l^{th} path
$SINR_{opt}$	Optimum SINR
\mathcal{B}	Complex scalar
\mathcal{D}	Complex scalar
\mathbf{C}	A $M \times \mathcal{K}$ matrix having \mathcal{K} linearly independent constraint equations
\mathbf{p}	A $\mathcal{K} \times 1$ constraint response vector
$F(\mathbf{w})$	The cost function
$G(\mathbf{w})$	The constraint function
\mathbf{b}	The Lagrange multiplier vector
\mathbf{A}	A $M \times \mathcal{K}$ matrix of rank \mathcal{K} where $\mathbf{V}\Sigma\mathbf{U}^\dagger$
\mathbf{V}	Left singular matrix of matrix \mathbf{A}
\mathbf{U}	Right singular matrix of matrix \mathbf{A}
Σ	The $\mathcal{K} \times \mathcal{K}$ diagonal matrix
\mathcal{H}	A scalar
\mathcal{I}	A scalar
ς	A scalar
μ	A scalar constant
S	Total frame used to estimate the covariance matrix \mathbf{R}_{xx}
α	The forgetting factor
E_b	Bit-energy
N_0	One-sided power spectral density (PSD) in W/Hz
N_{total}	Total interference-plus-noise energy
S	Signal power
J	Interference power
$c_i(t)$	PN sequence of the i^{th} mobile
$c_{i,n}$	Binary PN code of the n^{th} bit of the i^{th} mobile
T_c	Chip period
T_b	Information-bearing bit period
N	Total number of in-band transmitting mobiles

$p(t - nT_c)$	Pulse modulation with chip period T_c
$b_i(t)$	Binary information-bearing sequence of the i^{th} mobile
$b_{i,n}$	Binary information-bearing bit of the n^{th} bit of the i^{th} mobile
$q(t - nT_b)$	Pulse modulation with bit period T_b
$x_i(t)$	Received baseband signal reference to the i^{th} mobile's CDMA PN code
$z_i(n)$	Post-correlated baseband signal of the i^{th} mobile
$H_{ik}(t)$	The k^{th} diversity branch impulse response of a i^{th} mobile
$n_k(t)$	The interference-plus-noise signal of the k^{th} diversity branch
$n_{ik}(t)$	The Gaussian noise received at the k^{th} diversity branch of the i^{th} mobile
i_{ik}	The interference received at the k^{th} diversity branch of the i^{th} mobile
$g_k(t)$	The k^{th} diversity branch amplitude received corresponding to the i^{th} mobile
w_k	The weight at the k^{th} diversity branch
$P_{i,l}$	The received power of the i^{th} mobile's l^{th} multipath
$\mathbf{z}_{i,l}$	The PN post-correlation vector of the i^{th} mobile's l^{th} multipath
$\mathbf{R}_{zz_{i,l}}$	The post-correlation correlation matrix of $\mathbf{z}_{i,l}$
$\mathbf{R}_{IN_{i,l}}$	Interference-plus-noise correlation matrix of the i^{th} mobile's l^{th} path
\mathbf{A}	A square matrix of $M \times M$
\mathbf{B}	A square matrix of $M \times M$
\mathbf{C}	A diagonal matrix of $M \times M$
$\mathbf{e}_{i,l}$	Principal eigenvector estimate for the i^{th} mobile's l^{th} multipath
$\hat{\mathbf{R}}_{xx}(k)$	Autocorrelation of the received baseband signal vector $\mathbf{x}(k)$ at time index k
\mathbf{Q}_k	Eigenvectors matrix eigendecomposed from $\hat{\mathbf{R}}_{xx}(k)$ at time index $k - 1$
\mathbf{u}_m	Eigenvector corresponding to the m^{th} column of \mathbf{Q}_{k-1}
\mathbf{D}_k	Eigenvalues diagonal matrix eigendecomposed from $\hat{\mathbf{R}}_{xx}(k)$ at time index k
d_m	Eigenvalue corresponding to the m^{th} diagonal eigenvalue
$\mathbf{s}(t)$	Received signal vector at time t
$\mathbf{s}_i(t)$	Received signal vector of the i^{th} independent source
r	Independent signal received of $\mathbf{x}(t)$, i.e. rank of $\mathbf{R}_{xx}(t)$
$\sigma_n(t)^2$	Time varying noise power

$\mathbf{R}_{nn}(t)$	Noise covariance matrix equivalent to $\sigma_n^2(t)\mathbf{I}$
$\mathbf{R}_{ss}(t)$	Signal covariance matrix varies as a function of time t
β	Complex vector equivalent to $\mathbf{Q}_{k-1}^\dagger \mathbf{x}(k)$
\mathbf{e}_i	The i th column of a $M \times M$ identity matrix \mathbf{I}
γ	A real-valued $M \times 1$ vector equivalent to $\mathbf{G}^\dagger \beta$
$\gamma^{(s)}$	A real-valued $r \times 1$ vector of γ with r independent received-signals
$\gamma^{(n)}$	A real-valued $(M - r) \times 1$ vector of the noise subspace of γ
\mathbf{G}	Diagonal unitary transformation matrix
\mathbf{H}	Householder transformation matrix
$\mathbf{H}^{(s)}$	Signal subspace Householder transformation $r \times r$ matrix
$\mathbf{H}^{(n)}$	Noise subspace Householder transformation $(M - r) \times (M - r)$ matrix
$\mathbf{H}_{M-r}^{(n)}$	A noise subspace block Householder transformation (i.e. $\mathbf{H}^{(n)}$)
$\mathbf{H}_r^{(s)}$	A signal subspace block Householder transformation (i.e. $\mathbf{H}^{(s)}$)
\mathbf{I}_{M-r}	Identity $(M - r) \times (M - r)$ matrix
\mathbf{I}_r	Identity $r \times r$ matrix
$d^{(s)}$	The spherical subspaces of the signal eigenvalues of \mathbf{D}
$d^{(n)}$	The spherical subspaces of the noise eigenvalues of \mathbf{D}
$\mathbf{v}^{(n)}$	Equivalent to $\gamma^{(n)} + \text{sign}(\gamma_1^{(n)}) \ \gamma^{(n)}\ \mathbf{e}_1$ vector
$\mathbf{v}^{(s)}$	Equivalent to $\gamma^{(s)} + \text{sign}(\gamma_r^{(s)}) \ \gamma^{(s)}\ \mathbf{e}_r$ vector
η	Equivalent to $(1 - \alpha)^{\frac{1}{2}} \mathbf{H}^T \gamma$ vector
η_r	The r^{th} value of η equivalent to $\ \gamma^{(s)}\ $
η_{r+1}	The $(r + 1)^{\text{th}}$ value of η equivalent to $\ \gamma^{(n)}\ $
\mathbf{b}	A $M \times 1$ vector
ρ	An arbitrary value
κ	An arbitrary value
\mathbf{Q}_2	A 2×2 eigenvector matrix of $[\mathbf{q}_1, \mathbf{q}_2]$
\mathbf{q}_m	Eigenvector of the m^{th} column
$\tilde{\mathbf{D}}_i$	Equivalent to $\alpha \mathbf{D}_{k-1} - \lambda_i \mathbf{I}_2$
λ_i	The eigenvalue corresponding to the i^{th} column of \mathbf{D}_k

\mathbf{q}	Eigenvector
\mathbf{q}_i	Eigenvector corresponding to the i^{th} column of \mathbf{Q}
$\hat{\mathbf{Q}}_k^{(s)}$	Signal subspace eigenvectors $M \times r$ matrix
$\hat{\mathbf{Q}}_k^{(n)}$	Noise subspace eigenvectors $M \times (M - r)$ matrix
$\mathbf{G}^{(s)}$	Signal subspace unitary transformation $r \times r$ matrix
$\mathbf{G}^{(n)}$	Noise subspace unitary transformation $(M - r) \times (M - r)$ matrix
λ_1	Principal eigenvalue of \mathbf{D}_k
λ_2	Noise subspace eigenvalue of \mathbf{D}_k
\mathbf{R}_{xx_i}	Autocorrelation matrix of vector \mathbf{x}_i relative to the i^{th} mobile
P_i	Power received from the i^{th} mobile at the base-station
\mathbf{R}_{IN_i}	Autocorrelation matrix of the interference-plus-noise
$\mathbf{z}_i(n)$	Post-correlation vector of the i^{th} mobile at discrete time n
$b_i(n)$	Information bit of the i^{th} mobile at discrete time n
$\mathbf{a}_i(n)$	The array response vector of the i^{th} mobile at discrete time n
$\hat{\mathbf{a}}_i(n)$	Estimated array response vector of $\mathbf{a}_i(n)$
$c_i(t)$	PN chip of the i^{th} mobile received at time t
$\mathbf{R}_{zz_i}(n)$	Autocorrelation matrix of the i^{th} mobile's post-correlation vector
$\lambda_i(n)$	Principal eigenvalue of \mathbf{R}_{zz_i}
$\lambda_m(n)$	The m^{th} diagonal eigenvalue of \mathbf{R}_{zz_i}
$\mathbf{u}_m(n)$	The m^{th} column eigenvector corresponding to $\lambda_m(n)$
$\mathbf{R}_{ss_i}(n)$	The signal subspace estimated correlation matrix of \mathbf{R}_{zz_i}
$\mathbf{R}_{nn_i}(n)$	The noise subspace estimated correlation matrix of \mathbf{R}_{zz_i}
$\mathbf{x}_{i,l}(t)$	Pre-correlation vector of the i^{th} mobile's l^{th} multipath received
$b_{j,k}$	Information bit of the j^{th} mobile's k^{th} multipath received
$c_{j,k}$	PN chip of the j^{th} mobile's k^{th} multipath received
$A_{j,k}$	Signal amplitude of the j^{th} mobile's k^{th} multipath received
$\mathbf{z}_{i,l}$	Post-correlation vector of the i^{th} mobile's l^{th} multipath
$\mathbf{a}_{j,k}(n)$	Array response vector of the j^{th} mobile's k^{th} multipath at discrete time n
$\mathbf{a}_{j,k}(t)$	Array response vector of $\mathbf{a}_{j,k}$

$\mathbf{R}_{zzi,l}(n)$	Post-correlation matrix of the i^{th} mobile's l^{th} multipath
$\hat{\mathbf{R}}_{nni,l}(n)$	The estimated noise subspace covariance matrix of the i^{th} mobile's l^{th} path
$\hat{\mathbf{R}}_{\text{IN}}^{-1}(n)$	Estimated inverse of the interference-plus-noise correlation matrix
$\mathbf{r}_i(t)$	The DS-QPSK received signal of the i^{th} mobile
$\mathbf{x}_i^I(t)$	In-phase baseband pre-correlation signal of $\mathbf{r}_i(t)$
$\mathbf{x}_i^Q(t)$	Quadrature-phase baseband pre-correlation signal of $\mathbf{r}_i(t)$
$\mathbf{z}_i^I(n)$	In-phase post-correlation signal of \mathbf{x}_i^I
$\mathbf{z}_i^Q(n)$	Quadrature-phase post-correlation signal of $\mathbf{x}_i^Q(t)$
$y_i^I(n)$	Digital beamformed in-phase post-correlation signal of \mathbf{z}_i^I
$y_i^Q(n)$	Digital beamformed quadrature-phase post-correlation signal of \mathbf{z}_i^Q
$\mathbf{w}_i^I(n)$	In-phase weight vector
$\mathbf{w}_i^Q(n)$	Quadrature-phase weight vector
$c_j^I(t)$	In-phase PN sequence of the j^{th} mobile
$d_j^{\text{IS}}(t)$	In-phase short code PN sequence of the j^{th} mobile
d_j^{L}	Long code PN sequence of the j^{th} mobile
$\mathbf{n}^I(t)$	In-phase noise vector
$c_j^Q(t)$	Quadrature-phase PN sequence of the j^{th} mobile
$d_j^{\text{QS}}(t)$	Quadrature-phase short code PN sequence of the j^{th} mobile
$\mathbf{n}^Q(t)$	Quadrature-phase noise vector
$\mathbf{R}_{vv_i}(k)$	The FWFPC correlation matrix of the i^{th} mobile
α_v	The memory factor used to deemphasize old data
$\mathbf{v}_i(r)$	The FWFPC vector
λ_s	Signal subspace eigenvalue
λ_n	Noise subspace eigenvalue
$\hat{\mathbf{D}}_{v_i}(k)$	Estimated eigenvalues matrix of $\mathbf{v}_i(r)$
$\hat{\mathbf{Q}}_{v_i}(k)$	Estimated eigenvectors matrix $\mathbf{v}_i(r)$

Operations and Conventions

$(\cdot)^{\text{T}}$ Transpose of (\cdot)

$(\cdot)^*$	Complex conjugate of (\cdot)
$(\cdot)^\dagger$	Complex conjugate transpose of (\cdot)
$\text{Re}[\cdot]$	Real part of $[\cdot]$
$\mathbf{E}\{\cdot\}$	The expected value of $\{\cdot\}$
\mathcal{R}	Real number domain
\mathcal{C}	Complex number domain
$e(\cdot)$	Exponential to the (\cdot)
$\cos(\cdot)$	Cosine of (\cdot)
$\sin(\cdot)$	Sine of (\cdot)
$\log_{10}\{\cdot\}$	Logorithm of base 10
$\ln[\cdot]$	Natural logorithm of base e of $[\cdot]$
$ \cdot ^2$	Magnitude square
$\ (\cdot)\ $	Magnitude of (\cdot)
$\min_{(\cdot)} \mathbf{F}$	Minimum of function \mathbf{F} with respect to variable (\cdot)
$\nabla^2(\cdot)$	The Hessian matrix of (\cdot)
$\nabla(\cdot)$	Gradient vector of (\cdot)
$\hat{\nabla}_{\mathbf{w}(k)}(\cdot)$	Estimate Gradient vector of (\cdot) w.r.t. $\mathbf{w}(k)$
$\mathcal{L}[(\cdot)]$	Likelihood function of (\cdot)
$\frac{\partial}{\partial(\cdot)} \mathbf{F}$	Differentiating function \mathbf{F} with respect to variable (\cdot)
$\int_a^b(\cdot)$	Integate from a to b
$\sqrt{(\cdot)}$	Square root of (\cdot)
$\delta[t]$	Impulse function
$\sum_{m=1}^{m=M}$	Summation from $m = 1$ up to $m = M$
$P_{\mathbf{s}}\{\cdot\}$	Probability w.r.t. signal \mathbf{s}
$\exp\{\cdot\}$	Exponential function of $\{\cdot\}$
$[\cdot]^{-1}$	Inverse of $[\cdot]$
$O(\cdot)$	Computation of order of (\cdot)
$\lim_{k \rightarrow \infty}(\cdot)$	Limit of (\cdot) as k tends to infinity
$\text{trace}\{(\cdot)\}$	Trace of matrix (\cdot)

$\det(\cdot)$	Determinant of matrix (\cdot)
$\text{rank}(\cdot)$	The rank of (\cdot) matrix
$\Lambda(\cdot)$	The triangular function
$\mathbf{PEV}(\cdot)$	The principal eigenvalue of matrix (\cdot)

Chapter 1

Introduction

The information era has introduced the urgent need for a communication system which can provide flexible and high quality service in the form of a personal communication system capable of carrying voice, data and video signals. In recent years, the growth of mobile phone subscribers has demonstrated the potential market demand for the future. However, due to limited spectrum availability for cellular communications, technology improvements and breakthroughs are the keys to provide the future capacity which can handle the potentially significant number of simultaneous users within a cell. There are a number of proposals for increasing cell capacity, such as reducing the cell size (pico or micro cells), reducing the frequency reuse factor to 4 instead of 7, using time division multiple access (TDMA) instead of the analog advanced mobile phone service (AMPS), using code division multiple access (CDMA) technology to simultaneously share the available radio spectrum with other users, using diversity combiners, using antenna array beamformers, and so on. Physical communication channels pose fundamental limitations on the radio link for mobile communications due to fading, shadowing, the near-far effect, and other factors.

In order to cope with the ever-increasing number of subscribers per cell and finite frequency spectrum resources, the application of Direct Sequence Multiple Access (DSMA)/Code Division Multiple Access (CDMA) into a cellular system has attracted many researchers, especially throughout North America. DS/CDMA efficiently uses the available spectrum by allowing multiple subscribers to simultaneously access the

network. Since the frequency spectral band that is available for the wireless cellular communication systems is limited, using a code division multiple access (CDMA) system can efficiently utilize the available bandwidth.

This thesis has investigated a numerically stable and efficient digital signal processing solution using a digital beamforming technique in a CDMA cellular communications system for the reverse link. The goal is to increase the cell capacity and reduce the number of base station required by exploiting both space and time diversity at the receiver.

1.1 Motivation

With current technology, it is now possible to economically implement very sophisticated and computationally intensive digital signal processing algorithms for practical cellular communications operations. In addition, comprehensive investigations have been conducted on the integration of a “smart” antenna array into the base station for optimal directional receiving and transmitting in order to further increase cell capacity. These “smart” array signal processing techniques extract information from the output of the antenna array and track the energy sources as they move in space. To further increase cell capacity, it has been demonstrated that adaptive or self-adjusted antenna array beamformers hold great potential for improving SINR and hence achieving higher cell capacities [25] [27] [26] [9] [39]. In addition, a modified code filtering algorithm which increases the processing gain has been introduced for application in the North American standard IS-95 CDMA system [9].

With computationally efficient and noniterative eigendecomposition subspace methods [6] [46] and a CDMA system which extracts the desired signal power from the noise-like interfering signals, we are motivated to investigate the novel application of a noniterative subspace eigendecomposition method to a CDMA system.

1.2 Summary of Contributions

The goal of this research is to reduce the amount of computation required and increase stability in order to realize a future real time CDMA cellular system which suppresses interference signals by using digital adaptive beamforming at the base-station antenna array. Only the uplink, i.e. reverse link, of a cellular CDMA system is considered since it presents the most difficult challenge in a CDMA cellular system due to its asynchronous access, near/far effect and the limited power that can be generated by a mobile.

In summary, the contributions of this thesis are as follows:

- A noniterative subspace spherical tracking algorithm to the base-station antenna array of a CDMA cellular communications system was applied in order to reduce computation and enable real-time operation. In particular, a narrowband IS-95 and a generic CDMA system model were used to evaluate the performance of such algorithm.
- The application constraints of using a subspace tracking method under a zero time delay spread (flat fading) and non-zero time delay spread (frequency selective) fading propagation models were derived.
- The array response estimate NR1SSU tracking was evaluated (through the DOA representation for easy visualization) for the weight vectors updating at the rate of one IS-95 frame with the rank-one update of the FWPC vectors in an IS-95 CDMA system and at the rate of one information bit with the rank-one update of the PN chip post-correlation vectors in a generic CDMA system.
- The performance of using a beamforming only receiver to a beamsteered-RAKE receiver structure under a frequency selective fading propagation model was compared.
- The performance of using a beamforming receiver to a diversity combiner under a flat fading propagation model was compared.

- Implementing a beamformer at each diversity branch to further increase the signal-to-interference-plus-noise ratio was proposed.

1.3 Thesis Organization

This chapter introduces the motivation behind this thesis and summarizes the overall contributions made. Chapter 2 reviews the fundamentals for array signal processing techniques and, in particular, digital beamforming techniques. Chapter 3 reviews the background of cellular communication systems and the current application of CDMA technology to cellular communications using beamformers and beamsteered-RAKE receiver structures. Chapter 4 introduces the novel application of a noniterative subspace tracking method with analytical derivations of the constraints involved with applying such a subspace method in a CDMA communication system. Chapter 5 presents simulation results for the application of a NR1SSU algorithm under both IS-95 and a generic CDMA system with either flat fading or frequency selective fading propagation models. Chapter 6 concludes this thesis and presents future directions for research.

Chapter 2

Antenna Arrays and Digital Beamforming

2.1 Introduction

This chapter reviews and explores conventional antenna array processing concepts and delay-and-sum adaptive beamforming techniques. Section 2.2 introduces antenna array processing concepts, and the spatial filtering capability of an antenna array is presented in Section 2.3. Different performance criteria for estimating statistically optimum beamforming weight vectors are reviewed in Section 2.4. It is interesting that all of the criteria considered here converge toward the same steady-state Wiener solution, within a constant scalar factor. Finally, conventional adaptive beamforming algorithms are reviewed in Section 2.5.

2.2 Antenna Arrays

Sensor arrays have been in use for several decades in many practical signal processing applications such as radar, sonar, communications, imaging, geophysical exploration, astrophysical exploration, biomedical, etc. Antenna arrays offer two basic improvements over the signal processing capabilities of a single antenna. First, an array permits some bearing-resolving capability whereas a single sensor cannot. Second, it

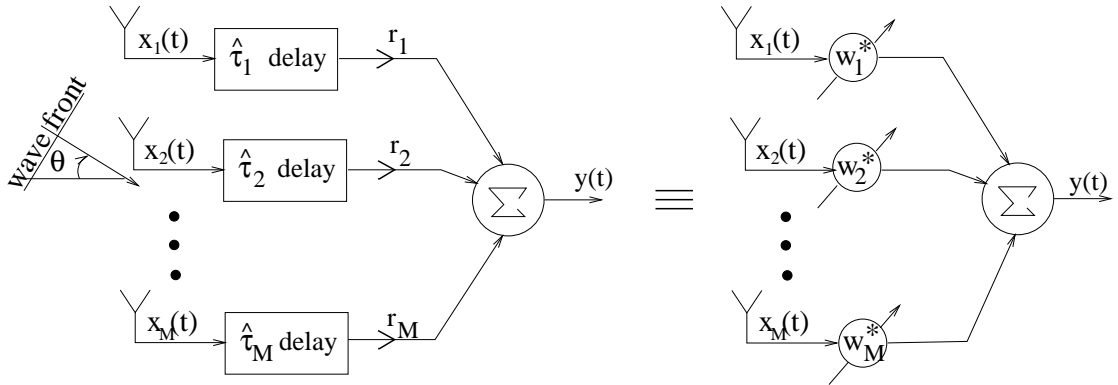


Figure 2.1: A beamformer which combines antenna outputs after a delay and scale weighting has been applied.

increases the signal-to-interference-noise ratio (SINR) when the weighting of delays at the antenna array match the actual delays of the desired signal as received at each antenna element. This results in coherent combining of the components of the desired signal. Antenna arrays used in conjunction with appropriate array signal processing techniques offer the possibility of overcoming the sensitivity and beamwidth limitations of a single antenna as well as allowing modification of the array beam shape. This can enhance the reception or transmission of a desired signal by suppressing interfering signals or spatial filtering.

In recent years, adaptive signal processing at the antenna array in cellular communication systems for optimal directional transmission and reception in order to improve SINR has attracted much research interest [20] [27] [26] [24] [33]. Figure 2.1 shows a general complex-weighted M-element antenna array which produces a single output [23] [17],

$$y(t) = \mathbf{w}^\dagger \mathbf{x}(t) = \sum_{m=1}^M w_m^* x_m(t) = \sum_{m=1}^M r_m x_m(t - \hat{\tau}_m) \quad (2.1)$$

where $y(t)$ is the weighted antenna array complex-valued scalar output at time t , $\mathbf{w} = [w_1, w_2, \dots, w_M]^T$ is the $M \times 1$ complex weight vector, $\mathbf{x}(t) = [x_1(t), x_2(t), \dots, x_M(t)]^T$ is the $M \times 1$ antenna array received signal output vector at time t , r_m is the amplitude weighting of the complex weight applied to the m^{th} antenna element output, and $\hat{\tau}_m$ is the corresponding time delay. The amplitude weighting vector $[r_1, r_2, \dots, r_M]^T$

is sometimes called the array's shading or taper [23]. Array signal processing algorithms which focus on the array's signal-capturing abilities in a particular direction are termed *beamforming*. Therefore, Figure 2.1 also represents a beamformer.

2.2.1 Antenna Array Signal Model

In order to introduce a signal model, a simple scenario is considered where only a RF signal of an i^{th} mobile, $s_i(t)$, is transmitting and impinging the antenna array as narrowband plane-waves¹. The superposition principle of plane-waves traveling in space can then be applied to this plane-waves model for receiving multiple signals. A signal is considered to be narrowband when the band of frequencies occupied by the received signals is small relative to the carrier frequency f_c [29]. The narrowband assumption can also be applied to wideband signals, as in the case of CDMA, provided that the propagation time across the array is small compared to the inverse bandwidth of the signal and that the frequency response of each antenna element is approximately flat over the signal bandwidth [24].

From the above assumptions and the fact that the output of a bandpass system is a bandpass signal [29], the signal vector received at the antenna array of the transmitted signal $s_i(t)$ can be expressed as

$$\begin{aligned}
 \mathbf{r}(t) &= s_i(t) * h(\tau; t) + \mathbf{n}(t) \\
 &= \text{Re} \left[\sum_{k=1}^{J_i} \varrho_{i,k}(t) e^{-j\omega_c \tau_{ik}} \mathbf{a}_{i,k}(\Theta) u_i(t - \tau_{ik}) e^{j\omega_c t} \right] + \mathbf{n}(t) \\
 &= \text{Re} \left[\sum_{k=1}^{J_i} \varrho_{i,k}(t) e^{-j\omega_c \tau_{ik}} \mathbf{a}_{i,k}(t) u_i(t - \tau_{ik}) e^{j\omega_c t} \right] + \mathbf{n}(t) \tag{2.2}
 \end{aligned}$$

where [29]

$$h(\tau; t) = \sum_{k=1}^{J_i} \varrho_k(t) e^{-j\omega_c \tau_{ik}} \delta[t - \tau_{ik}] \tag{2.3}$$

¹Since an electromagnetic wave propagates spherically in space, the plane-wave assumption is valid for the far-field signal. However, for a near-field signal, a spherical wave impinges on the antenna array. The plane-wave assumption can be relaxed at the expense of complicating the array response model, in which for near-field signals and a 2-D array, the azimuth and range of the signal have to be considered.

is the time-variant channel impulse response with the total number of the resolvable multipaths, J_i , received from the i^{th} transmitted mobile ($J_i = 1$ represents a flat fading channel and $J_i > 1$ represents a frequency-selective fading channel) [29] [43], $\rho_{i,k}(t)$ is the time-varying channel amplitude gain of the i^{th} mobile's k^{th} multipath, τ_{ik} is the channel time delay of the k^{th} multipath of the i^{th} transmitting mobile, $s_i(t) = \text{Re}[u_i(t)e^{j\omega_c t}]$ is the transmitted RF signal with carrier frequency ω_c , $u_i(t)$ is the transmitted baseband signal of the i^{th} transmitting mobile, $\mathbf{n}(t) \in \mathcal{N}(\mathbf{0}, \sigma^2 \mathbf{I})$ is the noise vector received at the antenna array, $\delta[t]$ is the impulse function, and $\mathbf{a}_{i,k}(\Theta) = \mathbf{a}_{i,k}(t)$ is the array response vector corresponding to the i^{th} mobile's k^{th} received multipath (which will be defined in Section 2.2.2). Details of the multipath propagation channel modeling will be reviewed in Chapter 3.

2.2.2 Array Response Vector

An array response vector [23] [24] of a signal impinging on an array at broadside time-varying direction-of-arrival (DOA), $\theta(t) = \theta$, and having a carrier frequency $\omega_c = 2\pi f_c$ can be expressed as

$$\mathbf{a}(t) = \mathbf{a}(\Theta) = [G_1(\omega_c, \theta, \Omega_1)e^{-j\omega_c \tau_1(\theta, \Omega_2)}, \dots, G_M(\omega_c, \theta, \Omega_M)e^{-j\omega_c \tau_M(\theta, \Omega_M)}]^T \quad (2.4)$$

where Θ denotes the set of variables that the array response vector depends on (the set of variables of Θ are the angle of DOA θ , the carrier frequency ω_c , each antenna element's mutual coupling resistance Ω_m , time t , and etc.), $G_m(\omega_c, \theta, \Omega_m)$ is the m^{th} antenna's amplitude response, and $\tau_m(\theta, \Omega_m) = \tau_m$ is the m^{th} element's time delay response [17] [37]. Note that the angle θ are measured with respect to the normal of an antenna array which is called the broadside DOA.

In order to present the DOA tracking results in Chapter 5, the beamforming simulation results of the array response vectors presented in Chapter 5 had been parameterized to the direction of arrival, θ . Parameterization was done based on the assumption that the antenna array was ideally calibrated, in which the amplitude response $G_m(\omega_c, \theta, \Omega_m)$ is calibrated to unity with respect to the carrier frequency

ω_c , the mutual coupling effect Ω_m , and the direction of arrival θ . In addition, it is assumed that the time delay between antenna elements is linear with respect to the mutual coupling effect. Therefore, the array response vector can be written in terms of the time delay as

$$\mathbf{a}(\theta, \omega_c) = [e^{-j\omega_c\tau_1}, e^{-j\omega_c\tau_2}, \dots, e^{-j\omega_c\tau_M}]^T \quad (2.5)$$

where τ_m simply represents the time delays. Note that, the principal eigenvectors decomposed from the eigendecomposition method of the autocorrelation matrix of a received signal vector with signal power higher than that of the interference-plus-noise is an accurate array response vector estimate which does not required an antenna array to be calibrated. The principal eigenvectors of such decomposition are an accurate array response vector estimate of Equation (2.4) [17]. The evaluation of the applied algorithm in terms of the DOA estimated is for easier visual presentation only.

The estimated time-varying DOA, $\hat{\theta}$, of an uniformly calibrated circular array (UCA) in Chapter 5 are parameterized based on Equation 2.6 referring to Figure 2.2

$$\begin{aligned} \tau_m &= \frac{R}{c} \cos\left(\frac{\pi}{2} - \hat{\theta} - \psi_m\right) \\ &= \frac{1}{c} \frac{d}{2 \sin \frac{\pi}{M}} \sin\left(\hat{\theta} + \frac{2\pi(m-1)}{M}\right) \end{aligned} \quad (2.6)$$

where R is the radius of the UCA, d is the equal antenna spacing between adjacent antenna elements, c is speed of light, M is the total number of antenna elements of the UCA, $\psi_m = 2\pi(m-1)/M$ for $m = 1, 2, \dots, M$ is the angle of the m^{th} antenna element with respect to the center of the UCA measured counterclockwise from the x-axis, and $\hat{\theta}$ is the estimated DOA which measured from the normal of the x-axis as shown in Figure 2.2.

The estimated time-varying DOA, $\hat{\theta}$, of an uniformly calibrated linear array (ULA) are parameterized base on the equation below with graphical presentation shown in Figure 2.3

$$\tau_m = (m-1) \frac{d}{c} \sin \hat{\theta} \quad (2.7)$$

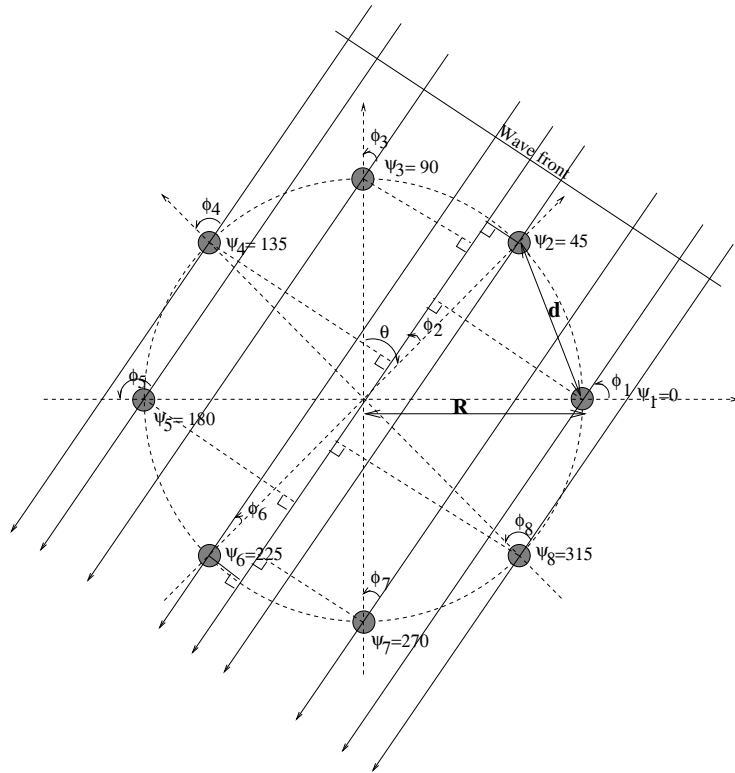


Figure 2.2: An eight-element circular array of DOA θ , assuming the reference point is the center of this circular array

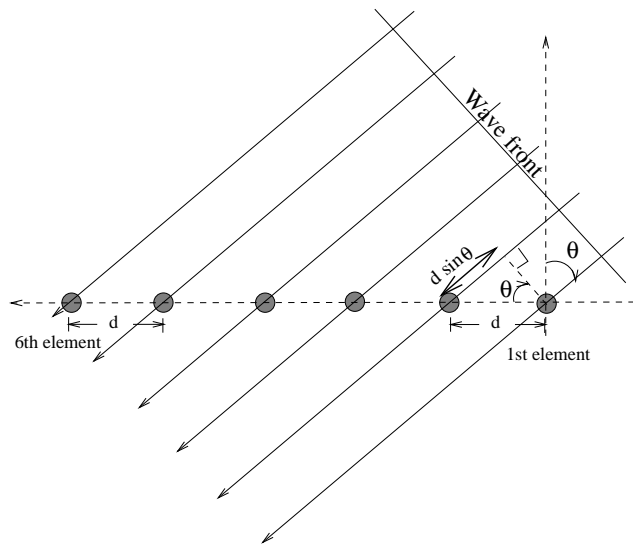


Figure 2.3: A six-element uniform linear array with a plane wave impinging from DOA θ

where $\frac{d}{c} \sin \hat{\theta}$ is the time delay between equi-spaced adjacent antenna elements, c is the speed of light, d is the equi-spaced inter-element distance, and $\hat{\theta}$ is the broadside DOA to be estimated.

2.2.3 Spatial Resolution

The spatial passband and stopband of an antenna array can be affected by the choice of array geometry, spatial aperture, and antenna weights. The angular resolution of an antenna array can be used to evaluate its ability to accurately attenuate powers from directions other than the desired direction. High angular resolution improves the maximum output signal-to-interference-plus-noise ratio (SINR) when the angular separation between the desired and undesired signals is small. The reciprocal of the 3 dB beamwidth/spatial passband of the main lobe (the principal lobe) of the antenna array's beam pattern is the array's angular resolution. In other words, the narrower the main lobe, the better the spatial filtering capability of the antenna array. Note that the main lobe of an array's directivity pattern is called a *beam*. A directivity pattern is also called the *beam pattern* [23].

2.3 Antenna Array Spatial Filtering Capability

Antenna arrays equipped with appropriate weightings can be utilized to obtain some degree of spatial filtering or directional sensitivity over incoming signals. The directional/beam pattern [23] [42] of a weighted antenna array, which represents the relative sensitivity of a response to signals coming from DOA θ and having an array response vector of $\mathbf{a}(\Theta)$, can be defined as

$$A(\Theta) = \mathbf{w}^\dagger \mathbf{a}(\Theta) = \sum_{m=1}^M w_m^* e^{-j\omega_c \tau_m} = \sum_{m=1}^M r_m e^{-j\omega_c (\tau_m - \hat{\tau}_m)} \quad (2.8)$$

where $w_m = r_m e^{j\omega_c \hat{\tau}_m}$ is the complex weight with shading r_m and a time delay of $\hat{\tau}_m$ that is applied to the m^{th} antenna element's output as shown in Figure 2.1, τ_m is the time delay of a plane-wave impinging on the array measure from the array reference

point, and M is the number of antenna array elements. Equation (2.8) can be easily understood as stacking the M phase-shifted and amplitude-weighted received signals to create nulls or peaks.

Using the directional pattern defined in equation (2.8), the normalized directional pattern or normalized gain $G(\Theta)$ [23] [42] of an M -element array can be expressed as

$$G(\Theta) = 10 \log_{10} \left\{ \frac{|A(\Theta)|^2}{(\sum_{m=1}^M r_m)^2} \right\} \quad (2.9)$$

since $A(\Theta)$ maximized when $\tau_m = \hat{\tau}_m$.

Using the normalized directional pattern, we can now explore the effects on the beam pattern (spatial filtering capability) caused by different choices for the antenna array spatial aperture d , array geometry (UCA or ULA and/or the number of antenna elements used), and weighting vectors $\mathbf{w} = [w_1, w_2, \dots, w_M]^T$. The antennas considered here are omnidirectional and the array response time delays τ_m of an UCA and ULA follows Equations (2.6) and (2.7), respectively, for presentation purposes. The normalized directional pattern, showing the relative sensitivity of the spatial array response to incoming DOAs θ , are evaluated over a range of $-180^\circ \leq \theta \leq 180^\circ$ which includes plane-waves impinging on the array from every angle.

2.3.1 Effect of antenna time-delay weight

First, we consider the beam pattern with $r_m = 1$ for $m = 1, 2, \dots, M$, that is, no shading is applied. The directivity pattern can then be written as

$$A(\Theta) = \sum_{m=1}^M e^{-j\omega_c(\tau_m - \hat{\tau}_m)} \quad (2.10)$$

Equation (2.10) suggests that the maximum spatial response to a particular DOA, θ_0 , occurs when $\hat{\tau}_m = \tau_m$. This in turn produces the ability to steer beams. Referencing Equation (2.6), to steer a beam of UCA to the DOA θ_0 , $\hat{\tau}_m$ is set to

$$\hat{\tau}_m = \frac{d}{c2 \sin(\pi/M)} \sin \left(\theta_0 + \frac{2\pi(m-1)}{M} \right) \quad (2.11)$$

referring to Equation (2.6) and the phasor of equation (2.10) becomes

$$= \frac{\omega_c(\tau_m - \hat{\tau}_m)}{\lambda_c} \frac{d}{2 \sin(\pi/M)} \left(\sin \left(\theta + \frac{2\pi(m-1)}{M} \right) - \sin \left(\theta_0 + \frac{2\pi(m-1)}{M} \right) \right) \quad (2.12)$$

and similarly, by referencing Equation (2.7), a ULA can steer the beam to DOA θ_0 , with the phasor of equation (2.10) becoming

$$\omega_c(\tau_m - \hat{\tau}_m) = \omega_c(m-1)(\beta - \hat{\beta}) = (m-1) \frac{2\pi}{\lambda_c} d(\sin \theta - \sin \theta_0)$$

Figure 2.4 and 2.5 show the beam steering ability of a UCA and a ULA, respectively, when the steering angle θ_0 equals 20° , 50° , 100° , -50° . Note that the beam of a UCA retains the same 3 dB beamwidth while it is steering; however, the beamwidth of a ULA gradually increases as the beam steers away from broadside. It can be reasoned that the directivity gain pattern of a ULA, in response to a DOA, θ , with the time delays $\hat{\tau}_m$ being designed to steer at θ_0 , can be written as

$$\begin{aligned} A(\Theta) &= \sum_{m=1}^M e^{-j\omega_c(\tau_m - \hat{\tau}_m)} = \sum_{m=1}^M e^{-j(m-1)(\beta - \hat{\beta})} \\ &= \frac{\sin \frac{M(\beta - \hat{\beta})}{2}}{\sin \frac{(\beta - \hat{\beta})}{2}} = \frac{\sin \frac{M\pi d}{\lambda_c} (\sin \theta - \sin \theta_0)}{\sin \frac{\pi d}{\lambda_c} (\sin \theta - \sin \theta_0)} \end{aligned} \quad (2.13)$$

by using the equality $\sum_{m=0}^{M-1} a^m = (1 - a^M)/(1 - a)$. From equation (2.13), we see that the normalized beam pattern value depends on the difference between the sines of the angles (a change of sign will occur when the DOAs are off-broadside) rather than on the difference between the angles themselves (when θ_0 is close to broadside, $\sin \theta_0 \approx \theta_0$). Therefore, the array pattern plots have different shapes depending on the value of the steered angle θ_0 [17]. Thus, a ULA beam pattern has a larger main beamlobe asymmetry for a larger off-broadside steering angle θ_0 .

Note that lobes which have a gain level much below that of the mainlobe are called sidelobes and lobes which have the same gain level as the mainlobe are called grating lobes. Grating lobes are usually undesirable and are also classified as interferometer effects [23].

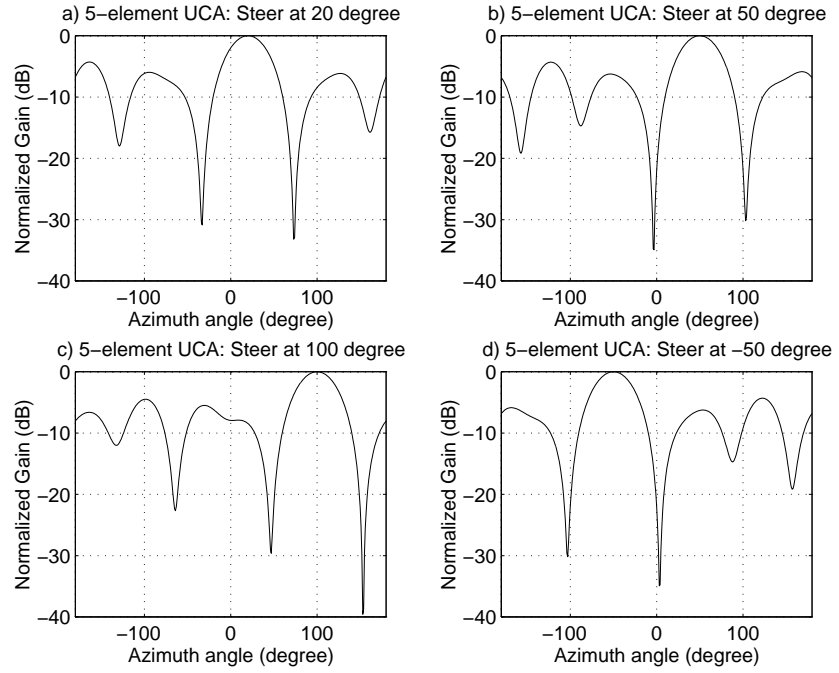


Figure 2.4: A 5-element UCA beam steering at different DOAs with $d = 0.5\lambda$.

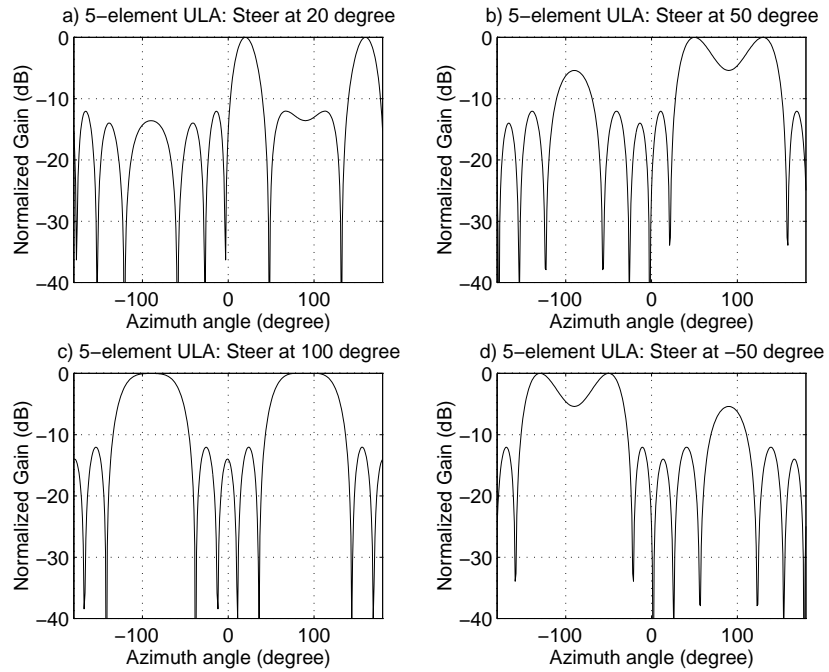


Figure 2.5: A 5-element ULA beam steering at different DOAs with $d = 0.5\lambda$.

Therefore, antenna arrays equipped only with phase shifting (time delays) at each array element output provide a steering ability of their spatial filter beam patterns. In order to observe the effect of employing time delays in isolation, the antenna element spacing was kept constant at one-half the carrier wavelength and the total number of antenna elements used was five in Figures 2.4 and 2.5, the mainlobe steered correspondingly to the steered angle θ_0 as θ_0 varies.

2.3.2 Effect of number of antenna elements

The effect on the beam pattern of using different numbers of antenna elements is now considered. Again, the antenna spacing d is kept constant at one-half the carrier wavelength, the steering angle is kept at zero broadside or DOA $\theta_0 = 0$, and shading is not considered (i.e. $r_m = 1$ for all m). Performing a similar comparison between a one-dimensional linear array and a 2-dimensional circular array, Figures 2.6 and 2.7 show the beam patterns for 3, 4, 5, and 10-element UCAs and ULAs respectively. It is clear that increasing the number of antenna elements improves the resolution which in turn improves the spatial filtering performance. In Figure 2.7(c), the 3 dB beamwidth of a 5-element ULA is about 20° compared to the 10° 3 dB beamwidth of the 10-element ULA in Figure 2.7(d).

In addition, using different array geometries, such as a one-dimensional ULA, produces different beam patterns and beamwidths than, for example, a 2-dimensional planar UCA. The 3 dB beamwidth of a 5-element ULA as shown in Figure 2.7(c) is about 20° while the 3dB beamwidth of a 5-element UCA is about 50° degrees as shown in Figure 2.6(c).

2.3.3 Effect of shading

We now consider the effect of adding shading to the beam pattern. The shading or windowing of the amplitudes at the antenna outputs permits trading off the mainlobe beamwidth against sidelobe levels [14]. As shown in Figures 2.8 and 2.9, 10-point Blackman and Hamming windows are used to demonstrate how shading can shape

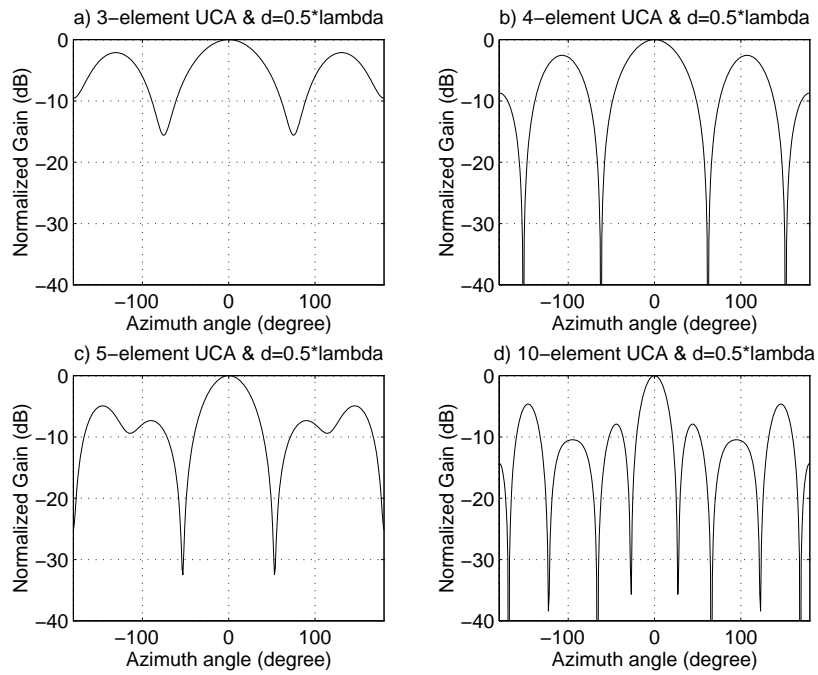


Figure 2.6: UCA 3, 4, 5, and 10 antenna elements with equi-spaced antenna elements of one-half carrier wavelength a) 3-element b) 4-element c) 5-element d) 10-element

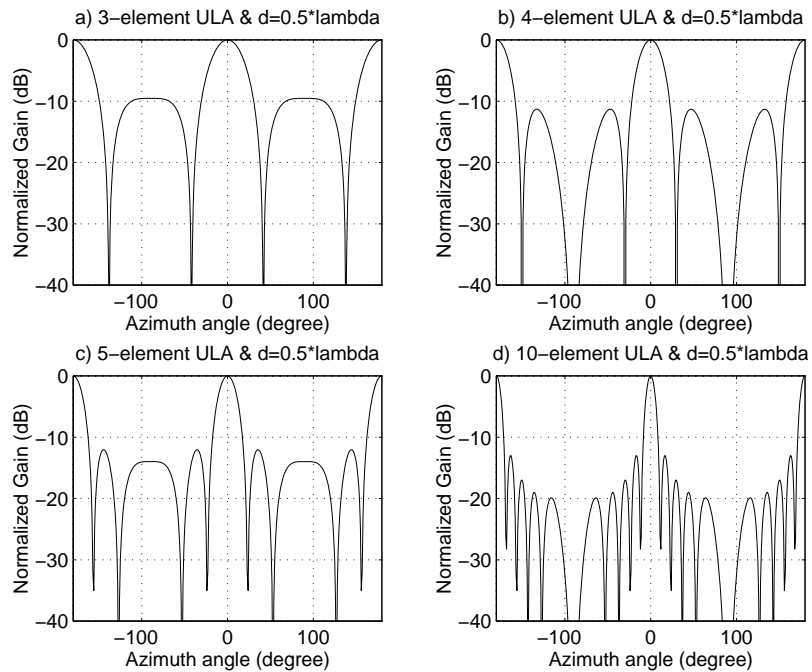


Figure 2.7: ULA 3, 4, 5, and 10 antenna elements with equi-spaced antenna elements of one-half carrier wavelength a) 3-element b) 4-element c) 5-element d) 10-element

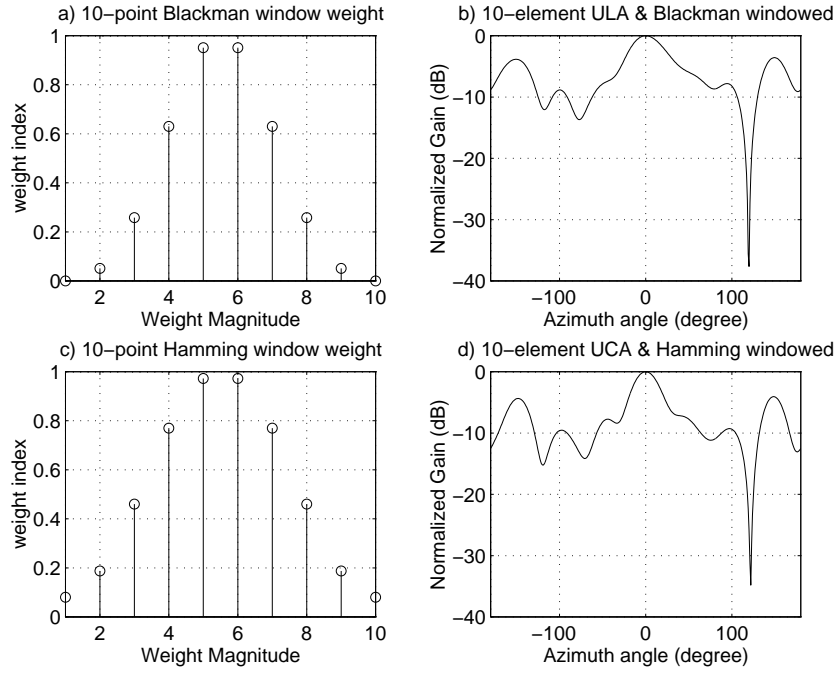


Figure 2.8: Using shading weights to shape the beampattern of a UCA

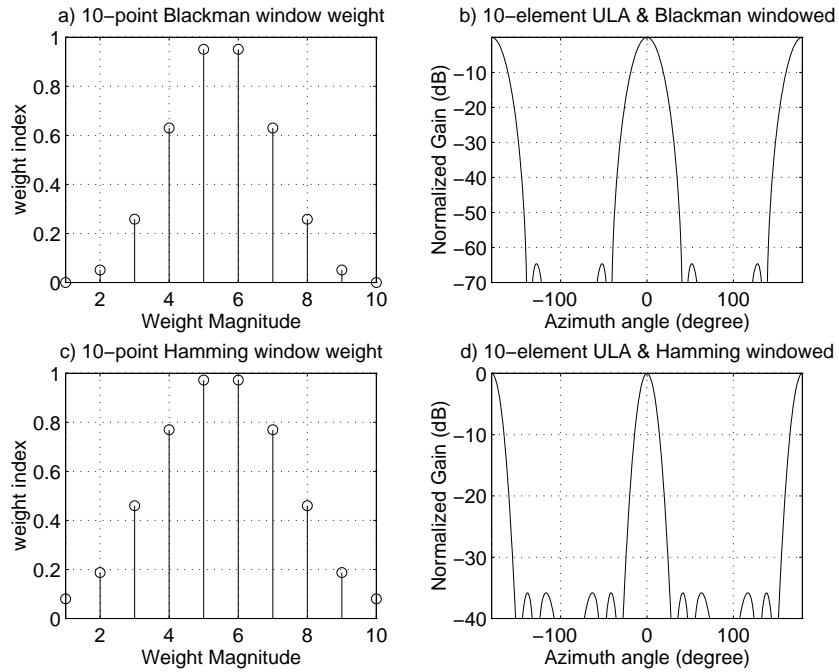


Figure 2.9: Using shading weights to shape the beampattern of a ULA

the beampattern. When comparing Figure 2.9(b) to 2.7(d), Blackman windowing attenuated the sidelobe levels by as much as 50 dB from the original sidelobe levels. However, the 3 dB beamwidth in Figure 2.9(b) is now about 22° wider than that of the original 3 dB beamwidth of about 10° in Figure 2.7(d). Again, the other variable quantities have been constant one-half carrier wavelength equi-spaced 10-element ULA and UCA, and array steering at $\theta_0 = 0$.

Thus, without physically changing the directivity of an antenna or the number of antenna elements, the array can steer or shape the array beam pattern by incorporating time delays and shading at the outputs of an antenna array.

2.3.4 Effect of antenna element spacing

Finally, the effect of array spatial aperture, that is, the separation between elements is considered. Figures 2.10 and 2.11 show the effects of varying the spatial aperture of a 5-element ULA and UCA, respectively, while keeping the array shading at $r_m = 1$ for $m = 1, 2, \dots, M$, and steering at $\theta_0 = 0$. Note that the absolute separation between antenna elements is not important; rather, its size as measured in carrier wavelengths [23]. These plots show that as the spatial aperture increases, the main lobe beam gets narrower. However, this trades-off with the grating lobes becoming more significant. These effects will lead to a degradation of the weighted output SINR since interfering signals will be passed through the grating lobes with a high spatial gain. To avoid grating lobe or interferometer effects for omnidirectional antennas, a maximum element spacing of $\lambda_c/2$ is usually used and such an array is called a “filled array”. Filled arrays, however, need a larger number of antenna elements to obtain resolution than is available with a wider spatial aperture. Also, the antenna spacing should not be less than $\lambda_c/4$, which is considered to be inefficient since there is very little difference in the directional pattern as compared to that of a single element antenna [23].

When element spacing is allowed to be larger than one-half wavelength, nonuniformly spaced array elements can be employed to disrupt the periodic beam pattern

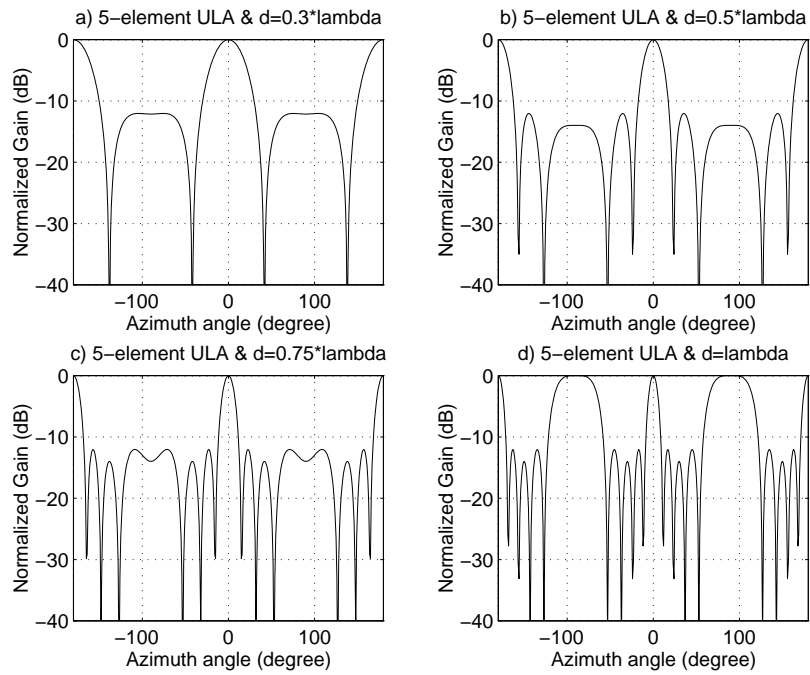


Figure 2.10: A 5-element ULA: a) spatial aperture d is 0.3 carrier wavelength λ_c , b) d is $0.5 \lambda_c$, c) d is $0.75 \lambda_c$, d) d is λ_c

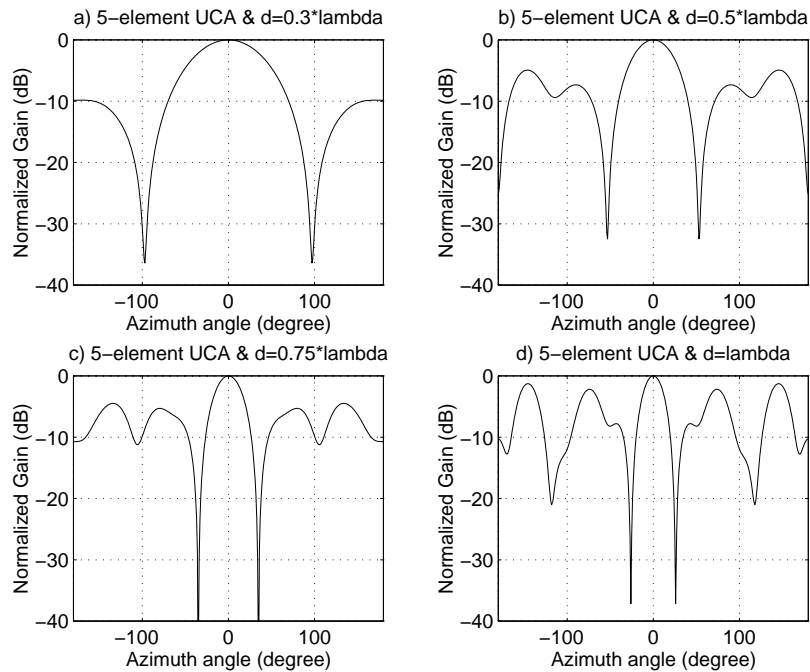


Figure 2.11: A 5-element UCA: a) spatial aperture d is 0.3 carrier wavelength λ_c , b) d is $0.5 \lambda_c$, c) d is $0.75 \lambda_c$, d) d is λ_c

structure. The wider the antenna element spacing, the less correlation between the received signals at adjacent antenna elements. In this case, the plane wave assumption will no longer hold. Large antenna element spacing will produce space diversity where each element's received signals are mutually uncorrelated or with a very low correlation of less than 0.5 [33]. Instead of using omnidirectional antennas, directional antennas (as used in sectorization) can also improve SINR performance since grating nulls can be eliminated. However, in a cellular communication systems the increased number of hand-offs required between sectors could reduce overall system performance.

In practice, the correlation of signals received at adjacent antennas is related to the antenna element spacing and the angle spread of the received signal [21] [22] [33]. In order for the plane-wave assumption to hold, an uniform antenna element spacing of one-half the wavelength or less is generally maintained to obtain high correlation (at least 0.8) between the signals sampled at each element. As with the narrowband assumption made previously, the plane-wave signal assumption will still hold provided that the propagation time across the array is much less than the inverse of the channel bandwidth. Therefore, throughout this thesis for beamforming environment, it is assumed that the channel produces J_i multipath of the i^{th} transmitting mobile that impinging on the array, where each corresponding information-bearing plane-wave has a different channel gain $\rho_{i,k}(t)$ and phase shift τ_{ik} for different DOA θ_k within the angle spread for each k^{th} multipath.

2.3.5 Summary of effects of antenna array variables

In summary, the antenna array spatial filtering resolution increases as the number of antenna elements increases. As antenna element spacing (the spatial aperture) increases, resolution will also increase, but this trade-offs with the presence of grating lobes. Shading can suppress the spatial gain of sidelobes while trading off resolution. The resolution of a ULA decreases as it steers off-broadside, while a UCA appears to have the same resolution as it steers around its full angular range. Also, different

types of array geometries, such as ULA and UCA, provide different resolutions and beam patterns.

2.4 Statistically Adaptive Optimum Beamforming Weight Vectors

Depending on how the beamforming weights are chosen, beamformers can be classified either as data independent or statistically optimum. The weights in a data independent beamformer do not depend on the received array data and are chosen to present a specified response for all signal and interference scenarios. In practice, propagating waves are perturbed by the propagation medium or the receive mechanism. In this case, the plane-wave assumption may no longer hold and weight vectors that assumed plane-wave time delays between adjacent elements will not combine the waves of the desired signal coherently.

Matching of a randomly perturbed signal with arbitrary characteristics can be realized only in a statistical sense by using a matrix weighting of input data which adapts to the received signal's characteristics [23]. This is called statistically optimum beamforming. In this case, the weight vectors are chosen based on the statistics of the received data. The weights are selected to optimize the beamformer response so that the array output contains minimal contributions due to noise and signals arriving from directions other than the desired signal direction [42].

Any performance degradation resulting from a deviation of the actual operating conditions from the assumed ideal conditions is minimized by the use of complementary methods that introduce constraints. Due to our interest in applying array signal processing techniques in cellular CDMA communications where mobiles can be located anywhere in the cell, statistically optimum beamformers provide the ability to adapt to the statistics of different subscribers.

The performance criteria described are applicable to continuous-time as well as discrete-time beamforming. We assume that each antenna has the necessary receiver

electronics and an analog-to-digital converter for performing digital beamforming. The steady-state statistically optimum beamforming weight vectors discussed in this section are based on different criteria and assume knowledge of the asymptotic second-order statistics of the received array data. It is important to determine the steady-state performance limits for different types of optimum weight measures since such limits provide an indication of how well the selected design will perform.

There are different criteria for determining statistically-optimum beamformer weights, several of which are reviewed in this section. The criteria measured presented here include minimum mean square error (MMSE), maximization of signal-to-interference-plus-noise ratio (SINR), maximum likelihood (ML), and linearly constrained minimum variance (LCMV).

In deriving the following optimum weights, it is convenient to represent the signal envelopes as well as the adaptive weights in their complex envelope form [23]. In any system only real signals actually appear, and the relationship between the real and corresponding complex signal is defined as

$$\text{actual signal} = \mathbf{Re}\{\text{complex signal envelope } e^{j\omega_c t}\}$$

Therefore, equation (2.2) can be rewritten as

$$\mathbf{r}(t) = \mathbf{Re} \left[\mathbf{x}(t)e^{j\omega_c t} \right] \quad (2.14)$$

where $\mathbf{x}(t)$ is the complex envelope of the received signal $\mathbf{r}(t)$. The output of the weighted antenna array then follows as

$$y(t) = \mathbf{Re} \left[\mathbf{w}(t)^\dagger \mathbf{x}(t)e^{j\omega_c t} \right] \quad (2.15)$$

where $\mathbf{w}(t)^\dagger \mathbf{x}(t)$ is the complex envelope representation of $y(t)$.

Throughout this thesis, the signal envelopes and the weights are all represented by the complex envelope of the actual signal.

2.4.1 Minimum mean square error (MMSE)

If sufficient knowledge of the desired signal is available, a reference signal y_d can then be generated. These reference signals are used to determine the optimal weight vector

$\mathbf{w}_{\text{MSE}} = [w_1, w_2, \dots, w_M]^T$ by minimizing the mean square error (MMSE) of the M -element antenna array [44]. Figure 2.12 shows a block diagram of an adaptive system using reference signals. Mathematically, the MMSE criteria can be expressed as

$$\min_{\mathbf{w}} E\{|y_d - y|^2\} = \min_{\mathbf{w}} \mathbf{E}\{\varepsilon^2\} \quad (2.16)$$

where $y = \mathbf{w}^\dagger \mathbf{x} = \sum_{m=1}^M w_m^* x_m$ is the weighted array output, and $\mathbf{x} = [x_1, x_2, \dots, x_M]^T$ is the signal received at the antenna array. The minimum of equation (2.16) can be found by differentiation with respect to \mathbf{w} and then setting the result equal to zero. The Hessian matrix $\mathbf{E}\{\varepsilon^2\}$ is $\nabla^2 \mathbf{E}\{\varepsilon^2\} = \mathbf{E}\{\mathbf{x}\mathbf{x}^\dagger\} = \mathbf{R}_{xx}$ which is greater than zero since \mathbf{R}_{xx} is a positive-definite matrix. A matrix \mathbf{R}_{xx} is positive-definite if $\mathbf{x}^\dagger \mathbf{R}_{xx} \mathbf{x} > 0$ for all nonzero \mathbf{x} vectors. There exists a computationally stable factorization $\mathbf{R}_{xx} = \mathbf{L}\mathbf{D}\mathbf{L}^\dagger$ for a symmetric matrix $\mathbf{R}_{xx} = \mathbf{E}\{\mathbf{x}\mathbf{x}^\dagger\}$ where \mathbf{L} is the lower triangular matrix and $\mathbf{D} = \text{diag}(d_1, d_2, \dots, d_M)$ is a diagonal matrix [13]. The additive white Gaussian noise (AWGN) received vector $\mathbf{n}(t) \sim (0, \sigma_n^2 \mathbf{I})$ where σ_n^2 is the nonzero noise power implies that $\mathbf{D} > 0$ always; therefore, \mathbf{R}_{xx} is positive-definite.

Consider the gradient vector of $\mathbf{E}\{\varepsilon^2\}$ with respect to \mathbf{w}

$$\nabla \mathbf{E}\{y_d^2 + \mathbf{w}^\dagger \mathbf{x}\mathbf{x}^\dagger \mathbf{w} - 2\mathbf{w}^\dagger \mathbf{x}y_d\} = 2\mathbf{R}_{xx}\mathbf{w} - 2\mathbf{r}_{xd} = 0 \quad (2.17)$$

where $\mathbf{R}_{xx} = \mathbf{E}\{\mathbf{x}\mathbf{x}^\dagger\}$ is the autocorrelation matrix and $\mathbf{r}_{xd} = \mathbf{E}\{\mathbf{x}y_d\}$ is the cross-correlation matrix. Thus, the optimal MMSE weight solution is

$$\mathbf{w}_{\text{MSE}} = \mathbf{R}_{xx}^{-1} \mathbf{r}_{xd} \quad (2.18)$$

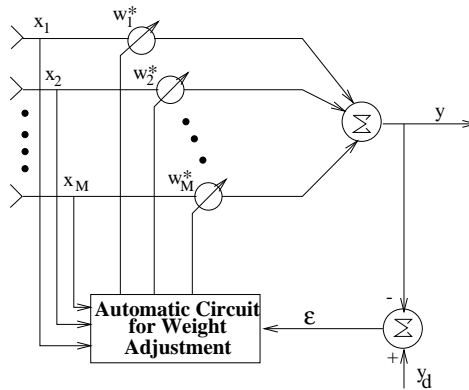


Figure 2.12: Reference signal adaptive antenna

and is called the Wiener solution.

The advantage of using a reference signal is that the desired signal bearing can be unknown. The disadvantage of using this method is generating an accurate reference signal based on limited knowledge at the receiver.

2.4.2 Maximization of signal-to-interference-plus-noise ratio (SINR)

The weighted array output of a beamformer can be expressed as

$$\mathbf{y} = \mathbf{w}^\dagger (\mathbf{s} + \mathbf{i} + \mathbf{n}) = \mathbf{y}_s + \mathbf{y}_{\text{IN}} \quad (2.19)$$

where $\mathbf{s} = \sigma_s u_s(t) \mathbf{a}(t)$ is assumed to be the signal vector, σ_s is the signal amplitude, $u_s(t)$ the binary baseband signal information, $\mathbf{a}(t)$ represents the array response vector of the signal arriving from DOA θ_0 , $\mathbf{y}_s = \mathbf{w}^\dagger \mathbf{s}$ is the desired signal array response weighted output, $\mathbf{y}_{\text{IN}} = \mathbf{w}^\dagger (\mathbf{i} + \mathbf{n})$ is the interference-plus-noise total array response weighted output, \mathbf{s} is the $M \times 1$ desired signal array response vector, \mathbf{i} is the $M \times 1$ total interference signal power array response vector, and \mathbf{n} is the $M \times 1$ noise array response vector. Consequently, the weighted array signal output power is

$$E\{|y_s|^2\} = \mathbf{w}^\dagger \mathbf{E}\{\mathbf{s}\mathbf{s}^\dagger\} \mathbf{w} = \mathbf{w}^\dagger \mathbf{R}_{ss} \mathbf{w} \quad (2.20)$$

where \mathbf{R}_{ss} is the autocorrelation matrix of the signal vector \mathbf{s} and the weighted array interference-plus-noise output power is

$$E\{|y_{\text{IN}}|^2\} = \mathbf{w}^\dagger \mathbf{E}\{(\mathbf{i} + \mathbf{n})(\mathbf{i} + \mathbf{n})^\dagger\} \mathbf{w} = \mathbf{w}^\dagger \mathbf{R}_{\text{IN}} \mathbf{w} \quad (2.21)$$

\mathbf{R}_{IN} is the autocorrelation matrix of $\mathbf{n} + \mathbf{i}$. Therefore, the weighted output SINR can then be expressed as

$$\text{SINR} = \frac{\mathbf{w}^\dagger \mathbf{R}_{ss} \mathbf{w}}{\mathbf{w}^\dagger \mathbf{R}_{\text{IN}} \mathbf{w}} \quad (2.22)$$

Since \mathbf{R}_{IN} is an N-by-N symmetric positive-definite matrix, there exists a unique symmetric positive-definite matrix $\mathbf{X} = \mathbf{R}_{\text{IN}}^{1/2}$ such that $\mathbf{R}_{\text{IN}} = \mathbf{R}_{\text{IN}}^{\dagger/2} \mathbf{R}_{\text{IN}}^{1/2} = \mathbf{X}^\dagger \mathbf{X} =$

\mathbf{X}^2 [13]. By substituting $\mathbf{z} = \mathbf{R}_{\text{IN}}^{1/2} \mathbf{w}$, equation (2.22) can be rewritten as

$$\text{SINR} = \frac{\mathbf{z}^\dagger \mathbf{R}_{\text{IN}}^{-\dagger/2} \mathbf{R}_{ss} \mathbf{R}_{\text{IN}}^{-1/2} \mathbf{z}}{\mathbf{z}^\dagger \mathbf{z}} \quad (2.23)$$

Equation (2.23) may be recognized as a standard quadratic form and is bounded by the minimum and maximum of the eigenvalues of the symmetric matrix $\mathbf{R}_{\text{IN}}^{-\dagger/2} \mathbf{R}_{ss} \mathbf{R}_{\text{IN}}^{-1/2}$. Let λ be the eigenvalues of $\mathbf{Y} = \mathbf{R}_{\text{IN}}^{-\dagger/2} \mathbf{R}_{ss} \mathbf{R}_{\text{IN}}^{-1/2}$ and \mathbf{v} be the corresponding eigenvectors. It then follows that in order to maximize the SINR, we need to solve the generalized eigenproblem

$$\mathbf{R}_{\text{IN}}^{-\dagger/2} \mathbf{R}_{ss} \mathbf{R}_{\text{IN}}^{-1/2} \mathbf{v} = \lambda \mathbf{v} \quad (2.24)$$

The eigenvector corresponding to the maximum eigenvalue λ_{max} of equation (2.24) is then the optimal weight vector \mathbf{w}_{SINR} according to the maximization of SINR criterion. $\mathbf{R}_{\text{IN}}^{-\dagger/2} \mathbf{R}_{ss} \mathbf{R}_{\text{IN}}^{-1/2} = \mathbf{Y}$ implies that

$$\mathbf{R}_{ss} \mathbf{R}_{\text{IN}}^{-1/2} = \mathbf{R}_{\text{IN}}^{\dagger/2} \mathbf{Y} \quad (2.25)$$

Since both $\mathbf{R}_{\text{IN}}^{-1/2}$ and \mathbf{R}_{ss} are symmetric square matrices

$$\mathbf{R}_{\text{IN}}^{-1/2} \mathbf{R}_{ss} = \mathbf{R}_{\text{IN}}^{\dagger/2} \mathbf{Y} \quad (2.26)$$

which gives

$$\mathbf{R}_{\text{IN}}^{-1} \mathbf{R}_{ss} = \mathbf{R}_{\text{IN}}^{-\dagger/2} \mathbf{R}_{ss} \mathbf{R}_{\text{IN}}^{-1/2} = \mathbf{Y} \quad (2.27)$$

Therefore it is more convenient to find the optimal SINR weight vector by solving the generalized eigenproblem of

$$\mathbf{R}_{\text{IN}}^{-1} \mathbf{R}_{ss} \mathbf{w}_{\text{SINR}} = \lambda_{max} \mathbf{w}_{\text{SINR}} \quad (2.28)$$

Let SINR be the SINR value that satisfies equation (2.22). This gives the following equality

$$\mathbf{R}_{ss} \mathbf{w} = (\text{SINR}) \mathbf{R}_{\text{IN}} \mathbf{w} \quad (2.29)$$

At the optimum SINR (denoted by SINR_{opt}), we have

$$\begin{aligned}\mathbf{R}_{ss}\mathbf{w}_{\text{SINR}} &= \text{SINR}_{opt}\mathbf{R}_{\text{IN}}\mathbf{w}_{\text{SINR}} \\ &= \frac{\mathbf{w}_{\text{SINR}}^\dagger\mathbf{R}_{ss}\mathbf{w}_{\text{SINR}}}{\mathbf{w}_{\text{SINR}}^\dagger\mathbf{R}_{\text{IN}}\mathbf{w}_{\text{SINR}}}\mathbf{R}_{\text{IN}}\mathbf{w}_{\text{SINR}}\end{aligned}\quad (2.30)$$

Since $\mathbf{s}^\dagger\mathbf{w}_{\text{SINR}}$ is a complex scalar, it then follows that

$$\mathbf{s} = \sigma_s u_s(t)\mathbf{a}(t) = \frac{\mathbf{w}_{\text{SINR}}^\dagger\mathbf{s}}{\mathbf{w}_{\text{SINR}}^\dagger\mathbf{R}_{\text{IN}}\mathbf{w}_{\text{SINR}}}\mathbf{R}_{\text{IN}}\mathbf{w}_{\text{SINR}}\quad (2.31)$$

The ratio $\left(\mathbf{w}_{\text{SINR}}^\dagger\mathbf{s}\right) / \left(\sigma_s u_s(t)\mathbf{w}_{\text{SINR}}^\dagger\mathbf{R}_{\text{IN}}\mathbf{w}_{\text{SINR}}\right)$ is also a complex scalar value and can be denoted by a complex scalar \mathcal{B} . Thus

$$\mathbf{w}_{\text{SINR}} = \frac{1}{\mathcal{B}}\mathbf{R}_{\text{IN}}^{-1}\mathbf{a}(t)\quad (2.32)$$

which again is a Wiener solution multiplied by a scalar. Again, Equation (2.32) performs first prewhitening and then matching with the signal.

The advantage of using maximal SINR weight adaptation to the received array data is that these weights give the true maximization of SINR. The disadvantage of using this performance measure is having to solve a generalized eigenproblem. The convergence time for determining the eigenvectors depends on the eigenvalue spread. The smaller the eigenvalue spread, the slower the convergence of the adaptive weight vector [23]. Determining the optimal weight vector for maximum SINR requires good estimates of the second-order statistics such as the desired signal autocorrelation matrix, \mathbf{R}_{ss} , and the autocorrelation interference-plus-noise matrix \mathbf{R}_{IN} .

2.4.3 Maximum likelihood (ML)

If we assume that the interference-plus-noise components are multivariate Gaussian, the likelihood function of the input signal vector can be written as

$$\mathcal{L}[\mathbf{x}] = P_{\mathbf{s}}\{\mathbf{x}|\mathbf{s}\}\quad (2.33)$$

$$= \frac{1}{(2\pi)^{M/2}|\mathbf{R}_{\text{IN}}|^{1/2}} \exp\left\{-\frac{1}{2}(\mathbf{x} - \mathbf{s})^\dagger\mathbf{R}_{\text{IN}}^{-1}(\mathbf{x} - \mathbf{s})\right\}\quad (2.34)$$

Assume the signal vector $\mathbf{s} = \sigma_s u_s(t) \mathbf{a}(t)$ where σ_s is the signal amplitude, $u_s(t)$ is the transmitted binary baseband signal information, $\mathbf{a}(t)$ is the signal array response vector corresponding to the desired signal's DOA θ . It follows that the log likelihood is

$$\ln[\mathcal{L}[\mathbf{x}]] = -\frac{1}{2}(\mathbf{x} - \sigma_s u_s(t) \mathbf{a}(t))^\dagger \mathbf{R}_{\text{IN}}^{-1} (\mathbf{x} - \sigma_s u_s(t) \mathbf{a}(t)) \quad (2.35)$$

which gives the likelihood equation as

$$\frac{\partial}{\partial \sigma_s u_s(t)} \ln \mathcal{L}[\mathbf{x}] = -\mathbf{a}(t)^\dagger \mathbf{R}_{\text{IN}}^{-1} \mathbf{x} + \sigma_s u_s(t) \mathbf{a}(t)^\dagger \mathbf{R}_{\text{IN}}^{-1} \mathbf{a}(t) \quad (2.36)$$

Setting the likelihood equation to zero gives the maximum likelihood estimates of $\hat{\sigma}_s \hat{u}_s(t)$

$$\hat{\sigma}_s \hat{u}_s(t) = \frac{\mathbf{a}(t)^\dagger \mathbf{R}_{\text{IN}}^{-1} \mathbf{x}}{\mathbf{a}(t)^\dagger \mathbf{R}_{\text{IN}}^{-1} \mathbf{a}(t)} = \mathbf{w}_{\text{ML}}^\dagger \mathbf{x} \quad (2.37)$$

since $\mathbf{a}(t)^\dagger \mathbf{R}_{\text{IN}}^{-1} \mathbf{a}(t)$ is a scalar. The maximum likelihood weight vector is obtained as

$$\mathbf{w}_{\text{ML}} = \frac{1}{\mathbf{a}(t)^\dagger \mathbf{R}_{\text{IN}}^{-1} \mathbf{a}(t)} \mathbf{R}_{\text{IN}}^{-1} \mathbf{a}(t) \quad (2.38)$$

Maximum likelihood is well-suited in situations when the desired signal's waveform is completely unknown. Then, the desired signal may be regarded as a time function which is to be estimated [23]. However, the constraint of a multivariate Gaussian interference-plus-noise distribution restricts the application of the ML criterion.

2.4.4 Linearly constrained minimum variance (LCMV)

LCMV requires knowledge or prior estimation of the desired signal array response vector $\mathbf{a}(t) = [e^{j\omega_c \tau_1}, e^{j\omega_c \tau_2}, \dots, e^{j\omega_c \tau_M}]^T$ with DOA θ and temporal frequency ω_c . LCMV constrains the response of the beamformer so that signals from the direction of interest are passed through the array with a specified gain and phase [11]. The LCMV weights are chosen to minimize the expected value of the output power/variance subject to the response constraints. That is

$$\min_{\mathbf{w}} \{\mathbf{w}^\dagger \mathbf{R}_{\text{xx}} \mathbf{w}\} \quad \text{subject to} \quad \mathbf{C}^\dagger \mathbf{w} = \mathbf{g}^* \quad (2.39)$$

where \mathbf{w} is the $M \times 1$ array weighting vector to be determined, $\mathbf{R}_{xx} = \mathbf{E}\{\mathbf{x}\mathbf{x}^\dagger\}$ is the $M \times M$ autocorrelation matrix of the antenna array output, \mathbf{C} is a $M \times \mathcal{K}$ matrix having \mathcal{K} linearly independent constraint equations, and \mathbf{p} is the $\mathcal{K} \times 1$ constraint response vector.

The constraints have an effect of preserving the desired signal while minimizing contributions to the array output due to interfering signals and noise arriving from directions other than the direction of interest. Let $F(\mathbf{w}) = \mathbf{w}^\dagger \mathbf{R}_{xx} \mathbf{w}$ be the cost function and $G(\mathbf{w}) = \mathbf{C}^\dagger \mathbf{w} - \mathbf{p}^*$ be the constraint function. By using a $\mathcal{K} \times 1$ Lagrange multiplier vector \mathbf{b} , the following is obtained

$$H(\mathbf{w}) = \frac{1}{2}F(\mathbf{w}) + \mathbf{b}G(\mathbf{w}) = \frac{1}{2}\mathbf{w}^\dagger \mathbf{R}_{xx} \mathbf{w} + \mathbf{b}^\dagger (\mathbf{C}^\dagger \mathbf{w} - \mathbf{g}^*) \quad (2.40)$$

$F(\mathbf{w})$ has its minimum or maximum value at a point \mathbf{w} subject to the constraint $G(\mathbf{w}) = \mathbf{C}^\dagger \mathbf{w} - \mathbf{p}^* = 0$, i.e. when $H(\mathbf{w}) = 0$. Therefore, to find the minimum point of equation (2.40) we differentiate it with respect to \mathbf{w} and set it equal to zero. For $H(\mathbf{w}) = 0$, it follows that

$$\mathbf{w}_{opt} = -\mathbf{R}_{xx}^{-1} \mathbf{C} \mathbf{b} \quad (2.41)$$

where the $M \times 1$ Lagrange multiplier \mathbf{b} still needs to be determined. Substituting \mathbf{w}_{opt} back into the constraint equation yields

$$\mathbf{C}^\dagger \mathbf{w}_{opt} = \mathbf{C}^\dagger [-\mathbf{R}_{xx}^{-1} \mathbf{C} \mathbf{b}] = \mathbf{p}^* \quad (2.42)$$

and the Lagrange multiplier vector is found to be

$$\mathbf{b} = -[\mathbf{C}^\dagger \mathbf{R}_{xx}^{-1} \mathbf{C}]^{-1} \mathbf{p}^* \quad (2.43)$$

where the existence of $[\mathbf{C}^\dagger \mathbf{R}_{xx}^{-1} \mathbf{C}]^{-1}$ follows from the facts that \mathbf{R}_{xx} is positive-definite and \mathbf{C} is full-rank. Therefore, the LCMV estimate of the weight vector is

$$\mathbf{w}_{opt} = \mathbf{R}_{xx}^{-1} \mathbf{C} [\mathbf{C}^\dagger \mathbf{R}_{xx}^{-1} \mathbf{C}]^{-1} \mathbf{p}^* \quad (2.44)$$

As a special case in constraining only one desired signal array response gain, a LCMV problem [42] can be expressed as

$$\min_{\mathbf{w}} \mathbf{w}^\dagger \mathbf{R}_{xx} \mathbf{w} \quad \text{subject to} \quad \mathbf{C}^\dagger \mathbf{w} = \mathbf{a}(t)^\dagger \mathbf{w} = p^* \quad (2.45)$$

where g is a complex scalar which constrains the output response to $\mathbf{a}(t)$. Using a Lagrange multiplier, the LCMV weight estimate of equation (2.45) is then

$$\mathbf{w}_{opt} = \mathbf{R}_{xx}^{-1} \mathbf{a}(t) [\mathbf{a}(t)^\dagger \mathbf{R}_{xx}^{-1} \mathbf{a}(t)]^{-1} p^* \quad (2.46)$$

For the case of only one constraint vector, $\mathbf{a}(t)^\dagger \mathbf{R}_{xx}^{-1} \mathbf{a}(t)$ is a complex scalar, and we can write

$$\mathbf{w}_{opt} = \frac{g^*}{\mathbf{a}(t)^\dagger \mathbf{R}_{xx}^{-1} \mathbf{a}(t)} \mathbf{R}_{xx}^{-1} \mathbf{a}(t) \quad (2.47)$$

since p is a scalar. If $p = 1$, equation (2.45) is termed a minimum variance distortionless response (MVDR) beamformer. By substituting $\mathbf{R}_{xx} = \mathbf{R}_{IN} + \sigma^2 \mathbf{a}(t) \mathbf{a}(t)^\dagger$ and applying Matrix Inversion Lemma [17], it can be shown that equation (2.47) is equivalent to the maximum SINR solution (details are derived in section 2.4.5).

The advantage of using a LCMV criteria is its general constraint approach that permits extensive control over the adapted response of the beamformer. This technique is flexible and does not require knowledge of the desired signal autocorrelation matrix \mathbf{R}_{ss} , the interference-plus-noise autocorrelation matrix \mathbf{R}_{IN} , or any reference signal y_d . However the disadvantage of using a LCMV is the computation complexity of the constraint weight vector.

The constraint matrix allows the beamformer to be designed to attain a certain level of beamforming performance. There are several different constraint matrix designs for the LCMV performance measure such as point constraints, eigenvector constraints, etc. [42]

2.4.4.1 Point constraints

Point constraints fix the beamformer response at points of spatial direction and temporal frequency [42]. Here, we present an example of using point constraint for LCMV criteria.

Considering constraining the array response corresponding to three DOAs θ_0 , θ_1 and θ_2 , in which we would like to have distortionless processing of incoming signals

from DOA θ_0 and θ_1 while nulling DOA θ_2 . The LCMV estimate of the optimal weight vector involves solving equation (2.48) and the LCMV optimal weight is as in equation (2.46).

$$\min_{\mathbf{w}} \mathbf{w}^\dagger \mathbf{R}_{xx} \mathbf{w} \quad \text{subject to} \quad \mathbf{C}^\dagger \mathbf{w} = \begin{bmatrix} \mathbf{a}(\theta_0, \omega_c)^\dagger \\ \mathbf{a}(\theta_1, \omega_c)^\dagger \\ \mathbf{a}(\theta_2, \omega_c)^\dagger \end{bmatrix} \mathbf{w} = \begin{bmatrix} p_0^* \\ p_1^* \\ 0 \end{bmatrix} = \mathbf{p}^\dagger \quad (2.48)$$

Each linear constraint uses one degree of freedom for minimizing power; therefore, if there are \mathcal{K} linear constraints, only $M - \mathcal{K}$ degrees of freedom are available for minimizing the variance. For an M -element antenna array, if $\mathcal{K} = M$ linear constraints are used, there are no degrees of freedom left for power minimization and the statistical beamformer becomes a data-independent beamformer.

2.4.4.2 Eigenvector constraints

Eigenvector constraints are typically used to control beamformer response over regions of directions and/or frequencies [16] [42]. The eigenvector constraints for the LCMV problem can be formulated as

$$\min_{\mathbf{w}} \mathbf{w}^\dagger \mathbf{R}_{xx} \mathbf{w} \quad \text{subject to} \quad \mathbf{V}^\dagger \mathbf{w} = \Sigma_{\mathcal{K}}^{-1} \mathbf{U}^\dagger \mathbf{r}_d \quad (2.49)$$

where the singular value decomposition of a rank \mathcal{K} $M \times \mathcal{K}$ matrix \mathbf{A} can be expressed as $\mathbf{A} = \mathbf{V} \Sigma \mathbf{U}^\dagger$. \mathbf{V} and \mathbf{U} are the left and right singular matrix of \mathbf{A} , respectively, and Σ is the $\mathcal{K} \times \mathcal{K}$ diagonal matrix containing the \mathcal{K} largest singular values of \mathbf{A} . The vector $\mathbf{r}_d = [\mathbf{w}^\dagger \mathbf{a}(\theta_1, \omega_c), \mathbf{w}^\dagger \mathbf{a}(\theta_2, \omega_c), \dots, \mathbf{w}^\dagger \mathbf{a}(\theta_{\mathcal{K}}, \omega_c)]^T$ is the weighted array response vector constraint vector. The $M \times \mathcal{K}$ matrix $\mathbf{A} = [\mathbf{a}(\theta_1, \omega_c), \mathbf{a}(\theta_2, \omega_c), \dots, \mathbf{a}(\theta_{\mathcal{K}}, \omega_c)]^T$ represents the \mathcal{K} array response vector constraints where $\mathbf{a}_m(\theta_m, \omega_c)$ is the array response of the m^{th} DOA θ_m array response constraint.

This is called an eigenvector constraint approach since the column vectors of \mathbf{V} correspond to the eigenvectors of the full rank matrix $\mathbf{A} \mathbf{A}^\dagger$. Note that when it is a narrowband signal arrived at an antenna array, $\mathbf{A} \mathbf{A}^\dagger$ equals the spatial autocorrelation matrix $\mathbf{R}_{xx} = \mathbf{A} \mathbf{A}^\dagger$ of \mathcal{K} signals with unity power impinging on the array.

Criteria	MMSE	SINR	ML	LCMV (one constraint)
\mathbf{w}_{opt}	$\mathbf{R}_{xx}^{-1}\mathbf{r}_{xd}$	$\frac{1}{\mathcal{B}}\mathbf{R}_{IN}^{-1}\mathbf{a}(t)$	$\frac{1}{\mathcal{D}-1}\mathbf{R}_{IN}^{-1}\mathbf{a}(t)$	$\frac{1}{\mathcal{D}-1}\mathbf{R}_{IN}^{-1}\mathbf{a}(\theta, \omega_c)$

Table 2.1: Summary of the statistically optimum weight vector estimates

2.4.5 Summary – Unifying optimum weight solution

We apply the Matrix Inversion Lemma [17] to the narrowband data covariance matrix $\mathbf{R}_{xx} = \mathbf{R}_{IN} + \sigma_s^2\mathbf{a}(t)\mathbf{a}(t)^\dagger$ where \mathbf{R}_{IN} is the interference-plus-noise matrix and σ_s^2 is the total received signal power [23]. It then follows that

$$\begin{aligned}\mathbf{R}_{xx}^{-1} &= \mathbf{R}_{IN}^{-1} - \frac{\sigma_s^2\mathbf{R}_{IN}^{-1}\mathbf{a}(t)\mathbf{a}(t)^\dagger\mathbf{R}_{IN}^{-1}}{1 + \sigma_s^2\mathbf{a}(t)^\dagger\mathbf{R}_{IN}^{-1}\mathbf{a}(t)} \\ &= \frac{1}{1 + \sigma_s^2\mathbf{a}(t)^\dagger\mathbf{R}_{IN}^{-1}\mathbf{a}(t)}\mathbf{R}_{IN}^{-1} = \frac{1}{\mathcal{D}}\mathbf{R}_{IN}^{-1}\end{aligned}\quad (2.50)$$

where $1 + \sigma_s^2\mathbf{a}(t)^\dagger\mathbf{R}_{IN}^{-1}\mathbf{a}(t)$ is a complex scalar and can be represented by \mathcal{D} .

It is a remarkable fact that all the different performance measure criteria considered here converge to the same steady-state Wiener solution within a constant scale factor as shown in Table 2.1. This introduces a more general concept of a unified approach to adaptive beamforming

$$\mathbf{w}_{opt} = \varsigma\mathbf{R}_{xx}^{-1}\mathbf{r}_{xd} = \mathcal{H}\mathbf{R}_{IN}^{-1}\mathbf{a}(t) = \mathcal{I}\mathbf{R}_{xx}^{-1}\mathbf{a}(t) \quad (2.51)$$

where ς is a scalar, \mathcal{I} is a scalar, \mathcal{H} is also a scalar, \mathbf{R}_{xx}^{-1} is the inverse of the data array autocorrelation matrix, and \mathbf{R}_{IN}^{-1} is the inverse of the interference-plus-noise autocorrelation matrix. All of these optimum weight vector matrix filter operators embody the principle of first prewhitening the spatial correlation matrix and then spatially matching the signals received at each antenna to obtain an undistorted representation of the desired signal.

2.5 Adaptive Algorithm for Beamforming

Section 2.4 showed that statistically optimum weight vectors for adaptive beamforming can be calculated by the Wiener solution; however, the knowledge of the asymptotic second-order statistics of the signal and the interference-plus-noise was assumed to be available. These statistics are usually not known, but with the assumption of ergodicity where the time average equals the ensemble average, the second-order statistics can be estimated from available data. For time-varying signal environments, such as wireless cellular communications systems, statistics change with time as the target mobile and interferers move around the cell. For the time-varying signal propagation environment, a recursive update of the weight vector is needed to track a moving mobile so that the spatial filtering beam will adaptively steer to the target mobile's time-varying DOA, thus resulting in optimal transmission/reception of the desired signal. To solve the problem of time-varying statistics, weight vectors are typically determined by adaptive algorithms which adapt to the changing environments.

Figure 2.13 shows a generic adaptive antenna array system consisting of an M -element antenna array with a real-time adaptive array signal processor containing an update control algorithm. Using data samples collected from the antenna array, the signal processor automatically proceeds to adjust the weight vector towards optimization of the selected criteria. These antenna systems are sometimes referred to as “smart” antenna arrays.

Steady-state and transient-state are the two classifications of the requirement of an adaptive antenna array. These two classifications depend on whether the array weights have reached their steady-state values in a stationary environment or are being adjusted in response to a change in the signal environment. In order to determine an algorithm for adapting the weight vector to the time-varying environment at each sample, the least mean square (LMS) and the recursive least squares (RLS) adaptive updating algorithm can be used. The LMS algorithm converges to the steady-state Wiener solution much more slowly than does RLS [23] [42]. The computation for the RLS update algorithm, however, requires a computation of order $O(M^2)$ while

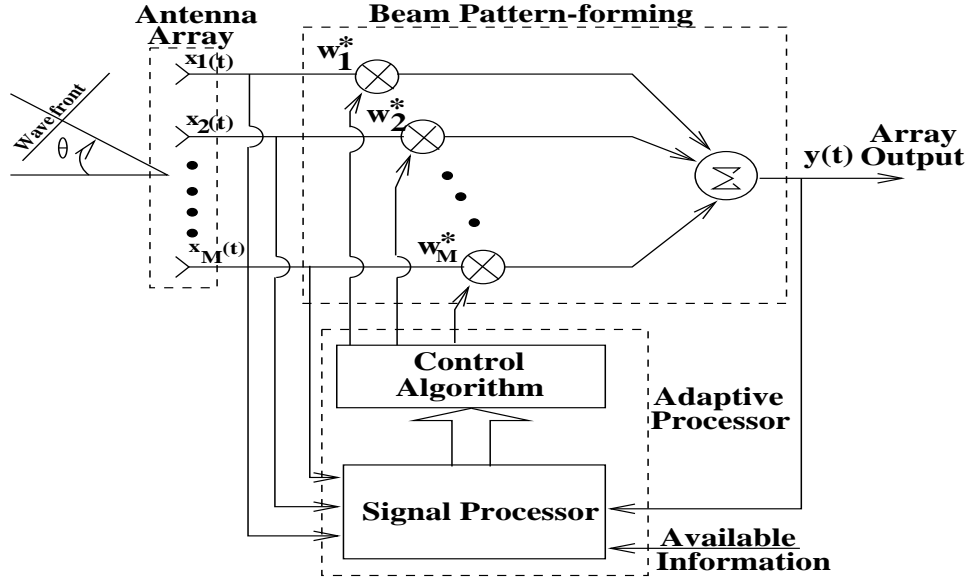


Figure 2.13: Functional diagram of a M-element adaptive array

the LMS update algorithm only requires a computation of order $O(M)$. The LMS iterative algorithm is presented first, followed by the RLS algorithm.

2.5.1 Least mean square (LMS) adaptive algorithm

The LMS algorithm linearly minimizes the mean-square error while also incorporating new observations and iteratively solving the minimization problem [17] [23] [44].

LMS changes the weight vector along the direction of the estimated gradient based on the steepest descent method. The steepest descent algorithm converges most rapidly in the direction of the negative gradient [13]. By the quadratic characteristics of a mean square error function $\mathbf{E}\{\varepsilon(k)^2\}$ that has only one minimum, the steepest descent is guaranteed to converge.

At adaptation index k , given a mean-square-error (MSE) function $\mathbf{E}\{\varepsilon(k)^2\} = \mathbf{E}\{|y_d(k) - \mathbf{w}(k)^\dagger \mathbf{x}(k)|^2\}$, the LMS algorithm updates the weight vector according to

$$\mathbf{w}(k+1) = \mathbf{w}(k) + \mu \hat{\nabla}_{\mathbf{w}(k)} \mathbf{E}\{\varepsilon(k)^2\} \quad (2.52)$$

where μ is the scalar constant which controls the rate of convergence and stability

($\mu < 0$ is required for the weight update to converge), $\mathbf{w}(k+1)$ is the weight vector after adaptation, $\mathbf{w}(k)$ is the weight vector before adaptation, and $\hat{\nabla}_{\mathbf{w}(k)} \mathbf{E}\{\varepsilon(k)^2\}$ is the estimated gradient vector of $\mathbf{E}\{\varepsilon(k)^2\}$.

The gradient estimate is found by differentiating $\mathbf{E}\{\varepsilon(k)^2\}$ with respect to the weight vector $\mathbf{w}(k)$ which gives

$$\hat{\nabla}_{\mathbf{w}(k)} \mathbf{E}\{\varepsilon(k)^2\} = 2\varepsilon(k) \nabla[\varepsilon(k)] = -2[y_d(k) - \mathbf{w}(k)^\dagger \mathbf{x}(k)] \mathbf{x}(k) \quad (2.53)$$

The gradient estimation in equation (2.53) is unbiased since it equals the true value of the gradient of the expected value of the mean-square-error (MSE).

Thus, equation (2.52) becomes

$$\mathbf{w}(k+1) = \mathbf{w}(k) - 2\mu[y_d(k) - \mathbf{w}(k)^\dagger \mathbf{x}(k)] \mathbf{x}(k) \quad (2.54)$$

2.5.1.1 Convergence of the LMS update algorithm

By taking the expected value of equation (2.54), it follows that

$$\mathbf{E}\{\mathbf{w}(k+1)\} = [\mathbf{I} + 2\mu \mathbf{R}_{xx}] \mathbf{E}\{\mathbf{w}(k)\} - 2\mu \mathbf{r}_{xd} \quad (2.55)$$

where $\mathbf{R}_{xx} = \mathbf{E}\{\mathbf{x}(k) \mathbf{x}(k)^\dagger\}$ is the autocorrelation matrix, and $\mathbf{r}_{xd} = \mathbf{E}\{y_d(k) \mathbf{x}(k)\}$ is the cross-correlation matrix of $\mathbf{x}(k)$ and $y_d(k)$.

By setting the initial weight vector to $\mathbf{w}(0)$, equation (2.54) can be rewritten as

$$\mathbf{E}\{\mathbf{w}(k+1)\} = [\mathbf{I} + 2\mu \mathbf{R}_{xx}]^{k+1} \mathbf{w}(0) - 2\mu \sum_{i=0}^k [\mathbf{I} + 2\mu \mathbf{R}_{xx}]^i \mathbf{r}_{xd} \quad (2.56)$$

Since $\mathbf{R}_{xx} = \mathbf{E}\{\mathbf{x} \mathbf{x}^\dagger\}$ is a symmetric matrix, the eigendecomposition of \mathbf{R}_{xx} always exists and the diagonal eigenvalue matrix \mathbf{D} is real-valued and positive-definite [13].

$$\mathbf{R}_{xx} = \mathbf{Q}^\dagger \mathbf{D} \mathbf{Q} \quad (2.57)$$

where \mathbf{Q} is the orthonormal eigenvector matrix of \mathbf{R}_{xx} . It then follows that

$$\mathbf{E}\{\mathbf{w}(k+1)\} = [\mathbf{I} + 2\mu \mathbf{Q}^\dagger \mathbf{D} \mathbf{Q}]^{k+1} \mathbf{w}(0) - 2\mu \sum_{i=0}^k [\mathbf{I} + 2\mu \mathbf{Q}^\dagger \mathbf{D} \mathbf{Q}]^i \mathbf{r}_{xd} \quad (2.58)$$

$$= \mathbf{Q}^\dagger [\mathbf{I} + 2\mu \mathbf{D}]^{k+1} \mathbf{Q} \mathbf{w}(0) - 2\mu \mathbf{Q}^\dagger \sum_{i=0}^k [\mathbf{I} + 2\mu \mathbf{D}]^i \mathbf{Q} \mathbf{r}_{xd} \quad (2.59)$$

If the diagonal matrix $\mathbf{I} + 2\mu\mathbf{D}$ has a magnitude less than unity, as the current iteration k increases

$$\lim_{k \rightarrow \infty} [\mathbf{I} + 2\mu\mathbf{D}]^{k+1} \rightarrow 0 \quad (2.60)$$

and

$$\lim_{k \rightarrow \infty} \sum_{i=0}^k [\mathbf{I} + 2\mu\mathbf{D}]^i = -[2\mu\mathbf{D}]^{-1} \quad (2.61)$$

using the equality $\sum_{i=0}^{N-1} a^i = [1 - a^N]/[1 - a]$.

Thus, in the limit as the iterations increase

$$\lim_{k \rightarrow \infty} \mathbf{E}\{\mathbf{w}(k+1)\} = \mathbf{Q}^\dagger \mathbf{D}^{-1} \mathbf{Q} \mathbf{r}_{xd} = \mathbf{R}_{xx}^{-1} \mathbf{r}_{xd} \quad (2.62)$$

which implies that the weight vector converges to the Wiener solution provided that sufficient iterations have been performed.

The requirement on the diagonal matrix that $|\mathbf{I} + 2\mu\mathbf{D}| < 1$ sets the bound of the constraint parameter μ of the LMS update algorithm in order for it converge to the optimum Wiener solution.

Since \mathbf{R}_{xx} is positive-definite, the eigenvalues of \mathbf{D} are all positive, and the bound on μ is given by the largest eigenvalue λ_{max} of \mathbf{D} where

$$|1 + 2\mu\lambda_{max}| < 1 \quad (2.63)$$

or

$$\frac{-1}{\lambda_{max}} < \mu < 0 \quad (2.64)$$

Alternatively, in terms of the total power of vector \mathbf{x} ,

$$\lambda_{max} \leq \text{trace}\{\mathbf{R}_{xx}\} \quad (2.65)$$

where $\text{trace}\{\mathbf{R}_{xx}\} = \mathbf{E}\{x_i^2\}$ is the total input power.

Therefore, a condition for satisfactory Wiener solution convergence of the mean of the LMS weight vector is

$$\frac{-1}{\sum_{i=1}^M \mathbf{E}\{x_i^2\}} < \mu < 0 \quad (2.66)$$

where M is the number of antenna elements in the array.

LMS is a simple adaptive algorithm whose convergence characteristics depend on the shape of the error surface and therefore the eigenstructure of R_{xx} . Its convergence can be slow if the eigenvalues are widely spread. When the covariance matrix eigenvalues differ by orders of magnitude, the algorithm convergence time can be exceedingly long, and in any case is highly data dependent [23]. Therefore, in practice, depending on the eigenvalue spread, the LMS algorithm may not have sufficient iteration time for the weight vector to converge to the statistically optimum solution and adaptation to the time-varying environment will not be able to be performed in real time. LMS weights/filter coefficients do not converge to a stable set of values even when the observations are stationary since the filter coefficients depend on new observations and are continually updated via the estimate of the gradient. In addition, employing the LMS algorithm assumes that enough knowledge of the desired signal is known so to generate reference signal sequences. Acquiring this knowledge could be expensive for wireless communications systems.

2.5.2 Recursive least squares (RLS) adaptive algorithm

In contrast to the LMS algorithm, a RLS adaptive algorithm approximates the Wiener solution directly without imposing the additional burden of approximating an optimization procedure such as gradient estimation [42]. This more direct approach results in filters with better convergence properties than the LMS but at the expense of computational complexity. Recalling that the statistically optimum Wiener solution is

$$\mathbf{w} = \mathbf{R}_{xx}^{-1} \mathbf{r}_{xd} \quad (2.67)$$

There are two commonly used methods of estimating the covariance matrix \mathbf{R}_{xx} in equation (2.67). The first method time averages the outer product of the received output vector over S frames. The next optimal weight vector is predicted based on the current received data. Therefore, regardless of which method is chosen to estimate

the covariance matrix, the estimate at index k must only depend on the observations obtained before that time. At adaptation time index k , the covariance matrix can be estimated from the last S frames of time as

$$\hat{\mathbf{R}}_{xx}(k) = \frac{1}{S} \sum_{i=k-S}^{k-1} \mathbf{x}(i)\mathbf{x}(i)^\dagger \quad (2.68)$$

Note that $S \geq M$ is required to obtain an invertible covariance matrix from this moving average [17].

The second method uses an exponentially-weighted estimate where

$$\hat{\mathbf{R}}_{xx}(k) = \sum_{i=0}^{k-1} \alpha^{k-i} \mathbf{x}(i)\mathbf{x}(i)^\dagger \quad (2.69)$$

This can be rewritten in a simple rank-one update recursive form

$$\hat{\mathbf{R}}_{xx}(k) = \alpha \hat{\mathbf{R}}_{xx}(k-1) + \mathbf{x}(k-1)\mathbf{x}(k-1)^\dagger \quad (2.70)$$

Similar to the moving average estimate, an invertible estimate occurs when $k \geq M$. Because of this recursive form, application of the Matrix Inversion Lemma [17] permits the inverse of $\hat{\mathbf{R}}_{xx}$ to be expressed as

$$\begin{aligned} \hat{\mathbf{R}}_{xx}^{-1}(k) &= \frac{1}{\alpha} \left[\hat{\mathbf{R}}_{xx}^{-1}(k-1) - \frac{\hat{\mathbf{R}}_{xx}^{-1}(k-1)\mathbf{x}(k-1)\mathbf{x}(k-1)^\dagger \hat{\mathbf{R}}_{xx}^{-1}(k-1)}{\alpha + \mathbf{x}(k-1)^\dagger \hat{\mathbf{R}}_{xx}^{-1}(k-1)\mathbf{x}(k-1)} \right] \\ &= \frac{1}{\alpha} \left[\hat{\mathbf{R}}_{xx}^{-1}(k-1) - \mathbf{g}(k)\mathbf{x}(k-1)^\dagger \hat{\mathbf{R}}_{xx}^{-1}(k-1) \right] \end{aligned} \quad (2.71)$$

where

$$\mathbf{g}(k) = \frac{\hat{\mathbf{R}}_{xx}^{-1}(k-1)\mathbf{x}(k-1)}{\alpha + \mathbf{x}(k-1)^\dagger \hat{\mathbf{R}}_{xx}^{-1}(k-1)\mathbf{x}(k-1)} \quad (2.72)$$

Similarly, the second-order statistics vector \mathbf{r}_{xd} in equation (2.67) can be estimated by

$$\hat{\mathbf{r}}_{xd}(k) = \alpha \hat{\mathbf{r}}_{xd}(k-1) + y_d(k)\mathbf{x}(k-1) \quad (2.73)$$

Therefore, at time index k , the prediction of the weight vector at time $k+1$ can be written in a recursive form as

$$\mathbf{w}(k+1) = \hat{\mathbf{R}}_{xx}^{-1}(k)\hat{\mathbf{r}}_{xd}(k) \quad (2.74)$$

Substituting the exponentially weighted estimate from equations (2.71) and (2.73) into equation (2.74), we have

$$\begin{aligned}
\mathbf{w}(k+1) &= \hat{\mathbf{R}}_{xx}^{-1}(k)\hat{\mathbf{r}}_{xd}(k) \\
&= \frac{1}{\alpha} \left[\hat{\mathbf{R}}_{xx}^{-1}(k-1) - \mathbf{g}(k)\mathbf{x}(k-1)\dagger\hat{\mathbf{R}}_{xx}^{-1}(k-1) \right] [\alpha\hat{\mathbf{r}}_{xd}(k-1) + y_d(k)\mathbf{x}(k-1)] \\
&= \hat{\mathbf{R}}_{xx}^{-1}(k-1)\hat{\mathbf{r}}_{xd}(k-1) - \mathbf{g}(k)(\hat{\mathbf{R}}_{xx}^{-1}(k-1)\hat{\mathbf{r}}_{xd}(k-1))\dagger\mathbf{x}(k-1) \\
&\quad - \frac{1}{\alpha}y_d(k)\hat{\mathbf{R}}_{xx}^{-1}(k-1)\mathbf{x}(k-1) + \frac{1}{\alpha}y_d(k)\mathbf{g}(k)\mathbf{x}(k-1)\dagger\hat{\mathbf{R}}_{xx}^{-1}(k-1)\mathbf{x}(k-1) \\
&= \mathbf{w}(k) - \mathbf{g}(k)\mathbf{w}(k)\dagger\mathbf{x}(k-1) + y_d(k)\mathbf{g}(k) \\
&\quad + \frac{1}{\alpha}y_d(k)\mathbf{g}(k)\mathbf{x}(k-1)\dagger\mathbf{R}_{xx}^{-1}(k-1)\mathbf{x}(k-1) \\
&\quad - \frac{1}{\alpha}y_d(k)\mathbf{g}(k)\mathbf{x}(k-1)\dagger\hat{\mathbf{R}}_{xx}^{-1}(k-1)\mathbf{x}(k-1) \\
&= \mathbf{w}(k) + \mathbf{g}(k)[y_d(k) - \mathbf{w}(k)\dagger\mathbf{x}(k-1)]
\end{aligned} \tag{2.75}$$

Therefore, RLS directly updates the weight vector estimate where the weight vector for each adaptation time index is

$$\mathbf{w}(k+1) = \mathbf{w}(k) + \mathbf{g}(k)[y_d(k) - \mathbf{w}(k)\dagger\mathbf{x}(k-1)] \tag{2.76}$$

where $\mathbf{g}(k) = [\hat{\mathbf{R}}_{xx}^{-1}\mathbf{x}(k-1)]/[\alpha + \mathbf{x}(k-1)\dagger\hat{\mathbf{R}}_{xx}^{-1}\mathbf{x}(k-1)]$, and α is the parameter that controls the effective amount of data used in the averaging and hence the degree to which the algorithm can track variations in signal characteristics.

As long as $0 < \alpha < 1$, the RLS weight update algorithm always converges. The initial covariance matrices \mathbf{R}_{xx} and \mathbf{r}_{xd} in equations (2.70) and (2.73), respectively, are initialized to a constant a times the identity matrix ($a\mathbf{I}$). An estimate of the signal power σ^2 is usually used for this constant. The initial weight vector $\mathbf{w}(0)$ in equation (2.76) is set to zero.

Typically, the RLS algorithm requires about 2M adaptation steps to converge which is much faster than the LMS algorithm. However, this is at the price of increased computational complexity. In addition, the difference equation in equation (2.71) for updating the inverse of the covariance matrix is sensitive to numerical roundoff. This numerical computational issue can be approached using so-called

square-root algorithms that update the matrix square root of the covariance matrix [17].

2.6 Summary

This chapter has reviewed the fundamental concepts of antenna arrays and digital beamforming. In particular, we have explored several different parameter estimation methods for generating statistically optimum beamforming weight vectors. Adaptive algorithms for beamforming were also discussed.

Chapter 3

CDMA Cellular Communication Systems

3.1 Introduction

This chapter reviews Direct Sequence/Code Division Multiple Access (DS/CDMA) signal applications in cellular communication systems and the current state-of-the-art in the application of array signal processing to base station antenna arrays. Section 3.2 reviews the spread spectrum signals and their application to CDMA for digital communications systems. A signal multipath fading model is described in Section 3.3. The second-generation IS-95 CDMA cellular standard is outlined in Section 3.5. In Section 3.6, current state-of-the-art array signal processing techniques using base station antenna arrays and 2D RAKE receivers are reviewed.

3.2 Spread Spectrum Signals

In spread spectrum, a previously modulated signal is modulated a second time to a much greater bandwidth of W_{ss} by using a pseudo random noise (PN) sequence. Figure 3.1 illustrates the basic elements of a spread spectrum digital communications system [29]. As shown, the information signal sequence has bandwidth B and the spread signal has bandwidth W_{ss} . The ratio $B_e = W_{ss}/B$ is called the bandwidth expansion factor or processing gain, and is designed to be much greater than unity, that is, $W_{ss} \gg B$.

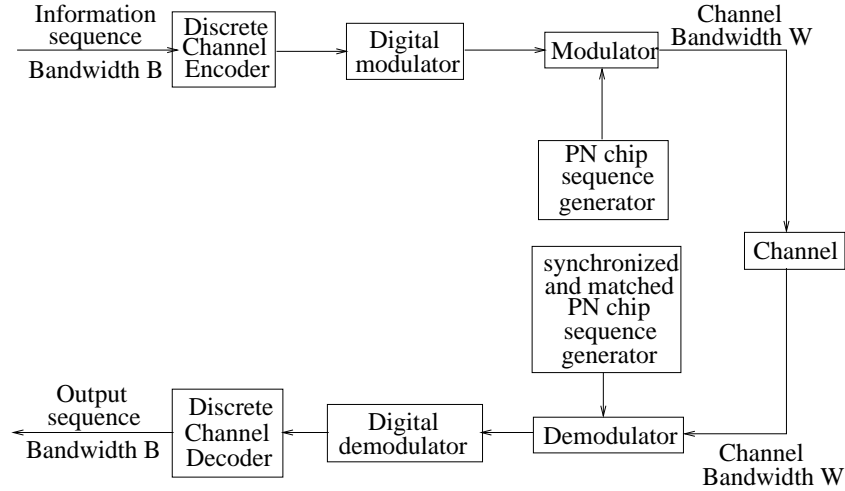


Figure 3.1: Model of spread spectrum digital communication system

The discrete channel encoder shown in Figure 3.1 at the transmitter introduces redundancy into the information sequences. This combats noise and interference in the channel and increases the reliability of data transmitted through the channel. Most importantly, this redundancy at the transmitter aids the receiver in correctly decoding the degraded received signals. A discrete channel encoding technique may involve grouping k information bits adjacent in time and mapping each k -bit sequence into a unique n -bit sequence, called a code word, that introduces redundancy. The digital modulator shown in Figure 3.1 converts a binary digital information sequence into a waveform that is compatible with the characteristics of the channel, thereby allowing the digital signal to be transmitted through the real channel. The waveform modulated signal is then further spread by the PN sequence.

Direct sequence spread spectrum requires the synchronization and matching of the transmitted PN sequence in order to demodulate or despread the received signal back to the transmitted information sequence of bandwidth B . The despreading operation compresses the desired signal back to its original bandwidth B while simultaneously spreading the undesired noise bandwidth by the same amount W_{ss} , thus reducing the power spectral density of the interference. Consequently, despreading diminishes the effect of interference by spreading the interference power over the wider bandwidth

W_{ss} and the interfering signals then appear as noise. The performance of spread spectrum signalling is limited by the interference power after despreading.

3.2.1 Bit-energy-to-total-noise ratio of a spread spectrum modulated signal

To illustrate the concept of ideal despreading of signals at the receiver, consider a desired signal of power S Watts (W) at bit rate $1/B$ with the total received additive channel interference power of J Watts with bandwidth W_{ss} Hz after despreading. Assume that the channel also introduces additive gaussian white noise (AGWN) with a one-sided power spectral density (PSD) of N_0 W/Hz. Therefore, the bit-energy-to-total noise ratio [15] is then

$$\frac{E_b}{N_{total}} = \frac{S/B}{(N_0 W_{ss})/W_{ss} + J/W_{ss}} = \frac{S/B}{N_0 + J/W_{ss}} \quad (3.1)$$

When the interference signal power is much higher than the thermal noise (AWGN) power (i.e. $J/W_{ss} \gg N_0$), then eqn.(3.1) can be approximated as

$$\frac{E_b}{N_{total}} \approx \frac{S/B}{J/W_{ss}} = \frac{S}{J} \frac{W_{ss}}{B} \quad (3.2)$$

where W_{ss}/B is the processing gain, and J/S is the interference-to-signal ratio (ISR). Since the ultimate probability of error depends on E_b/N_{total} , the bit-energy-to-total-noise ratio of a spectrum receiver can be improved by maximizing the processing gain and minimizing the ISR.

Due to spread spectrum's wideband pseudo-random PN sequence spreading and despreading effect on interference power, employing this type of modulation has the following advantages: (1) suppressing interference from self-interference due to multi-path propagation or jamming interferers or interference from other users in a channel, (2) hiding a signal in the presence of background noise by transmitting it at a low power, and (3) securing privacy in a digital communications system.

Spread spectrum in conjunction with phase shift keying (PSK) or frequency shift keying (FSK) modulation are the two most popular types of spread spectrum modulation techniques used in digital communications systems. In PSK spread spectrum,

the phase of the PSK signal is shifted pseudo-randomly according to the PN sequence pattern, and the resulting modulated signal is also called a direct sequence (DS) or a pseudo-noise (PN) spread spectrum signal. When the available channel bandwidth is subdivided into a large number of contiguous frequency slots, the transmitting frequency of an M-ary FSK is specified pseudo-randomly according to the PN sequence pattern. This is called frequency-hopped (FH) spread spectrum.

PSK spread spectrum is applied when phase coherence between the transmitted and the received signal can be maintained over a time interval that is relatively long as compared to the reciprocal of the transmitted signal bandwidth. FH spread spectrum signalling is appropriate to use in applications where phase coherence cannot be maintained due to extremely rapid time-varying effects in the communications link.

3.2.2 Code division multiple access (CDMA)

In digital cellular communication systems, the available frequency bands are limited and expensive. In order to cope with the ever-increasing number of subscribers and limited frequency bands, applying of DSMA/CDMA to increase capacity in future commercial digital cellular personal communication services (PCS) has attracted much investigation. In addition to DS spread spectrum's features, CDMA provides superior efficient usage of the available frequency band by assigning each user a specified PN sequence which allows multiple users to simultaneously transmit on the same channel. In a CDMA communications network, each user has a transmitter and corresponding receiver intended for modulating and demodulating respectively with the assigned PN sequence.

Mathematically, the assigned PN sequence $c_i(t)$ for the i^{th} mobile of a CDMA network can be expressed as

$$c_i(t) = \sum_{n=-\infty}^{\infty} c_{i,n} p(t - nT_c) \quad (3.3)$$

where $c_{i,n} \in \{1, -1\}$ is the assigned binary PN code sequence for the i^{th} mobile, and $p(t)$ is pulse modulation with pulse rate $1/T_c = W_{ss}$.

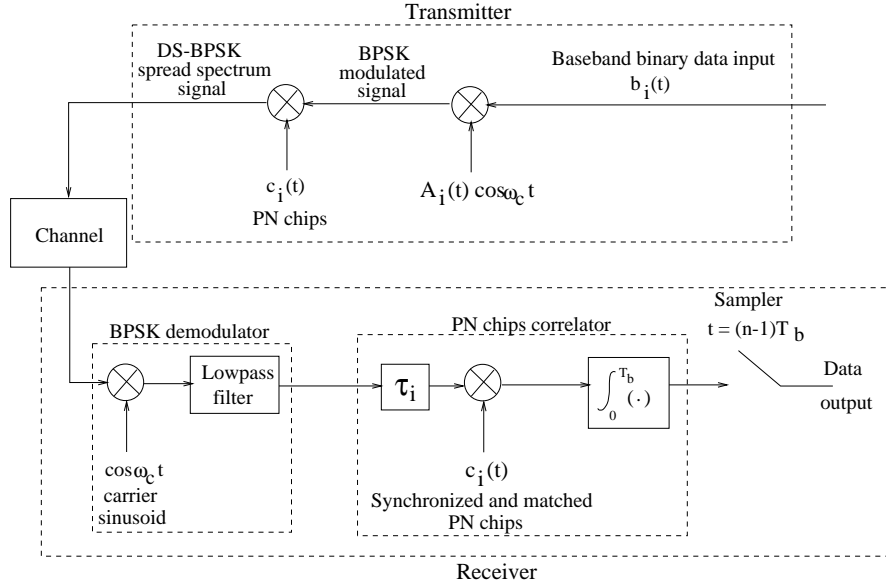


Figure 3.2: DS-BPSK digital spread spectrum system model

The baseband information bit sequence of period T_b can be expressed as

$$b_i(t) = \sum_{n=-\infty}^{\infty} b_{i,n} q(t - nT_b) \quad (3.4)$$

where $b_{i,n} \in \{-1, 1\}$ is the i^{th} user's binary-valued information-bearing signal sequence, and $q(t)$ is a pulse modulation with pulse rate $1/T_b$. Note that T_b may not necessarily equal $1/B$ since after the digital channel encoder, the information sequence may be encoded to a higher code word bit rate by the digital channel encoder as shown in Figure 3.1. However, spread spectrum modulation always has $T_b \gg T_c$. Therefore, the equivalent baseband transmitted signal combining the PN chips and the information bits can be expressed as

$$u_i(t) = \sum_{n=-\infty}^{\infty} c_{i,n} b_{i,n} p(t - nT_c) \quad (3.5)$$

In order to formulate equations for a CDMA cellular system, direct-sequence binary phase shift keying (DS-BPSK) spread spectrum is considered and is shown in Figure 3.2 [38]. Substituting equations (3.3) and (3.4) into Figure 3.2, the DS-BPSK modulated signal of the i^{th} mobile can be written as

$$s_i(t) = \text{Re}\{u_i(t)e^{j\omega_c t}\} = \text{Re}\{A_i(t)c_i(t)b_i(t)e^{j\omega_c t}\}$$

$$\begin{aligned}
&= A_i(t)c_i(t)b_i(t)\cos(\omega_c t) \\
&= \sum_{n=-\infty}^{\infty} A_i(t)c_{i,n}b_{i,n}p(t-nT_c)\cos(\omega_c t)
\end{aligned} \tag{3.6}$$

where $A_i(t)$ is the i^{th} mobile's transmitted signal amplitude, and $\text{Re}\{\cdot\}$ denotes the real part of $\{\cdot\}$.

Assume that there are N mobiles transmitting signals to the base-station, including the desired mobile. Also assume for now that the channel does not introduce multi-path, so each transmitted signal is received with only one path and a time-varying complex channel gain $\rho_k(t)e^{-j\omega_c\tau_k(t)}$. At the i^{th} correlator of a CDMA network, after synchronization with the i^{th} mobile, the complex envelope of the received signal can be expressed as

$$x_i(t) = \sum_{k=1}^N \rho_k(t)e^{-j\omega_c\tau_{i,k}(t)} A_i(t)c_i(t - \tau_{i,k}(t))b_i(t - \tau_{i,k}(t)) + n(t) \tag{3.7}$$

where $\rho_k(t)$ is the channel attenuation factor, $\phi_k = \omega_c\tau_k$ is the channel phase shift, $\tau_{i,k}(t) = \tau_k(t) - \tau_i(t)$ is the time delay of the k^{th} mobile relative to the i^{th} mobile and $|\tau_{i,k}(t)| \in (0, T_c]$ with $\tau_{i,i} = 0$ if self-synchronization is assumed, T_c is the chip rate of the PN sequence, $n(t) \in \mathcal{N}(0, \sigma_n^2)$ is the zero-mean additive white gaussian noise (AWGN) due to thermal noise.

Therefore, after ideal despreading with the designated i^{th} mobile's PN sequence, the despread received signal [27] [47] becomes

$$\begin{aligned}
z_i(n) &= \frac{1}{\sqrt{T_b}} \int_{nT_b}^{(n+1)T_b} x_i(t)c_i(t)dt \\
&= \frac{1}{\sqrt{T_b}} \int_{nT_b}^{(n+1)T_b} \sum_{k=1}^N \rho_k(t)e^{-j\omega_c\tau_{i,k}(t)} A_k(t)c_k(t - \tau_{i,k})b_k(t - \tau_{i,k})c_i(t)dt \\
&\quad + \frac{1}{\sqrt{T_b}} \int_{nT_b}^{(n+1)T_b} n(t)c_i(t)dt \\
&= \sqrt{T_b}\rho_i(t)A_i b_i(t) + \frac{1}{\sqrt{T_b}} \int_{nT_b}^{(n+1)T_b} n(t)c_i(t)dt \\
&\quad + \frac{1}{\sqrt{T_b}} \int_{nT_b}^{(n+1)T_b} \sum_{k=1, k \neq i}^N \rho_k(t)e^{-j\omega_c\tau_{i,k}(t)} A_k(t)c_k(t - \tau_{i,k})b_k(t - \tau_{i,k})c_i(t)dt
\end{aligned} \tag{3.8}$$

In equation (3.8), it is shown that the second and third terms are spread by a bandwidth $W_{ss} = 1/T_c$, while the desired despread signal bandwidth has been reduced back to its original bandwidth of $1/T_b$.

3.3 Multipath Fading Channel Models

Unlike wired channels whose parameters are stationary and predictable, wireless channels place fundamental limitations on the performance of a mobile communications system due to the dynamic time-varying nature of the transmission path and the relative speed between the transmitter and the receiver. In order to predict the average received signal strength for a given distance between transmitter and receiver and to estimate the radio coverage in a particular channel, sophisticated radio channel modelling and statistical analysis tools are required to characterize channels for practical radio receiver design in different communications systems [15] [22] [29].

The physical mechanisms of electromagnetic wave propagation in space are diverse, and are dominated by reflection, scattering, and diffraction. These propagation effects cause a transmitted signal $s(t)$ to arrive at the receiver over several paths with different channel gains $\rho_l e^{j\omega_c \tau_l}$ and within a time spread T_m . The time spread parameter characterizes the time-dispersive nature of the multipath fading channel.

To construct a model for the multipath fading environment of a CDMA cellular communication system [29], consider only one sequence of the bandpass DS-BPSK described in Figure 3.2 as transmitted by the i^{th} mobile with a signal of the form

$$\begin{aligned}
 s_i(t) &= \text{Re}\{A_i(t)c_i(t)b_i(t)e^{j\omega_c t}\} \\
 &= A_i(t)c_i(t)b_i(t) \cos(\omega_c t) \\
 &= \text{Re}\{u(t)e^{j\omega_c t}\}
 \end{aligned} \tag{3.9}$$

where $c_i(t)$ represents the direct sequence PN chips, $b_i(t)$ is the binary information bit, $A_i(t)$ is the transmitted signal amplitude, and $u(t) = A_i(t)c_i(t)b_i(t)$ is the baseband information signal that is transmitted with a carrier frequency of $\omega_c = 2\pi f_c$.

Assuming that the multipath channel introduces J distinct components which arrive at the receiver, each path l experiences a channel attenuation factor of $\varrho_{i,l}(t)$ and a channel propagation delay of $\tau_{il}(t)$. Therefore, the received bandpass signal resulting from the i^{th} mobile's transmitted signal sequence $s_i(t)$ can be expressed as

$$r_i(t) = \operatorname{Re} \left\{ \sum_{l=1}^J \varrho_{i,l}(t) e^{-j\omega_c \tau_{il}(t)} u(t - \tau_{il}(t)) e^{j\omega_c t} \right\} \quad (3.10)$$

The equivalent complex envelope/baseband received signal is then

$$x_i(t) = \sum_{l=1}^J \varrho_{i,l}(t) e^{-j\omega_c \tau_{il}(t)} u(t - \tau_{il}(t)) \quad (3.11)$$

It follows that the channel impulse response can be represented by

$$h(\tau_{il}; t) = \sum_{l=1}^J \varrho_{i,l}(t) e^{-j\omega_c \tau_{il}(t)} \delta(t - \tau_{il}(t)) \quad (3.12)$$

It requires requires large dynamic changes in the medium to cause significant changes in the channel attenuation $\varrho_{i,l}(t)$ of the received signal [29]. Conversely, the channel phase shift of the l^{th} path $\phi_{il} = \omega_c \tau_{il}(t)$ can change dramatically even for a relatively minor change in the propagation delay $\tau_{il}(t)$. In fact, since $\tau_{il}(t)$ changes at different rates and in an unpredictable manner, therefore, the channel phase shift can be modeled as a random process. For a large number of multipaths J , the Central Limit Theorem can be applied, where the channel impulse response $h(\tau_{il}; t)$ can be modeled as a complex-valued Gaussian random variable [28] [29].

When the impulse response $h(\tau_{il}; t)$ is modeled as a zero-mean complex-valued Gaussian process, the channel is called a Rayleigh-fading channel since the amplitude of the impulse response $|h(\tau_{il}; t)|$ at any time instant t is Rayleigh-distributed. Urban cellular mobile communication channels, where no direct line of sight (LOS) between the transmitter and receiver exists, can be modeled by a Rayleigh-fading channel where the channel phase shift is uniformly distributed over $[0, 2\pi)$.

A channel has Rician fading when the impulse response is modeled as a non-zero complex-valued Gaussian random variable. A satellite communication channel can be modeled as a Rician fading channel where a LOS exists between the transmitter

and receiver. The channel phase shift is no longer uniformly distributed over 2π , but is localized to a certain phase corresponding to the LOS direction. Rayleigh-fading channels model the most severe fading environment and appear to be a realistic cellular communication system multipath signal model [29] [43].

There are two types of channel distortions to the channel impulse response: frequency selectivity and fading [29]. Frequency selectivity distortion depends on the multipath delay spread T_m or, equivalently, depends on the coherence bandwidth B_m of the channel relative to the transmitted signal bandwidth W_{ss} . Fading channel distortion depends on the time variations of the channel that are characterized by the coherence time T_D or, equivalently, by the Doppler spread B_D .

The frequency selectivity of a channel can be affected by scattering and reflecting in the environment. First, we discuss the frequency selectivity nature of a channel, as parameterized by the delay spread and coherence bandwidth. The delay spread of a transmitted signal propagating through a multipath channel can be determined by the autocorrelation function of the channel impulse response $\Phi(\tau_1, \tau_2; \Delta t)$ based on a wide-sense-stationary (WSS) assumption [29].

$$\begin{aligned}\Phi(\tau_1, \tau_2; \Delta t) &= \mathbf{E}\{h(\tau_1; t)h(\tau_2; t + \Delta t)^*\} \\ &= \Phi(\tau_1; \Delta t)\delta(\tau_1 - \tau_2)\end{aligned}\tag{3.13}$$

When Δt is zero, the autocorrelation function $\Phi(\tau; 0)$ is simply the average power output of the channel impulse response at time delay τ . $\Phi(\tau; 0)$ is also called the channel multipath intensity profile (MIP) or the delay power profile (DPP). The range of τ over which the DPP is essentially nonzero is called the multipath spread or delay spread of the channel as denoted by T_m . The DPP power output value is at $\tau = 0$ when the first multipath signal is received, so the power amplitude decreases as τ increases. Therefore, the longer the path propagates through space, the more its power dissipates to the environment before reception. An urban environment typically provides differential path time delays ranging from less than $1\mu s$ up to $10 - 20\mu s$ [30] [32].

Taking the Fourier transform of the DPP, the space-frequency autocorrelation

Frequency-nonselective channel	Frequency-selective channel
symbol period $T \gg$ delay spread T_m	symbol period $T \ll$ delay spread T_m
Signal BW $W_{ss} \ll$ Coherence BW B_m	Signal BW $W_{ss} \gg$ Coherence BW B_m

Table 3.1: Criteria for frequency-nonselective and frequency-selective channel

function can be expressed as

$$\Phi(f; 0) = \int_{-\infty}^{\infty} \Phi(\tau; 0) e^{-j\omega_c \tau} d\tau \quad (3.14)$$

which gives a measure of the channel's coherence bandwidth $B_m \approx 1/T_m$. The coherence bandwidth denotes the frequency range over which the correlation is close to unity. In other words, two sinusoids with a frequency separation greater than B_m will be affected differently by the channel.

A channel is called frequency-nonselective or flat fading when $B_m \gg W_{ss}$, that is, when the coherence bandwidth B_m is large in comparison to the bandwidth of the transmitted signal W_{ss} [29]. On the other hand, a channel is called frequency-selective when $B_m \ll W_{ss}$, that is, when the coherence bandwidth B_m is small in comparison to W_{ss} .

In fact, in a frequency-nonselective channel where $W_{ss} \ll B_m$, the received signal can be modelled as simply the transmitted signal multiplied by a complex-valued Gaussian random process of the channel impulse response [29]

$$h(0; t) = \rho(t) e^{j\omega_c t} \quad (3.15)$$

which means that the signals in a flat fading channel experience the same fading/channel gain. In this case, the multipath components are not resolvable because $W_{ss} T_m \ll 1$. Therefore, $1/W_{ss}$ represents the time resolution, i.e., the minimum time delay between received paths that is required at the receiver before the paths can be distinguished.

When the channel is frequency-selective, i.e. when $W_{ss} \gg B_m$, there typically exist at least $J = W_{ss}/B_m = T_m W_{ss}$ resolvable paths [29]. Two multipaths are said to be

Fast fading channel	Slow fading channel
High Doppler spread	Low Doppler spread
Coherence time $T_D < \text{Symbol period } T$	Coherence time $T_D > \text{Symbol period } T$

Table 3.2: Criteria for fast fading and slow fading channel

resolvable when they fade independently, with each k^{th} multipath of the i^{th} mobile experiencing different channel gain of $\rho_{ik}(t)e^{-j\omega_c\tau_{ik}}$. Therefore, the use of wideband signals, such as CDMA, may be viewed as another method for obtaining frequency diversity of order J [29]. The optimum receiver for processing the frequency-selective wideband signal is called a RAKE correlator or a RAKE matched filter [29].

Second, the time-variation of the channel due to Doppler effects can be characterized by the Doppler spread and coherence time. The time-varying nature of the channel can be caused either by the relative motion between the mobile and base station, or by the movement of objects in the channel. The Doppler spread B_D and coherence time T_D are parameters which describe the time-varying nature of the channel in a small-scale region. For a mobile communications channel, the maximum Doppler spread in Hz is calculated as [22]

$$B_D = \frac{v f_c}{c} \quad (3.16)$$

where v is the mobile velocity assuming the base station is stationary, c is the speed of light for electromagnetic waves traveling in space, and f_c is the carrier frequency of the signal. The coherence time can be approximated as [29]

$$T_D \approx \frac{1}{B_D} \quad (3.17)$$

The Doppler spread is a measure of the spectral broadening caused by the change of the mobile radio channel and is defined as the range of frequencies over which the received Doppler spectrum is essentially non-zero. Table 3.2 summarizes the criteria for fast and slow fading channels. If the baseband signal bandwidth W_{ss} is much greater than B_D , then the Doppler spread effects are negligible at the receiver [32].

3.4 Linear Diversity Combining

As discussed, wireless propagation introduces amplitude fluctuations and phase shifts to transmitted signals such as short-term Rayleigh fading which may introduce a severe performance degradation. A most common and widely used receiver structure to combat the short-term fading effect is to employ a diversity combining technique.

The diversity operations presume the availability of M distinguishable independently faded signal-transmission channels, referred to as diversity branches. In particular, for a space diversity receiver topology, these M diversity branches are widely spaced antennas where independent faded signals are received at each antenna element. In this thesis, the space diversity receiver topology is considered only for linear diversity combining. Note that diversity combining techniques assume that long-term fading affects all diversity branches identically. Thus, diversity combining techniques compensate only for short-term fading effects [1] [35].

A general linear combining technique of M diversity branches involves combining each branch with a weight, $w_k(t)$, in order to improve reception SINR gain.

$$y(t) = \sum_{k=1}^{k=M} w_k(t)^* x_k(t) \quad (3.18)$$

where $w_k(t)$ is the k^{th} branch's weight, $(\cdot)^*$ represents the conjugate of (\cdot) , M is the number of diversity branch available, and the k^{th} received baseband signal is represented as

$$\begin{aligned} x_{ik}(t) &= \varrho_{i,k}(t) e^{-j\omega_c \tau_{ik}} A_i(t) u_i(t) + i_{ik}(t) + n_{ik}(t) \\ &= H_{ik}(t) A_i(t) u_i(t) + n_k(t) \\ &= g_k(t) u_i(t) + n_k(t) \end{aligned} \quad (3.19)$$

where $u_i(t)$ is the baseband transmitted binary information signal equivalent at all diversity branches, $A_i(t)$ is the transmitted signal power of the i^{th} mobile which is same at all diversity branches, $H_{ik}(t)$ is the k^{th} diversity branch impulse response that composed of a channel gain $\varrho_{i,k}(t)$ and a channel phase shift $\omega_c \tau_{ik}$, $n_{ik}(t)$ is the k^{th}

branch Additive Gaussian white noise of the i^{th} mobile and $n_k(t)$ is the interference-plus-noise signal. Thus, the linearly diversity combined signal-to-interference-plus-noise ratio can be expressed as

$$SINR = \frac{|\sum_{k=1}^{k=M} w_k(t)^* g_k(t)|^2}{|\sum_{k=1}^{k=M} w_k(t)^* n_k(t)|^2} \quad (3.20)$$

The well-known and widely used linear diversity combining techniques are selection combining (SC), maximal-ratio combining (MRC), and equal-gain combining (EGC), which are reviewed briefly.

3.4.1 Selection Combining

In a selection combining, the receiver switches to the highest signal-to-interference-plus-noise signal branch received from these M diversity branches at any instant of time. That is

$$w_k = \begin{cases} 1 & \text{for } k = j \\ 0 & \text{for } k \neq j \end{cases} \quad (3.21)$$

in Equation (3.18) with $x_k(t) > x_j(t)$ for all $j = 1, 2, \dots, M$ and $k \neq j$.

The concept of selection combining is that when there is at least one diversity branch receiving relatively high SINR, then the selection combiner could maintain a higher quality of reception as compared to a single antenna reception topology. The advantage of a selection combiner is the high probability of not having every diversity branch signal experiencing a deep fade of the transmitted signals. The disadvantage of using selection combining is that the receiver system is dependent on the propagation channels; if the channels are all experiencing deep fades, there will no longer be adequate SINR.

3.4.2 Maximal-ratio Combining

In a maximal-ratio combining (MRC) receiver, weights are determined at each diversity branch so to maximize the signal-to-interference-plus-noise power. In this thesis,

CDMA binary information baseband signal $u_i(t)$ is spread by its PN code and orthogonal Walsh functions are considered where the interferer signals are assumed mutually uncorrelated. Therefore, the interference-plus-noise components $n_k(t)$ are uncorrelated and the requirements for employing a MRC are achieved [1]. The maximal-ratio diversity combining can be achieved when each k^{th} branch weight in Equation (3.18) is proportional to the root mean square of the desired signal power at the k^{th} branch and inversely proportional to the mean square noise in that branch. Mathematically,

$$w_k(t) = \frac{g_k(t)^*}{\mathbf{E}\{|n_k(t)|^2\}} \quad \text{for all } k = 1, 2, \dots, M \quad (3.22)$$

where $g_k(t)^*$ is the conjugate of $g_k(t)$ which phase aligns every branch and allows coherent addition of the signals from each branch, $\mathbf{E}\{(\cdot)\}$ represents the expectation operation. The maximal-ratio combined signal SINR can be shown to be

$$SINR = \sum_{k=1}^{k=M} SINR_k \quad (3.23)$$

where $SINR_k = \frac{\mathbf{E}\{|g_k(t)|^2\}}{\mathbf{E}\{|n_k(t)|^2\}}$ is the signal-to-interference-plus-noise ratio of the k^{th} branch signal received.

The advantage of using maximal ratio combining is that it provides the maximum SINR gain compared to using other classical types of combining. The disadvantage of MRC is the intensive signal processing required to estimate the channel parameters including gain, phase shift as well as the averaged interference-plus-noise power. Note that MRC is similar to optimal SINR beamforming.

3.4.3 Equal-gain Combining

Equal-gain combining (EGC) sets all branch weights amplitudes to unity and sets the weight phase opposite to that of the signal in the respective branches [35]. That is setting

$$\mathbf{w}(t) = [e^{j\phi_1(t)}, e^{j\phi_2(t)}, \dots, e^{j\phi_M(t)}]^T \quad (3.24)$$

in Equation (3.18). EGC is simply a phase-locked addition of all branches that incoherently summing the noise and coherently summing the signals. The advantage

of using the EGC is its simplicity and is statistically effective in achieving diversity results. However, when there are relatively deep faded signal branches that are being combined, the resultant equal-gain combined signal will reduce the overall signal-to-interference-plus-noise ratio. Therefore, the assumption of equal noise levels in all branches is crucial to proper operation of this EGC [35].

3.5 The IS-95 reverse link

The second-generation IS-95 CDMA common air interface standard proposed by Qualcomm was formally adopted as the North American digital cellular standard IS-95 on July 16, 1993. Preliminary field trials of IS-95 have demonstrated that a CDMA cellular system can increase capacity by 10 to 20 times over that of an analog cellular system under realistic channel conditions [30].

The rest of this thesis investigates array signal processing applications to an antenna array at the base station of a CDMA cellular system. This can further improve the received SINR at the base station which will in turn increase the cell capacity. Only the reverse link (mobile-to-base-station) of the IS-95 standard is reviewed here. It is assumed that only the base station is equipped with an antenna array but not the handset due to cost and power consumption limitations.

3.5.1 The reverse link/uplink channel waveform

The IS-95 uplink employs PN spread spectrum modulation using a length $2^{15} - 1$ short code sequence of chip rate 1.2288Mcps. The standard $2^{15} - 1$ short code states are augmented with the 0 state to obtain a sequence of length 32768. Note that the short code used here is the same as the short code used for the forward (base-to-mobile) link where the base station distinguishes different mobiles by the use of a very long ($2^{42} - 1$) PN sequence with each user having a different time offset and code word. Therefore, each user has his/her own unique long code PN sequence.

The information bits are transmitted at 9.6kbps and are segmented into 50 frames

of 192 bits each, corresponding to 20ms in time. Each frame is then convolutionally encoded using a rate 1/3 code (three encoded binary symbols per information bit) of constraint length 9 giving an encoded bit rate of 28.8kbps. The convolutionally-encoded information is then grouped in sets of six symbols to form code words. These code words are used to select between 64 different orthogonal Walsh function chip sequences of chip rate 307.2kcps for transmission via 64-ary orthogonal modulation. The Walsh chips are then direct-sequence spread with the mobile's long code sequence at 1.2288Mcps. The data stream is then split into in-phase and quadrature phase streams where each is further modulated with the short codes at chip rate 1.2288Mcps and then modulated with a carrier frequency at 1.9GHz. It can be noted that the spreading gain provided by the IS-95 uplink is only $1228800/307200 = 4$. The rest of the performance gain can be attributed to coding.

To maximize system capacity, the reverse link imposes power control where the handset transmission powers are adjusted so that the received signal-to-noise ratios E_b/N_0 at the base station are equal for every handset. Power control combats the performance impairment known as the near-far problem when interfering mobiles near the base station create more interference for more distant mobiles.

3.5.1.1 Base-station receiver

For uplink reception, the base station uses dual antenna diversity in each 120° sector to provide path diversity. Path diversity of independently faded paths can be artificially obtained by widely separating the antennas for each sector. Path diversity can also be used on individual antenna elements in frequency selective mobile channels in which more than one signal path will be received as reviewed in the previous section. Multipaths arriving at the antenna array with more than one chip delay T_c will fade independently because PN sequences have nearly zero correlation for time offsets greater than one chip. The RAKE receiver for combining the orthogonal signals is called a non-coherent RAKE [29].

For a given desired i^{th} mobile, a corresponding i^{th} non-coherent RAKE receiver

with correlators J_c is used to despread J_c paths. Then, a front-end scanner continuously monitor all six antenna outputs for multipath signals and chooses the $J < J_c$ strongest multipaths for RAKE combining, based on received signal power.

3.6 State-of-the-Art Array Signal Processing applications to CDMA Cellular Communication Systems

As reviewed here and in the previous chapter, adaptive antenna array beamforming in cellular CDMA communication systems holds great potential for improving signal-to-interference-noise ratios and thereby achieving higher cell capacity. An adaptive beamforming network spatially filters the in-band interfering mobiles by adaptively updating the weight vector of each beamformer so as to steer the main beam lobe to the direction-of-arrival (DOA) of the desired mobile. Traditional eigen-based beamforming techniques require iterative and computationally-expensive batch processing [23] [24] [25]. The goal of this research is to achieve higher capacity and coverage in future multimedia cellular CDMA systems by using an adaptive antenna array beamforming network at the base station. Motivated by adaptive beamforming techniques, we review here related state-of-the-art adaptive beamforming techniques for base-station antenna arrays.

Naguib and Paulraj [24] [25] showed that updating beamforming weights for each mobile in a multi-beamforming network can be expensive depending on how the estimates are being calculated. From Chapter 2, the signal-to-interference-noise ratio (SINR) optimum beamforming weight $\mathbf{w}_{\text{opt}_{i,l}}$ for the i^{th} mobile and l^{th} path requires: (i) the array response, $\mathbf{a}_{i,l} \in \mathcal{C}^{M \times 1}$, and (ii) the inverse of the batch processing interference-noise covariance matrix, $\mathbf{R}_{\text{IN},i,l}^{-1} \in \mathcal{C}^{M \times M}$, i.e.,

$$\mathbf{w}_{\text{opt}_{i,l}} = \zeta \mathbf{R}_{\text{IN},i,l}^{-1} \mathbf{a}_{i,l} \tag{3.25}$$

where $\mathbf{a}_{i,l} = [a_1, \dots, a_M]^T \in \mathcal{C}^{M \times 1}$ is the i^{th} mobile's l^{th} multipath unit channel array response vector, M is the number of antenna elements, ζ is a scalar, and \mathcal{C} is the complex domain. The estimation of (i) & (ii) requires the formation of a pre-correlation autocovariance matrix \mathbf{R}_{xx} as well as the i^{th} mobile's l^{th} multipath post-correlation autocovariance matrix $\mathbf{R}_{zz_{i,l}}$ [24] [25].

The adaptive beamforming method proposed in [24][25][27] for a CDMA environment is computationally very expensive, since there are 1228800 (PN chips per second) pre-correlation vectors $\mathbf{x}(t)$ per user per second and 307200 (Walsh chips per second) post-correlation vectors $\mathbf{z}_i(n)$ per user per second in IS-95. As shown in [25] and [24], Naguib and Paulraj had formulated the pre-correlation matrix as

$$\mathbf{R}_{xx} = \mathbf{E}\{\mathbf{x}\mathbf{x}^\dagger\} = P_{i,l}\mathbf{a}_{i,l}\mathbf{a}_{i,l}^\dagger + \mathbf{R}_{\text{IN}_{i,l}} \quad (3.26)$$

where L is the spread spectrum processing gain, $P_{i,l}$ is the total receiving power of the i^{th} mobile's l^{th} path, and \mathbf{R}_{IN} is the interference-plus-noise correlation matrix. They also formulated the post-correlation matrix is as

$$\mathbf{R}_{zz_{i,l}} = LP_{i,l}\mathbf{a}_{i,l}\mathbf{a}_{i,l}^\dagger + \mathbf{R}_{\text{IN}_{i,l}} = (L-1)\mathbf{a}_{i,l}\mathbf{a}_{i,l}^\dagger + \mathbf{R}_{xx} \quad (3.27)$$

These pre-correlation and post-correlation matrices give

$$\mathbf{R}_{zz_{i,l}} - \mathbf{R}_{xx} = (L-1)\mathbf{a}_{i,l}\mathbf{a}_{i,l}^\dagger \quad (3.28)$$

and the estimate of the interference-plus-noise correlation matrix $\hat{\mathbf{R}}_{\text{IN}_{i,l}}$ as

$$\hat{\mathbf{R}}_{\text{IN}_{i,l}} = \frac{L}{L-1}(\mathbf{R}_{xx} - \frac{1}{L}\mathbf{R}_{zz_{i,l}}) \quad (3.29)$$

From equation (3.30), it then follows that

$$\mathbf{R}_{zz_{i,l}}\mathbf{a}_{i,l} - \mathbf{R}_{xx}\mathbf{a}_{i,l} = (L-1)\mathbf{a}_{i,l} \quad (3.30)$$

Therefore, the channel array response vector can be estimated by solving for the principal eigenvector corresponding to the maximum eigenvalue λ_{max} of the matrix pencil of $\mathbf{R}_{zz_{i,l}}\mathbf{a}_{i,l} - \lambda\mathbf{R}_{xx}\mathbf{a}_{i,l}$. A matrix pencil represents the set of all matrices of

the form $\mathbf{A} - \lambda\mathbf{B}$ where \mathbf{A} and \mathbf{B} are two $M \times M$ matrices with $\lambda \in \mathbf{C}$ [13]. The eigenvalues of the pencil elements of the set $\lambda(\mathbf{A}, \mathbf{B})$ are defined by

$$\lambda(\mathbf{A}, \mathbf{B}) = \{\lambda \in \mathbf{C} : \det(\mathbf{A} - \lambda\mathbf{B}) = 0\} \quad (3.31)$$

That is, if $\lambda \in \lambda(\mathbf{A}, \mathbf{B})$ and

$$\mathbf{A}\mathbf{v} = \lambda\mathbf{B}\mathbf{v} \quad \text{where} \quad \mathbf{v} \neq 0 \quad (3.32)$$

then \mathbf{v} is referred to as an eigenvector of $\mathbf{A} - \lambda\mathbf{B}$. Solving for the principal eigenvector of equation (3.32) is equivalent to solving a generalized eigenvalue problem of

$$\mathbf{R}_{zz_{i,l}} \mathbf{a}_{i,l} = \lambda \mathbf{R}_{xx} \mathbf{a}_{i,l} \quad (3.33)$$

To avoid accumulation of numerical errors generated from recursive updating of the estimated covariance matrices by eqn.(2.69), the square matrix of \mathbf{R}_{xx} is used. The square root $\mathbf{R}_{xx}^{1/2}$ of a positive definite matrix \mathbf{R}_{xx} always exists [13]. \mathbf{R}_{xx} is defined as positive definite matrix due to white additive Gaussian noise.

$$\left(\mathbf{R}_{xx}^{-1/2} \mathbf{R}_{zz_{i,l}} \mathbf{R}_{xx}^{-\dagger/2} \right) \left(\mathbf{R}_{xx}^{1/2} \mathbf{a}_{i,l} \right) = \lambda \left(\mathbf{R}_{xx}^{1/2} \mathbf{a}_{i,l} \right) \quad (3.34)$$

Therefore the channel array response vector can be estimated from Equation (3.34) as

$$\hat{\mathbf{a}}_{i,l} = \mathbf{R}_{xx}^{-1/2} \mathbf{e}_{i,l} \quad (3.35)$$

The iterative power method is used to calculate the principal eigenvector $\mathbf{e}_{i,l}$ corresponding to the largest eigenvalue of $\mathbf{R}_{xx}^{-*/2} \mathbf{R}_{zz_{i,l}} \mathbf{R}_{xx}^{1/2}$.

One drawback of an iterative eigen-decomposition method, such as the power method, is that its computational complexity may be unbounded, depending on the eigenvalue spread.

3.6.1 2D-RAKE Receiver for Frequency-selective fading

For the CDMA IS-95 standard, a one-chip path differential delay corresponds to a differential path distance of 250 meters. Therefore, signals arriving at the base-station

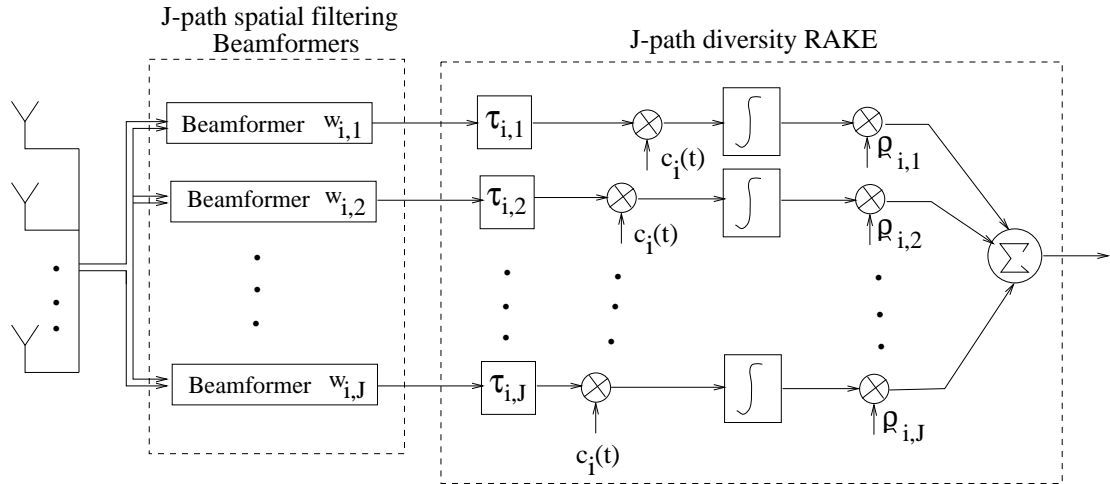


Figure 3.3: 2D-RAKE receiver

with a differential delay of more than one chip will very likely be coming from different directions [30]. This effect is especially pronounced in heavily built-up urban areas. Therefore, angle-of-arrival diversity techniques can also be used for the optimal RAKE receiver in an IS-95 system.

Khalaj, Paulraj and Kailath introduce the concept of a 2D RAKE receiver to construct a space-time receiver [20]. The 2D RAKE can exploit the temporal and spatial structure of the individual paths arriving at the receiver by first beamforming each of the J paths from the M -element array, then delaying each by the estimated channel delay, and finally coherently combining the J paths in order to further improve the SINR. Figure 3.3 shows a 2D-RAKE receiver structure where spatial filtering is performed for each path before combining [20].

3.7 Summary

This chapter has reviewed CDMA direct sequence modulation techniques and concepts, and has also examined a general Rayleigh multipath environment for a cellular system. Current state-of-the-art array signal processing techniques for digital beamforming with base station antenna arrays were also outlined. These computationally-expensive methods motivate a new approach toward a computationally efficient and

statistically stable noniterative beamforming algorithms.

Chapter 4

Noniterative Rank-1 Signal Subspace Update Algorithm

In this chapter, we describe a Noniterative Rank-1 Signal Subspace eigenstructure Update (NR1SSU) algorithm and apply it to a beamforming network in a CDMA cellular communication system. The application of NR1SSU is motivated by the intensive computation required in array signal processing. In addition, using an iterative eigendecomposition method could lead to unbounded computational complexity when the largest eigenvalues differ by an arbitrarily small amount [23]. Section 4.1 states the existing limitations on digital beamforming algorithms which inspired the recent work by Naguib and Paulraj [25] [27] [26] [24]. The concept of noniterative, numerically stabilized, and efficient subspace tracking is reviewed in Section 4.2. Section 4.3 derives and develops the mathematical model of the received signal vector at the base station. The noniterative subspace tracking is then incorporated into a generic CDMA system as well as the IS-95 CDMA system. In addition, an eigenbased inverse covariance matrix is computed to achieve maximum signal-to-interference-plus-noise ratio (SINR). Section 4.6 presents the NR1SSU computation complexity per weight vector update.

4.1 Motivation of using NR1SSU

In practice, the performance of an adaptive array critically depends on the convergence rate that can be achieved. As reviewed in Chapter 2, the iterative power method and the LMS algorithm may result in slow adaptive weight vector convergence to the optimum Wiener solution depending on the eigenvalue spread of the estimated correlation matrix used [23]. One way to circumvent the convergence rate dependence on eigenvalue distribution is to employ a direct method of adaptive weight computation, based on the sample covariance matrix of the signal environment. One example is the RLS algorithm discussed in Chapter 2. The RLS algorithm directly estimates the second-order statistics for the optimum Wiener solution when a reference signal is provided. The RLS algorithm computation is independent of the eigenvalue spread, and often converges much faster than the power method or the LMS algorithm. However, the RLS algorithm is computationally expensive and the difference equations for updating the inverse covariance matrix in equation (2.71) are numerically unstable [17].

From Chapter 2, the adaptive Wiener solution to the optimum beamformer requires knowledge of the desired signal array response vector. In [25] [24] [26], as reviewed in Chapter 2, the weight vector update method proposed by Naguib and Pauraj shows that the desired signal channel array response vector can be estimated by the principal eigenvector of $\mathbf{R}_{xx}^{-1/2} \mathbf{R}_{zz_{i,l}} (\mathbf{R}_{xx}^{1/2})^\dagger$, i.e.,

$$\left(\mathbf{R}_{xx}^{-1/2} \mathbf{R}_{zz_{i,l}} (\mathbf{R}_{xx}^{-1/2})^\dagger \right) \left(\mathbf{R}_{xx}^{1/2} \mathbf{a}_{i,l} \right) = \lambda \left(\mathbf{R}_{xx}^{1/2} \mathbf{a}_{i,l} \right) \quad (4.1)$$

Naguib and Paulraj employ the iterative power method to solve this generalized eigenvalue problem which possesses unbounded complexity and slow convergence. Although [25] uses a recursive direct inversion method to estimate the optimal weight vector for beamforming, it is again eigenvalue-spread dependent.

This eigenvalue convergence problem motivates us to investigate a noniterative subspace decomposition method [6] for data-adaptive optimal beamforming for base-station antenna arrays in a CDMA cellular communication system. The NR1SSU

algorithm efficiently computes rank-one updates of the eigenstructure of matrices and is numerically stable [5] [6], as discussed in the next section. This novel application of subspace decomposition forms the core of this thesis investigation. Section 4.3 presents our formulation of the noniterative subspace update algorithm and its application to a generic CDMA system as described in Chapter 2 and to the IS- 95 cellular communication system.

4.1.1 Rank-one update for time-varying statistics

In a mobile communication channel, mobile user signal statistics are time-varying, depending on the motion of the user as well as the changing environment. The time-varying covariance matrix can be estimated by an exponentially-weighted rank-one covariance matrix which adapts to time-varying statistics [5] [6] [34]. The memory factor, α , of an exponentially-weighted rank-one covariance matrix deemphasizes old data while updating the covariance matrix by adding the outer product of the new received array vector. The covariance matrix of the received array signal can be estimated by exponentially weighting the rank-one update covariance matrix as reviewed in Chapter 2, equation (2.70). The recursive exponentially weighted covariance estimate $\hat{\mathbf{R}}_{xx}(k)$ at time index k can be expressed as

$$\begin{aligned}\hat{\mathbf{R}}_{xx}(k) &= \mathbf{E}\{\mathbf{x}(k)\mathbf{x}(k)^\dagger\} = (1 - \alpha) \sum_{n=1}^k \alpha^{k-n} \mathbf{x}(k)\mathbf{x}(k)^\dagger \\ &= \alpha \hat{\mathbf{R}}_{xx}(k-1) + (1 - \alpha) \mathbf{x}(k)\mathbf{x}(k)^\dagger\end{aligned}\quad (4.2)$$

where the memory factor $0 < \alpha < 1$, $\mathbf{x}(k)$ is the k^{th} snapshot of array output data, and the recursion is initialized at time zero with $\hat{\mathbf{R}}_{xx}(0) = \mathbf{0}$. Note that the larger the memory factor, the less deemphasis of old data, while the smaller the memory factor, the greater the deemphasis on old data. This memory factor controls the amount of data used in the averaging process and hence the degree to which the covariance estimate can adapt to the time variations in the signal. In extreme case of $\alpha = 0$, the covariance estimate totally ignores the old data. However, this will cause rapidly varying estimates of the covariance matrix because of the lack of averaging of the

stochastic process. When the memory factor equals unity, there is no adaptation to new data of the time-varying covariance matrix estimate. This again fails to estimate the covariance matrix. Therefore, the appropriate memory factor must be chosen to properly trade-off between stability and adaptation speed.

The matrix in Equation (4.2) can also be estimated through a rank-one eigenstructure update that recursively uses the previous known or estimated eigendecomposition of the covariance matrix, $\hat{\mathbf{R}}_{xx}(k-1) = \mathbf{Q}_{k-1}\mathbf{D}_{k-1}\mathbf{Q}_{k-1}^\dagger$ to estimate the current eigendecomposition $\hat{\mathbf{R}}_{xx}(k) = \mathbf{Q}_k\mathbf{D}_k\mathbf{Q}_k^\dagger$.

Mathematically, a rank-one eigenstructure update of equation (4.2) can be expressed as

$$\hat{\mathbf{R}}_{xx}(k) = \alpha\mathbf{Q}_{k-1}\mathbf{D}_{k-1}\mathbf{Q}_{k-1}^\dagger + (1-\alpha)\mathbf{x}(k)\mathbf{x}(k)^\dagger \quad (4.3)$$

where $\mathbf{D}_{k-1} = \text{diag}(d_1, d_2, \dots, d_M) \in \mathcal{R}^{M \times M}$ is the real-valued diagonal eigenvalue matrix. Note that the eigenvalues of a covariance matrix represent the power of the received signal vector which is always positive semi-definite, and $\mathbf{Q}_{k-1} = [\mathbf{u}_1, \mathbf{u}_2, \dots, \mathbf{u}_M] \in \mathcal{C}^{M \times M}$ consists of the corresponding orthonormal eigenvectors $\mathbf{u}_m \in \mathcal{C}^{M \times 1}$ for $m = 1, 2, \dots, M$.

4.2 Noniterative spherical subspace rank-one eigenstructure update

A noniterative subspace rank-one eigenstructure update can be applied to a time-varying additive-noise signal model of an M-element antenna array received signal output [6] [5]

$$\mathbf{x}(t) = \mathbf{s}(t) + \mathbf{n}(t) \quad (4.4)$$

where the $M \times 1$ signal vector $\mathbf{s}(t)$ may be composed into a sum of r independent signal vectors

$$\mathbf{s}(t) = \sum_{i=1}^r \mathbf{s}_i(t) \quad (4.5)$$

The correlation matrix $\mathbf{R}_{ss}(t) = \mathbf{E}\{\mathbf{s}(t)\mathbf{s}(t)^\dagger\}$ is of rank r and positive semi-definite

$$\text{rank}(\mathbf{R}_{ss}(t)) \approx r < M \quad (4.6)$$

and the $M \times 1$ noise vector $\mathbf{n}(t)$ is assumed to be white or has been prewhitened so that the noise variance matrix is

$$\mathbf{R}_{nn}(t) = \sigma_n^2(t)\mathbf{I} \quad (4.7)$$

where the noise power $\sigma_n^2(t)$ may be time-varying. In other words, the noise vector $\mathbf{n}(t)$ is assumed to be uncorrelated with the signal vector $\mathbf{s}(t)$ such that

$$\mathbf{E}\{\mathbf{s}(t)\mathbf{n}(t)^\dagger\} = \mathbf{0} \quad (4.8)$$

The correlation matrix of $\mathbf{x}(t)$ can then be decomposed as

$$\begin{aligned} \mathbf{R}_{xx}(t) &= \mathbf{E}\{\mathbf{x}(t)\mathbf{x}(t)^\dagger\} = \mathbf{E}\{\mathbf{s}(t)\mathbf{s}(t)^\dagger\} + \mathbf{E}\{\mathbf{n}(t)\mathbf{n}(t)^\dagger\} \\ &= \mathbf{R}_{ss}(t) + \mathbf{R}_{nn}(t) \end{aligned} \quad (4.9)$$

Assuming that the time-varying stochastic process $\mathbf{x}(t)$ is ergodic for $1/(1 - \alpha)$ time steps, complex-valued, and zero-mean, the covariance matrix of $\mathbf{x}(t)$ can then be estimated recursively by the rank-one eigenstructure update as stated in equation (4.3). Therefore, at the discrete update time index k , equation (4.9) can be expressed as

$$\hat{\mathbf{R}}_{xx}(k) = \alpha \mathbf{Q}_{k-1} \mathbf{D}_{k-1} \mathbf{Q}_{k-1}^\dagger + (1 - \alpha) \mathbf{x}(k) \mathbf{x}(k)^\dagger \quad (4.10)$$

where $\mathbf{Q}_{k-1} = [\mathbf{u}_1, \mathbf{u}_2, \dots, \mathbf{u}_M]$ are the eigenvectors corresponding to the eigenvalues $\mathbf{D}_{k-1} = \text{diag}(d_1, d_2, \dots, d_M) \in \mathcal{R}^{M \times M}$. Note that for a signal subspace of r independent signal vectors, the eigenvalues are indexed in the order $d_1 \geq d_2 \geq \dots \geq d_r \geq d_{r+1} \approx d_{r+2} \approx \dots \approx d_M$ where the largest r eigenvalues correspond to the r independent signals powers and the smallest $M - r$ eigenvalues correspond to the noise power of $\mathbf{n}(t)$. Specifically, $d_{r+1} \approx d_{r+2} \dots \approx d_M \approx \sigma_n^2$ is the noise power.

By substituting the complex vector $\mathbf{g} = \sqrt{(1-\alpha)}\mathbf{Q}_{k-1}^\dagger \mathbf{x}(k)$ or equivalently $\mathbf{x}(k) = \mathbf{Q}_{k-1}\mathbf{g}/\sqrt{(1-\alpha)}$, equation (4.10) becomes

$$\hat{\mathbf{R}}_{xx}(k) = \mathbf{Q}_{k-1}(\alpha\mathbf{D}_{k-1} + \mathbf{g}\mathbf{g}^\dagger)\mathbf{Q}_{k-1}^\dagger \quad (4.11)$$

Using the diagonal unitary transformation

$$\mathbf{G} = \text{diag}\left(\frac{g_1}{|g_1|}, \frac{g_2}{|g_2|}, \dots, \frac{g_n}{|g_n|}\right) \quad (4.12)$$

the complex-valued matrix $(\alpha\mathbf{D}_{k-1} + \mathbf{g}\mathbf{g}^\dagger)$ can be transformed into a real valued matrix [6] [34]. That is, by substituting the real-valued vector $[\gamma_1, \gamma_2, \dots, \gamma_M]^\text{T} = \boldsymbol{\gamma} = \mathbf{G}^\dagger\mathbf{g}$, equation (4.11) can be written as

$$\begin{aligned} \hat{\mathbf{R}}_{xx}(k) &= \mathbf{Q}_{k-1}\mathbf{G}(\alpha\mathbf{D}_{k-1} + \boldsymbol{\gamma}\boldsymbol{\gamma}^\text{T})\mathbf{G}^\dagger\mathbf{Q}_{k-1}^\dagger \\ &= \mathbf{Q}_k(\alpha\mathbf{D}_{k-1} + \boldsymbol{\gamma}\boldsymbol{\gamma}^\text{T})\mathbf{Q}_k^\dagger \\ &= \mathbf{Q}_k\mathbf{D}_k\mathbf{Q}_k^\dagger \end{aligned} \quad (4.13)$$

where $\mathbf{D}_{k-1} = \mathbf{G}^\dagger\mathbf{D}_{k-1}\mathbf{G}$ since $\hat{\mathbf{R}}_{xx}(k)$ is symmetric and positive semi-definite.

Equation (4.13) shows that the updated eigenvalue matrix $\mathbf{D}_k = \text{diag}(\tilde{d}_1, \tilde{d}_2, \dots, \tilde{d}_M)$ at time index k is obtained by a rank-one modification of the eigenvalue matrix $\mathbf{D}_{k-1} = \text{diag}(d_1, d_2, \dots, d_M)$ at time $k-1$.

In fact, there are three properties [2] [3] that will help reduce computation in modifying the eigenstructure using a rank-one modification of an eigenvalue matrix with $\mathbf{D}_k = \alpha\mathbf{D}_{k-1} + |\gamma|^2(\boldsymbol{\gamma}/|\boldsymbol{\gamma}|)(\boldsymbol{\gamma}^\text{T}/|\boldsymbol{\gamma}|) = \alpha\mathbf{D}_{k-1} + \rho\mathbf{f}\mathbf{f}^\text{T}$ where $\mathbf{f} = \boldsymbol{\gamma}/|\boldsymbol{\gamma}|$ with $|\mathbf{f}| = 1$ and $\rho = |\gamma|^2$:

i) When $f_i = 0$ for some $i \in \{1, 2, \dots, M\}$, the corresponding i^{th} eigenvalue and eigenvector remain unchanged since $\alpha\mathbf{D}_k\mathbf{e}_i = (\alpha\mathbf{D}_{k-1} + \mathbf{f}\mathbf{f}^\text{T})\mathbf{e}_i = \alpha\mathbf{D}_{k-1}\mathbf{e}_i + \mathbf{f}f_i = \alpha\mathbf{D}_{k-1}\mathbf{e}_i$ where \mathbf{e}_i is the i^{th} column of $M \times M$ identity matrix, \mathbf{I}_M .

ii) When $|f_i| = 1$ for some i , i.e. $f_j = 0$ for $j \neq i$ because $|\mathbf{f}| = 1$ and \mathbf{D}_{k-1} is semi-definite, the eigenvalues become $\alpha\tilde{d}_i = \alpha d_i + \rho$ and $\alpha\tilde{d}_j = \alpha d_j$ with all the corresponding j eigenvectors remain unchanged for $j \neq i$.

iii) When eigenvalues in \mathbf{D}_{k-1} have multiplicity $(M - r) \geq 2$, the vector \mathbf{f} can be reflected/rotated to give $M - r - 1$ zero components and hence by property i) $M - r - 1$ eigenvalues and eigenvectors remain unchanged.

The signal model in equation (4.13) represents a multiplicity of $M - r$ equal noise power spherical subspace eigenvalues, and by property iii) the vector γ can be rotated/reflected to form an vector $\eta = \mathbf{H}^T \gamma$ with $r + 1$ non-zero components and $M - r - 1$ zero components. The vector γ can then be grouped into two subspaces

$$\gamma = \begin{bmatrix} \gamma^{(s)} \\ \gamma^{(n)} \end{bmatrix} \quad (4.14)$$

where the $r \times 1$ vector $\gamma^{(s)}$ corresponds to the signal subspace of r independent received-signals and the vector $(M - r) \times 1$, $\gamma^{(n)}$, corresponds to the white noise subspace.

A noise subspace block Householder transformation $\mathbf{H}_{M-r}^{(n)}$ can be applied to reflect/rotate the multiple $M - r$ dimensional noise subspace components into a single component [13] [5] which can be defined as

$$\mathbf{H}_{M-r}^{(n)} = \mathbf{I}_{M-r} - 2 \frac{\mathbf{v}^{(n)}(\mathbf{v}^{(n)})^T}{(\mathbf{v}^{(n)})^T \mathbf{v}^{(n)}} \quad (4.15)$$

where

$$\mathbf{v}^{(n)} = \gamma^{(n)} + \text{sign}(\gamma_1^{(n)}) \|\gamma^{(n)}\| \mathbf{e}_1 \quad (4.16)$$

where \mathbf{e}_1 is the first column vector of an $(M - r) \times (M - r)$ identity matrix \mathbf{I}_{M-r} , $\gamma_1^{(n)}$ is the first component of $\gamma^{(n)}$, and $\mathbf{v}^{(n)} \in \mathcal{R}^{(M-r) \times 1}$. The Householder transformation is stable and by using the signum function $\text{sign}(\cdot)$ large errors are avoided in the factor $2/(\mathbf{v}^T \mathbf{v})$ when $\gamma^{(n)}$ is close to a multiple of \mathbf{e}_1 [13]. Note that the Householder transformation does not change the span of these subspaces and that the Householder transformation is computationally efficient and numerically stable [6] [13] [5].

A Householder transformation

$$\mathbf{H} = \begin{bmatrix} \mathbf{I}_r & \mathbf{0} \\ \mathbf{0} & \mathbf{H}_{M-r}^{(n)} \end{bmatrix} \quad (4.17)$$

deflates an $M \times M$ eigenproblem into an $(r + 1) \times (r + 1)$ eigenproblem, where $\mathbf{H}_{M-r}^{(n)}$ defined in Equation (4.15).

As to further reduce computation, when the signal subspace can be approximated by a multiplicity of r eigenvalues, an $M \times M$ eigenproblem can be deflated into a 2×2 noniterative closed-form eigenproblem [6]. This 2×2 closed-form eigendecomposition is obtained by averaging the eigenvalues of the signal subspace and applying the signal subspace block Householder transformation to the r components of $\gamma^{(s)}$ [6] [18].

After taking at least M snapshots at the antenna array output, the spherical subspaces of the signal eigenvalues and noise eigenvalues contained in diagonal matrix \mathbf{D}_{k-1} of the r signal subspace eigenvalues are replaced by $d^{(s)} = (d_1 + d_2 + \dots + d_r)/r$ and the $M - r$ noise subspace eigenvalues are replaced by $d^{(n)} = (d_{r+1} + d_{r+2} + \dots + d_M)/(M - r)$ where the rank of the signal subspace has to be less than the total number of antenna elements. The deflation operation can be expressed as

$$\alpha \mathbf{D}_{k-1} = \begin{bmatrix} d_1 & 0 & 0 & 0 \\ 0 & d_2 & 0 & 0 \\ 0 & 0 & \dots & 0 \\ 0 & 0 & 0 & d_M \end{bmatrix} \approx \alpha \begin{bmatrix} d^{(s)} \mathbf{I}_r & \mathbf{0} \\ \mathbf{0} & d^{(n)} \mathbf{I}_{M-r} \end{bmatrix} \quad (4.18)$$

It has been shown that sphericalizing a signal subspace can enhance the robustness of signal subspace eigenvector estimation especially at low SNR [6] [31]. When the signal power is close to the noise power, the signal array response vector can be lost in the noise subspace. By averaging the signal subspace eigenvalues, the ‘‘averaged’’ signal dimensions will be tracked as long as the signal subspace has higher eigenvalues/power than the noise subspace. This is the case since eigenvectors with closely spaced eigenvalues are more sensitive to perturbations than eigenvectors with well-separated eigenvalues.

In a manner analogous to the noise subspace, the signal subspace block Householder matrix is defined as [6]

$$\mathbf{H}_r^{(s)} = \mathbf{I}_r - 2 \frac{\mathbf{v}^{(s)}(\mathbf{v}^{(s)})^T}{(\mathbf{v}^{(s)})^T \mathbf{v}^{(s)}} \quad (4.19)$$

where \mathbf{I}_r is a $r \times r$ identity matrix, $\mathbf{v}^{(s)} \in \mathcal{R}^{r \times 1}$, and

$$\mathbf{v}^{(s)} = \gamma^{(s)} + \text{sign}(\gamma_r^{(s)}) \|\gamma^{(s)}\| \mathbf{e}_r \quad (4.20)$$

that \mathbf{e}_r is the r^{th} column vector of a $r \times r$ identity matrix and $\gamma_r^{(s)}$ is the r^{th} component of $\gamma^{(s)}$.

Equations (4.19) and (4.15) can then be combined to form a block Householder transformation

$$\mathbf{H} = \begin{bmatrix} \mathbf{H}_r^{(s)} & \mathbf{0} \\ \mathbf{0} & \mathbf{H}_{M-r}^{(n)} \end{bmatrix} \quad (4.21)$$

that deflates the $M \times M$ eigenproblem of equation (4.13) to a 2×2 closed-form eigenproblem. In fact, \mathbf{H} serves to concentrate all the power in the vector γ into two scalar components representing spherical signal and noise subspaces, respectively.

By substituting the block Householder deflation matrix into the rank-one eigenvalue matrix update [6],

$$\begin{aligned} \eta &= \mathbf{H}^T \gamma = \mathbf{H} \gamma \\ &= [0, \dots, 0, \eta_r, \eta_{r+1}, 0, \dots, 0]^T \\ &= [0, \dots, 0, \|\gamma^{(s)}\|, \|\gamma^{(n)}\|, 0, \dots, 0]^T \end{aligned} \quad (4.22)$$

where $\|\gamma^{(s)}\| = (\sum_{j=1}^r \gamma_j^2)^{\frac{1}{2}} = \eta_r$ and $\|\gamma^{(n)}\| = (\sum_{j=(r+1)}^n \gamma_j^2)^{\frac{1}{2}} = \eta_{r+1}$. The real-valued rank-one update eigenvalue matrix of equation (4.13) becomes

$$\begin{aligned} & \alpha \mathbf{D}_{k-1} + \gamma \gamma^T \\ &= \alpha \begin{bmatrix} d^{(s)} \mathbf{I}_r & \mathbf{0} \\ \mathbf{0} & d^{(s)} \mathbf{I}_{M-r} \end{bmatrix} + (1 - \alpha) \gamma \gamma^T \\ &= \begin{bmatrix} \mathbf{H}_r^{(s)} & \mathbf{0} \\ \mathbf{0} & \mathbf{H}_{M-r}^{(n)} \end{bmatrix} \left(\alpha \begin{bmatrix} d^{(s)} \mathbf{I}_r & \mathbf{0} \\ \mathbf{0} & d^{(n)} \mathbf{I}_{M-r} \end{bmatrix} + \eta \eta^T \right) \begin{bmatrix} \mathbf{H}_r^{(s)} & \mathbf{0} \\ \mathbf{0} & \mathbf{H}_{M-r}^{(n)} \end{bmatrix}^T \\ &= \mathbf{H} \begin{bmatrix} \alpha d^{(s)} \mathbf{I}_{r-1} & \mathbf{0} & \mathbf{0} & \mathbf{0} \\ \mathbf{0} & \alpha d^{(s)} + \eta_r^2 & \eta_r \eta_{r+1} & \mathbf{0} \\ \mathbf{0} & \eta_{r+1} \eta_r & \alpha d^{(n)} + \eta_{r+1}^2 & \mathbf{0} \\ \mathbf{0} & \mathbf{0} & \mathbf{0} & \alpha d^{(n)} \mathbf{I}_{M-r-1} \end{bmatrix} \mathbf{H}^T \end{aligned}$$

$$\begin{aligned}
&= \mathbf{H} \begin{bmatrix} \alpha d^{(s)} \mathbf{I}_{r-1} & \mathbf{0} & \mathbf{0} \\ \mathbf{0} & \mathbf{Q}_2 \begin{bmatrix} \lambda_1 & 0 \\ 0 & \lambda_2 \end{bmatrix} \mathbf{Q}_2^T & \mathbf{0} \\ \mathbf{0} & \mathbf{0} & \alpha d^{(n)} \mathbf{I}_{M-r-1} \end{bmatrix} \mathbf{H}^T \\
&= \mathbf{H} \begin{bmatrix} \mathbf{I}_{r-1} & \mathbf{0} & \mathbf{0} \\ \mathbf{0} & \mathbf{Q}_2 & \mathbf{0} \\ \mathbf{0} & \mathbf{0} & \mathbf{I}_{M-r-1} \end{bmatrix} \begin{bmatrix} \alpha d^{(s)} \mathbf{I}_{r-1} & \mathbf{0} & \mathbf{0} & \mathbf{0} \\ \mathbf{0} & \lambda_1 & \mathbf{0} & \mathbf{0} \\ \mathbf{0} & \mathbf{0} & \lambda_2 & \mathbf{0} \\ \mathbf{0} & \mathbf{0} & \mathbf{0} & \alpha d^{(n)} \mathbf{I}_{M-r-1} \end{bmatrix} \\
&\quad \begin{bmatrix} \mathbf{I}_{r-1} & \mathbf{0} & \mathbf{0} \\ \mathbf{0} & \mathbf{Q}_2 & \mathbf{0} \\ \mathbf{0} & \mathbf{0} & \mathbf{I}_{M-r-1} \end{bmatrix}^T \mathbf{H}^T \quad (4.23)
\end{aligned}$$

The whole problem is now deflated to a 2x2 eigenproblem

$$\alpha \mathbf{D}_{k-1}^{(2)} + \eta^{(2)} (\eta^{(2)})^T = \begin{bmatrix} \alpha d^{(s)} + \eta_r^2 & \eta_r \eta_{r+1} \\ \eta_{r+1} \eta_r & \alpha d^{(n)} + \eta_{r+1}^2 \end{bmatrix} = \mathbf{Q}_2 \begin{bmatrix} \lambda_1 & 0 \\ 0 & \lambda_2 \end{bmatrix} \mathbf{Q}_2^T \quad (4.24)$$

where $\eta^{(2)} = [\eta_r \eta_{r+1}]^T$,

$$\mathbf{D}_{k-1}^{(2)} = \begin{bmatrix} d^{(s)} & 0 \\ 0 & d^{(n)} \end{bmatrix} \quad (4.25)$$

the 2×2 eigenvectors matrix $\mathbf{Q}_2 = [\mathbf{q}_1 \mathbf{q}_2]$ and the corresponding two eigenvalues, λ_1 and λ_2 , can be solved for in closed-form.

The eigenvalues can be determined through the determinant of equation (4.24)

$$\begin{vmatrix} \alpha d^{(s)} + \eta_r^2 - \lambda_i & \eta_r \eta_{r+1} \\ \eta_{r+1} \eta_r & \alpha d^{(n)} + \eta_{r+1}^2 - \lambda_i \end{vmatrix} = 0 \quad (4.26)$$

which involves solving the characteristic equation for $i = 1, 2$

$$\lambda_i^2 - \left(\alpha (d^{(s)} + d^{(n)}) + \eta_r^2 + \eta_{r+1}^2 \right) \lambda_i + \alpha^2 d^{(s)} d^{(n)} + \alpha (d^{(s)} \eta_{r+1}^2 + d^{(n)} \eta_r^2) = 0 \quad (4.27)$$

Consequently, for $i = 1, 2$, the eigenvalues can be found in closed-form by

$$\lambda_i = \frac{-b \pm \sqrt{b^2 - 4ac}}{2a} \quad (4.28)$$

where $a = 1$, $b = \alpha(d^{(s)} + d^{(n)}) + \eta_r^2 + \eta_{r+1}^2$, and $c = \alpha^2 d^{(s)} d^{(n)} + \alpha(d^{(s)} \eta_{r+1}^2 + d^{(n)} \eta_r^2)$.

The eigendecomposition of the 2×2 matrix in equation (4.24) can be represented as

$$\left(\alpha \mathbf{D}_{k-1}^{(2)} + \eta^{(2)} (\eta^{(2)})^T \right) \mathbf{q}_i = \begin{bmatrix} \alpha d^{(s)} + \eta_r^2 & \eta_r \eta_{r+1} \\ \eta_{r+1} \eta_r & \alpha d^{(n)} + \eta_{r+1}^2 \end{bmatrix} \mathbf{q}_i = \lambda_i \mathbf{q}_i \quad (4.29)$$

for $i = 1, 2$. Equivalently,

$$\left(\alpha \mathbf{D}_{k-1}^{(2)} - \lambda_i \mathbf{I}_2 + \eta^{(2)} (\eta^{(2)})^T \right) \mathbf{q}_i = \left(\tilde{\mathbf{D}}_i + \eta^{(2)} (\eta^{(2)})^T \right) \mathbf{q}_i = 0 \quad (4.30)$$

where $\tilde{\mathbf{D}}_i = \alpha \mathbf{D}_{k-1}^{(2)} - \lambda_i \mathbf{I}_2$.

Theorem 5 in [3] states that for an invertible matrix $\mathbf{A} \in \mathcal{R}^{M \times M}$, $\mathbf{u} \in \mathcal{R}^{M \times 1}$, and an arbitrary scalar $\rho \neq 0$, given any vector $\mathbf{b} \in \mathcal{R}^{M \times 1}$ the following two equations are equivalent

$$\left(\mathbf{A} + \rho \mathbf{u} \mathbf{u}^T \right) \mathbf{q} = \mathbf{b} \quad (4.31)$$

and

$$\mathbf{q} = \mathbf{A}^{-1} \mathbf{b} - \kappa \mathbf{A}^{-1} \mathbf{u} \quad (4.32)$$

where κ is arbitrary scalar.

Therefore, setting $\mathbf{A} = \tilde{\mathbf{D}}_i$, $\rho = 1$, $\mathbf{u} = \eta^{(2)}$, $\mathbf{b} = \mathbf{0}$, and $\mathbf{q} = \mathbf{q}_i$, the orthonormal eigenvectors of equation (4.24) can be determined in closed-form for $i = 1, 2$ as

$$\begin{aligned} \mathbf{q}_i &= \frac{-\tilde{\mathbf{D}}_i^{-1} \eta^{(2)}}{|\tilde{\mathbf{D}}_i^{-1} \eta^{(2)}|} = \frac{-(\alpha \mathbf{D}_{k-1} - \lambda_i \mathbf{I}_2)^{-1} \eta}{|(\alpha \mathbf{D}_{k-1} - \lambda_i \mathbf{I}_2)^{-1} \eta|} \\ &= \frac{\left(\alpha \begin{bmatrix} d^{(s)} & 0 \\ 0 & d^{(n)} \end{bmatrix} - \lambda_i \mathbf{I}_2 \right)^{-1} \begin{bmatrix} \|\gamma^{(s)}\| \\ \|\gamma^{(n)}\| \end{bmatrix}}{\left| \left(\alpha \begin{bmatrix} d^{(s)} & 0 \\ 0 & d^{(n)} \end{bmatrix} - \lambda_i \mathbf{I}_2 \right)^{-1} \begin{bmatrix} \|\gamma^{(s)}\| \\ \|\gamma^{(n)}\| \end{bmatrix} \right|} \end{aligned} \quad (4.33)$$

The updated eigenvector matrix estimate $\hat{\mathbf{Q}}_k$ will then be

$$\hat{\mathbf{Q}}_k = [\mathbf{Q}_{k-1}^{(s)} \mathbf{G}^{(s)} \mathbf{H}^{(s)}, \mathbf{Q}_{k-1}^{(n)} \mathbf{G}^{(n)} \mathbf{H}^{(n)}] \begin{bmatrix} \mathbf{I}_{r-1} & \mathbf{0} & \mathbf{0} \\ \mathbf{0} & \mathbf{Q}_2 & \mathbf{0} \\ \mathbf{0} & \mathbf{0} & \mathbf{I}_{M-r-1} \end{bmatrix} \quad (4.34)$$

Note that because of the Householder transformation matrix property of rank-one modification of an identity matrix, the signal subspace Householder post-multiplication

$$\mathbf{Q}_{k-1}^{(s)} \mathbf{G}^{(s)} \mathbf{H}^{(s)} = \mathbf{Q}_{k-1}^{(s)} \mathbf{G}^{(s)} - \frac{2}{(\mathbf{v}^{(s)})^T \mathbf{v}^{(s)}} \left(\mathbf{Q}_{k-1}^{(s)} \mathbf{G}^{(s)} \mathbf{v}^{(s)} \right) (\mathbf{v}^{(s)})^T \quad (4.35)$$

requires only $8Mr + 2r + 1$ real-real multiplications (flops), where $\mathbf{Q}_{k-1}^{(s)}$ is an $M \times r$ complex matrix, $\mathbf{G}^{(s)}$ is the unitary transformation complex-valued diagonal matrix of $r \times r$, and $\mathbf{v}^{(s)}$ is the real-valued $r \times 1$ vector. Note that a "flop" represents a real-real multiplications throughtout this thesis. Arithmetic additions or subtractions are not included in the computation.

The noise subspace Householder post-multiplication is given by

$$\mathbf{Q}_{k-1}^{(n)} \mathbf{G}^{(n)} \mathbf{H}^{(n)} = \mathbf{Q}_{k-1}^{(n)} \mathbf{G}^{(n)} - \frac{2}{(\mathbf{v}^{(n)})^T \mathbf{v}^{(n)}} \left(\mathbf{Q}_{k-1}^{(n)} \mathbf{G}^{(n)} \mathbf{v}^{(n)} \right) (\mathbf{v}^{(n)})^T \quad (4.36)$$

with $\mathbf{Q}_{k-1}^{(n)}$ a $M \times (M - r)$ complex-valued matrix, $\mathbf{G}^{(n)}$ an unitary transformation $(M - r) \times (M - r)$ complex-valued diagonal matrix, $\mathbf{v}^{(n)}$ a $(M - r) \times 1$ real-valued vector, and $\mathbf{H}^{(n)}$ a real-valued $(M - r) \times (M - r)$ matrix. This update requires $8M(M - r) + 2(M - r) + 1$ flops.

Multiplying a complex valued $M \times M$ matrix \mathbf{A} as

$$\mathbf{A} \begin{bmatrix} \mathbf{I}_{r-1} & \mathbf{0} & \mathbf{0} \\ \mathbf{0} & \mathbf{Q}_2 & \mathbf{0} \\ \mathbf{0} & \mathbf{0} & \mathbf{I}_{M-r-1} \end{bmatrix} \quad (4.37)$$

requires $4M$ flops. Therefore, the total number of flops required to update the eigenvectors matrix, $\hat{\mathbf{Q}}_k$, is $8M^2 + 18M + 2$. Consequently, noniterative subspace tracking requires a computation of $\mathbf{O}(M^2)$.

To maintain subspace sphericity and avoid eigenvalue iteration, the signal and noise eigenvalues must be re-averaged before the next noniterative update can be accomplished. For $\lambda_1 > \lambda_2$, the next spherical eigenvalue subspace matrix \mathbf{D}_k is obtained by re-averaging the spherical signal subspace eigenvalue

$$d^{(s)} = \frac{\lambda_1 + (r - 1)d^{(s)}}{r} \quad (4.38)$$

and the spherical noise subspace eigenvalue

$$d^{(n)} = \frac{\lambda_2 + (M - r - 1)d^{(n)}}{M - r} \quad (4.39)$$

If re-averaging the eigenvalue subspace matrix is not performed before the next recursion, the rank-one eigenstructure update process reverts to an iterative one. This noniterative subspace update [6] has an ability to switch between noniterative subspace and iterative eigenstructure updates. This ability may allow for practical compromises in implementation if eigenvalues need to be calculated.

To further reduce computation, the smaller subspace may only be tracked [6], and the larger subspace is not computed. For a signal subspace of rank r , the computation reduces to $\mathbf{O}(Mr)$.

Noniterative tracking is generally much faster than iterative tracking and calculates the eigendecomposition of the covariance matrix without dependence on eigenvalue spread. The noniterative eigenvalue information is tracked only in an average sense and is a stable process because of the well-separated signal and noise subspaces.

4.3 Application of Noniterative subspace tracking to the CDMA System Model

We now apply the computationally efficient and numerically stable subspace tracking method discussed in Section 4.2 to adaptive array response estimation in a CDMA system [36].

First, a generic CDMA system model is considered to develop the conditions required for application of the subspace tracking method. Through the modelling and analysis in Section 4.4 which is verified later by computer simulations in Chapter 5, we demonstrate that the signal subspace eigenvector corresponding to the largest eigenvalue of the post-correlation autocorrelation matrix is an accurate estimate of the desired mobile's array response vector as long as the "code filtering" processing gain is high enough to separate the signal and noise subspace.

The NR1SSU algorithm and its application to IS-95 are described in Section 4.5 where a detailed computational analysis is provided. This NR1SSU algorithm has also been tested on a PN chip-level IS-95 CDMA simulator [8] and the simulation results are presented in Chapter 5.

4.4 DS-BPSK CDMA system model

First we consider a direct sequence binary phase-shift-keying (DS-BPSK) CDMA system model for cellular communications applications in which each user is assigned a distinct pseudo-noise (PN) code that modulates a binary phase shift keying (BPSK) modulated signal. A block diagram of this DS-BPSK is shown in Figure 3.2 of Chapter 3. Two system environments that perturb the transmitted signals before reception at the base-station antenna arrays will be considered. Section 4.4.1 presents the application of a NR1SSU to a flat slow fading propagation model that has a small multipath time delay spread where effectively only one path is received at the antenna array of each mobile's transmitted signal. The application is then generalized to a frequency selective slow fading propagation model in section 4.4.2, in which there are multiple echos of a transmitted signal received at the base-station antenna array. Each replica is attenuated with a different channel gain and phase shift since these replicas of the transmitted signal experience different propagation paths before reaching the base-station.

4.4.1 Case of zero multipath time delay spread propagation model

We consider a transmitted signal that propagates in a wireless communication channel with zero multipath time delay spread where only one path of a transmitted signal is received. This propagation channel is classified as a frequency-nonselective or flat fading channel as discussed in Chapter 3.

Similar to the DS-BPSK signal model of equation (3.7) in Chapter 3, the baseband

signal vector $\mathbf{x}_i(t)$ received at the M - element antenna array of the i^{th} branch of a DS-BPSK CDMA network is

$$\begin{aligned}
\mathbf{x}_i(t) &= [x_{i,1}(t), x_{i,2}(t), \dots, x_{i,M}(t)]^T \\
&= \sum_{j=1}^N \varrho_j(t) e^{j\omega_c \tau_{i,j}} A_j(t) c_j(t - \tau_{i,j}) b_j(t - \tau_{i,j}) \mathbf{a}_j(t) + \mathbf{n}(t) \\
&= \sum_{j=1}^N \sqrt{P_j(t)} c_j(t - \tau_{i,j}) b_j(t - \tau_{i,j}) \mathbf{a}_j(t) + \mathbf{n}(t)
\end{aligned} \tag{4.40}$$

where N is the total number of in-band mobiles, $c_j(t - \tau_{i,j}) \in \{1, -1\}$ represents the PN chips of the j^{th} mobile with a chip period of $T_c = 1/W_{ss}$, W_{ss} is the spread spectrum bandwidth, $b_j(t - \tau_{i,j}) \in \{1, -1\}$ is the j^{th} mobile's information bit sequence with information period $T_b = 1/B$, B is the information bit bandwidth, $|\tau_{i,j}| \in \mathcal{U}(0, T_c)$ is the uniformly distributed differential time delay of the j^{th} mobile relative to the i^{th} mobile, column vector $\mathbf{n}(t) = [n_1(t), \dots, n_M(t)]^T \sim \mathcal{N}(\mathbf{0}, \sigma_n^2 \mathbf{I})$ represents independent and identically distributed Gaussian thermal noise, M is the number of antenna elements in the base station array or sector, $P_j(t) = \varrho_j^2 A_j(t)^2$ is the total power received at the base station from the j^{th} mobile's DOA, $\mathbf{a}_j(t) = [a_1(\theta_j(t)), \dots, a_M(\theta_j(t))]^T \in \mathcal{C}^{M \times 1}$ is the time-varying array response of the j^{th} mobile, $\theta_j(t)$ is the time-varying DOA of the j^{th} mobile, and $[\cdot]^T$ denotes transpose of $[\cdot]$.

Without loss of generality, for all $i = 1, 2, \dots, N$ and $j = 1, 2, \dots, N$, we assume perfect self-synchronization to the i^{th} desired mobile at each i^{th} branch of the network, i.e., $\tau_{i,i} = 0$, and the signal $b_j(t - \tau_{i,j})$, chip $c_j(t - \tau_{i,j})$ and noise $\mathbf{n}(t)$ are mutually uncorrelated. The array response vectors $\mathbf{a}_j(t)$ are assumed to be unchanged over one information bit period T_b .

Under the above assumptions and the derivations in Appendix A, the pre-correlation vector $\mathbf{x}_i(t)$ of eqn.(4.40) is zero-mean and the pre-correlation covariance matrix is

$$\begin{aligned}
\mathbf{R}_{xx_i}(t) = \mathbf{E}\{\mathbf{x}_i(t)\mathbf{x}_i(t)^\dagger\} &= P_i(t)\mathbf{a}_i(t) * \mathbf{a}_i(t)^\dagger + \sum_{j=1, j \neq i}^N P_j(t)\mathbf{a}_j(t) * \mathbf{a}_j(t)^\dagger + \sigma_n^2 \mathbf{I} \\
&= P_i(t)\mathbf{a}_i(t) * \mathbf{a}_i(t)^\dagger + \mathbf{R}_{\text{IN}_i}(t)
\end{aligned} \tag{4.41}$$

where $\mathbf{R}_{\text{IN}_i}(t)$ denotes the interference-plus-noise covariance matrix, \mathbf{I} is the $M \times M$

identity matrix, $(\cdot)^\dagger$ denotes transpose conjugate. At information bit n , the i^{th} mobile's PN post-correlation vector, $\mathbf{z}_i(n)$ of $\mathbf{x}_i(t)$ over time interval T_b is

$$\begin{aligned}
\mathbf{z}_i(n) &= \sqrt{T_b} \varrho_i(t) A_i(t) b_i(n) \mathbf{a}_i(n) + \frac{1}{\sqrt{T_b}} \int_{nT_b}^{(n+1)T_b} \mathbf{n}(t) c_i(t) dt \\
&\quad + \sum_{j=1, j \neq i}^N \frac{1}{\sqrt{T_b}} \int_{nT_b}^{(n+1)T_b} \varrho_j(t) e^{j\omega_c \tau_{i,j}} A_j(t) b_j(t - \tau_{i,j}) c_j(t - \tau_{i,j}) c_i(t) \mathbf{a}_j(n) dt \\
&= \sqrt{T_b} \varrho_i(t) A_i(t) b_i(n) \mathbf{a}_i(n) + \frac{1}{\sqrt{T_b}} \int_{nT_b}^{(n+1)T_b} \mathbf{n}(t) c_i(t) dt \\
&\quad + \sum_{j=1, j \neq i}^N \frac{1}{\sqrt{T_b}} \int_{nT_b}^{(n+1)T_b} \varrho_j(t) e^{j\omega_c \tau_{i,j}} A_j(t) b_j(t - \tau_{i,j}) c_j(t - \tau_{i,j}) c_i(t) \mathbf{a}_j(n) dt \\
&= \sqrt{T_b} \varrho_i(t) A_i(t) b_i(n) \mathbf{a}_i(n) + MAI + \frac{1}{\sqrt{T_b}} \int_{nT_b}^{(n+1)T_b} \mathbf{n}(t) c_i(t) dt \tag{4.42}
\end{aligned}$$

where MAI stands for multiple-access interference from other users.

The i^{th} mobile's post-correlation autocovariance matrix can be defined as

$$\mathbf{R}_{\mathbf{z}_i}(n) \equiv \mathbf{E}\{\mathbf{z}_i(n) * \mathbf{z}_i(n)^\dagger\} \frac{1}{T_c} \tag{4.43}$$

where $L = T_b/T_c$ is the ‘‘code filtering’’ processing gain. Using results in [41] [19],

$$\frac{1}{T_b} \mathbf{E} \left[\int_0^{T_b} c_i(\tau) c_j(\tau - \tau_{i,j}) d\tau \right]^2 = \frac{2}{T_b} \left[\frac{T_b^2}{3L} - \frac{T_b^2}{12L^2} \right] \simeq \frac{2T_b}{3L} \tag{4.44}$$

After integration, eqn.(4.43) becomes, (see Appendix A)

$$\begin{aligned}
\mathbf{R}_{\mathbf{z}_i}(n) &= LP_i(n) \mathbf{a}_i(n) * \mathbf{a}_i(n)^\dagger + \frac{2}{3} \sum_{j=1, j \neq i}^N P_j(n) \mathbf{a}_j(n) * \mathbf{a}_j(n)^\dagger + \frac{\sigma_n^2}{T_c} \mathbf{I} \\
&= LP_i(n) \mathbf{a}_i(n) * \mathbf{a}_i(n)^\dagger + \frac{2}{3} \left(\sum_{j=1, j \neq i}^N P_j(n) \mathbf{a}_j(n) * \mathbf{a}_j(n)^\dagger + \sigma_n^2 \mathbf{I} \right) - \frac{2\sigma_n^2}{3} \mathbf{I} + \frac{\sigma_n^2}{T_c} \mathbf{I} \\
&= LP_i(n) \mathbf{a}_i(n) * \mathbf{a}_i(n)^\dagger + \frac{2}{3} \mathbf{R}_{\text{IN}_i}(n) + \left(\frac{3 - 2T_c}{3T_c} \right) \sigma_n^2 \mathbf{I} \tag{4.45}
\end{aligned}$$

where $P_j(n) = \varrho_j(t)^2 A_j(t)^2$ is the total received power of the j^{th} mobile.

If L is large enough, such that

$$\text{PEV} \left(LP_i(n) \mathbf{a}_i(n) * \mathbf{a}_i(n)^\dagger \right) \gg \text{PEV} \left(\frac{2}{3} \sum_{j=1, j \neq i}^N P_j(n) \mathbf{a}_j(n) * \mathbf{a}_j(n)^\dagger \right) \tag{4.46}$$

where $\text{PEV}(\cdot)$ represents the principal eigenvalue of matrix (\cdot) . We can consider eqn.(4.45) as a signal-plus-noise spherical subspace problem, with

$$\begin{aligned}\mathbf{R}_{zz_i}(n) &= LP_i(n)\mathbf{a}_i(n) * \mathbf{a}_i(n)^\dagger + \frac{2}{3} \sum_{j=1, j \neq i}^N P_j(n)\mathbf{a}_j(n) * \mathbf{a}_j(n)^\dagger + \frac{\sigma_n^2}{T_c} \mathbf{I} \\ &= \mathbf{R}_{ss_i}(n) + \hat{\mathbf{R}}_{nn}(n) \\ &= \lambda_s(n)\hat{\mathbf{a}}_i(n) * \hat{\mathbf{a}}_i(n)^\dagger + \sum_{m=2}^M \lambda_m(n)\mathbf{u}_m(n) * \mathbf{u}_m(n)^\dagger\end{aligned}\quad (4.47)$$

where $\lambda_s(n)$ is the i^{th} mobile's estimated channel attenuated despread signal amplitude, $\hat{\mathbf{a}}_i(n)$ is the estimated array response vector of the desired i^{th} mobile at time n , λ_m are the eigenvalues of $\mathbf{R}_{zz_i}(n)$ and $\mathbf{u}_m(n)$ are the corresponding eigenvectors for $m = 1, 2, \dots, M$ and $s = 1$ is the signal subspace. In eqn.(4.47), the signal covariance matrix is of rank one with

$$\mathbf{R}_{ss_i}(n) = LP_i(n)\mathbf{a}_i(n) * \mathbf{a}_i(n)^\dagger = \lambda_s(n)\hat{\mathbf{a}}_i(n) * \hat{\mathbf{a}}_i(n)^\dagger \quad (4.48)$$

and the multiple access interference-noise covariance matrix is

$$\hat{\mathbf{R}}_{nn_i}(n) = \frac{2}{3} \sum_{j=1, j \neq i}^N P_j(n)\mathbf{a}_j(n) * \mathbf{a}_j(n)^\dagger + \frac{\sigma_n^2}{T_c} \mathbf{I} \quad (4.49)$$

which is now approximately a spherical noise covariance matrix $\hat{\mathbf{R}}_{nn_i}(n)$ for large processing gain L .

Therefore subspace tracking can be employed successfully in a CDMA system when equation (4.46) is satisfied. That is the principal eigenvector $\hat{\mathbf{a}}_i(n)$ corresponding to the largest eigenvalue of $\mathbf{R}_{zz_i}(n)$ is an accurate signal subspace array response vector estimate when eqn.(4.46) holds. Simulations results presented in Chapter 5 verify this noniterative subspace tracking application.

From equation (4.47), the signal-to-interference-plus-noise ratio of the weighted post-correlation vector $\mathbf{w}_i(n)^\dagger \mathbf{z}_i(n)$ is

$$\begin{aligned}\text{SINR}_i &= \frac{\mathbf{w}_i(n)^\dagger \left(LP_i(n)\mathbf{a}_i(n) * \mathbf{a}_i(n)^\dagger \right) \mathbf{w}_i(n)}{\mathbf{w}_i(n)^\dagger \left(\frac{2}{3} \sum_{j=1, j \neq i}^N P_j(n)\mathbf{a}_j(n) * \mathbf{a}_j(n)^\dagger + \frac{\sigma_n^2}{T_c} \mathbf{I} \right) \mathbf{w}_i(n)} \\ &= \frac{\mathbf{w}_i(n)^\dagger \left(P_i(n)\mathbf{a}_i(n) * \mathbf{a}_i(n)^\dagger / B \right) \mathbf{w}_i(n)}{\mathbf{w}_i(n)^\dagger \left(\frac{2}{3W_{ss}} \sum_{j=1, j \neq i}^N P_j(n)\mathbf{a}_j(n) * \mathbf{a}_j(n)^\dagger + \sigma_n^2 \mathbf{I} \right) \mathbf{w}_i(n)}\end{aligned}$$

$$= \frac{\mathbf{w}_i(n)^\dagger \mathbf{R}_{ss_i}(n) \mathbf{w}_i(n)}{\mathbf{w}_i(n)^\dagger \hat{\mathbf{R}}_{nn_i}(n) \mathbf{w}_i(n)} \quad (4.50)$$

4.4.2 Case of non-zero multipath time delay spread propagation model

When the channel produces multiple replicas of a transmitted signal, each with different channel gain, the propagation channel model is classified as frequency-selective with non-zero multipath time delay spread. Frequency-selective fading channel occurs when the system signalling bandwidth W_{ss} is greater than the channel coherence bandwidth, i.e. $W_{ss} > B_m$ as discussed in Chapter 3. The frequency-selective fading propagation channel considered here assumed all multipaths received are resolvable [40] [29] with time resolution $T_c = 1/W_{ss}$. Therefore, the number of resolvable paths under this frequency-selective fading propagation model is $W_{ss}T_m \approx W_{ss}/B_m$ [29].

The received baseband pre-correlation signal of the i^{th} mobile's l^{th} path in a frequency selective propagation model having N transmitting in-band mobiles can be expressed as

$$\begin{aligned} \mathbf{x}_{i,l}(t) &= \sum_{j=1}^N \sum_{k=1}^{J_j} \varrho_{j,k}(t) e^{j\omega_c \tau_{il,jk}} A_{j,k}(t) c_{j,k}(t - \tau_{il,jk}) b_{j,k}(t - \tau_{il,jk}) \mathbf{a}_{j,k}(t) + \mathbf{n}(t) \\ &= \varrho_{i,l}(t) A_{i,l}(t) c_{i,l}(t) b_{i,l}(t) \mathbf{a}_{i,l}(t) + \mathbf{n}(t) \\ &\quad + \sum_{k=1, k \neq l}^{J_i} \varrho_{j,k}(t) e^{j\omega_c \tau_{il,jk}} A_{j,k}(t) c_{j,k}(t - \tau_{il,jk}) b_{j,k}(t - \tau_{il,jk}) \mathbf{a}_{j,k}(t) \\ &\quad + \sum_{j=1, j \neq i}^N \sum_{k=1}^{J_j} \varrho_{j,k}(t) e^{j\omega_c \tau_{il,jk}} A_{j,k}(t) c_{j,k}(t - \tau_{il,jk}) b_{j,k}(t - \tau_{il,jk}) \mathbf{a}_{j,k}(t) \end{aligned} \quad (4.51)$$

for $j = 1, 2, \dots, N$ and $k = 1, 2, \dots, J_j$ where J_j is the total number of resolvable multipaths of the j^{th} mobile received at the base station, $\tau_{il,jk}$ is the differential time delay of the j^{th} mobile's k^{th} multipath relative to the i^{th} mobile's l^{th} path with self-synchronization $\tau_{il,il} = 0$, $\varrho_{j,k}(t)$ is the channel attenuation factor of the j^{th} mobile's k^{th} path, $\omega_c \tau_{il,jk}$ is the channel phase shift of the j^{th} mobile's k^{th} multipath, $c_{j,k}(t)$ is the j^{th} mobile's k^{th} multipath's PN sequence of period T_c second, $b_{j,k}(t)$ is the j^{th} mobile's k^{th} multipath's information bit of duration T_b , $\mathbf{n}(t) = [n_1(t), n_2(t), \dots, n_M(t)]^T \sim$

$\mathcal{N}(\mathbf{0}, \sigma_n^2 \mathbf{I})$ is the independent identically distributed Gaussian thermal noise, and $\mathbf{a}_{j,k}(t) = [a_1(t), a_2(t), \dots, a_M(t)]^T$ is the time-varying array response vector which may be more appropriately called the time-varying channel vector.

Again without loss of generality, for all $i = 1, 2, \dots, N$, $j = 1, 2, \dots, N$, multipath $k = 1, 2, \dots, J_j$ from the j^{th} mobile, and multipath index $p = 1, 2, \dots, J_j$ from the j^{th} mobile, the signal information bit $b_{j,k}(t - \tau_{il,jk}(t))$, chip $c_{j,k}(t - \tau_{il,jk}(t))$ and noise vector $\mathbf{n}(t)$ are mutually uncorrelated. For mobile m not equal mobile j , i.e. $m \neq j$, information bits $b_{j,k}(t - \tau_{il,jk}(t))$ and $b_{m,p}(t - \tau_{il,mp}(t))$ are assumed uncorrelated as well as $c_{j,k}(t - \tau_{il,jk}(t))$ and $c_{m,p}(t - \tau_{il,mp}(t))$ for all $m = 1, 2, \dots, N$. The array response vectors $\mathbf{a}_{j,k}(t)$ are assumed to be unchanged over one information bit period T_b .

At information bit n , the post-correlation signal is then

$$\begin{aligned}
\mathbf{z}_{i,l}(n) &= \int_{nT_b}^{(n+1)T_b} \varrho_{i,l}(t) A_{i,l}(t) c_{i,l}(t) b_{i,l}(t) \mathbf{a}_{i,l}(t) c_{i,l}(t) dt + \int_{nT_b}^{(n+1)T_b} \mathbf{n}(t) c_{i,l}(t) dt \\
&+ \int_{nT_b}^{(n+1)T_b} \sum_{k=1, k \neq l}^{J_i} \varrho_{j,k}(t) e^{j\omega_c \tau_{il,jk}} A_{j,k}(t) c_{j,k}(t - \tau_{il,jk}) b_{j,k}(t - \tau_{il,jk}) \mathbf{a}_{j,k}(t) c_{i,j}(t) dt \\
&+ \int_{nT_b}^{(n+1)T_b} \sum_{j=1, j \neq i}^N \sum_{k=1}^{J_j} \varrho_{j,k}(t) e^{j\omega_c \tau_{il,jk}} A_{j,k}(t) c_{j,k}(t - \tau_{il,jk}) b_{j,k}(t - \tau_{il,jk}) \mathbf{a}_{j,k}(t) c_{i,j}(t) dt \\
&= \sqrt{T_b} \varrho_{i,l}(t) A_{i,l}(t) b_{i,l}(t) \mathbf{a}_{i,l}(t) + SI + MAI + \int_{nT_b}^{(n+1)T_b} \mathbf{n}(t) c_{i,l}(t) dt \quad (4.52)
\end{aligned}$$

where the SI term represents self-interference of the i^{th} mobile's l path and the MAI term represents multiple access interference from other users.

Referring to the detailed derivation in Appendix B, the pre-correlation covariance matrix with J_j resolvable multipaths for the j^{th} mobile can be generalized from (4.41) to

$$\begin{aligned}
\mathbf{R}_{\text{xx},i,l}(t) &= \sum_{j=1}^N \sum_{k=1}^{J_j} P_{j,k}(t) \mathbf{a}_{j,k}(t) * \mathbf{a}_{i,k}(t)^\dagger + \sigma_n^2 \mathbf{I} \\
&= P_{i,l}(n) \mathbf{a}_{i,l}(n) * \mathbf{a}_{i,l}(n)^\dagger + \mathbf{R}_{\text{IN},i,l}(n) \quad (4.53)
\end{aligned}$$

where $P_{j,k}(n) = \varrho_{j,k}(t)^2 A_{j,k}(t)^2$ is the total received power of the j^{th} mobile's k^{th} path and assumed to be unchanged over an information bit period T_b , i.e. slow fading.

And the post-correlation covariance matrix is generalized from (4.45) to

$$\begin{aligned} \mathbf{R}_{zz_{i,l}}(n) &= LP_{i,l}(n)\mathbf{a}_{i,l}(n) * \mathbf{a}_{i,l}(n)^\dagger + \frac{2}{3} \sum_{k=1, k \neq l}^{J_i} P_{i,k}(n)\mathbf{a}_{i,k}(n) * \mathbf{a}_{i,k}(n)^\dagger \\ &\quad + \frac{2}{3} \sum_{j=1, j \neq i}^N \sum_{k=1}^{J_j} P_{j,k}(n)\mathbf{a}_{j,k}(n) * \mathbf{a}_{j,k}(n)^\dagger + \frac{\sigma_n^2}{T_c} \mathbf{I} \end{aligned} \quad (4.54)$$

where the power of the time-delayed multipath signal is determined by the delay power profile of the channel.

Again, if L is large enough that

$$\begin{aligned} \text{PEV} \left(LP_{i,l}(n)\mathbf{a}_{i,l}(n) * \mathbf{a}_{i,l}(n)^\dagger \right) &\gg \text{PEV} \left(\frac{2}{3} \sum_{k=1, k \neq l}^{J_i} P_{i,k}(n)\mathbf{a}_{i,k}(n) * \mathbf{a}_{i,k}(n)^\dagger \right. \\ &\quad \left. + \frac{2}{3} \sum_{j=1, j \neq i}^N \sum_{k=1}^{J_j} P_{j,k}(n)\mathbf{a}_{j,k}(n) * \mathbf{a}_{j,k}(n)^\dagger \right) \end{aligned} \quad (4.55)$$

then eqn.(4.54) can again be considered as a signal plus noise subspace problem and the noniterative spherical subspace tracking can be applied to estimate the array response vector for the post-correlation covariance matrix

$$\begin{aligned} \mathbf{R}_{zz_{i,l}}(n) &= \mathbf{R}_{ss_{i,l}}(n) + \hat{\mathbf{R}}_{nn_{i,l}}(n) \\ &= LP_{i,l}(n)\mathbf{a}_{i,l}(n) * \mathbf{a}_{i,l}(n)^\dagger + \frac{2}{3} \mathbf{R}_{IN_{i,l}}(n) + \left(\frac{3 - 2T_c}{3T_c} \right) \sigma_n^2 \mathbf{I} \\ &= \lambda_{i,l}(n)\hat{\mathbf{a}}_{i,l}(n) * \hat{\mathbf{a}}_{i,l}(n)^\dagger + \sum_{m=2}^M \lambda_m(n)\mathbf{u}_m(n) * \mathbf{u}_m(n)^\dagger \end{aligned} \quad (4.56)$$

where the rank of $\mathbf{R}_{ss_{i,l}}(n)$ is one and the eigenvector $\hat{\mathbf{a}}_{i,l}(n)$ corresponding to the largest eigenvalue of $\mathbf{R}_{zz_{i,l}}(n)$ in eqn.(4.56) is again an accurate array response estimate of one of the resolvable multipath DOA's of the i^{th} mobile as long as L is large enough such that eqn.(4.55) holds.

The weighted signal-to-interference-plus-noise ratio for non-zero time spread multipath case is then

$$\begin{aligned} \text{SINR}_{i,l} &= \frac{\mathbf{w}_{i,l}(n) \left(LP_{i,l}(n)\mathbf{a}_{i,l}(n) * \mathbf{a}_{i,l}(n)^\dagger \right) \mathbf{w}_{i,l}(n)}{\mathbf{w}_{i,l}(n)^\dagger \hat{\mathbf{R}}_{nn_{i,l}}(n) \mathbf{w}_{i,l}(n)} \\ &= \frac{\mathbf{w}_{i,l}(n)^\dagger \mathbf{R}_{ss_{i,l}}(n) \mathbf{w}_{i,l}(n)}{\mathbf{w}_{i,l}(n)^\dagger \hat{\mathbf{R}}_{nn_{i,l}}(n) \mathbf{w}_{i,l}(n)} \end{aligned} \quad (4.57)$$

where

$$\begin{aligned} \hat{\mathbf{R}}_{nn_i,l}(n) &= \frac{2}{3} \sum_{k=1, k \neq l}^{J_i} P_{i,k}(n) \mathbf{a}_{i,k}(n) * \mathbf{a}_{i,k}(n)^\dagger \\ &+ \frac{2}{3} \sum_{j=1, j \neq i}^N \sum_{k=1}^{J_j} P_{j,k}(n) \mathbf{a}_{j,k}(n) * \mathbf{a}_{j,k}(n)^\dagger + \frac{\sigma_n^2}{T_c} \mathbf{I} \end{aligned} \quad (4.58)$$

Experiments conducted in metropolitan Ottawa [45] have shown that the first three multipaths received of a transmitted signal capture at least 80% of the delay power profile. Also, experiments measured in metropolitan Toronto [4] show that with a power control scheme at a bandwidth of 1.25 MHz, a three-arm (artificial multipath) RAKE receiver performs at most 1.8 dB worse than an all-path RAKE receiver. Therefore, in the case of either using a 2D-RAKE receiver or a diversity RAKE receiver, a 3-arm RAKE receiver will be assumed to sufficiently combat multipath fading. In addition, these delay spread measurement experiments provide us with important information of the application of noniterative subspace tracking. That is, it gives an approximate upper bound of the number of multipaths that increase either the self multipath interference or the multiple access interference.

4.4.3 Interference-plus-noise matrix inverse estimation

From eqns.(4.41) and (4.45) or eqns.(4.53) and (4.56), $\mathbf{R}_{IN_i}(n)^{-1}$ or $\mathbf{R}_{IN_i,l}(n)^{-1}$ can be estimated from their respective pre- and post-correlation matrices for both zero and non-zero multipath time spreads:

$$\hat{\mathbf{R}}_{IN_i}^{-1}(n) = \left[\frac{3L}{3L-2} \left(\mathbf{R}_{xx_i}(n) - \frac{\mathbf{R}_{zz_i}(n)}{L} \right) + \left(\frac{3-2T_c}{3T_b-2T_c} \right) \sigma_n^2 \mathbf{I} \right]^{-1} \quad (4.59)$$

which is computationally very expensive. The matrix subtraction in eqn.(4.59) also poses numerical problems. From eqns.(4.47) and (4.56), we propose an alternative method to estimate the inverse of $\mathbf{R}_{IN_i}(n)$ by

$$\hat{\mathbf{R}}_{IN_i}^{-1}(n) = \sum_{m=1}^M \frac{\mathbf{u}_m(n) * \mathbf{u}_m(n)^\dagger}{\frac{3}{2}(\bar{\lambda}_m(n) - \frac{(3-2T_c)\sigma_n^2}{3T_c})} \quad (4.60)$$

where $\bar{\lambda}_1 = 0$ and $\bar{\lambda}_m = \lambda_m$ for $m = 2, 3, \dots, M$. This eliminates the batch processing and dramatically reduces the adaptive beamforming weight computation. However,

accurate eigenvalues estimates will be needed since a small error in λ_m will generate a large error in $\hat{\mathbf{R}}_{\text{IN}_i}^{-1}(n)$. There is a trade-off between computation efficiency and optimum SINR spatial filtering for the beamforming adaptation algorithm. We may even choose $\mathbf{w}_i(\mathbf{k}) = \mathbf{a}_i(\mathbf{k})$, since in practice, the number of samples are limited, and the inverse of the interference-noise covariance matrix cannot accurately be estimated. We instead propose to update the weight vector with an optimum SNR criterion instead of an optimum SINR criterion (a suboptimal solution for the weighting vector).

4.5 DS-QPSK CDMA system model

Recall from Chapter 3 that IS-95 CDMA system is a North American second generation CDMA cellular communications standard. IS-95 uses direct-sequence quadrature phase shift keying (DS-QPSK) where the uplink mobile transmitted signal modulation is summarized in the block diagram as shown in Figure 4.1.

The DS-QPSK received signal for the i^{th} mobile demodulator at the antenna array is expressed in

$$\mathbf{r}_i(t) = \mathbf{x}_i^I(t) \cos(\omega_c t) + \mathbf{x}_i^Q(t) \sin(\omega_c t) \quad (4.61)$$

where $\mathbf{x}_i^I(t)$ is the in-phase received baseband signal and $\mathbf{x}_i^Q(t)$ is the quadrature-phase received baseband signal. A base-station receiver structure for the i^{th} mobile is presented in the block diagram in Figure 4.2.

The digital beamformed received-signals of the in-phase $y_i^I(n)$ and quadrature-phase $y_i^Q(n)$ can be expressed, respectively, as

$$y_i^I(n) = \mathbf{w}_i^I(n)^\dagger \mathbf{z}_i^I(n) \quad (4.62)$$

and

$$y_i^Q(n) = \mathbf{w}_i^Q(n)^\dagger \mathbf{z}_i^Q(n) \quad (4.63)$$

where $\mathbf{w}_i^I(n) = [w_i^{I1}(n), w_i^{I2}(n), \dots, w_i^{IM}(n)]^T$ is the in-phase weight vector, $\mathbf{w}_i^Q(n) = [w_i^{Q1}(n), w_i^{Q2}(n), \dots, w_i^{QM}(n)]^T$ is the quadrature-phase weight vector, $\mathbf{z}_i^I(n)$ is the in-phase and $\mathbf{z}_i^Q(n)$ is the quadrature-phase discrete post-correlation signal after short

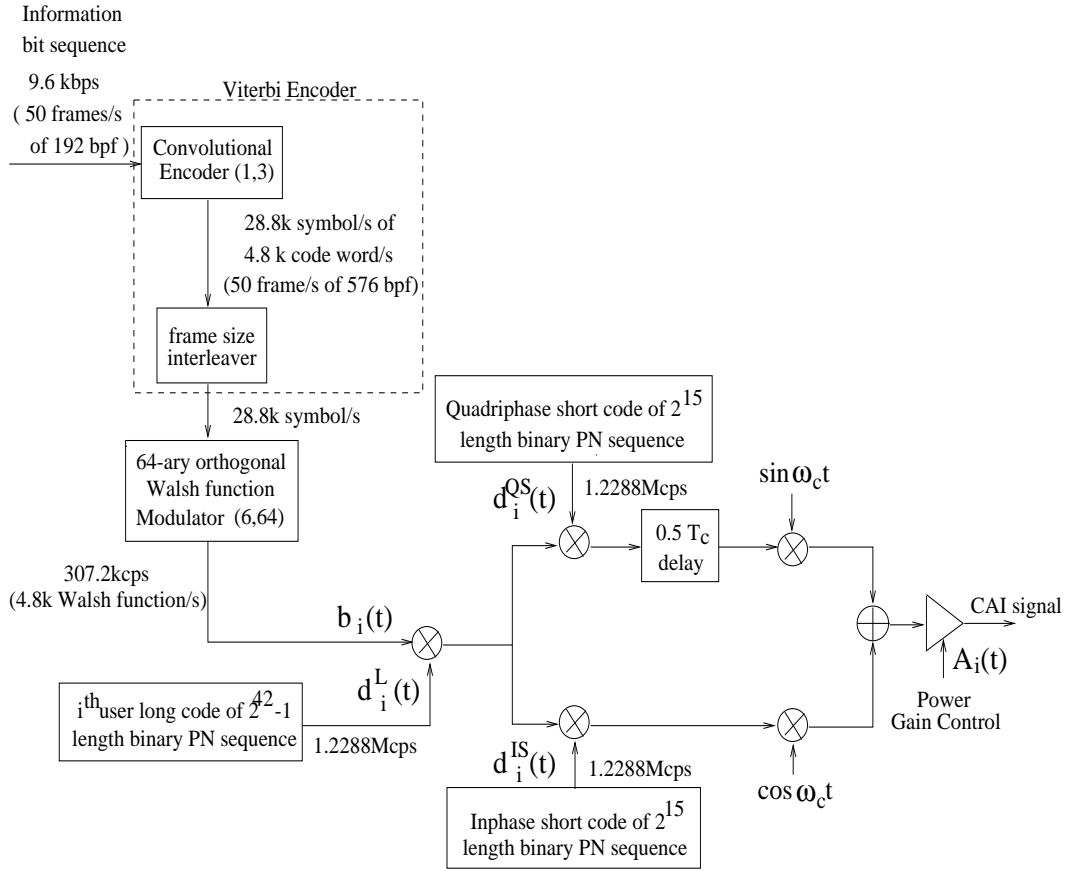


Figure 4.1: IS-95 reverse link mobile modulated signal

and long code correlation with a code-filtering processing gain of four. Again the algorithm controlling the weights that adaptively and optimally combines the signals received from each antenna elements determines the possible available cell-capacity.

Considering a zero delay spread propagation model with N in-band transmitting mobiles, the received in-phase baseband pre-correlation vector for the i^{th} mobile can be expressed as

$$\begin{aligned}
 \mathbf{x}_i^I(t) &= [x_i^{I1}(t), x_i^{I2}(t), \dots, x_i^{IM}(t)]^T \\
 &= \sum_{j=1}^N \varrho_j(t) e^{j\omega_c \tau_{i,j}} A_j(t) c_j^I(t - \tau_{i,j}) b_j(t - \tau_{i,j}) \mathbf{a}_j(t) + \mathbf{n}^I(t) \\
 &= \sum_{j=1}^N \varrho_j(t) e^{j\omega_c \tau_{i,j}} A_j(t) d_j^{IS}(t - \tau_{i,j}) d_j^L(t - \tau_{i,j}) b_j(t - \tau_{i,j}) \mathbf{a}_j(t) + \mathbf{n}^I(t)
 \end{aligned}$$

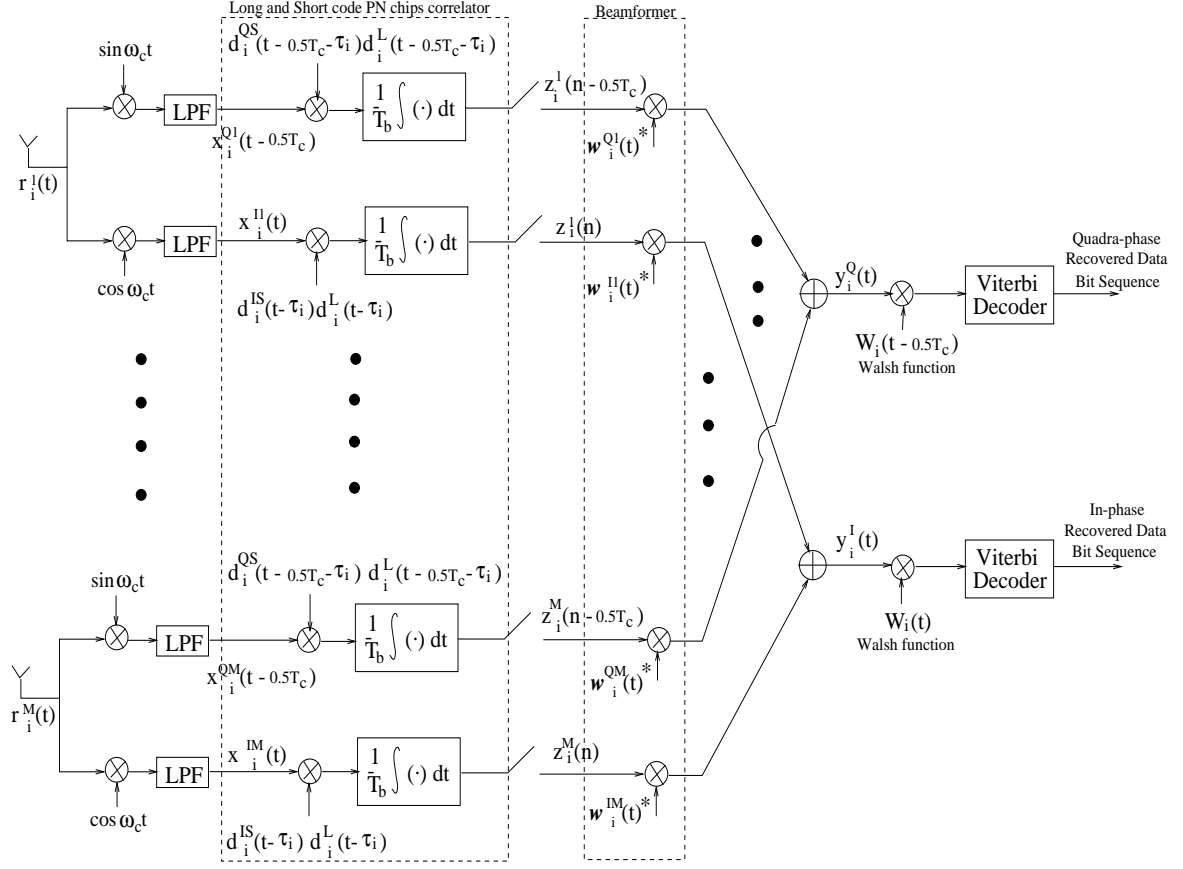


Figure 4.2: IS-95 CDMA base-station M-antenna array i^{th} mobile receiver model

$$= \sum_{j=1}^N \sqrt{P_j(t)} c_j^I(t - \tau_{i,j}) b_j(t - \tau_{i,j}) \mathbf{a}_j(t) + \mathbf{n}^I(t) \quad (4.64)$$

which is the same as the DS-BPSK in equation (4.40) but with Walsh function modulated information sequence $b_j(t)$ and the PN sequence $c_j^I(t - \tau_{i,j})$ now being the product of the j^{th} mobile's in-phase short code $d_j^{IS}(t - \tau_{i,j})$ and the long code $d_j^L(t - \tau_{i,j})$ PN sequences, $\tau_{i,j}$ is the time delay (channel phase shift) of the j^{th} mobile relative to the i^{th} mobile, $\rho_j(t)$ is the channel attenuation, $A_j(t)$ is the j^{th} mobile's transmitted signal amplitude, $\mathbf{a}_j(t)$ is the signal array response vector of the j^{th} mobile, $b_j(t)$ is the orthogonal Walsh function encoded information bit sequence and $\mathbf{n}^I(t)$ is the in-phase received signal additive white Gaussian noise array response vector.

Similarly, the received quadrature-phase baseband pre-correlation vector can be

expressed as

$$\begin{aligned}
& \mathbf{x}_i^Q(t) \\
&= [x_i^{Q1}(t), x_i^{Q2}(t), \dots, x_i^{QM}(t)]^T \\
&= \sum_{j=1}^N \varrho_j(t) e^{j\omega_c \tau_{i,j}} A_j(t) c_j^Q(t - \tau_{i,j}) b_j(t - T_c/2 - \tau_{i,j}) \mathbf{a}_j(t) + \mathbf{n}^Q(t) \\
&= \sum_{j=1}^N \sqrt{P_j(t)} d_j^{\text{QS}}(t - T_c/2 - \tau_{i,j}) d_j^{\text{L}}(t - T_c/2 - \tau_{i,j}) b_j(t - T_c/2 - \tau_{i,j}) \mathbf{a}_j(t) \\
&\quad + \mathbf{n}^Q(t) \\
&= \sum_{j=1}^N \sqrt{P_j(t)} c_j^Q(t - \tau_{i,j}) b_j(t - T_c/2 - \tau_{i,j}) \mathbf{a}_j(t) + \mathbf{n}^Q(t) \tag{4.65}
\end{aligned}$$

which again is the same as the DS-BPSK in equation (4.40) and the in-phase received signal of equation (4.64) but with a quadrature phase shifted Walsh function information sequence $b_j(t - T_c/2 - \tau_{i,j})$ and the PN sequence $c_j^Q(t - T_c/2 - \tau_{i,j})$ of the j^{th} mobile's quadrature-phase short code $d_j^{\text{QS}}(t - T_c/2 - \tau_{i,j})$ and the long code $d_j^{\text{L}}(t - T_c/2 - \tau_{i,j})$ PN sequences product, and $\mathbf{n}^Q(t)$ is the quadrature-phase received signal additive white Gaussian noise array response vector.

Therefore the in-phase $\mathbf{z}_i^I(t)$ and quadrature-phase $\mathbf{z}_i^Q(t)$ post-correlation vector can be expressed by equation (4.42) with the PN sequence $c_i(t)$ and the AWGN $\mathbf{n}(t)$ modified as follows. For the in-phase post-correlation vector, the PN sequence is replaced by

$$c_i(t) = c_i^I(t) = d_j^{\text{IS}}(t - \tau_{i,j}) d_j^{\text{L}}(t - \tau_{i,j}) \tag{4.66}$$

and the AWGN is now the in-phase part

$$\mathbf{n}(t) = \mathbf{n}^I(t) \tag{4.67}$$

For the quadrature-phase post-correlation vector, the PN sequence is replaced by

$$c_i(t) = c_i^Q(t - T_c/2) = d_j^{\text{QS}}(t - T_c/2 - \tau_{i,j}) d_j^{\text{L}}(t - T_c/2 - \tau_{i,j}) \tag{4.68}$$

and the AWGN is now the quadrature-phase part

$$\mathbf{n}(t) = \mathbf{n}^Q(t) \tag{4.69}$$

As presented above, the IS-95 in-phase and quadrature-phase DS-QPSK can be considered with the DS-BPSK on each in-phase and quadrature-phase demodulated signal as shown in section 4.3. Most importantly the NR1SSU algorithm can be applied to each of the in-phase and quadrature-phase channels independently to achieve more reliable estimation under either a zero or non-zero multipath time delay spread propagation models.

4.5.1 NR1SSU for IS-95

We remark that the conventional IS-95 CDMA system only gives a PN chip spreading gain of $L = 4$ [30], which is insufficient for equations (4.46) and (4.55) to be satisfied. However, this problem may be overcome by feeding back the Walsh function correlation vector $\mathbf{v}_i(r)$ [9] [7]. As shown in Figure 4.3, regenerating the Walsh functions from the recovered information bits and then correlating with the PN chip post-correlated vector will yield a total code-filtering gain of 192.75 instead of 4. In [9] [7] it is shown that with an estimation delay of one frame (20 ms) the feedback Walsh function covariance matrix $\mathbf{R}_{\mathbf{v}_i}$ will increase the spatial processing gain L to nearly 200. Indeed, [9] [7] shows that

$$\begin{aligned} \frac{1}{T_c^2} R_{v_i}(k) &= \left(\frac{1}{4} N_w^2 N_F^2 + \frac{1}{4} N_w N_F \right) P_i(k) \mathbf{a}_i(k) * \mathbf{a}_i(k)^\dagger \\ &+ \frac{1}{3} N_w N_F \sum_{j=1, j \neq i}^N P_j(k) \mathbf{a}_j(k) * \mathbf{a}_j(k)^\dagger + \frac{1}{2T_c} N_w N_F \sigma_n^2 \mathbf{I} \quad (4.70) \end{aligned}$$

and $L \approx (\frac{1}{4} N_w^2 N_F^2 + \frac{1}{4} N_w N_F) / (\frac{1}{3} N_w N_F) = \frac{3}{4} (N_w N_F + 1) = 192.75$, in which $N_w = 4$ is the number of PN chips in one Walsh chip, $N_F = 64$ is number of Walsh chips in one Walsh function [9] [7]. The NR1SSU algorithm that uses the feedback Walsh function post-correlation (FWFPC) vector is summarized in the block diagram Figure 1.

Instead of employing batch covariance matrix processing [25], we employed a rank-one eigendecomposition model as described in Section 4.2 which adaptively updates the time-varying data covariance matrix [6] [25] that allows for modelling of the motion of mobiles. By using the FWFPC vector as the FWFPC covariance matrix

estimate update, the FWFPC covariance matrix can be estimated by the recursive exponentially weighted covariance matrix as

$$\begin{aligned}
\mathbf{R}_{\mathbf{v}\mathbf{v}_i}(\mathbf{k}) &= \alpha_v \mathbf{R}_{\mathbf{v}\mathbf{v}_i}(\mathbf{k}-1) + (1-\alpha_v) \mathbf{v}_i(r) * \mathbf{v}_i(r)^\dagger \\
&= \alpha_v \hat{\mathbf{Q}}(\mathbf{k}-1) \hat{\mathbf{D}}(\mathbf{k}-1) \hat{\mathbf{Q}}(\mathbf{k}-1)^\mathbf{T} + (1-\alpha_v) \hat{\mathbf{Q}}(\mathbf{k}-1) \mathbf{g} * \mathbf{g}^\dagger \hat{\mathbf{Q}}(\mathbf{k}-1)^\mathbf{T} \\
&= \hat{\mathbf{Q}}(\mathbf{k}-1) \mathbf{G} \mathbf{H} \mathbf{H}^\dagger (\alpha_v \hat{\mathbf{D}}(\mathbf{k}-1) + \mathbf{f} * \mathbf{f}^\dagger) \mathbf{H} (\mathbf{H}^\dagger \mathbf{G}^\dagger \hat{\mathbf{Q}}(\mathbf{k}-1)^\mathbf{T}) \\
&= \hat{\mathbf{Q}}(\mathbf{k}-1) \mathbf{G} \mathbf{H} \begin{bmatrix} \alpha_v d^{(s)} \mathbf{I}_{p-1} & \mathbf{0} & \mathbf{0} \\ \mathbf{0} & \mathbf{Q}^{(2)} \begin{bmatrix} \lambda_s & 0 \\ 0 & \lambda_n \end{bmatrix} \mathbf{Q}^{(2)\dagger} & \mathbf{0} \\ \mathbf{0} & \mathbf{0} & \alpha_v d^{(n)} \mathbf{I}_{M-p-1} \end{bmatrix} \\
&\quad \mathbf{H}^\dagger \mathbf{G}^\dagger \hat{\mathbf{Q}}(\mathbf{k}-1)^\mathbf{T}
\end{aligned}$$

where $\mathbf{Q}^{(2)} = [q_1, q_2]$ is the 2x2 eigenvector matrix and $0 \leq \alpha_v \leq 1$ is a memory factor used to deemphasize old data, $\mathbf{g} = \hat{\mathbf{Q}}(\mathbf{k}-1)^\mathbf{T} \mathbf{v}_i(r)$, $\mathbf{f} = \mathbf{G}^\dagger \mathbf{g}$, \mathbf{H} is the block Householder transformation matrix which deflates the MxM eigen-problem into a noniterative 2x2 quadratic eigenproblem as well as stabilizes the subspace tracking [6], and $\mathbf{G} = \text{diag}(\frac{g_1}{|g_1|}, \frac{g_2}{|g_2|}, \dots, \frac{g_M}{|g_M|})$ is the unitary transformation matrix.

The application of the NR1SSU algorithm to the IS-95 CDMA system is summarized in Tables 1 and 2 and the block diagram representation is shown in Figure 1. In Table 1, only the initialization phase at update time $\mathbf{k} = 0$ needs covariance matrix batch processing to generate the eigenstructure. From time $\mathbf{k} = 1$ onwards, no batch processing covariance matrix calculation is necessary. The NR1SSU algorithm is presented in Table 2.

Note that in step 11, we may further reduce computation by updating only one of the noise eigenvectors [3] [6], however simulation results show that this would lead to an inaccurate array response estimate due to the fact that the noise subspace is not perfectly spherical.

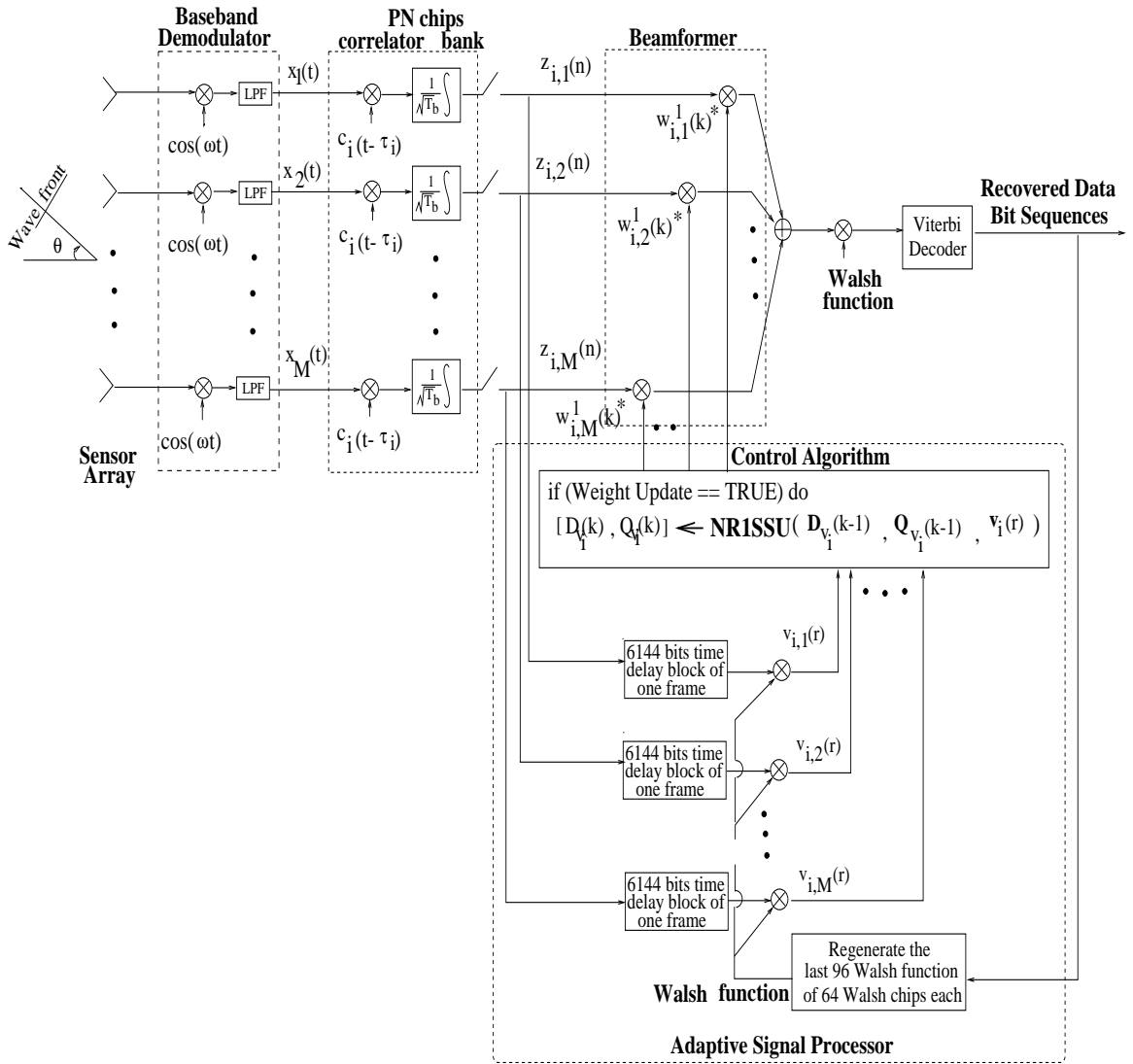


Figure 4.3: for tracking the i^{th} mobile's in phase branch (i^{th} in phase branch) of the network

For the i^{th} mobile of the CDMA network

- Initialization phase {1st frame of a new call},
 - 1 $k \leftarrow 0$ {weight update index}
 - 2 $[\mathbf{w}_i^1(k), \mathbf{w}_i^2(k), \dots, \mathbf{w}_i^p(k)] \leftarrow$ all ones
 - 3 $\mathbf{R}_{\mathbf{v}\mathbf{v}_i}(0) \leftarrow 0$
 - 4 **for** $r = 1$ to $r = 96$ {Walsh function index of 1 frame}
 - 5 **do** $\alpha_v \leftarrow \frac{r-1}{r}$
 - 6 $\mathbf{R}_{\mathbf{v}\mathbf{v}_i}(r) \leftarrow \alpha_v \mathbf{R}_{\mathbf{v}\mathbf{v}_i}(r-1) + (1 - \alpha_v) \mathbf{v}_i(r) \mathbf{v}_i(r)^\dagger$
 - 7 $[\hat{\mathbf{D}}_{\mathbf{v}_i}(k), \hat{\mathbf{Q}}_{\mathbf{v}_i}(k)] \leftarrow \text{ITER-EIGEN}(\mathbf{R}_{\mathbf{v}\mathbf{v}_i}(r))$
 - 8 $[\hat{\mathbf{D}}_{\mathbf{v}_i}(k), \hat{\mathbf{Q}}_{\mathbf{v}_i}(k)] \leftarrow \text{ORDER}(\hat{\mathbf{D}}_{\mathbf{v}_i}(k), \hat{\mathbf{Q}}_{\mathbf{v}_i}(k))$
 - 9 $\mathbf{w}_i^1(k) \leftarrow \hat{\mathbf{a}}_{i,1}(k)$
- Tracking phase {for the rest of the call}
 - 10 $d^{(s)} \leftarrow d_1$
 - 11 $d^{(n)} \leftarrow \frac{d_2 + d_3 + \dots + d_M}{M-1}$
 - 12 $\hat{\mathbf{D}}_{\mathbf{v}_i}(k) \leftarrow \begin{bmatrix} d^{(s)} & \mathbf{0} \\ \mathbf{0} & d^{(n)} \mathbf{I}_{M-1} \end{bmatrix}$
 - 13 **while** call \neq end
 - 14 **do if** $((r \text{ modulus } (96 * (\text{update rate}))) = 0)$
 - 15 **then** $k \leftarrow k + 1$
 - 16 $[\hat{\mathbf{D}}_{\mathbf{v}_i}(k), \hat{\mathbf{Q}}_{\mathbf{v}_i}(k)] \leftarrow$
 $\text{NR1SSU}(\hat{\mathbf{D}}_{\mathbf{v}_i}(k), \hat{\mathbf{Q}}_{\mathbf{v}_i}(k), \mathbf{v}_i(r), \alpha_v)$
 - 17 $\mathbf{w}_i^1(k) \leftarrow \hat{\mathbf{a}}_{i,1}(k)$ Principal Eigenvector

Table 1: The tracking algorithm for the weight vector update for the i^{th} mobile

```

NR1SSU( $\hat{\mathbf{D}}(k-1), \hat{\mathbf{Q}}(k-1), \mathbf{y}, \alpha$ )
1    $\mathbf{g} \leftarrow \sqrt{(1-\alpha)} \hat{\mathbf{Q}}(k-1)^\dagger \mathbf{y}$ 
2    $\mathbf{G} \leftarrow \text{diag}(\frac{g_1}{|g_1|}, \frac{g_2}{|g_2|}, \dots, \frac{g_M}{|g_M|})$ 
3    $\begin{bmatrix} \mathbf{f}^{(s)} \\ \mathbf{f}^{(n)} \end{bmatrix} = \mathbf{f} \leftarrow \mathbf{G}^\dagger \mathbf{g}$ 
4    $\mathbf{H} \leftarrow \text{HOUSEHOLDER-DEFLAT}(\mathbf{f}^{(s)}, \mathbf{f}^{(n)})$  [6]
5    $b \leftarrow \alpha(d^{(s)} + d^{(n)}) + |\mathbf{f}^{(s)}|^2 + |\mathbf{f}^{(n)}|^2$ 
6    $c \leftarrow \alpha^2 d^{(s)} d^{(n)} + \alpha(d^{(s)} |\mathbf{f}^{(n)}|^2 + d^{(n)} |\mathbf{f}^{(s)}|^2)$ 
7-8  $\lambda_1 \leftarrow \frac{1}{2}(b + \sqrt{b^2 - 4c}); \lambda_2 \leftarrow \frac{1}{2}(b - \sqrt{b^2 - 4c})$ 
9-10  $\mathbf{q}_j \leftarrow \frac{\left( \begin{bmatrix} d^{(s)} & 0 \\ \alpha & d^{(n)} \end{bmatrix} - \lambda_j \mathbf{I} \right)^{-1} \begin{bmatrix} |\mathbf{f}^{(s)}| \\ |\mathbf{f}^{(n)}| \end{bmatrix}}{\left\| \left( \begin{bmatrix} d^{(s)} & 0 \\ \alpha & d^{(n)} \end{bmatrix} - \lambda_j \mathbf{I} \right)^{-1} \begin{bmatrix} |\mathbf{f}^{(s)}| \\ |\mathbf{f}^{(n)}| \end{bmatrix} \right\|}; j = 1, 2$ 
11   $[\hat{\mathbf{Q}}^{(s)}(k), \hat{\mathbf{Q}}^{(n)}(k)] \leftarrow$ 
       $[\hat{\mathbf{Q}}^{(s)}(k-1) \mathbf{G}^{(s)} \mathbf{H}^{(s)}, \hat{\mathbf{Q}}^{(n)}(k-1) \mathbf{G}^{(n)} \mathbf{H}^{(n)}]$ 
       $\begin{bmatrix} [\mathbf{q}_1 & \mathbf{q}_2] & \mathbf{0} \\ \mathbf{0} & \mathbf{0} & \mathbf{I}_{M-2} \end{bmatrix}$ 
12   $d_{\text{new}}^{(s)} \leftarrow \lambda_1$ 
13   $d_{\text{new}}^{(n)} \leftarrow \frac{\lambda_2 + (M-2)d^{(n)}}{M-1}$ 
14   $\hat{\mathbf{D}}(k) \leftarrow \begin{bmatrix} d_{\text{new}}^{(s)} & \mathbf{0} \\ \mathbf{0} & d_{\text{new}}^{(n)} \mathbf{I}_{M-1} \end{bmatrix}$ 
15  return  $\hat{\mathbf{D}}(k), \hat{\mathbf{Q}}(k)$ 

```

Table 2: The NR1SSU procedure

4.6 Computational complexity of the NR1SSU algorithm

Referring to Table 2, the computation complexity in flops of the NR1SSU algorithm is shown in Table 3.

Flops per weight update	
Step # in Table 2	# of flops
1-10	$4M^2 + 14M + 40$
11	$8M^2 + 18M + 2$
12-14	2

Table 3: Total computation complexity of NR1SSU

where M is the number of antenna elements used and one flop represents a real-real multiplication as described earlier in Section 4.2.

In comparison, the Power method requires $4M^2 + 8M$ flops per iteration [25] which depends on the convergence factor $|\lambda_2|/|\lambda_1|$, where λ_1 is the largest eigenvalue and λ_2 is the second largest eigenvalue of the matrix under considerations. When the convergence factor $|\lambda_2|/|\lambda_1|$ is close to unity, the convergence rate of resolving the true eigenvalues are very slow. The eigendecomposition may not convergence at all when $|\lambda_2|/|\lambda_1|$ equals unity. Instead of depending on the eigenvalue spread, the NR1SSU updates the eigenvalues and the eigenvectors directly which takes a constant number of multiplications for each weight vector update.

4.7 Summary

In this chapter, a novel application of a subspace method to a generic CDMA and a IS-95 CDMA system has been proposed. In the IS-95 system, the in-phase and quadrature-phase signals can be used as two sources of independent data for channel array response vector estimation.

Table 3 shows that a total of $12M^2 + 32M + 44$ multiplications is required to perform a NR1SSU algorithm weight vector update (NR1SSU array response estimate) for either a generic CDMA system or IS-95 CDMA system. This direct eigenstructure rank-one update allows for real-time weight vector updates provided that the digital signal processor and the real-time signal processing cycle allows an additional $12M^2 + 32M + 44$ flops between weight vector updates.

Note also that the weight vector update rate can be adjusted to reflect different wireless communication environments. In the case of fast fading wireless communication links where transmitting signals fade rapidly and significantly due to surrounding scatter, reflectors, and moving objects or mobiles, the weight vector should be updated as frequently as possible. In the case of slow fading wireless communication links, the weight vector can be updated less frequently. In the IS-95 CDMA system that uses FWFPC vector to obtain sufficient processing gain as discussed in this chapter, the weight vector update rate is restricted to one weight update per frame. In a generic CDMA system that uses the PN post-correlation vector as discussed in this chapter, the weight vector can be adjusted to be updated as often as once per information bit provided that the processing gain constraint is satisfied and the real-time signal processing cycle and the DSP processor allow for the required computations.

In summary, NR1SSU allows real-time operations that efficiently and recursively compute the eigen-decomposition of either the post-correlation matrix or the feedback Walsh function post-correlation covariance matrix which accurately estimates the time-varying array response vector from the principal eigenvector.

In the next chapter, simulation results are presented for tracking performance verification.

Chapter 5

Performance of the NR1SSU Algorithm in CDMA

5.1 Introduction

In this chapter, the application of a noniterative subspace eigenstructure array signal processing technique to track the array response vector of a desired mobile for increasing the signal-to-interference-noise ratio (SINR) in a CDMA communication system is verified via simulations. Two systems, the North American CDMA standard IS-95 and a generic CDMA system, are used to evaluate the NR1SSU algorithm for tracking the array response vector. Two propagation models, a flat fading propagation model and a frequency-selective propagation model, are considered during the evaluation of the NR1SSU tracking application.

Increasing the received SINR essentially results in an increase in cell capacity. Therefore, in this thesis, only the SINR values are used for performance evaluation. To further increase the SINR to aid in combating short term fading effects, the NR1SSU algorithm is also evaluated with a beam-steered RAKE [20] receiver structure.

If the received electromagnetic waves impinging on each element of the antenna array are uncorrelated and/or if the inter-element spacing between antennas are large enough, the received signals at each antenna elements are no longer correlated and the combining of these uncorrelated signals is categorized as diversity combining.

Diversity combining that compensates for the channel gain and phase shift for each received path at each antenna element is called maximal-ratio-combining (see section 3.4.2) [15].

Due to the fact that urban wireless communication environments are harsh, it is possible that the received signals at each antenna element are uncorrelated even with only a small spacing between antennas [33]. In order to strive for a robust evaluation of beamforming strategies to increase cell capacity, this thesis also compares a spatially correlated beamforming receiver to an antenna diversity receiver structure. This evaluation is made by comparing a beamformer that receives spatially-correlated signals at a set of closely spaced antenna array elements with a diversity combiner that receives spatially uncorrelated signals at widely spaced base-station antenna elements.

The simulation results, presented in Sections 5.2 and 5.3, demonstrate the performance of the NR1SSU tracking algorithm for CDMA systems as well as verify the analytical constraints (equations (4.46) and (4.55)) derived in Chapter 4. A flat fading propagation model is used in Sections 5.2 and 5.3 except Section 5.3.3, which uses a frequency-selective fading propagation model to compare a spatial beamformer with a beamsteered-RAKE receiver.

In the case of spatially-correlated signals received for the closely-spaced antenna array, the NR1SSU estimated array response vector is parameterized in terms of the direction-of-arrival (DOA) for presentation purposes. This transformation from array response vector to DOA assumes that the antenna array has been calibrated. This allows for easier visual interpretation of the tracking of mobiles. The parameterization is achieved by averaging over the relative phase shift between adjacent antenna elements of an estimated array response vector. For an antenna array receiver with correlated signals, it is assumed that the received signal at each antenna element experiences the same channel gain and phase shift. For an antenna array receiver with uncorrelated signals, it is assumed that the received signals at each antenna element experience independent channel gains and phase shifts.

5.2 NR1SSU Application to a IS-95 CDMA System

In this section, a PN chip-level IS-95 CDMA uplink simulator [9] is used for evaluating the NR1SSU beamforming algorithm under a flat fading propagation model. This PN chip-level CDMA uplink simulator considers amplitude Rayleigh fading, propagation loss, shadowing, and power control (both perfect and imperfect) in a three-sector linear base-station antenna array receiver structure. In this IS-95 simulator [8], the received signals are assumed spatially-correlated due to the close spacing of the antenna elements. The flat fading and slow fading propagation model considered in this chip-level IS-95 system has zero-delay-spread [8]. Only the reverse link is considered; that is, the mobile to base station link.

5.2.1 Monte-Carlo array response tracking simulation results

First, the robustness of the NR1SSU array response vector for tracking a moving mobile is evaluated through 50 Monte-Carlo trials with 10 and 3 in-band moving mobiles, respectively. It is assumed that synchronization with the target mobile's pseudo-random noise (PN) long and short code sequences is achieved.

Figures 5.1 and 5.2 show, in terms of the mean and root mean square error (RMSE) of the tracked DOA estimates, the NR1SSU array response tracking performance that uses, respectively, the i^{th} target mobile's covariance matrix \mathbf{R}_{vv_i} of the feedback Walsh function post-correlation (FWFPC) vector \mathbf{v} [9], and the covariance matrix \mathbf{R}_{zz_i} of the short/long code post-correlation vector \mathbf{z} . This Monte-Carlo simulation in Figures 5.1 and 5.2 was evaluated over a duration of 200 IS-95 frames with NR1SSU tracking of a target moving mobile with 9 in-band interferers. Note that the weight vector is updated with the NR1SSU array response vector estimate only once per IS-95 frame. In this simulation, Rayleigh amplitude fading, fourth-order path loss propagation, and 8dB shadowing effect with perfect power control were utilized.

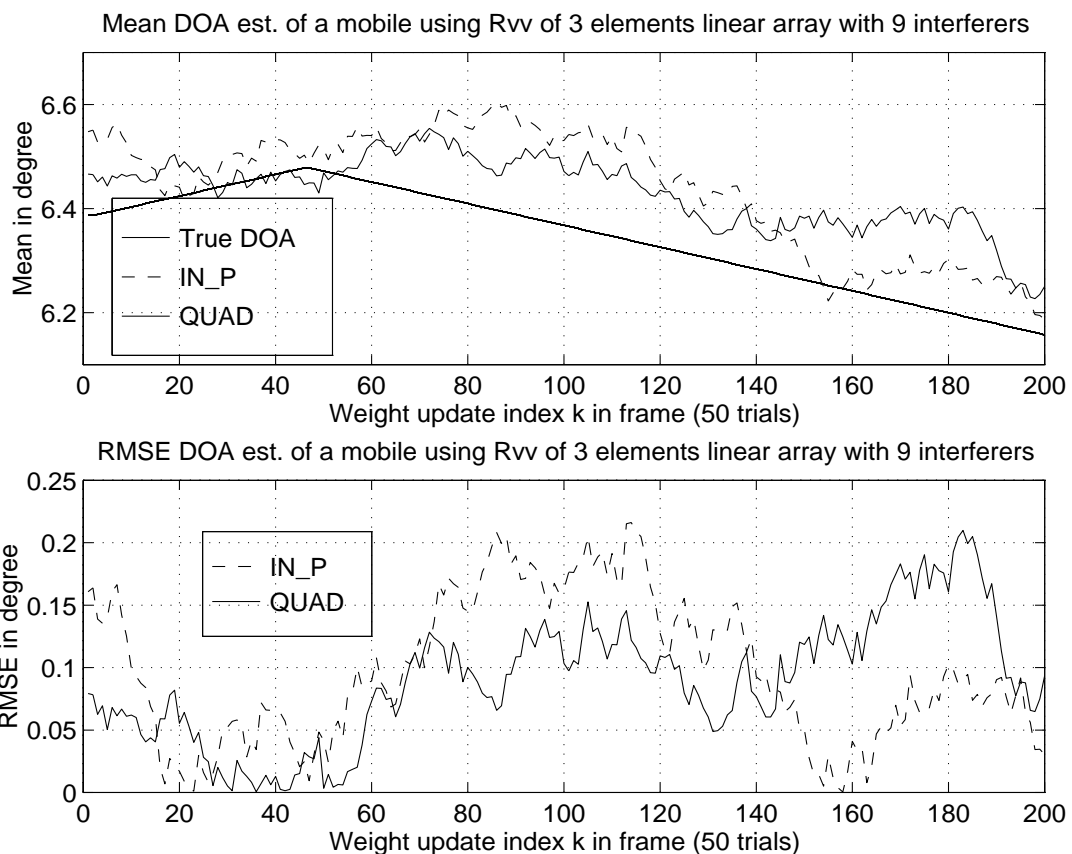


Figure 5.1: Monte-Carlo evaluation of a NR1SSU tracked moving mobile using the feedback Walsh function post-correlation (FWFPC) covariance matrix with perfect power control received at $\text{SNR} = 7\text{dB}$, 3-element 3-sector linear array having 9 moving interferers updated once per frame with 50 trials

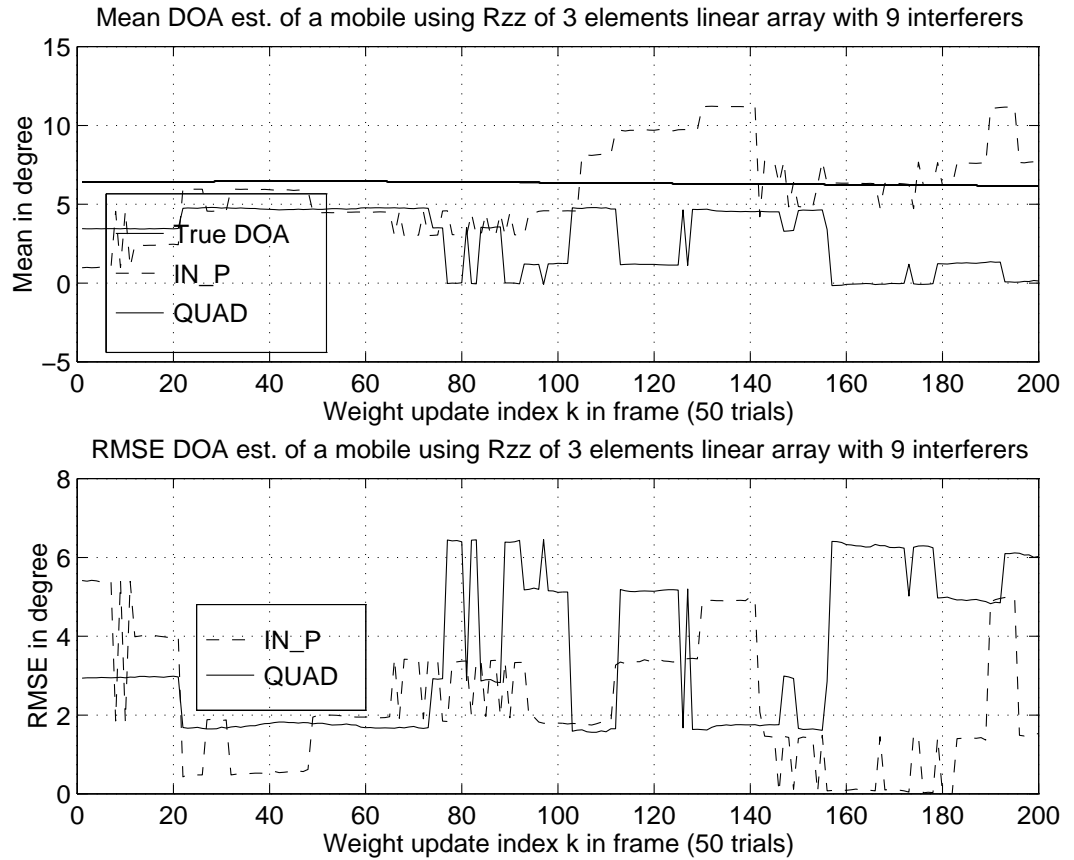


Figure 5.2: Monte-Carlo evaluation of a NR1SSU tracked moving mobile using the PN code post-correlation covariance matrix with perfect power control received at $\text{SNR} = 7\text{dB}$, 3-element 3-sector linear array having 9 moving interferers updated once per frame with the 50 trials of Figure 5.1

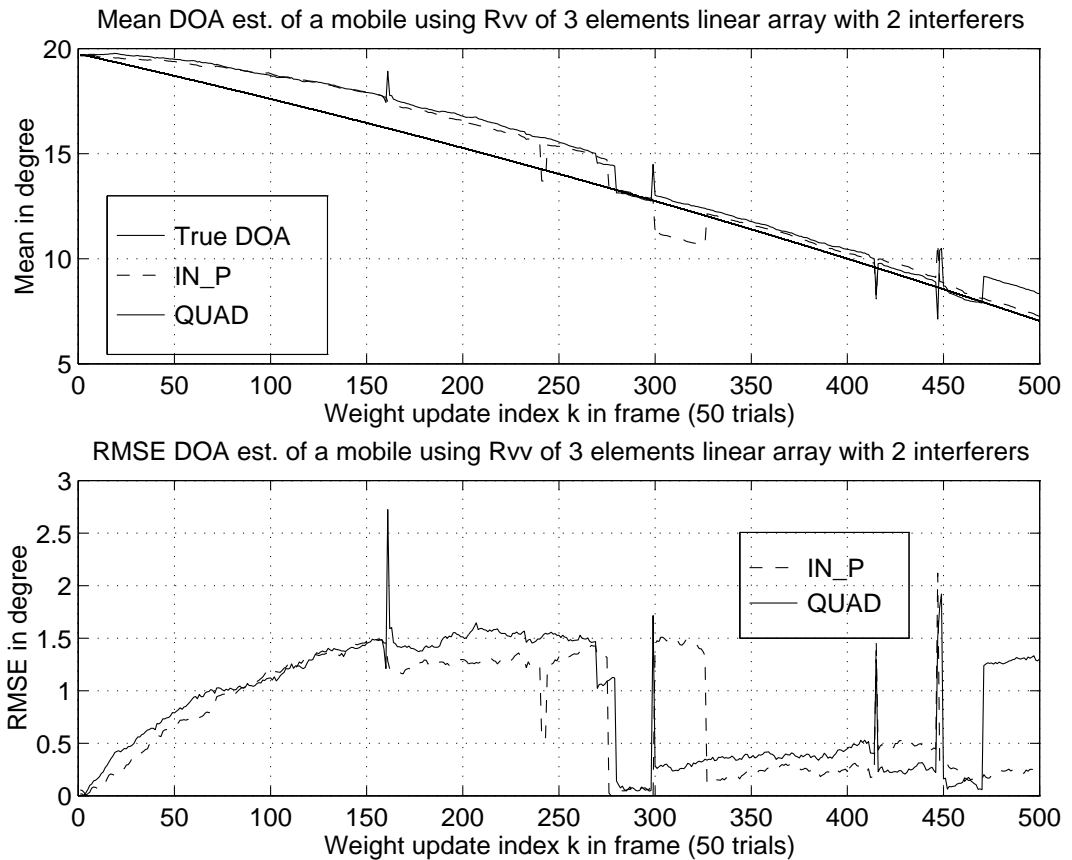


Figure 5.3: Monte-Carlo evaluation of a NR1SSU tracked moving mobile using the feedback Walsh function post-correlation (FWFPC) covariance matrix with perfect power control received at $\text{SNR} = 7\text{dB}$, 3-element 3-sector linear array having 2 faster moving interferers updated once per frame with 50 trials

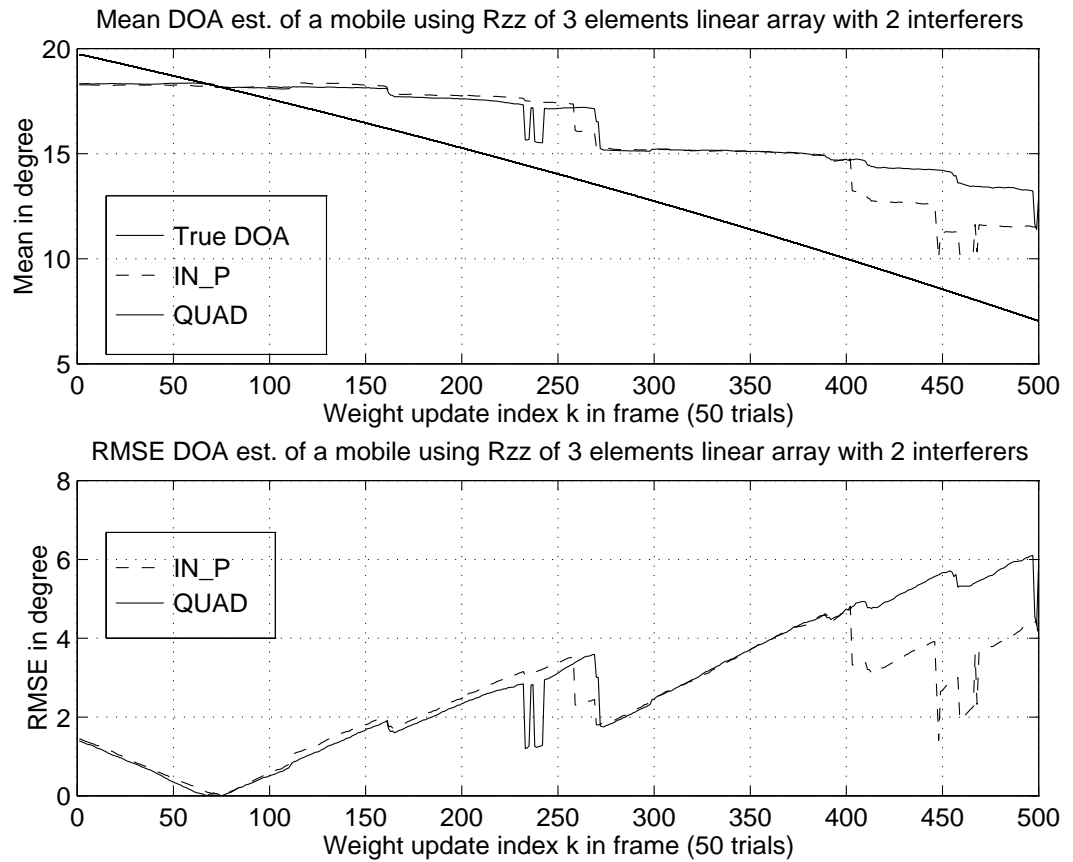


Figure 5.4: Monte-Carlo evaluation of a NR1SSU tracked moving mobile using the short and long PN code post-correlation covariance matrix with perfect power control received at $\text{SNR} = 7\text{dB}$, 3-element 3-sector linear array having 2 faster moving interferers updated once per frame with the 50 trials of Figure 5.3

Under the same run with 9 interferers, Figure 5.1 shows that the NR1SSU tracks the direction of arrival accurately within 0.25 degrees when using the FWFPC covariance matrix, while in comparison the NR1SSU tracks poorly when using the PN chip post-correlation matrix as shown in Figure 5.2. The reason for this is that the IS-95 system has a PN code spreading gain of 4 whereas the FWFPC vector increases the code-filtering processing gain to 192.75 by incurring an estimation delay of one frame (0.02 seconds) [9]. That is, Figures 5.1 and 5.2 exemplify the constraint of Equation (4.46) for a zero multipath time delay spread propagation model in that a higher processing gain results in better NR1SSU algorithm estimation.

The PN code post-correlation covariance matrix \mathbf{R}_{zz} is in fact the Walsh function covariance matrix of a IS-95 system where the Walsh functions of the reverse link carry information in the form of orthogonal functions. In fact, the higher the processing gain, the lower the despread interference power in comparison to the despread desired mobile signal since the spreading factor, L , determines how wide the interference power is spread over the frequency spectrum. Hence, the higher the processing gain, the more the despread interfering signals act as noise over the PN chip frequency band; however, it is a less efficient communications system in terms of the actual information transfer rate. CDMA is an interference-limited communication technique where each user transmits at the same carrier frequency with signal power superimposed at the receiver. Therefore, the higher the number of interferers, the higher the total noise-like power levels that are being added.

Figures 5.3 and 5.4 show the performance of NR1SSU tracking a faster moving mobile with two-inband interferers. These simulations used the FWFPC and the PN post-correlation vectors, respectively, over 500 frames for the channel array response vector estimation with weight updates once per frame. Using the FWFPC matrix \mathbf{R}_{vv_i} , NR1SSU tracks to within a root mean square error of 3 degrees. In comparison, by using the PN post-correlation covariance matrix \mathbf{R}_{zz_I} , NR1SSU tracks to within a root mean square error of 6.5 degrees. That is, when the approximations in Equation (4.46) are well-satisfied, NR1SSU will track accurately.

Figures 5.2 and 5.4 demonstrate the degradation in DOA estimation when constraint equation (4.46) is not satisfied. As shown, spike errors in DOA occur. The estimation errors in Figure 5.3 depict a situation where there is a deep fade over a period of time during which equation (4.46) fails to hold. This problem is magnified when the mobile is moving faster and covariance estimates are far from their asymptotic values. For example, in Figure 5.3 the mobile is moving at least 10 times faster than the mobile in Figure 5.1 resulting in larger errors.

For the IS-95 CDMA system, the direct calculation of the eigendecomposition using the noniterative subspace method will track the array response vector of a desired mobile accurately when the post-correlation vector being used has a high processing gain. This latter situation arises when applying the NR1SSU tracking algorithm using FWFPC as described earlier for the IS-95 system.

5.2.2 Perfect power control vs. imperfect power control

It is highly likely that signals received asynchronously at the base-station will deviate slightly from the desired power control level. Therefore, it is important to evaluate the NR1SSU algorithm with imperfect power control of the received signals at the base-station. Note that for the non-zero delay spread propagation model, the multipath echo signals received may result in a larger deviation from the desired power controlled signal. Therefore, comparison between systems that perform perfect and imperfect power control will demonstrate the robustness of the applied NR1SSU array response tracking algorithm in harsh propagation environments.

Figure 5.5 shows a tracked mobile with 39 in-band interferers with imperfect power control [7] and Figure 5.6 shows another tracked mobile in a similar situation as that of Figure 5.5. Figures 5.7 and 5.8 show two tracked mobiles with 39 in-band interferers under perfect power control.

By comparing Figures 5.5 and 5.6 (imperfect power control) to Figures 5.7 and 5.8 (perfect power control), it can be seen that the imperfect power control NR1SSU estimation error is only slightly larger than in the case of perfect power control.

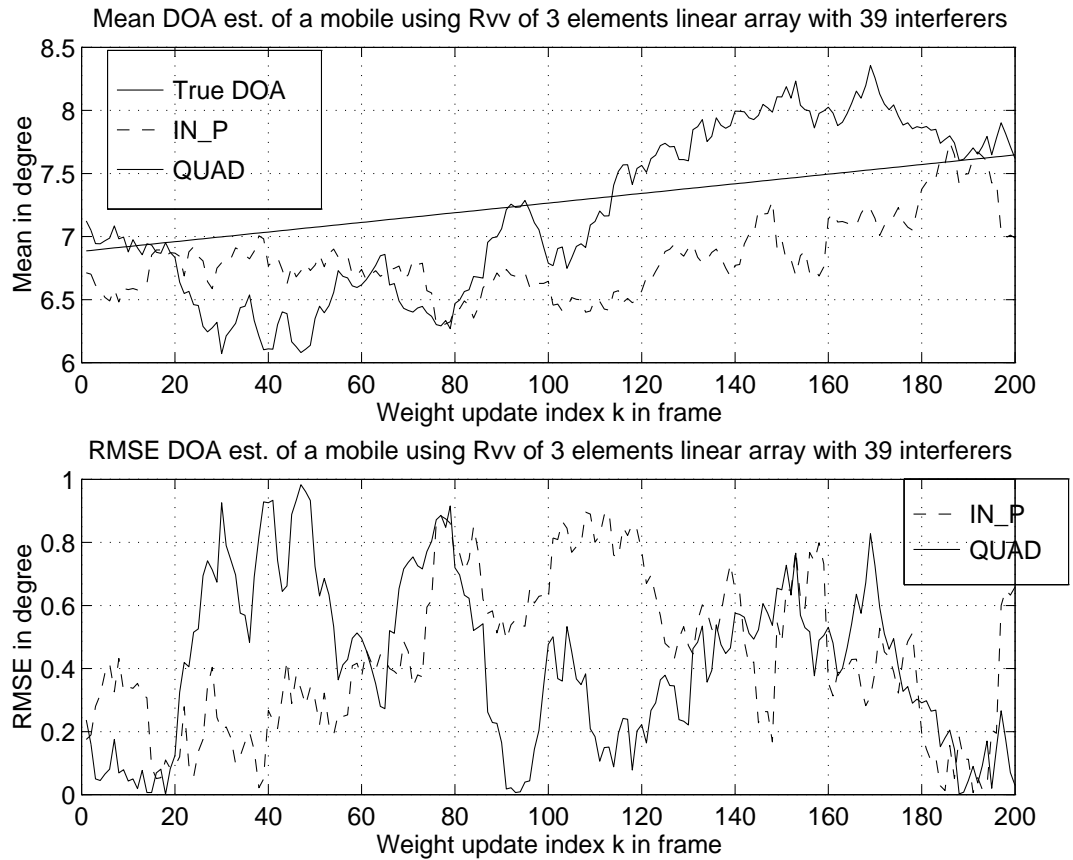


Figure 5.5: A tracked mobile's NR1SSU DOA estimates and root mean square error (RMSE) using the FWFPC covariance matrix with imperfect power control, 3-element, 3-sector linear array having 39 moving interferers

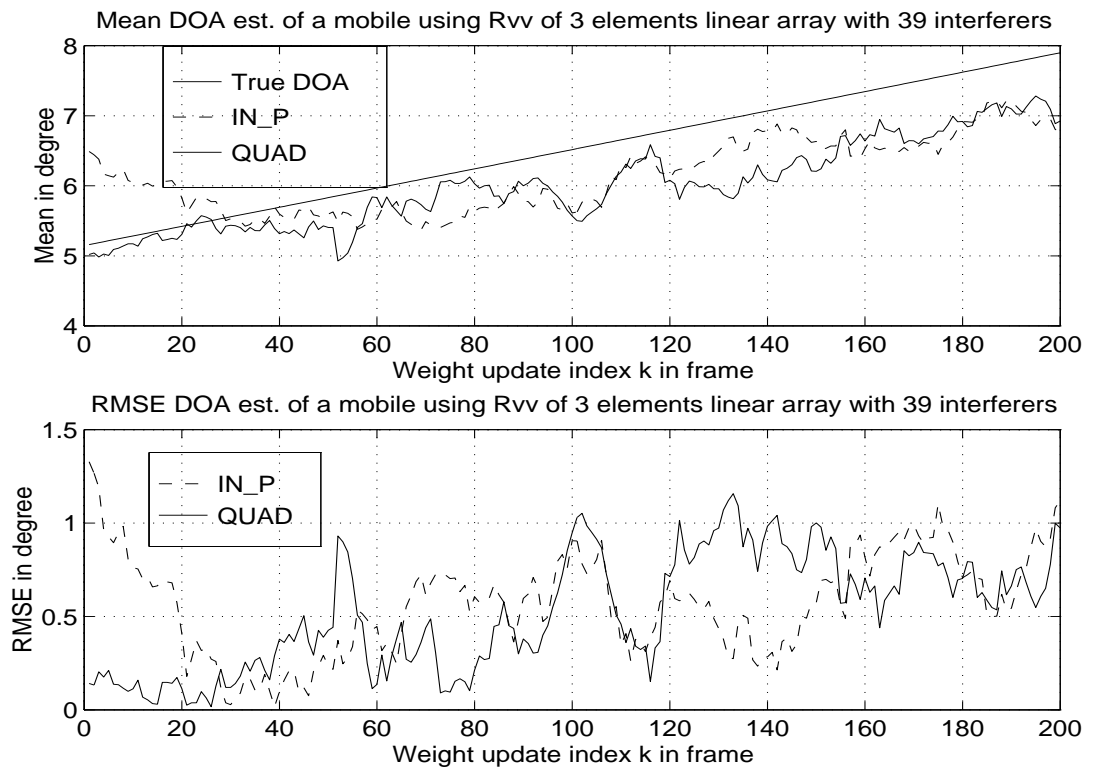


Figure 5.6: Another tracked mobile's NR1SSU DOA estimates and RMSE using the FWFPC covariance matrix with imperfect power control, 3-element, 3-sector linear array having the 39 moving interferers of Figure 5.5

Therefore, the NR1SSU tracking algorithm is able to accurately track a received signal under imperfect power control response. In fact, although the received signal power deviates from the desired power controlled level, the desired signal can still be tracked as long as the despread desired signal power is higher than the total interference-plus-noise power. Indeed, the condition for using the NR1SSU tracking algorithm can be empirically relaxed to

$$\text{PEV} \left(LP_i \mathbf{a}_i(n) * \mathbf{a}_i(n)^\dagger \right) > \text{PEV} \left(\frac{2}{3} \sum_{j=1, j \neq i}^N P_j(t) \mathbf{a}_i(n) * \mathbf{a}_i(n)^\dagger \right) \quad (5.1)$$

5.2.3 Different number of array antenna elements vs. performance

As discussed in Chapter 2, the greater the number of antenna elements used, the narrower the beamwidth of the spatial filter and the higher the SINR will be after beamforming; the SINR will be increased provided that the beamformer is directed to the desired mobile. Thus, the cell capacity can be increased by using a higher number of antenna elements. Therefore, it is valuable to consider the impact of increasing the number of antenna elements used with the NR1SSU algorithm for a CDMA communication system. Figures 5.9, 5.10, and 5.11 show a tracked mobile with 9 interferers using, respectively, a 4-element, 6-element, and 8-element base-station antenna linear array reception topology. These simulation results demonstrate that using a larger number of antenna elements improves the root mean square error on average over time. Therefore, it follows that using a base-station linear array topology with a higher number of antenna elements will provide extra beamforming gain.

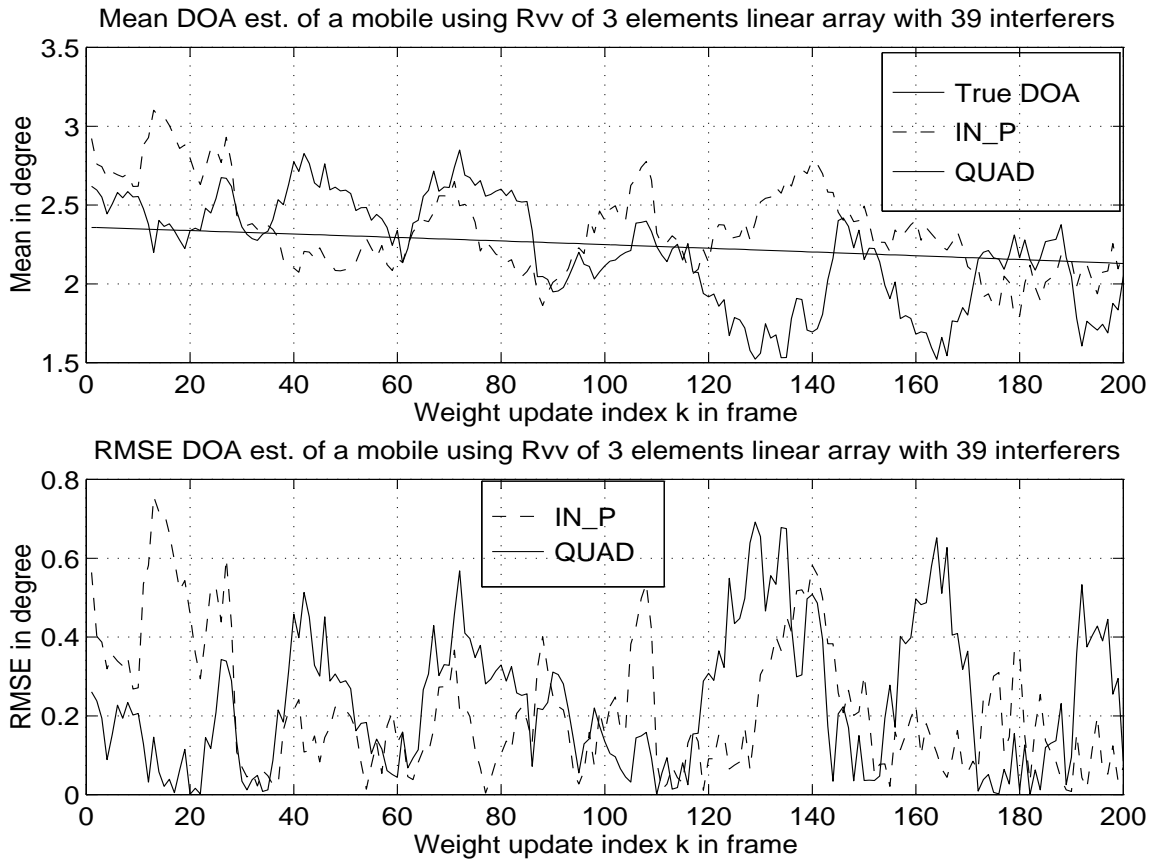


Figure 5.7: A tracked mobile's NR1SSU DOA estimates and RMSE using the FWFPC covariance matrix with perfect power control, 3-element, 3-sector linear array having 39 moving interferers

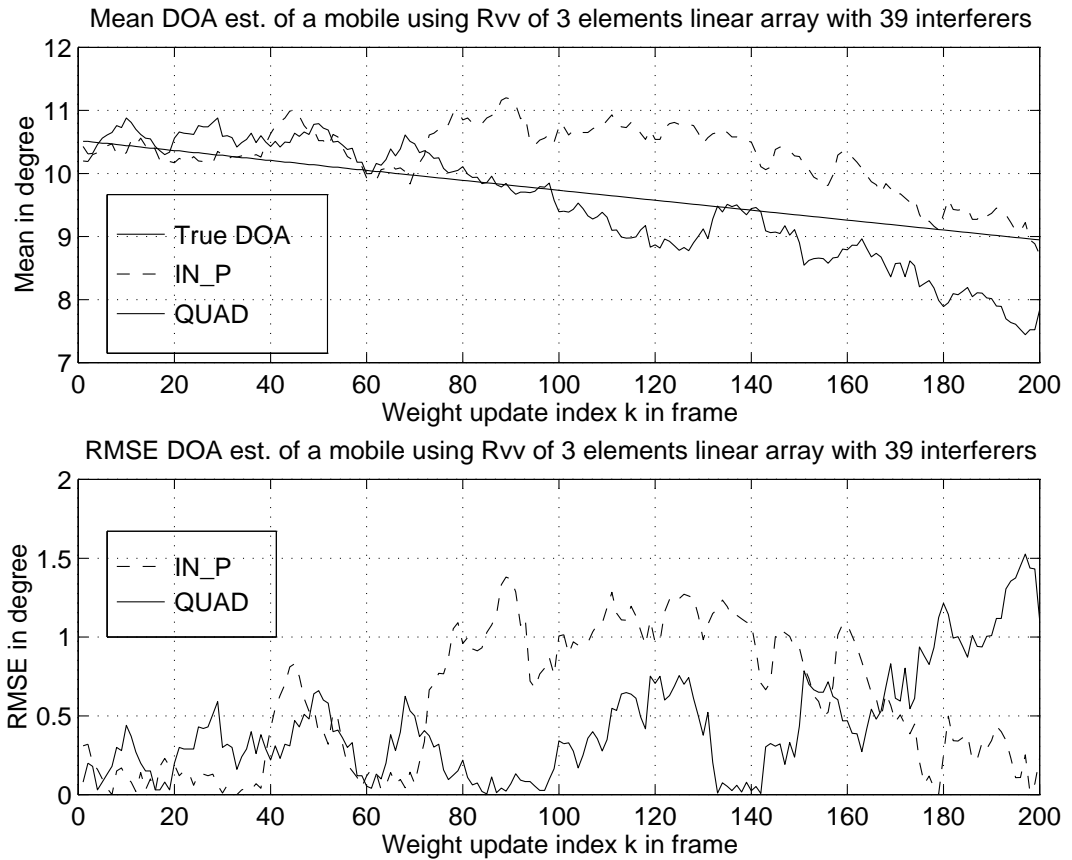


Figure 5.8: Another tracked mobile's NR1SSU DOA estimates and RMSE using the FWFPC covariance matrix with perfect power control, 3-element, 3-sector linear array having the 39 moving interferers of Figure 5.7

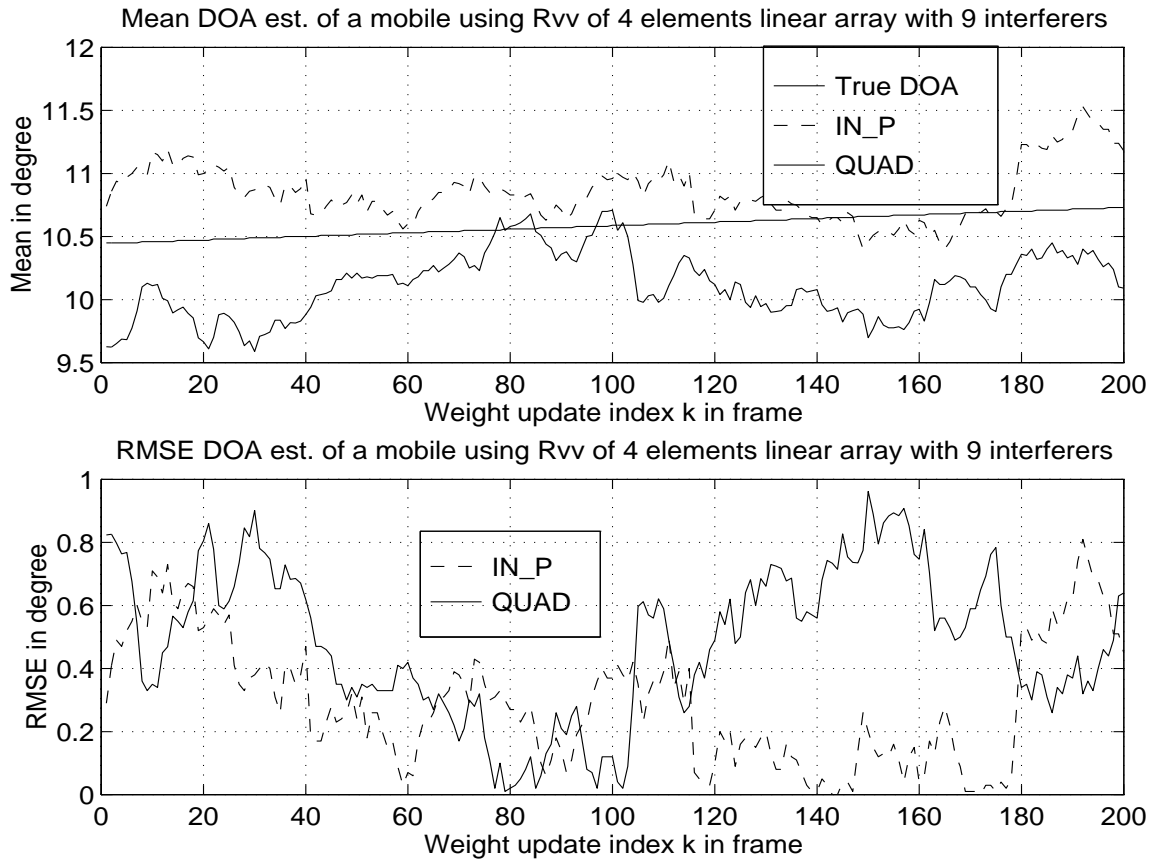


Figure 5.9: A tracked mobile's NR1SSU DOA estimates and RMSE using the FWFPC covariance matrix with perfect power control, 4-element, 3-sector linear array having 9 moving interferers

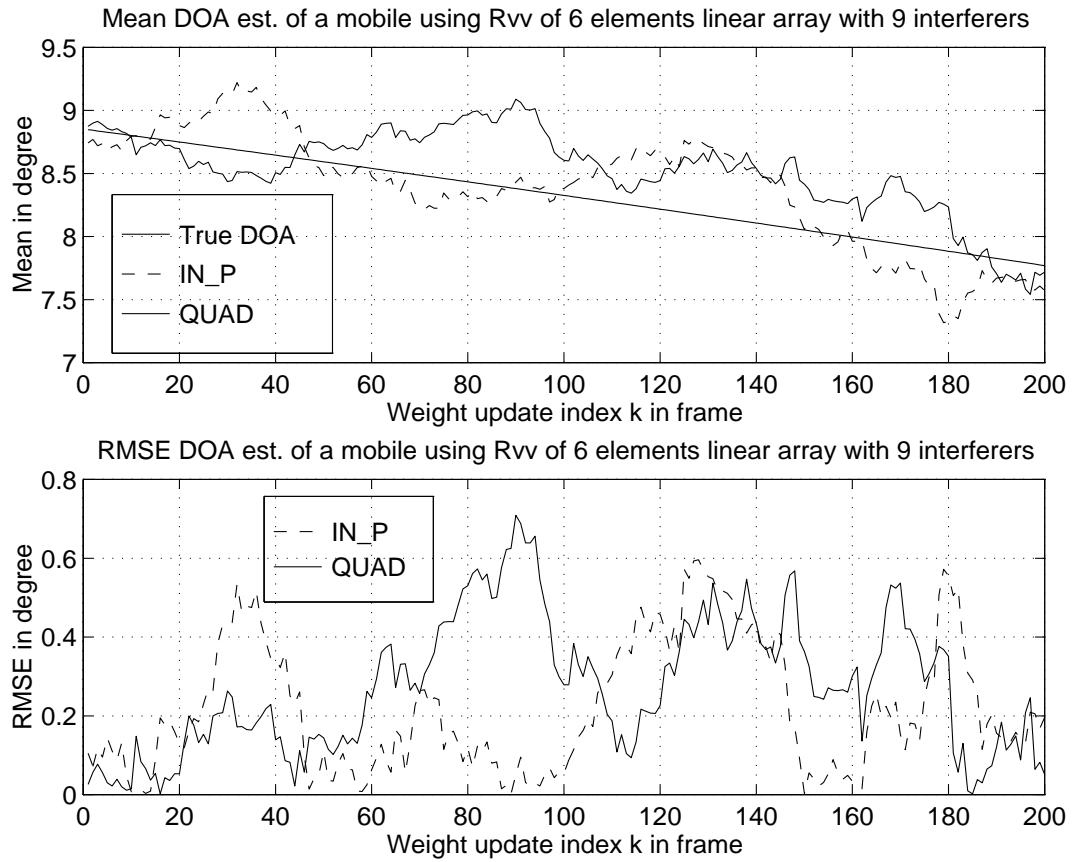


Figure 5.10: A tracked mobile's NR1SSU DOA estimates and RMSE using the FWFPD covariance matrix with perfect power control, 6-element, 3-sector linear array having 9 moving interferers

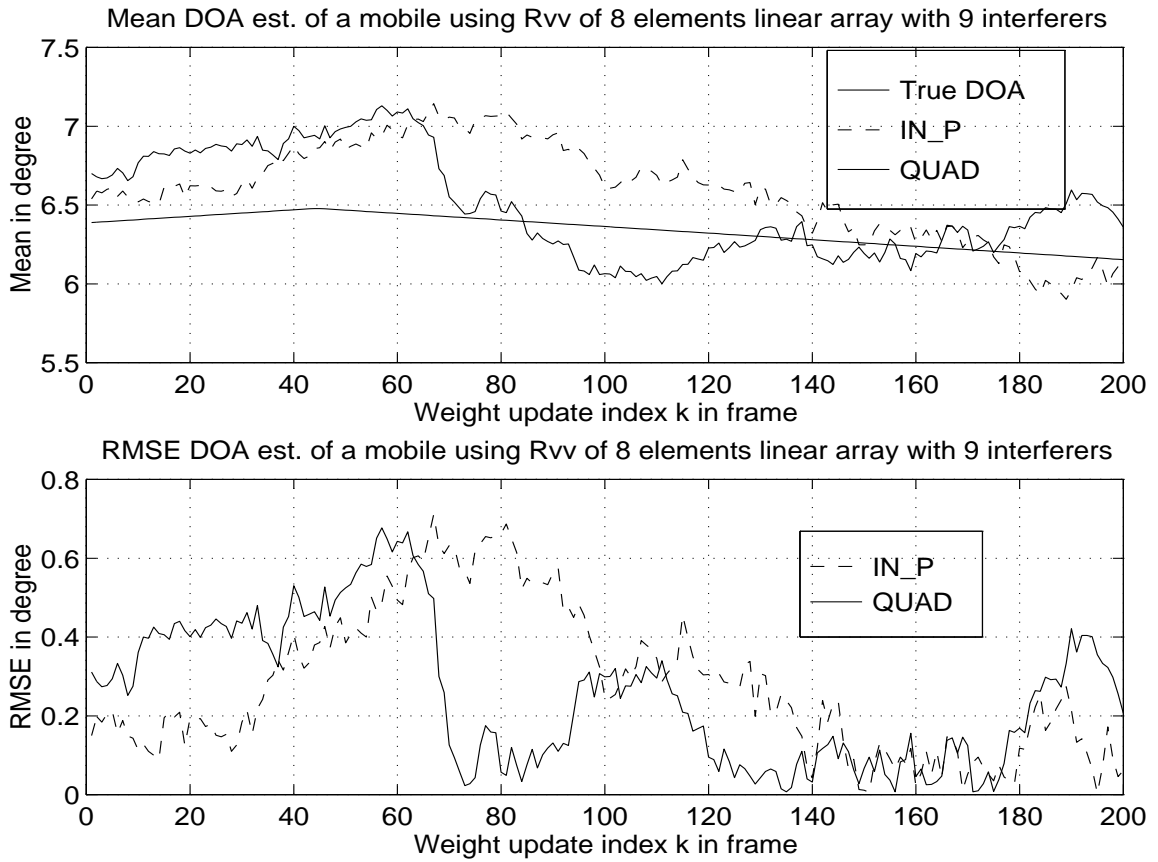


Figure 5.11: A tracked mobile's NR1SSU DOA estimates and RMSE using the FWFPD covariance matrix with perfect power control, 8-element, 3-sector linear array having 9 moving interferers

5.3 NR1SSU application to a generic CDMA system

In this section, a generic CDMA system is used to evaluate the NR1SSU algorithm under zero and non-zero time delay spread propagation models. These propagation models assumed short-term Rayleigh fading. Note that Rayleigh fading represents a worst case of multipath fading [29]. The following simulations were performed with a PN code filtering processing gain of 128. All of the NR1SSU array response vector estimates were obtained from the PN code filtering post-correlation covariance matrix of Equations (4.47) and (4.56) representing the zero-delay spread and non-zero delay spread propagation models respectively which presented in Chapter 4.

In the following subsections, a spatially-correlated receiver antenna linear array topology was used for beamforming with the signals received at each antenna element assumed to experience the same channel gain and phase shift. For diversity combining, spatially-uncorrelated receiver antenna array topology was used with the signals received at each widely-spaced antenna element assumed to experience independent channel gains and phase shifts.

5.3.1 Beamformer with optimum SINR versus optimum SNR

The performance of beamforming to a desired mobile's is compared for the cases of optimum SINR and optimum SNR beamforming criteria. The rationale for SNR beamforming is a reduction in computation. This section assumes a flat fading propagation model and spatially correlated signals reception at the base station antenna array, in which only one strong Rayleigh faded signal path is received at the antenna array from each transmitting in-band mobile. This is based on the assumption that mobile transmissions are power controlled to compensate for long-term channel fluctuations due to shadowing and propagation loss. Therefore, the simulations assume that all the mobiles' signals received at the base-station are independently short-term Rayleigh faded with a signal-to-noise power ratio that is power controlled to 7dB.

In the case of the optimum SINR beamforming, the adaptive weights are given by the Wiener solution

$$\mathbf{w}(t) = \mathbf{R}_{xx}^{-1} \mathbf{r}_{xd} = \zeta \mathbf{R}_{\text{IN}}^{-1} \mathbf{a}(t) = \mathcal{I} \mathbf{R}_{xx}^{-1} \mathbf{a}(t) \quad (5.2)$$

as reviewed in Chapter 2 (see Equation (2.51) and Table 2.1), where ζ and \mathcal{I} are scalars, \mathbf{r}_{xd} is the cross-correlation matrix of the pre-correlation vector and the desired signal vector, \mathbf{R}_{xx} is the pre-correlation covariance matrix, \mathbf{R}_{IN} is the interference-plus-noise covariance matrix, and $\mathbf{a}(t)$ is the array response vector corresponding to the narrowband frequency ω_c .

Based on the general assumption that the desired signal is uncorrelated with the interference and noise, the optimum SINR beamformer gives the desired mobile's beamformed SINR value as

$$\begin{aligned} \text{SINR} &= \frac{\mathbf{w}(t)^\dagger \mathbf{E}\{\mathbf{s}(t)\mathbf{s}(t)^\dagger\} \mathbf{w}(t)}{\mathbf{w}(t)^\dagger \mathbf{E}\{(\mathbf{i}(t) + \mathbf{n}(t))(\mathbf{i}(t) + \mathbf{n}(t))^\dagger\} \mathbf{w}(t)^\dagger} \\ &= \frac{\mathbf{a}(t)^\dagger \mathbf{R}_{xx}^{-1} \mathbf{E}\{\mathbf{s}(t)\mathbf{s}(t)^\dagger\} \mathbf{R}_{xx}^{-1} \mathbf{a}(t)}{\mathbf{a}(t)^\dagger \mathbf{R}_{xx}^{-1} \mathbf{E}\{(\mathbf{i}(t) + \mathbf{n}(t))(\mathbf{i}(t) + \mathbf{n}(t))^\dagger\} \mathbf{R}_{xx}^{-1} \mathbf{a}(t)} \end{aligned} \quad (5.3)$$

which is independent of any scalar ζ or \mathcal{I} , where $\mathbf{s}(t)$ is the $M \times 1$ desired signal vector, $\mathbf{i}(t)$ is the $M \times 1$ total interference signal vector, $\mathbf{n}(t)$ is the $M \times 1$ thermal noise vector, and M is the number of the antenna elements.

The adaptive weight vectors for an optimal maximum SNR beamformer presented as star-dotted lines that used in Figure 5.12 and 5.13 follow

$$\mathbf{w}(t) = \mathbf{a}(t) \quad (5.4)$$

where $\mathbf{a}(t)$ is the time-varying perfect array response vector. This SNR beamformer gives the desired mobile's beamformed SINR value as

$$\text{SINR} = \frac{\mathbf{a}(t)^\dagger \mathbf{E}\{\mathbf{s}(t)\mathbf{s}(t)^\dagger\} \mathbf{a}(t)}{\mathbf{a}(t)^\dagger \mathbf{E}\{(\mathbf{i}(t) + \mathbf{n}(t))(\mathbf{i}(t) + \mathbf{n}(t))^\dagger\} \mathbf{a}(t)} \quad (5.5)$$

First, Figure 5.12 demonstrates the fact that when there is only one antenna element at the base station, the beamformed SINR is the same no matter which

beamforming criterion is used. The reason being that the weights are now scalars and are cancelled out from the numerator and the denominator in Equations (5.3) and (5.5) for both optimum SINR and SNR beamforming. Thus, the SINR for spatial filtering with one antenna element reception depends only on the received signal's SINR where

$$\text{SINR} = \frac{\mathbf{E}\{\mathbf{s}(t)\mathbf{s}(t)^\dagger\}}{\mathbf{E}\{(\mathbf{i}(t) + \mathbf{n}(t))(\mathbf{i}(t) + \mathbf{n}(t))^\dagger\}} \quad (5.6)$$

Note that to explore the time diversity using taps, a one antenna element reception can increase the SINR.

Therefore, in a single antenna reception topology, the desired mobile's SINR only depends on the ratio of the received faded desired signal power to the total received interference-plus-noise power, as shown in Figures 5.12 and 5.13 with 9 and 24 interferers, respectively.

Antenna diversity with selection combining is the extension of single antenna reception where each base-station antenna is located far enough apart to obtain independently faded signals. The performance of a diversity combiner in a flat fading propagation model will be evaluated in Section 5.3.4.

With SINR beamforming weights for the linear array of each 120 degree sector, and 9 and 24 interferers, respectively, in Figures 5.12 and 5.13, the beamformed SINR for the 9 interferers case shows a larger performance gap between the maximum SINR and maximum SNR criteria. Note that the dot-dashed line represents beamformed SINR with adaptive weight vector update that follows $\mathbf{w}(t) = \hat{\mathbf{R}}_{xx}^{-1} \mathbf{a}(t)$ (the SINR beamforming criterion) and the star-dotted line represents beamformed SINR with adaptive weight vector update that follows $\mathbf{w}(t) = \mathbf{a}(t)$ (the SNR beamforming criterion), where $\mathbf{a}(t)$ is the perfect (actual) array response vector of the desired mobile and $\hat{\mathbf{R}}_{xx}^{-1}$ is the inverse of the received PN chip pre-correlation vector covariance matrix estimate using recursive exponentially weighted covariance estimate.

The performance trade off of not estimating the inverse of the covariance matrix, either \mathbf{R}_{xx}^{-1} or $\mathbf{R}_{\mathbb{N}}^{-1}$, for reducing computations is shown in Figures 5.12 and 5.13. Spatially nulling interferers clearly depends on the distribution of the interfering mobiles.

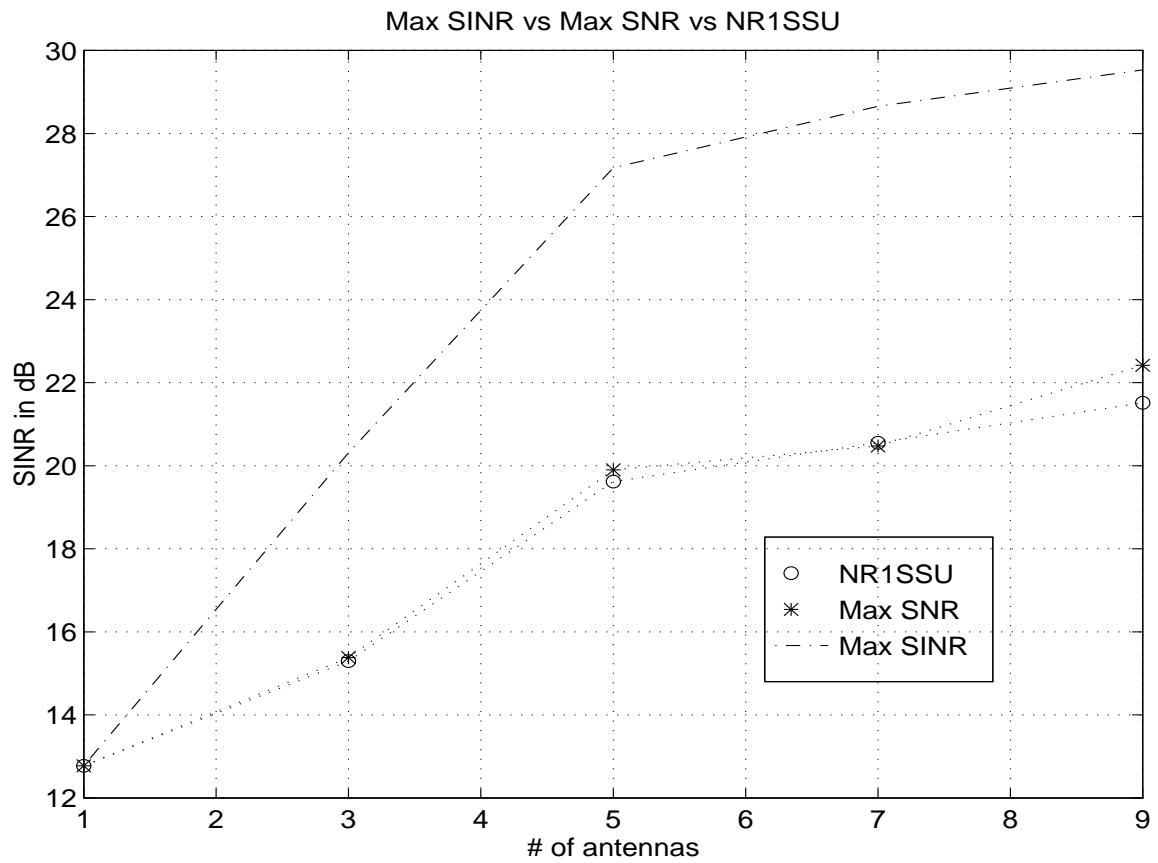


Figure 5.12: SINR vs SNR optimum (using perfect array response vector) vs NR1SSU with 10 mobiles in total

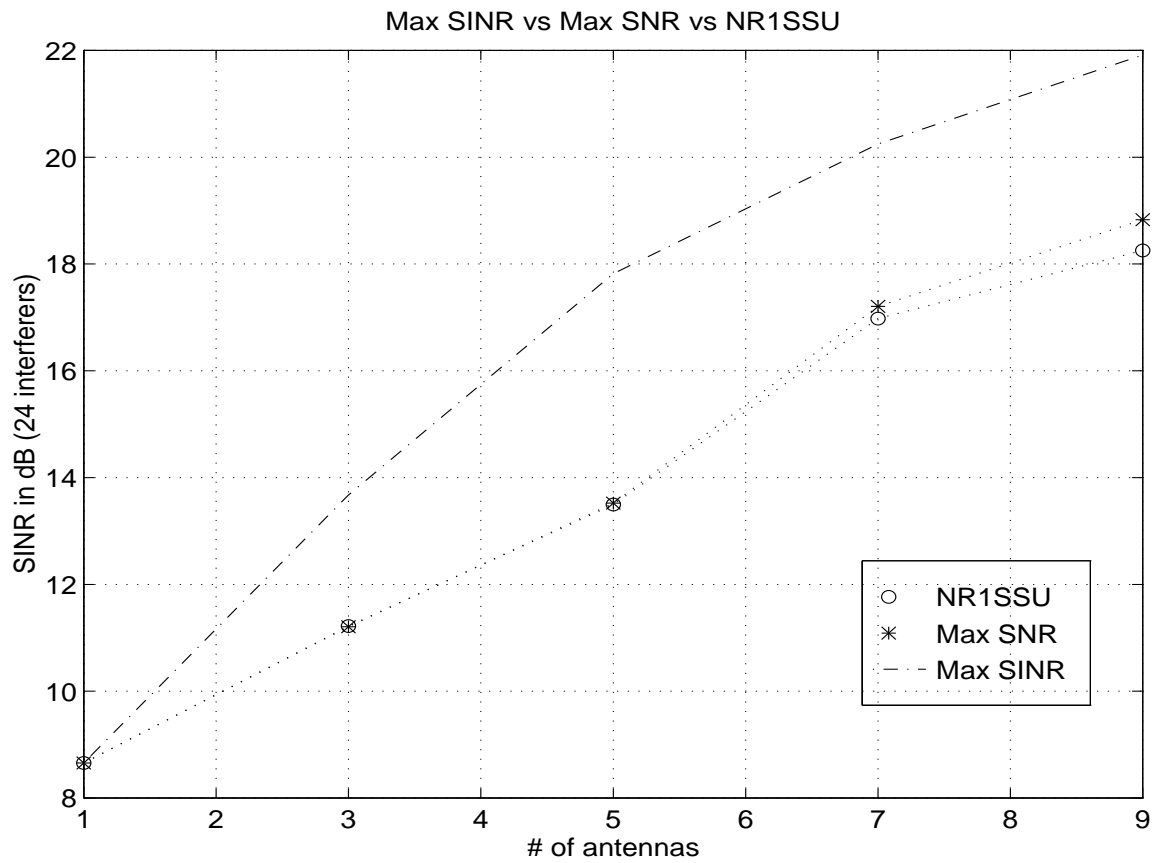


Figure 5.13: SINR vs SNR optimum (using perfect array response vector) vs NR1SSU with 25 mobiles in total

In cases where the interferers' effective DOA is close to that of the desired mobile, the spatial filter will not be able to discriminate the interferers from the desired mobile. In such a case, the received interferers and the desired mobile will experience similar spatial filtering; however, the desired signal will still be distinguishable from the interferers due to the assigned PN code by the virtue of a CDMA system.

In practice, the base-station antenna array beamforming algorithm is limited by the digital signal processor (DSP) available and the beamforming system's rate of adaptive weight vector update, where a trade-off between sophisticated signal processing algorithms and the DSP chip's available MIPS (million instruction per second) must be available to accomplish such signal processing algorithm. Figures 5.12 and 5.13 show that the beamformed power gain of using SNR beamforming with 24 interferers has almost half of the beamformed gain of using 9 interferers. Therefore, as the number of in-band mobiles increases to a certain level where the despread-beamformed interference signals can be modelled as white noise, then using SNR beamforming weights may be worth the relatively small performance penalty.

5.3.2 NR1SSU compared to true array response vector

Figures 5.12 and 5.13 also show that the beamforming weights using the NR1SSU array response estimates have negligible power loss compared to the beamforming weights obtained using the perfect array response vector. In Figures 5.12 and 5.13, the circle-dotted line represents the optimum SNR weight using $\mathbf{w} = \hat{\mathbf{a}}(t)$, where $\hat{\mathbf{a}}(t)$ is the adaptive array response vector estimate using the NR1SSU algorithm. The star-dotted line represents the beamformed SINR using the SNR beamforming criteria with the perfect array response as the adaptive beamforming weights, $\mathbf{w} = \mathbf{a}(t)$.

This clearly demonstrates that the NR1SSU array response estimate is an accurate estimate of the true array response vector, and results in negligible SINR loss.

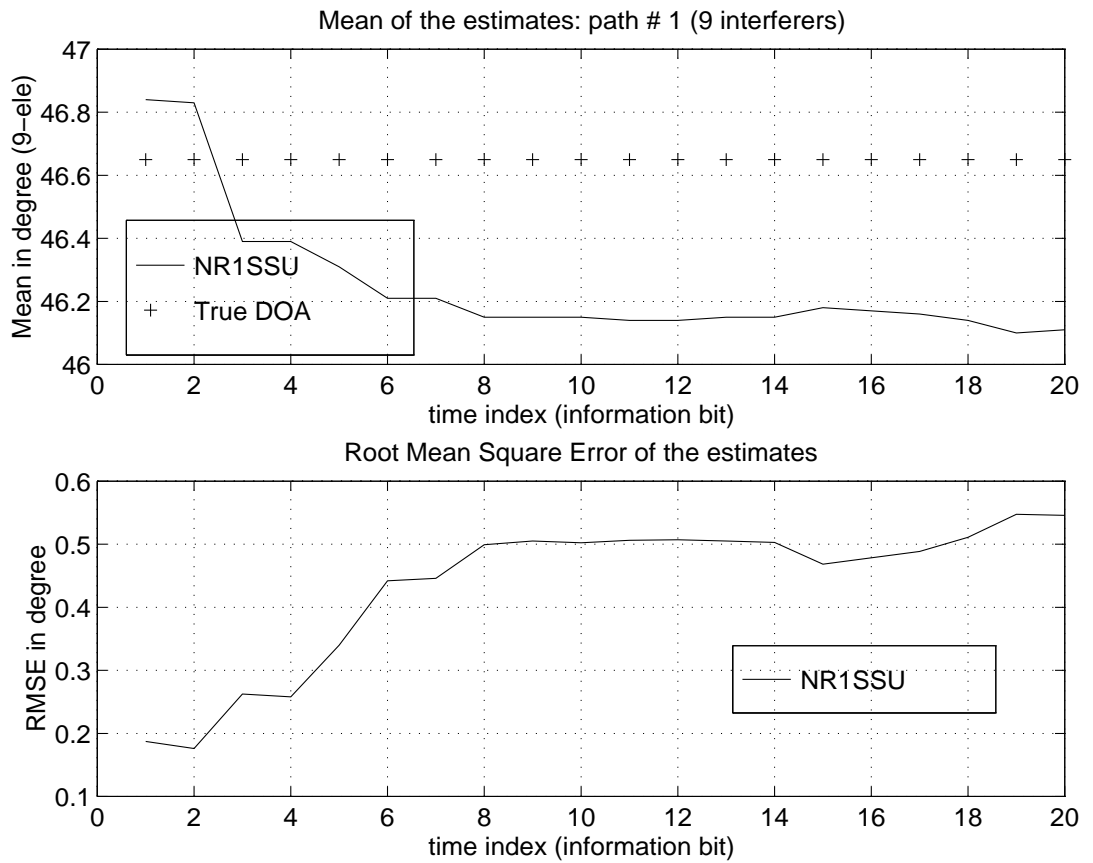


Figure 5.14: Exploiting delay spread with NR1SSU first multipath array response vector estimate in cellular channel, 10 mobiles in total

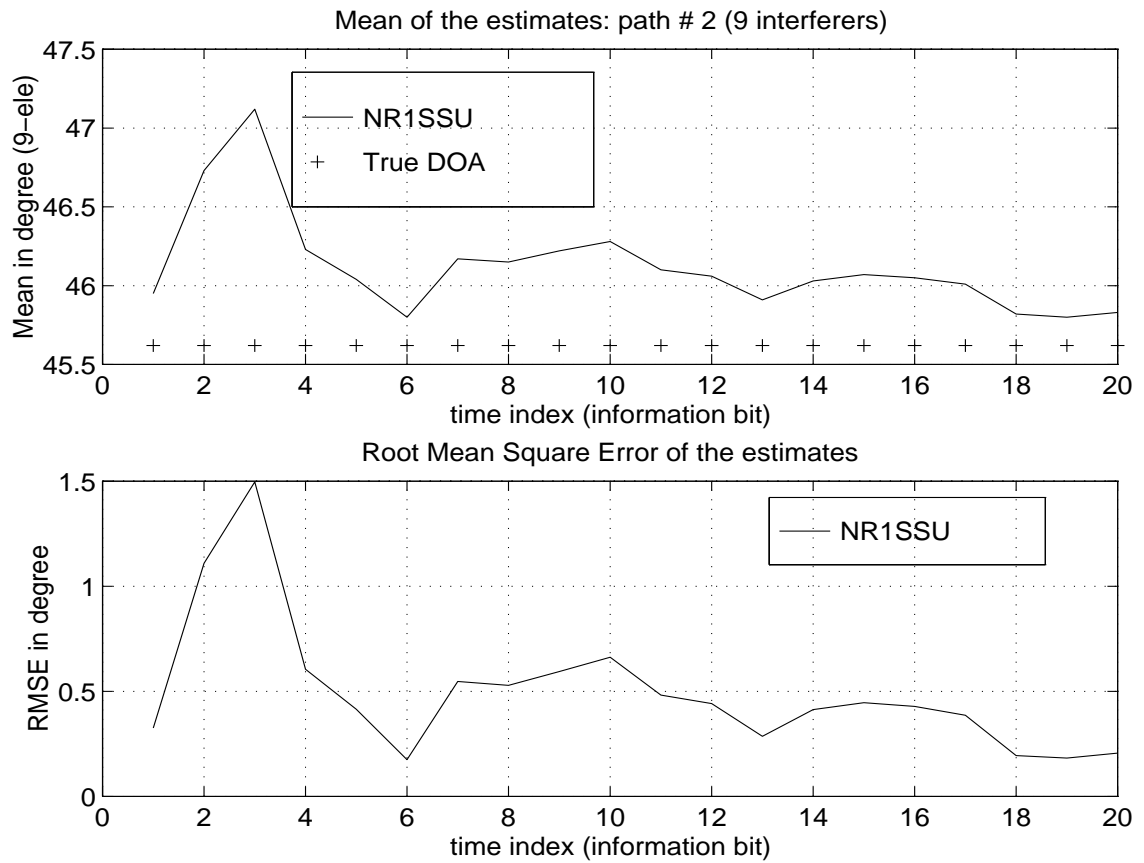


Figure 5.15: Exploiting delay spread with NR1SSU second multipath array response vector estimate in cellular channel, 10 mobiles in total

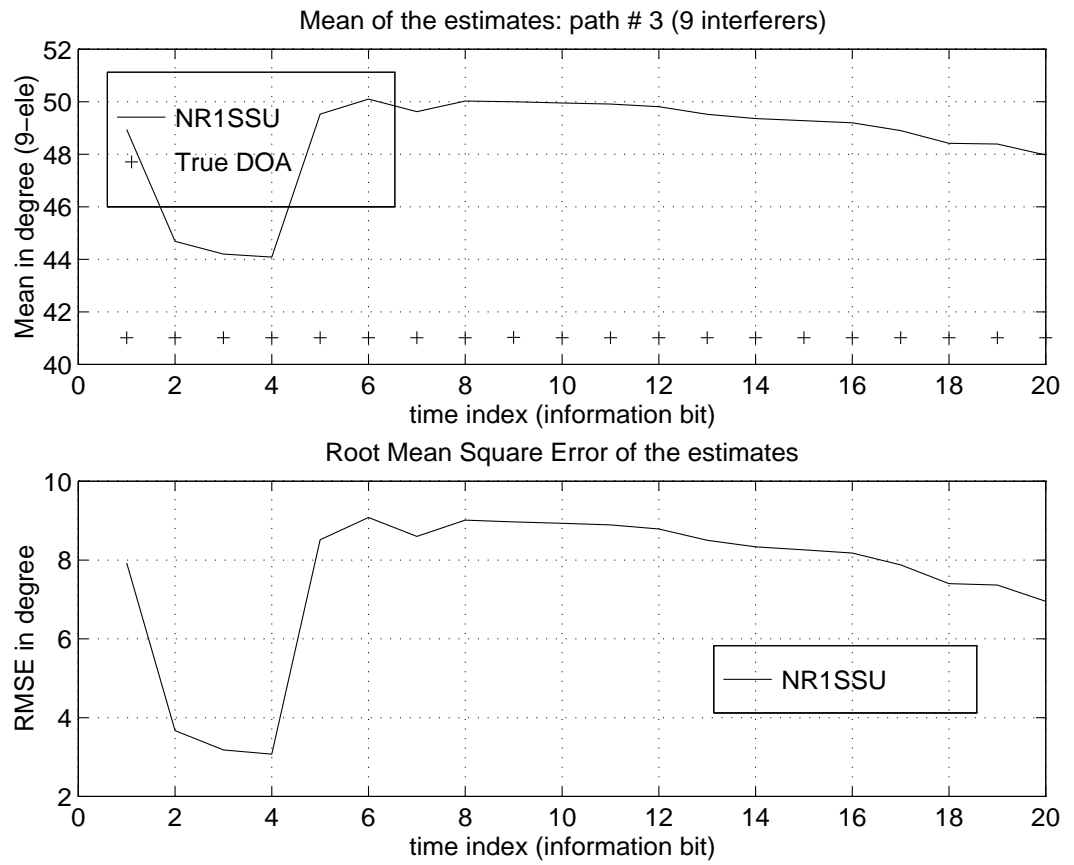


Figure 5.16: Exploiting delay spread with NR1SSU third multipath array response vector estimate in cellular channel, 10 mobiles in total

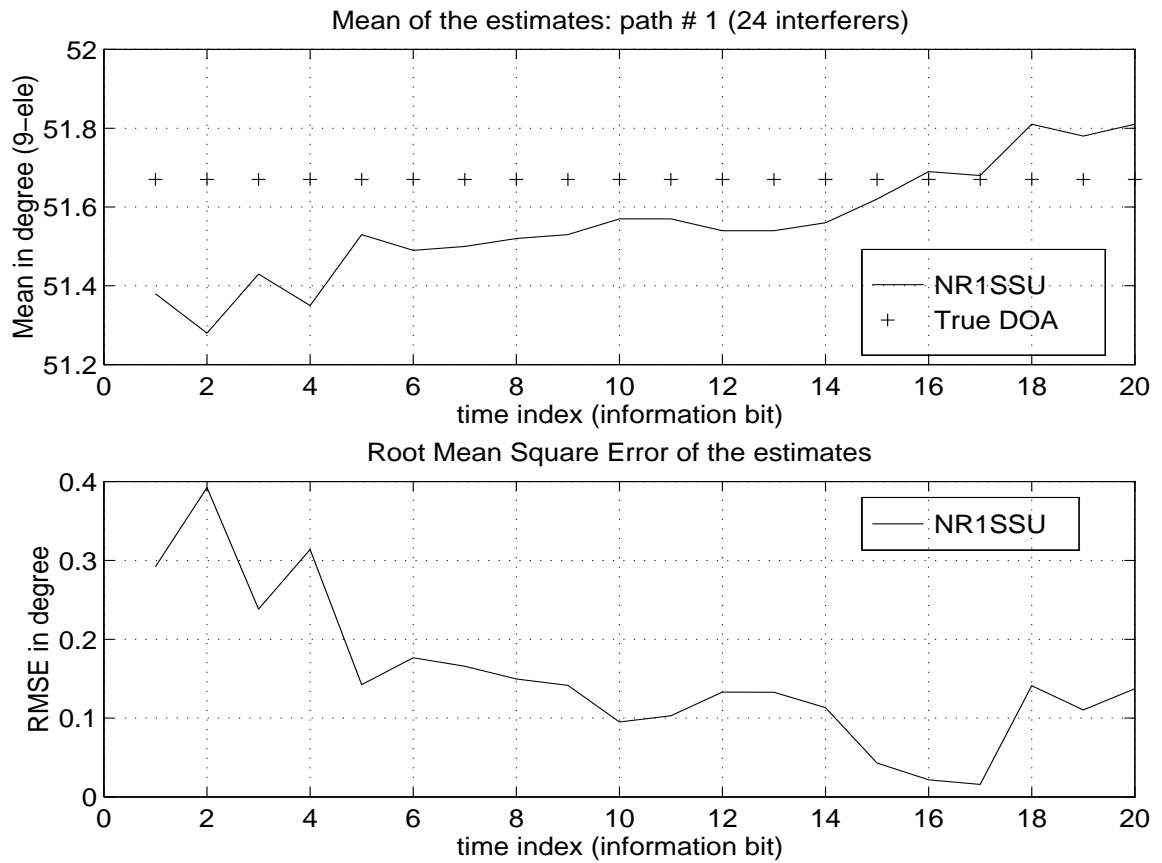


Figure 5.17: Exploiting delay spread with NR1SSU first multipath array response vector estimate in cellular channel, 25 mobiles in total

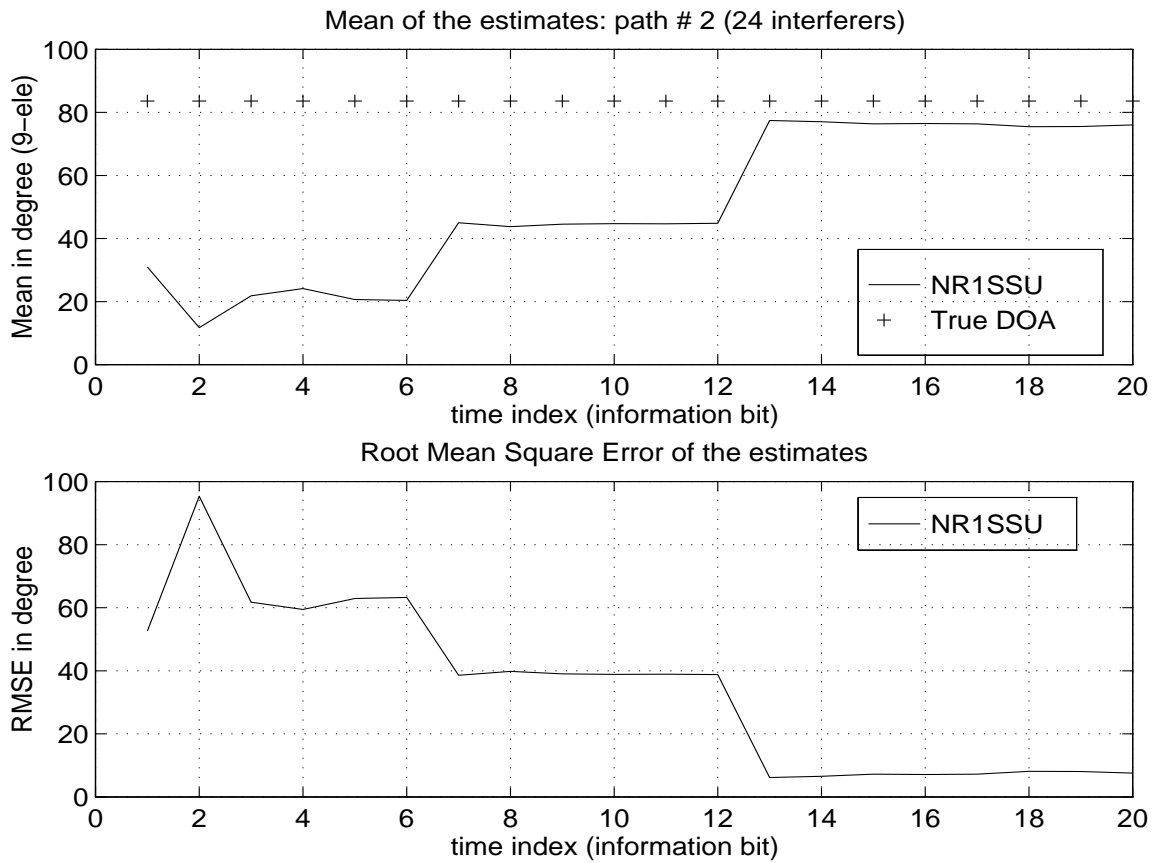


Figure 5.18: Exploiting delay spread with NR1SSU second multipath array response vector estimate in cellular channel, 25 mobiles in total

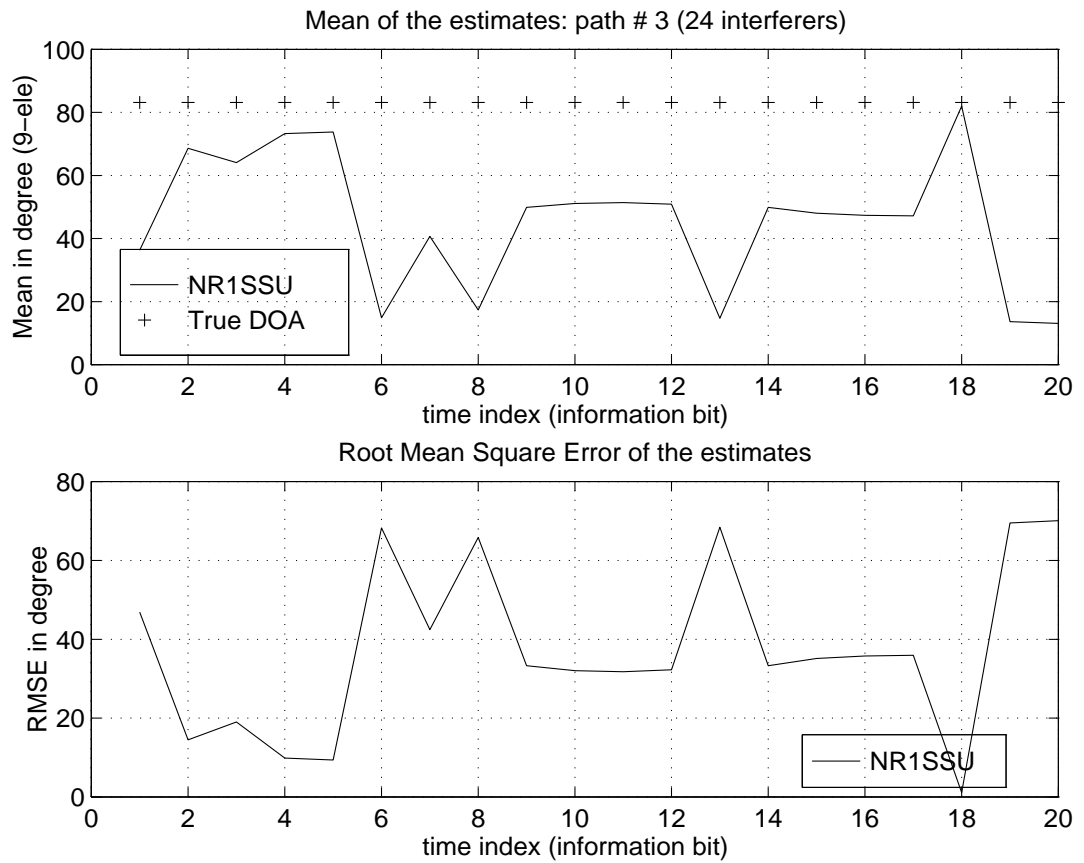


Figure 5.19: Exploiting delay spread with NR1SSU third multipath array response vector estimate in cellular channel, 25 mobiles in total

5.3.3 SNR vs. 2D-RAKE receiver

In this section, we assume a non-zero time delay spread propagation model in which there are three effective multipaths. Note that this is a valid assumption since the delay power profile (DPP) drops dramatically over consecutive path arrivals (field measurements show that multipaths arriving later than the third received path carries negligible power at a channel bandwidth of 1.25Mcps [45] [4]). Therefore, a three-arm RAKE receiver is sufficient to capture about 90% of the total power of a transmitted signal [45]. The power of each multipath is assumed to follow the delay power profile (DPP) of the first dominant received path which is assumed to be independently Rayleigh faded on a 7dB signal-to-noise ratio (SNR). The second received path assumes independent Rayleigh faded on a SNR of -2.5dB, and the third path is independently Rayleigh faded on a -5dB SNR path [45] [29]. It is assumed that power control has been applied to compensate for the long-term channel fluctuations due to propagation path loss and shadowing. Simulations were performed with both 10 and 25 in-band transmitting mobiles, where the number of signals received at the base-station at any time instant were 30 and 75 independently Rayleigh faded paths from 10 and 25 transmitting mobiles, respectively.

Figures 5.14-5.16 and 5.17-5.19 show tracking of the three dominant paths in a 9 and a 24 interferer environment, respectively. For the second strongest path shown in Figures 5.15 and 5.18, the received array response vector tracked fairly well in the 9-interferer environment, but not in the 24-interferer environment. This is due to the fact that the despread interference power plus thermal noise for 24 interferers has higher power level than or equals to the desired despread signal and Equation (4.55) no longer holds. Similarly, based on a -5 dB Rayleigh faded third path for both 9 and 24 interferers (respectively, Figures 5.16 and 5.19), the 9 interferers NR1SSU tracks poorly while the 24 interferers fails to track the very low power third path.

Figures 5.20 and 5.21 show the 3-arm beamsteered RAKE base-station receiver performance for the desired mobile as a function of the number of base-station antenna elements used. Again, the dotted line represents optimum SNR beamforming

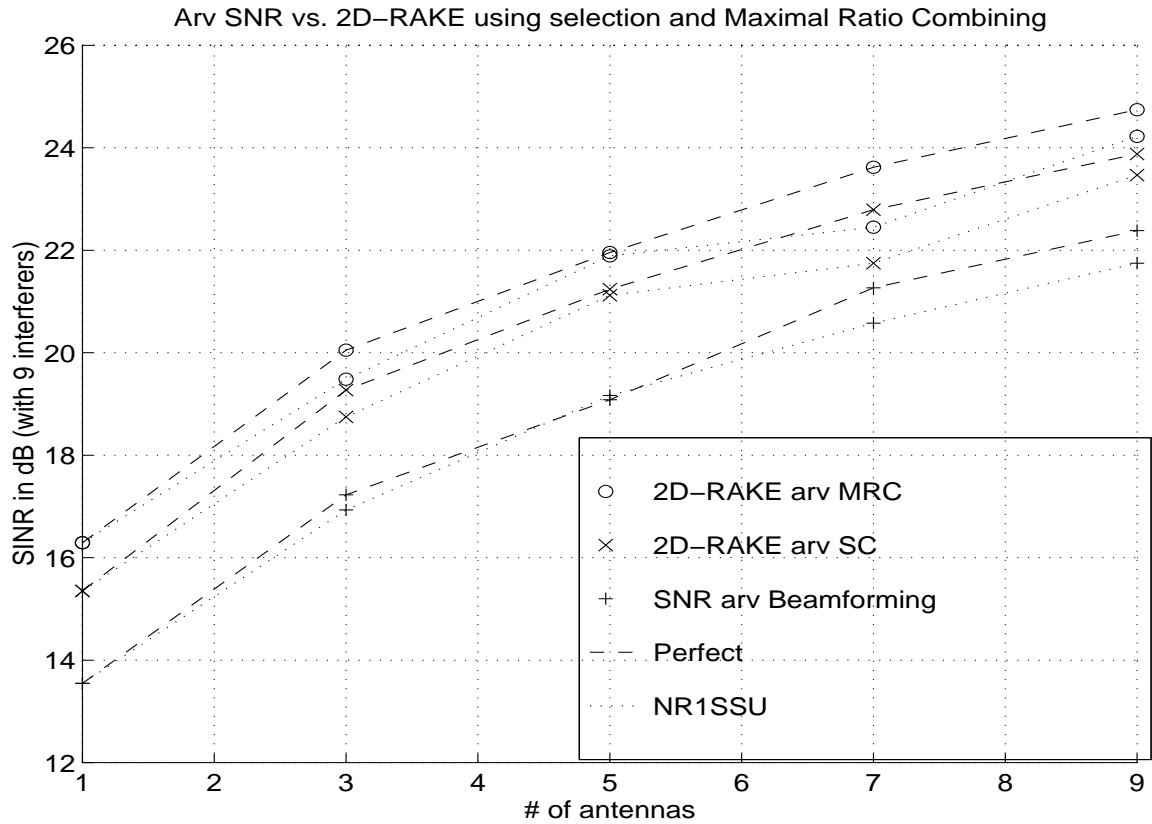


Figure 5.20: Exploiting delay spread with true array response and NR1SSU array response estimate in cellular channel, 10 mobiles in total with beamforming weight as true array response vector

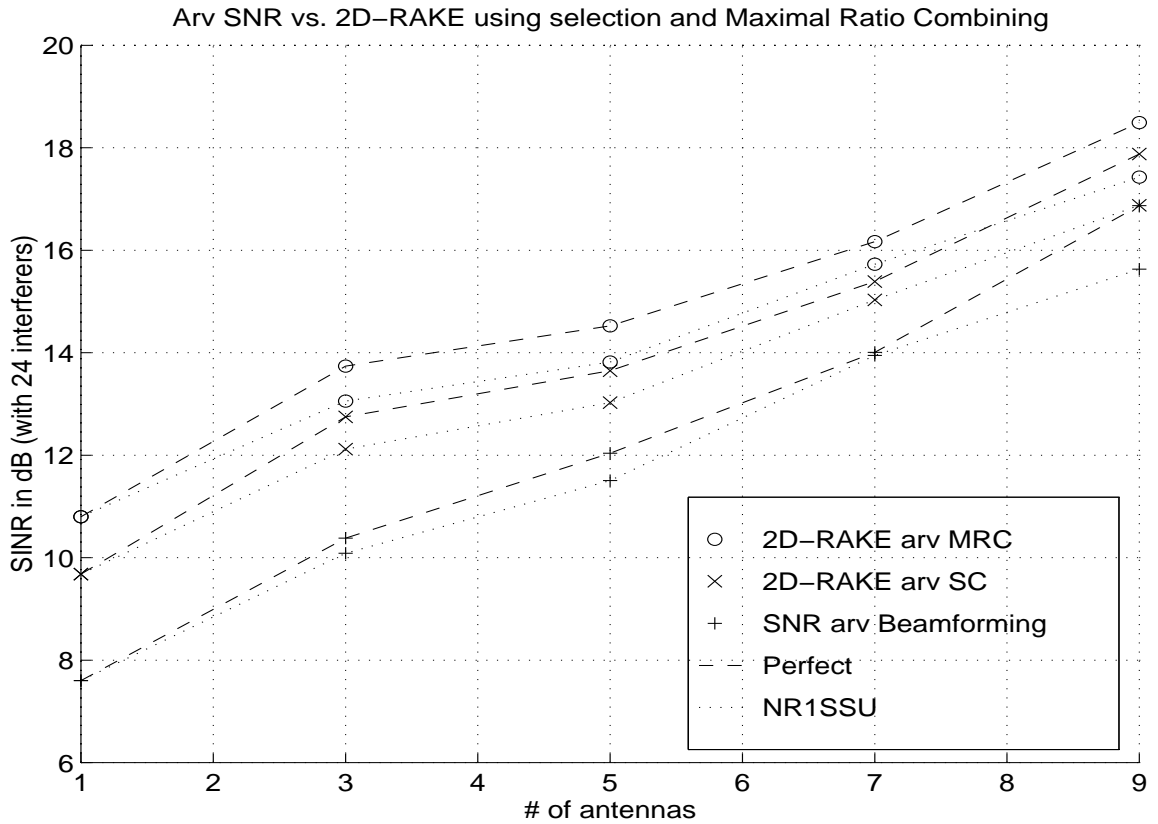


Figure 5.21: Exploiting delay spread with true array response and NR1SSU array response estimate in cellular channel, 25 mobiles in total with beamforming weight as true array response vector

using the NR1SSU tracked array response vector estimate, while the dashed line represents the optimum SNR beamforming using the perfect array response vector for the beamforming weights.

The plus-dotted and plus-dashed lines respectively represent the optimum SNR beamformed signal based on the first received path only with the NR1SSU estimate and the perfect array response vector as the beamforming weights. As shown in Figure 5.20 and 5.21, there is less than 1 dB loss incurred by using the NR1SSU array response vector estimate beamformed signal over the perfect array response vector beamformed signal for both 9 and 24 interferers, respectively.

Note that in this generic CDMA system with a non-zero time delay spread frequency-selective model, no Walsh function decision feedback is being used and the NR1SSU estimate does not incur a one frame time delay. The beamforming weight vector is being updated at a rate of every information bit in all the simulation results shown in Section 5.3.

The crossed-dotted line represents a 3-arm selection diversity combining NR1SSU array response estimate beamsteered-RAKE receiver which selects the highest beamformed signal power path out of the three beamformed time-delay received multipaths. The crossed-dashed line represent a 3-arm selection diversity combining perfect array response beamsteered-RAKE receiver which selects the highest beamformed signal power path out of the three beamformed time-delay received multipaths.

The circle-dotted line represents a 3-arm maximal ratio combining NR1SSU array response estimate beamsteered-RAKE receiver then maximally combines the three time delay NR1SSU beamformed multipath signals by weighting each arm with its multipath perfect channel parameters (channel gain and phase shift parameters). The circle-dashed line represents a 3-arm maximal ratio combining perfect array response beamsteered-RAKE receiver. Each multipath's channel gain and phase shift at every discretized instant of time is assume known for the maximal ratio combining (MRC) operation.

Overall, Figures 5.20 and 5.21 show the effect of exploiting the time delay spread

multipaths received at the base-station. A performance increase of about 2dB gain for selection combining RAKE and about 3dB for maximal-ratio combining RAKE is observed in both the 9 and 24 moving interferer scenarios. As shown, NR1SSU tracking is possible in the time delay spread environment.

5.3.4 Diversity combining

In the diversity combining receiver, it is assumed for each antenna element that the propagation model corresponds to a flat fading channel with zero time delay spread. The antenna array elements are assumed to be widely spaced so that independently faded signals are received at each antenna element. With this widely spaced antenna topology, the received signals at each antenna element are uncorrelated and act as artificial multipath to combat the fluctuating effects of fading.

Figures 5.22 and 5.23 show the simulation results for using maximal ratio diversity combining and selection diversity combining on the uncorrelated signals received at each antenna/channel for 49 and 24 interferers, respectively. For the simulated maximal ratio diversity combining, it has been assumed that the channel parameters are perfectly estimated, which corresponds to the upper bound of a linear diversity combiner [35]. In comparison, the ideal maximal ratio combiner provides about 2 to 3 dB SINR gain over the selection combiner. The above simulations assumed that power control compensates for the long-term fading effect. That is, each received signal is assumed to experience independent short-term Rayleigh fading on a 7dB average transmitted signal power. In other words, the received signal power at each antenna element is assumed to be independently Rayleigh faded on a 7dB signal power for these diversity combining simulations.

5.3.5 Beamforming against Diversity combining

In order to compare the performance of an antenna linear array topology with perfectly correlated fading against an uncorrelated fading signals received at each antenna array element, a beamformer and a diversity combiner were compared with respect to

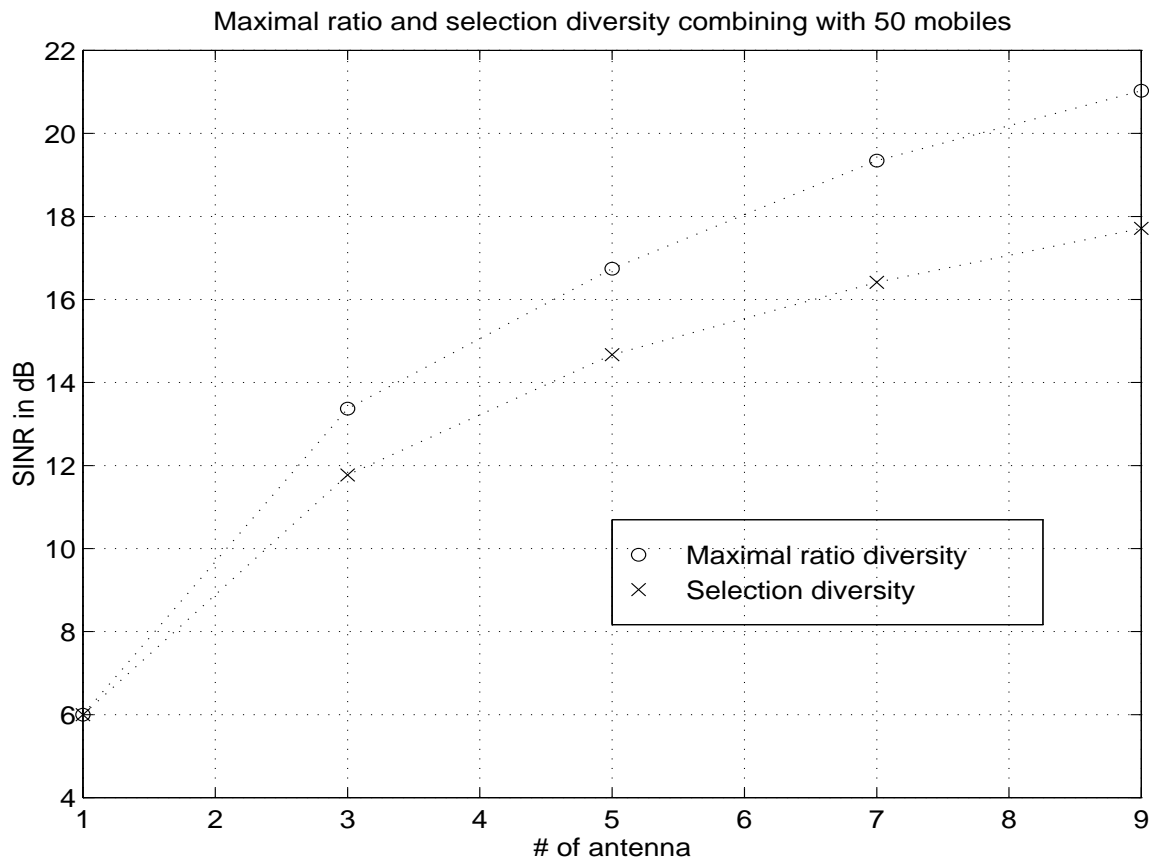


Figure 5.22: Diversity combining of a CDMA system with a single path propagation channel and 50 mobiles

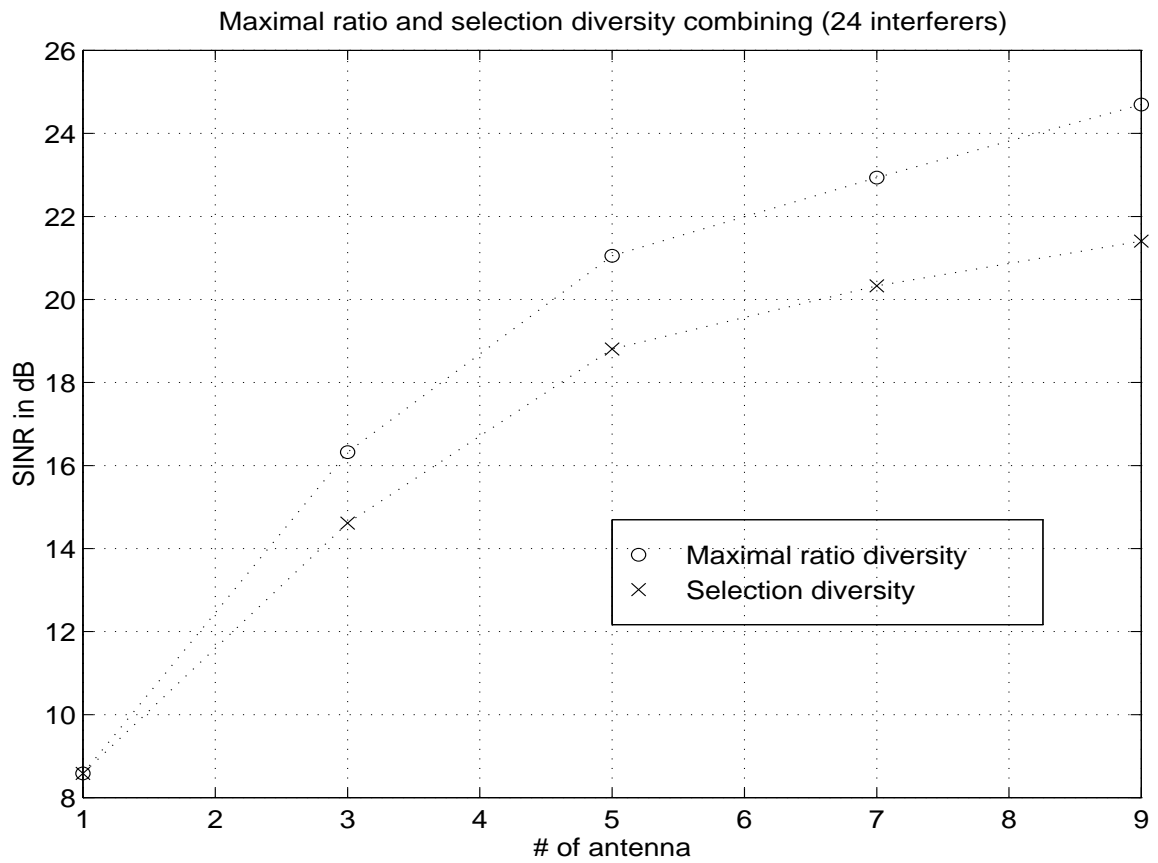


Figure 5.23: Diversity combining of a CDMA system with a single path propagation channel with 25 mobiles

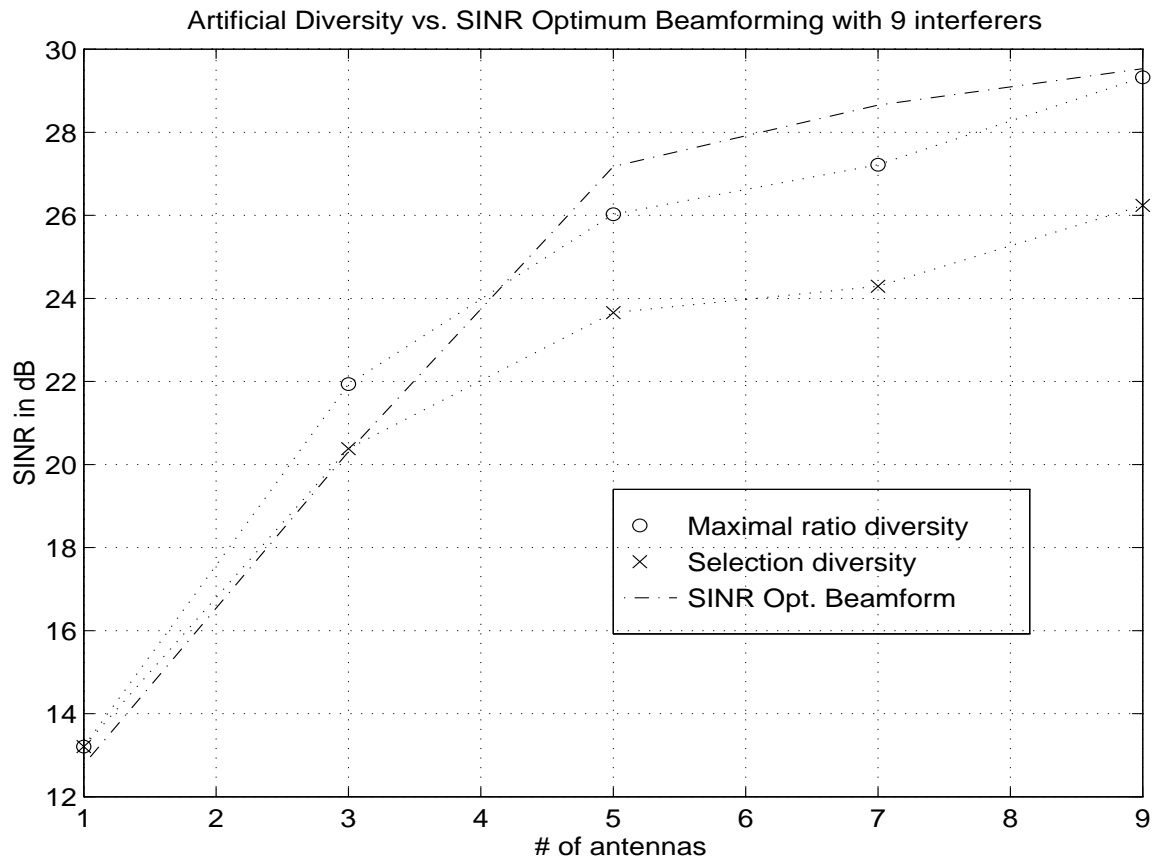


Figure 5.24: Artificial Diversity vs. SINR optimum Beamforming using perfect array response vectors with 10 mobiles in total

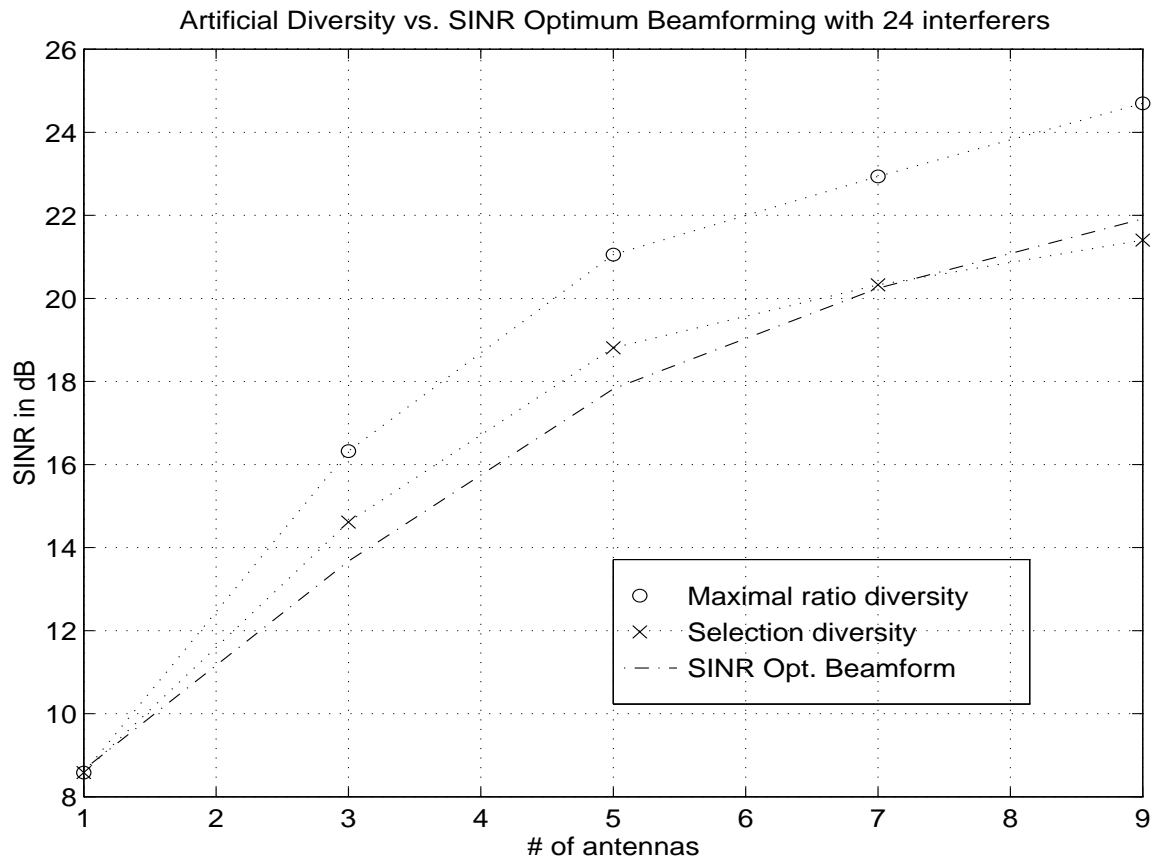


Figure 5.25: Artificial diversity vs. SINR optimum beamforming using perfect array response vector with 25 mobiles in total

their combined signal-to-interference-plus-noise ratio (SINR) under a flat slow fading propagation model. In Figures 5.24 and 5.25, the dashed line represents antenna array with closely-spaced elements with an optimum SINR beamformer which described in Section 5.3.1. The crossed-dotted line and circle-dotted line represent the selection diversity combined and the maximal ratio combined signals' SINR performances respectively using a widely-spaced antenna array. Figures 5.24 and 5.25 shows similar SINR performance at different interference levels of using both a spatial beamformer and a temporal diversity combiner.

5.4 Summary

This chapter has demonstrated through simulation results that the noniterative rank-one signal subspace eigenstructure update (NR1SSU) algorithm can be applied to track the array response vector of a desired signal using the post-correlation matrix. The simulation results also demonstrated that there is a negligible power loss when using the NR1SSU estimated array response vector as compared to the perfect array response vector for optimal SNR beamforming. The desired signal-to-interference-plus-noise performance gap between the optimum SNR and optimum SINR beamforming receivers is significant when the number of interferers is small. For channels with time delay spread, the beamsteered-RAKE receiver structure clearly improved the desired signal-to-interference-plus-noise ratio with about 1 to 2dB gain for selection combining and with about 2 to 3dB gain for maximal ratio combining. Also, spatial beamsteering (i.e. beamforming) was observed to have similar performance to diversity combining under a flat fading channel model.

In summary, NR1SSU algorithm for array response vector estimate can be applied to both zero delay spread flat fading and non-zero delay spread frequency selective fading propagation models.

Chapter 6

Conclusions

6.1 Thesis Conclusions

In conclusion, the noniterative signal subspace eigenstructure update (NR1SSU) algorithm can be applied to track an array response vector accurately with negligible performance loss as compared to the true array response vector in an optimum SNR beamformer. It has been shown that NR1SSU is a promising technique which may be used to track a desired mobile's array response vectors in both a generic CDMA system as well as a IS-95 CDMA system, as long as Walsh function feedback is used to provide a sufficiently large spatial processing gain L such that Equations (4.46) and (4.55) hold. With the proposed NR1SSU algorithm, the computationally expensive formation of a batch covariance matrix is required only at initialization, which occurs infrequently. In addition, NR1SSU sufficiently computes the weight vector update and is noniterative, thereby being highly applicable to real-time operations even for a large number of antenna elements. The performance gap between optimum SNR and optimum SINR beamformer is significant for the case of few interferers. A beam-steered Rake combiner improves beamforming at the receiver for the realistic delay spreads encountered in cellular channels.

The beamforming receiver has roughly equal performance to a diversity combiner for the same number of antennas over a flat fading channel. Therefore, enhancing a diversity system with a beamforming antenna array on each diversity branch should

provide a large potential gain on the desired signal. When a closely-spaced base-station antenna array receiver experiences a deep fade path from the desired mobile, the beamformer may not increase the relative desired despread signal power as much as an artificial diversity receiver would. This is because a diversity combiner exploits the independent fading channels that introduce a higher probability of having a better reception channel whereas a beamsteered-RAKE receiver exploits only the time delay multipath signals which depends on the delay power profile of the channel.

6.2 Summary of the Thesis Contributions

In summary, this thesis has made the following contributions:

- A noniterative subspace eigenstructure update algorithm was implemented in a novel application to track the array response vector of the desired signal in a CDMA system.
- The analytical conditions for applying a noniterative subspace method to a CDMA communication system were derived.
- The precise computational requirements of the NR1SSU algorithm (in flops) per optimum SNR beamforming weight vector update was evaluated.
- The performance of NR1SSU in both IS-95 and generic CDMA systems for the reverse link at the rate of one frame per weight vector update were evaluated.
- The differences between diversity combining and beamforming base-station receivers under a flat fading channel at the rate of one information bit per weight vector update were evaluated.
- The performance of a beamsteered-RAKE receiver which increases the desired received SINR gain by exploiting the time delay multipath under a frequency-selective fading channel at the rate of one information bit per weight vector update was evaluated.

6.3 Future work

Despite encouraging results, further improvements may be realized through estimating the interference-plus-noise covariance matrix for optimum SINR beamforming. The investigations described in this thesis could be extended to determine cell capacity.

Future investigations could be performed on a higher chip rate bandwidth CDMA system which would provide a higher processing gain and possible multimedia wireless communication such as high data rate video transmissions. Higher information bit transmission rates will have an advantage in a harsh propagation environment with small coherence time where the fading effect over an information bit is relatively flat, however, with relatively higher powers of consecutive multipaths and a proportionally larger number of non-negligible resolvable multipaths arriving [45], [29]. Relatively higher time delay multipaths implies that the Rake receiver will have a better advantage to combat the effects of fading which in turn should increase the SINR.

In addition, speed estimation or speed classifications of mobiles can serve to identify how frequent the weight vectors should be updated in order to reflect the correct slow or fast fading environment.

Appendix A

Zero time delay spread propagation model autocovariance matrix derivations

A.1 Pre-correlation and Post-correlation vectors

The baseband signal vector received at the base station antenna array is [29] [19] [27] [24]

$$\begin{aligned}\mathbf{x}_i(t) &= \sum_{j=1}^N \varrho_j(t) e^{-j\omega_c \tau_{i,j}} A_j(t) c_j(t - \tau_{i,j}) b_j(t - \tau_{i,j}) \mathbf{a}_j(t) + \mathbf{n}(t) \\ &= \sum_{j=1}^N \sqrt{P_j(t)} c_j(t - \tau_{i,j}) b_j(t - \tau_{i,j}) \mathbf{a}_j(t) + \mathbf{n}(t)\end{aligned}\quad (\text{A.1})$$

where N is the total number of mobiles in the current cell, $c_j(t - \tau_{i,j}) \in \{1, -1\}$ of period T_c is the pseudo noise (PN) code at time t for the j^{th} mobile with a time delay of $\tau_{i,j} \in (-T_c, T_c)$ relative to the i^{th} mobile's time delay, $b_j(t - \tau_{i,j}) \in \{1, -1\}$ of T_b period is the information bit of the j^{th} mobile, $\mathbf{n}(t) \in \mathcal{N}(0, \sigma^2 \mathbf{I})$ is the noise vector at time t , $\mathbf{a}_j(t)$ is the channel array response of the j^{th} mobile received at time t , and $\sqrt{P_j(t)} = \varrho_j(t) e^{-j\omega_c \tau_{i,j}} A_j(t)$ is the j^{th} mobile's received energy with channel gain $\varrho_j(t)$, channel phase shift $\omega_c \tau_{i,j}$, and transmitted amplitude $A_j(t)$.

Without loss of generality, it is assumed that for all $i = 1, 2, \dots, N$ and $j = 1, 2, \dots, N$, synchronization with the i^{th} mobile is possible, i.e. $\tau_{i,i} = 0$. Also, the information bits $b_i(t - \tau_{i,j})$ are assumed to be mutually uncorrelated with the noise

and the PN chip $c_i(t - \tau_{i,j})$ are assumed to be mutually uncorrelated with the noise, for all $i = 1, 2, \dots, N$ and $j = 1, 2, \dots, N$.

The PN code filtering post-correlation vector at discrete time n with a $(1/T_b)$ sampling rate is then

$$\begin{aligned}
\mathbf{z}_i(n) &= \frac{1}{\sqrt{T_b}} \int_{nT_b}^{(n+1)T_b} \mathbf{x}_i(t) c_i(t) dt \\
&= \frac{1}{\sqrt{T_b}} \int_{nT_b}^{(n+1)T_b} \sqrt{P_i(t)} b_i(t) c_i(t) c_i(t) \mathbf{a}_i(t) dt \\
&\quad + \frac{1}{\sqrt{T_b}} \sum_{j=1, j \neq i}^N \int_{nT_b}^{(n+1)T_b} \sqrt{P_j(t)} b_j(t - \tau_{i,j}) c_j(t - \tau_{i,j}) c_i(t) \mathbf{a}_j(t) dt \\
&\quad + \frac{1}{\sqrt{T_b}} \int_{nT_b}^{(n+1)T_b} c_i(t) \mathbf{n}(t) dt
\end{aligned} \tag{A.2}$$

The power $P_j(t)$ and the array response vector $\mathbf{a}_j(t)$ are assumed approximately do not change appreciably over the time period T_b (i.e. slow fading channel) for $j = 1, 2, \dots, N$. Then, the PN code despreading vector becomes

$$\begin{aligned}
\mathbf{z}_i(n) &= \sqrt{T_b} \sqrt{P_i(n)} b_i(n) \mathbf{a}_i(n) \\
&\quad + \frac{1}{\sqrt{T_b}} \sum_{j=1, j \neq i}^N \sqrt{P_j(n)} \mathbf{a}_j(n) \int_{nT_b}^{(n+1)T_b} b_j(t - \tau_{i,j}) c_j(t - \tau_{i,j}) c_i(t) dt \\
&\quad + \frac{1}{\sqrt{T_b}} \int_{nT_b}^{(n+1)T_b} c_i(t) \mathbf{n}(t) dt
\end{aligned} \tag{A.3}$$

A.1.1 The PN code pre-correlation matrix of the received stochastic signal vector

The mean of the pre-correlation signal is

$$\mathbf{E}\{\mathbf{x}_i(t)\} = \mathbf{0} \tag{A.4}$$

since the Pseudo-noise has an expected value of zero, $\mathbf{E}\{c_j(t)\} = 0$, and the thermal noise also has an expected value of zero, $\mathbf{E}\{\mathbf{n}(t)\} = 0$.

The autocovariance of the pre-correlation signal vector is then

$$\mathbf{R}_{xx_i}(t_1, t_2) = \mathbf{E}\{\mathbf{x}_i(t_1) \mathbf{x}_i(t_2)^\dagger\}$$

$$\begin{aligned}
&= \sum_{j=1}^N \sum_{k=1}^N \sqrt{P_j(t_1)P_k(t_2)} \mathbf{E}\{c_j(t_1 - \tau_{i,j})c_k(t_2 - \tau_{i,k})\} \mathbf{E}\{b_j(t_1 - \tau_{i,j})b_k(t_2 - \tau_{i,k})\} \\
&\quad \mathbf{a}_j(t_1)\mathbf{a}_k(t_2)^\dagger + \mathbf{E}\{\mathbf{n}(t_1)\mathbf{n}(t_2)^\dagger\}
\end{aligned}$$

Due to the fact that $c_j(t - \tau_j) = 0$ for $|\tau_j| > T_c$, therefore, the expected value of $c_j(t)$ and $c_i(t)$ is zero for $i \neq j$ and $i, j = 1, 2, \dots, N$. In addition, $b_j(t - \tau_j) = 0$ for $|\tau_j| > T_c$ and the expected value of $b_j(t)$ and $b_i(t)$ is zero for $i \neq j$ and $i, j = 1, 2, \dots, N$. This gives [29] [41] (also refer to Appendix C)

$$\mathbf{E}\{c_j(t_1 - \tau_{i,j})c_j(t_2 - \tau_{i,j})\} = \Lambda\left(\frac{t_1 - t_2}{T_c}\right) \quad (\text{A.5})$$

$$\mathbf{E}\{b_j(t_1 - \tau_{i,j})b_j(t_2 - \tau_{i,j})\} = \Lambda\left(\frac{t_1 - t_2}{T_b}\right) \quad (\text{A.6})$$

where it has been defined that

$$\Lambda\left(\frac{t_1 - t_2}{T_b}\right) = \begin{cases} 1 - \frac{|t_1 - t_2|}{T_b} & \text{for } |t_1 - t_2| < T_b \\ 0 & \text{elsewhere} \end{cases}$$

and

$$\Lambda\left(\frac{t_1 - t_2}{T_c}\right) = \begin{cases} 1 - \frac{|t_1 - t_2|}{T_c} & \text{for } |t_1 - t_2| < T_c \\ 0 & \text{elsewhere} \end{cases}$$

The pre-correlation covariance matrix becomes

$$\begin{aligned}
&\mathbf{R}_{xx_i}(t_1, t_2) \\
&= \sum_{j=1}^N \sqrt{P_j(t_1)P_j(t_2)} \mathbf{E}\{c_j(t_1 - \tau_{i,j})c_j(t_2 - \tau_{i,j})\} \mathbf{E}\{b_j(t_1 - \tau_{i,j})b_j(t_2 - \tau_{i,j})\} \\
&\quad \mathbf{a}_j(t_1)\mathbf{a}_j(t_2)^\dagger + \mathbf{E}\{\mathbf{n}(t_1)\mathbf{n}(t_2)^\dagger\} \\
&= \sum_{j=1}^N \sqrt{P_j(t_1)P_j(t_2)} \Lambda\left(\frac{t_1 - t_2}{T_c}\right) \Lambda\left(\frac{t_1 - t_2}{T_b}\right) \mathbf{a}_j(t_1)\mathbf{a}_j(t_2)^\dagger + \delta(t_1 - t_2)\sigma^2\mathbf{I} \quad (\text{A.7})
\end{aligned}$$

Therefore, the variance of the pre-correlation covariance matrix is then

$$\begin{aligned}
\mathbf{R}_{xx_i}(0) &= \mathbf{E}\{\mathbf{x}_i(t)\mathbf{x}_i(t)^\dagger\} = \mathbf{R}_{xx_i}(t, t) \\
&= \sum_{j=1}^N P_j(t)\mathbf{a}_j(t)\mathbf{a}_j(t)^\dagger + \sigma^2\mathbf{I} \quad (\text{A.8})
\end{aligned}$$

A.1.2 The PN code post-correlation covariance matrix of the received stochastic signal vector

The mean of the despread signal vector in Equation (A.3) is

$$\mathbf{E}\{\mathbf{z}_i(n)\} = \mathbf{0} \quad (\text{A.9})$$

and the autocovariance matrix of the despread random signal vector is defined as

$$\begin{aligned} \mathbf{R}_{z z_i}(n_1, n_2) &= \frac{1}{T_c} \mathbf{E}\{\mathbf{z}_i(n_1)\mathbf{z}_i(n_2)^\dagger\} \\ &= \frac{T_b}{T_c} \sqrt{P_i(n_1)P_i(n_2)} \mathbf{E}\{b_i(n_1)b_i(n_2)\} \mathbf{a}_i(n_1)\mathbf{a}_i(n_2)^\dagger \\ &\quad + \sum_{j=1, j \neq i}^N \sum_{k=1, k \neq i}^N \frac{\sqrt{P_j(n_1)P_k(n_2)}}{T_c T_b} \mathbf{w}_i(n_1)^\dagger \mathbf{a}_j(n_1)\mathbf{a}_k(n_2)^\dagger \mathbf{w}_i(n_2) \int_{nT_b}^{(n+1)T_b} \int_{nT_b}^{(n+1)T_b} \\ &\quad \mathbf{E}\{c_j(t_1 - \tau_{i,j})c_k(t_2 - \tau_{i,k})\} \mathbf{E}\{c_i(t_1)c_i(t_2)\} \mathbf{E}\{b_j(t - \tau_{i,j})b_k(t - \tau_{i,k})\} dt_1 dt_2 \\ &\quad + \frac{1}{T_c T_b} \int_{nT_b}^{(n+1)T_b} \int_{nT_b}^{(n+1)T_b} \mathbf{E}\{\mathbf{n}(t_1)\mathbf{n}(t_2)^\dagger\} \mathbf{E}\{c_i(t_1)c_i(t_2)\} dt_1 dt_2 \end{aligned} \quad (\text{A.10})$$

From Equations (A.5) and (A.6), the PN code post-correlation covariance matrix of the despread signal becomes

$$\begin{aligned} &\mathbf{R}_{z z_i}(n_1, n_2) \\ &= \frac{T_b}{T_c} \sqrt{P_i(n_1)P_i(n_2)} \mathbf{a}_i(n_1)\mathbf{a}_i(n_2)^\dagger \mathbf{\Lambda}\left(\frac{n_1 - n_2}{T_b}\right) \\ &\quad + \sum_{j=1, j \neq i}^N \sqrt{P_j(n_1)P_j(n_2)} \mathbf{a}_j(n_1)\mathbf{a}_j(n_2)^\dagger \left(\frac{1}{T_b T_c}\right) \int_{nT_b}^{(n+1)T_b} \int_{nT_b}^{(n+1)T_b} \\ &\quad \mathbf{\Lambda}\left(\frac{t_1 - t_2}{T_c}\right)^2 \mathbf{\Lambda}\left(\frac{t_1 - t_2}{T_b}\right) dt_1 dt_2 \\ &\quad + \frac{\sigma^2}{T_b T_c} \int_{nT_b}^{(n+1)T_b} \int_{nT_b}^{(n+1)T_b} \delta(t_1 - t_2) \mathbf{\Lambda}\left(\frac{t_1 - t_2}{T_c}\right) \mathbf{I} dt_1 dt_2 \end{aligned} \quad (\text{A.11})$$

Let $\xi = t_1 - t_2$ and $\eta = t_1 + t_2$, and by using the Jacobian transformation, the above equation becomes

$$\left| \frac{d(t_1, t_2)}{d(\xi, \eta)} \right| = \frac{1}{2}$$

The first integral in eqn.(A.11) can then be simplified to

$$Int_1 = \frac{1}{T_b} \int_{nT_b}^{(n+1)T_b} \int_{nT_b}^{(n+1)T_b} \mathbf{\Lambda}\left(\frac{t_1 - t_2}{T_c}\right)^2 \mathbf{\Lambda}\left(\frac{t_1 - t_2}{T_b}\right) dt_1 dt_2$$

$$\begin{aligned}
&= \frac{1}{T_b} \int_{-T_b}^{T_b} \int_{2nT_b+\xi}^{2nT_b+2T_b-\xi} \Lambda\left(\frac{\xi}{T_c}\right)^2 \Lambda\left(\frac{\xi}{T_b}\right) \left(\frac{1}{2}\right) d\eta d\xi \\
&= \frac{1}{T_b} \int_{-T_b}^{T_b} \Lambda\left(\frac{\xi}{T_c}\right)^2 \Lambda\left(\frac{\xi}{T_b}\right) (T_b - \xi) d\xi \\
&= \frac{1}{T_b} \int_{-T_c}^{T_c} \left(1 - \frac{|\xi|}{T_c}\right)^2 \left(1 - \frac{|\xi|}{T_b}\right) (T_b - \xi) d\xi \quad \text{for } |\xi| < T_c \text{ and } |\xi| < T_b \\
&= \frac{1}{T_b} \left(\int_{-T_c}^0 \left(1 - \frac{-\xi}{T_c}\right)^2 \left(1 - \frac{-\xi}{T_b}\right) (T_b - \xi) d\xi + \int_0^{T_c} \left(1 - \frac{\xi}{T_c}\right)^2 \left(1 - \frac{\xi}{T_b}\right) (T_b - \xi) d\xi \right) \\
&= \frac{1}{T_b} \int_0^{T_c} \left(1 - \frac{\xi}{T_c}\right)^2 \left(1 - \frac{\xi}{T_b}\right) (T_b + \xi + T_b - \xi) d\xi \\
&= 2 \int_0^{T_c} \left(1 - \frac{\xi}{T_c}\right)^2 \left(1 - \frac{\xi}{T_b}\right) d\xi
\end{aligned}$$

$T_b \gg T_c$ implies that $(T_c/T_b)^2 \approx 0$. Therefore, Int_1 becomes

$$\begin{aligned}
Int_1 &= 2 \int_0^{T_c} \left(1 - \frac{\xi}{T_b} + \frac{\xi^2}{T_c^2} - \frac{\xi^3}{T_c^2 T_b} - \frac{2\xi}{T_c} + \frac{2\xi^2}{T_c T_b}\right) d\xi \\
&= 2 \left[\xi - \frac{\xi^2}{2T_b} + \frac{\xi^3}{3T_c^2} - \frac{\xi^4}{4T_c^2 T_b} - \frac{\xi^2}{T_c} + \frac{2\xi^3}{3T_c T_b} \right]_0^{T_c} \\
&= 2 \left(T_c - \frac{T_c^2}{2T_b} + \frac{T_c}{3} - \frac{T_c^2}{4T_b} - T_c + \frac{2T_c^2}{3T_b} \right) \approx \frac{2T_c}{3} \tag{A.12}
\end{aligned}$$

Now we consider the integral of the third term in Equation (A.11). Again, by substituting $\xi = t_1 - t_2$ and $\eta = t_1 + t_2$, we have

$$\begin{aligned}
Int_2 &= \frac{1}{T_b} \int_{nT_b}^{(n+1)T_b} \int_{nT_b}^{(n+1)T_b} \delta(t_1 - t_2) \Lambda\left(\frac{t_1 - t_2}{T_c}\right) dt_1 dt_2 \\
&= \frac{1}{T_b} \int_{-T_b}^{T_b} \delta(\xi) \Lambda\left(\frac{\xi}{T_c}\right) (T_b - \xi) d\xi \\
&= \int_{-T_c}^{T_c} \delta(\xi) \Lambda\left(\frac{\xi}{T_c}\right) d\xi \\
&= 1 \tag{A.13}
\end{aligned}$$

Combining Equations (A.12) and (A.13), the autocovariance of the post-correlation in Equation (A.11) becomes,

$$\begin{aligned}
\mathbf{R}_{zz_i}(n_1, n_2) &= \frac{T_b}{T_c} \sqrt{P_i(n_1)P_i(n_2)} \mathbf{a}_i(n_1) \mathbf{a}_i(n_2)^\dagger \Lambda\left(\frac{n_1 - n_2}{T_b}\right) \\
&\quad + \frac{2}{3} \sum_{j=1, j \neq i}^N \sqrt{P_j(n_1)P_j(n_2)} \mathbf{a}_j(n_1) \mathbf{a}_j(n_2)^\dagger
\end{aligned}$$

$$+ \frac{\sigma^2}{T_c} \mathbf{I} \quad (\text{A.14})$$

Therefore, the variance of the post-correlation covariance matrix, $\mathbf{R}_{zz_i}(0)$, is

$$\begin{aligned} \mathbf{R}_{zz_i}(0) &= \mathbf{E}\{\mathbf{z}_i(n)\mathbf{z}_i(n)^\dagger\} = \mathbf{R}_{zz_i}(n, n) \\ &= \frac{T_b}{T_c} P_i(n) \mathbf{a}_i(n) \mathbf{a}_i(n)^\dagger + \frac{2}{3} \sum_{j=1, j \neq i}^N P_j(n) \mathbf{a}_j(n) \mathbf{a}_j(n)^\dagger \\ &\quad + \frac{1}{T_c} \sigma^2 \mathbf{I} \end{aligned} \quad (\text{A.15})$$

A.2 The SINR of the weighted post-correlation vector

From Equation (A.15), the weighted post-correlation vector's signal-to-interference-noise ratio (SINR) for the i^{th} mobile branch is

$$\begin{aligned} \text{SINR}_{\text{post}_i} &= \frac{\frac{T_b P_i(n)}{T_c} \mathbf{w}_i(n)^\dagger \mathbf{a}_i(n) \mathbf{a}_i(n)^\dagger \mathbf{w}_i(n)}{\sum_{j=1, j \neq i}^N \frac{2}{3} P_j(n) \mathbf{w}_i(n)^\dagger \mathbf{a}_j(n) \mathbf{a}_j(n)^\dagger \mathbf{w}_i(n) + \frac{1}{T_c} \sigma^2 \mathbf{w}_i(n)^\dagger \mathbf{w}_i(n)} \\ &= \frac{P_i(n) \|\mathbf{w}_i(n)^\dagger \mathbf{a}_i(n)\|^2 / B}{\sum_{j=1, j \neq i}^N \frac{2}{3 W_{ss}} P_j(n) \|\mathbf{w}_i(n)^\dagger \mathbf{a}_j(n)\|^2 + \sigma^2 \|\mathbf{w}_i(n)\|^2} \end{aligned} \quad (\text{A.16})$$

where $B = 1/T_b$ is the information bit bandwidth and W_{ss} is the PN chip bandwidth.

Appendix B

Non-zero time delay spread autocovariance derivations

B.1 Pre-correlation and Post-correlation vectors

For the non-zero time delay spread propagation model, the general form of the l^{th} arm of the RAKE received baseband signal vector at time t can be generalized to [25]

$$\begin{aligned}
\mathbf{x}_{i,l}(t) &= \sum_{j=1}^N \sum_{p=1}^{K_j} \sqrt{P_{j,p}(t)} c_j(t - pT_c - \tau_{il,jp}) b_j(t - pT_c - \tau_{il,jp}) \mathbf{a}_{j,p}(t) + \mathbf{n}(t) \\
&= \sum_{j=1}^N \sum_{p=1}^{K_j} \sqrt{P_{j,p}(t)} c_{j,p}(t - \tau_{il,jp}) b_j(t - pT_c - \tau_{il,jp}) \mathbf{a}_{j,p}(t) + \mathbf{n}(t) \\
&= \sqrt{P_{i,l}(t)} c_{i,l}(t) b_i(t - lT_c) \mathbf{a}_{i,l}(t) \\
&\quad + \sum_{p=1, p \neq l}^{K_i} \sqrt{P_{i,p}(t)} c_{i,p}(t - \tau_{il,ip}) b_i(t - pT_c - \tau_{il,ip}) \mathbf{a}_{i,p}(t) \\
&\quad + \sum_{j=1, j \neq i}^N \sum_{p=1}^{K_j} \sqrt{P_{j,p}(t)} c_{j,p}(t - \tau_{il,jp}) b_j(t - pT_c - \tau_{il,jp}) \mathbf{a}_{j,p}(t) + \mathbf{n}(t) \tag{B.1}
\end{aligned}$$

where $\forall j$, K_j is the number of resolvable multipaths arriving at the base station antenna array from the j^{th} mobile, N is the total number of mobiles in the cell, $c_{j,p}(t - \tau_{il,jp}) = c_j(t - pT_c - \tau_{il,jp}) \in \{1, -1\}$ are the j^{th} mobile's p^{th} path Pseudo-Noise (PN) code square pulses of period T_c at time t , $\tau_{il,jp} \in [-T_c, T_c]$ is the relative time delay of the j^{th} mobile's p^{th} path to the i^{th} mobile's l^{th} path, $b_j(t - pT_c - \tau_{il,jp}) \in \{1, -1\}$ is the j^{th} mobile's p^{th} multipath information bit square pulse of period T_b ,

$\mathbf{n}(t) \in \mathcal{N}(0, \sigma^2 \mathbf{I})$ is the noise vector received at time t , and $\mathbf{a}_{j,p}(t)$ is the j^{th} mobile's p^{th} path channel array response vector.

The baseband post-correlation signal vector sampled at discrete time $1/T_b$ synchronized to the i^{th} mobile's l^{th} multipath, i.e. $\tau_{il,il} = 0$, is then

$$\begin{aligned}
\mathbf{z}_{i,l}(n) &= \frac{1}{\sqrt{T_b}} \int_{nT_b}^{(n+1)T_b} x_{i,l}(t) c_{i,l}(t) dt \\
&= \frac{1}{\sqrt{T_b}} \int_{nT_b}^{(n+1)T_b} \sqrt{P_{i,l}(t)} b_i(t - lT_c) c_{i,l}(t) c_{i,l}(t) \mathbf{a}_{i,l}(t) dt \\
&\quad + \frac{1}{\sqrt{T_b}} \sum_{p=1, p \neq l}^{K_i} \int_{nT_b}^{(n+1)T_b} \sqrt{P_{i,p}(t)} b_i(t - pT_c - \tau_{il,ip}) c_{i,p}(t - \tau_{il,ip}) c_{i,l}(t) \mathbf{a}_{i,p}(t) dt \\
&\quad + \frac{1}{\sqrt{T_b}} \sum_{j=1, j \neq i}^N \sum_{p=1}^{K_j} \int_{nT_b}^{(n+1)T_b} \sqrt{P_{j,p}(t)} b_j(t - pT_c - \tau_{il,jp}) c_{j,p}(t - \tau_{il,jp}) c_{i,l}(t) \mathbf{a}_{j,p}(t) dt \\
&\quad + \frac{1}{\sqrt{T_b}} \int_{nT_b}^{(n+1)T_b} c_{i,l}(t) \mathbf{n}(t) dt \tag{B.2}
\end{aligned}$$

Assume that the power $P_{j,p}(t)$ and the channel array response vector $\mathbf{a}_{j,p}(t)$ do not change appreciably over period T_b , $\forall j, p$ (i.e. slow fading channel). Then the post-correlation signal vector for a non-zero time delay spread multipath model becomes

$$\begin{aligned}
\mathbf{z}_{i,l}(n) &= \sqrt{T_b} \sqrt{P_{i,l}(n)} b_i(n - lT_c) \mathbf{a}_{i,l}(n) \\
&\quad + \frac{1}{\sqrt{T_b}} \sum_{p=1, p \neq l}^{K_i} \sqrt{P_{i,p}(n)} \mathbf{a}_{i,p}(n) \int_{nT_b}^{(n+1)T_b} b_i(t - pT_c - \tau_{il,ip}) c_{i,p}(t - \tau_{il,ip}) c_{i,l}(t) dt \\
&\quad + \frac{1}{\sqrt{T_b}} \sum_{j=1, j \neq i}^N \sum_{p=1}^{K_j} \sqrt{P_{j,p}(n)} \mathbf{a}_{j,p}(n) \int_{nT_b}^{(n+1)T_b} b_j(t - pT_c - \tau_{il,jp}) c_{j,p}(t - \tau_{il,jp}) c_{i,l}(t) dt \\
&\quad + \frac{1}{\sqrt{T_b}} \int_{nT_b}^{(n+1)T_b} c_{i,l}(t) \mathbf{n}(t) dt \tag{B.3}
\end{aligned}$$

B.1.1 The PN code pre-correlation covariance matrix

The expected value of the baseband pre-correlation vector signal is

$$\mathbf{E}\{\mathbf{x}_{i,l}(t)\} = \mathbf{0} \tag{B.4}$$

since the expected value of the PN chip sequence is zero, $\mathbf{E}\{c_{j,p}(t - \tau_{il,jp})\} = 0$, and the expected value of the noise vector is also zero, $\mathbf{E}\{\mathbf{n}(t)\} = \mathbf{0}$.

Therefore, the autocovariance matrix of the baseband pre-correlation signal vector is

$$\begin{aligned}
\mathbf{R}_{xx_{i,l}}(t_1, t_2) &= \mathbf{E}\{\mathbf{x}_{i,l}(t_1)\mathbf{x}_{i,l}(t_2)^\dagger\} \\
&= \sqrt{P_{i,l}(t_1)P_{i,l}(t_2)}\mathbf{E}\{c_{i,l}(t_1)c_{i,l}(t_2)\}\mathbf{E}\{b_i(t_1 - lT_c)b_i(t_2 - lT_c)\}\mathbf{a}_{i,l}(t_1)\mathbf{a}_{i,l}(t_2)^\dagger \\
&\quad + \sum_{q=1, q \neq l}^{K_i} \mathbf{E}\{c_{i,l}(t_1)c_{i,q}(t_2 - \tau_{il,iq})\}\mathbf{E}\{b_i(t_1 - lT_c)b_i(t_2 - qT_c - \tau_{il,iq})\}\sqrt{P_{i,l}(t_1)P_{i,q}(t_2)} \\
&\quad \mathbf{a}_{i,l}(t_1)\mathbf{a}_{i,q}(t_2)^\dagger \\
&\quad + \sum_{p=1, p \neq l}^{K_i} \mathbf{E}\{c_{i,p}(t_1 - \tau_{il,ip})c_{i,l}(t_2)\}\mathbf{E}\{b_i(t_1 - pT_c - \tau_{il,ip})b_i(t_2 - lT_c)\}\sqrt{P_{i,p}(t_1)P_{i,l}(t_2)} \\
&\quad \mathbf{a}_{i,p}(t_1)\mathbf{a}_{i,l}(t_2)^\dagger \\
&\quad + \sum_{p=1, p \neq l}^{K_i} \sum_{q=1, q \neq l}^{K_i} \mathbf{E}\{c_{i,p}(t_1 - \tau_{il,ip})c_{i,q}(t_2 - \tau_{il,iq})\} \\
&\quad \mathbf{E}\{b_i(t_1 - pT_c - \tau_{il,ip})b_i(t_2 - qT_c - \tau_{il,iq})\}\sqrt{P_{i,p}(t_1)P_{i,q}(t_2)}\mathbf{a}_{i,p}(t_1)\mathbf{a}_{i,q}(t_2)^\dagger \\
&\quad + \sum_{j=1, j \neq i}^N \sum_{p=1}^{K_j} \sum_{q=1}^{K_j} \mathbf{E}\{c_{j,p}(t_1 - \tau_{il,jp})c_{j,q}(t_2 - \tau_{il,jq})\} \\
&\quad \mathbf{E}\{b_j(t_1 - pT_c - \tau_{il,jp})b_j(t_2 - qT_c - \tau_{il,jq})\}\sqrt{P_{j,p}(t_1)P_{j,q}(t_2)}\mathbf{a}_{j,p}(t_1)\mathbf{a}_{j,q}(t_2)^\dagger \\
&\quad + \mathbf{E}\{\mathbf{n}(t_1)\mathbf{n}(t_2)^\dagger\} \tag{B.5}
\end{aligned}$$

due to the fact that the expected value of the different pseudo random noise (PN) $c_{j,p}(t), c_{j,q}(t) \in \{1, -1\}$ [29], [41] is

$$\begin{aligned}
\mathbf{E}\{c_{j,p}(t_1)c_{j,q}(t_2)\} &= \delta(t_1 - t_2) \\
&= \begin{cases} \Lambda\left(\frac{t_1 - t_2}{T_c}\right) & \text{for } p = q \\ 0 & \text{for } p \neq q \end{cases}
\end{aligned}$$

and referring also to Appendix C. Note that for the multipath case, the information bit sequence may have a non-zero expected value due to the fact that $T_b > T_c$ where $\forall i, l, j, p, q$

$$\mathbf{E}\{b_j(t_1 - pT_c - \tau_{il,jp})b_j(t_2 - qT_c - \tau_{il,iq})\} = \Lambda\left(\frac{t_1 - t_2 - (p - q)T_c - (\tau_{il,jp} - \tau_{il,iq})}{T_b}\right) \tag{B.6}$$

Therefore, Equation (B.5) becomes

$$\mathbf{R}_{xx_{i,l}}(t_1, t_2) = \sqrt{P_{i,l}(t_1)P_{i,l}(t_2)}\Lambda\left(\frac{t_1 - t_2}{T_c}\right)\Lambda\left(\frac{t_1 - t_2}{T_b}\right)\mathbf{a}_{i,l}(t_1)\mathbf{a}_{i,l}(t_2)^\dagger$$

$$\begin{aligned}
& + \sum_{p=1, p \neq l}^{K_i} \Lambda\left(\frac{t_1 - t_2}{T_c}\right) \Lambda\left(\frac{t_1 - t_2}{T_b}\right) \sqrt{P_{i,p}(t_1)P_{i,p}(t_2)} \mathbf{a}_{i,p}(t_1) \mathbf{a}_{i,p}(t_2)^\dagger \\
& + \sum_{j=1, j \neq i}^N \sum_{p=1}^{K_j} \Lambda\left(\frac{t_1 - t_2}{T_c}\right) \Lambda\left(\frac{t_1 - t_2}{T_b}\right) \sqrt{P_{j,p}(t_1)P_{j,p}(t_2)} \mathbf{a}_{j,p}(t_1) \mathbf{a}_{j,p}(t_2)^\dagger \\
& + \delta(t_1 - t_2) \sigma^2 \mathbf{I}
\end{aligned}$$

Thus the variance of the stochastic pre-correlation signal vector is then

$$\begin{aligned}
& \mathbf{E}\{\mathbf{x}_{i,l}(t) \mathbf{x}_{i,l}(t)^\dagger\} = \mathbf{R}_{xx_{i,l}}(t, t) = \mathbf{R}_{xx_{i,l}}(0) \\
& = P_{i,l}(t) \mathbf{a}_{i,l}(t) \mathbf{a}_{i,l}(t)^\dagger \\
& \quad + \sum_{p=1, p \neq l}^{K_i} P_{i,p}(t) \mathbf{a}_{i,p}(t) \mathbf{a}_{i,p}(t)^\dagger + \sum_{j=1, j \neq i}^N \sum_{p=1}^{K_j} P_{j,p}(t) \mathbf{a}_{j,p}(t) \mathbf{a}_{j,p}(t)^\dagger + \sigma^2 \mathbf{I} \\
& = \sum_{j=1}^N \sum_{p=1}^{K_j} P_{j,p}(t) \mathbf{a}_{j,p}(t) \mathbf{a}_{j,p}(t)^\dagger + \sigma^2 \mathbf{I} \tag{B.7}
\end{aligned}$$

By comparing Equations (B.7) to (A.8), it indicates that a multipath environment creates additional interfering and self interfering signals relative to the desired j^{th} mobile's l^{th} multipath signal.

B.1.2 The PN code post-correlation covariance matrix

The mean of the post-correlation stochastic signal vector of Equation (B.3) is

$$\mathbf{E}\{\mathbf{z}_{i,l}(n)\} = \mathbf{0} \tag{B.8}$$

since for binary signalling the expected value of the binary information bit sequence is zero, $\mathbf{E}\{b_j(t - pT_c)\} = 0 \forall j, p$, and the expected value of the noise vector is also zero, $\mathbf{E}\{\mathbf{n}(t)\} = \mathbf{0}$.

Defining the autocovariance of the PN post-correlation covariance matrix as

$$\begin{aligned}
& \mathbf{R}_{zz_{i,l}}(n_1, n_2) = \frac{1}{T_c} \mathbf{E}\{\mathbf{z}_{i,l}(n_1) \mathbf{z}_{i,l}(n_2)^\dagger\} \\
& = \frac{T_b}{T_c} \sqrt{P_{i,l}(n_1)P_{i,l}(n_2)} \mathbf{E}\{b_i(n_1 - lT_c) b_i(n_2 - lT_c)\} \mathbf{a}_{i,l}(n_1) \mathbf{a}_{i,l}(n_2)^\dagger \\
& \quad + \frac{1}{T_c} \sum_{q=1, q \neq l}^{K_i} \sqrt{P_{i,l}(n_1)P_{i,q}(n_2)} \mathbf{a}_{i,l}(n_1) \mathbf{a}_{i,q}(n_2)^\dagger
\end{aligned}$$

$$\begin{aligned}
& \int_{nT_b}^{(n+1)T_b} \mathbf{E}\{b_i(t_1 - lT_c)b_i(t_2 - qT_c - \tau_{il,iq})\} \mathbf{E}\{c_{i,q}(t_2 - \tau_{i,l,iq})c_{i,l}(t_1)\} dt_2 \\
& + \frac{1}{T_c} \sum_{p=1, p \neq l}^{K_i} \sqrt{P_{i,p}(n_1)P_{i,l}(n_2)} \mathbf{a}_{i,p}(n_1) \mathbf{a}_{i,l}(n_2)^\dagger \\
& \int_{nT_b}^{(n+1)T_b} \mathbf{E}\{b_i(t_1 - pT_c - \tau_{il,ip})b_i(t_2 - lT_c)\} \mathbf{E}\{c_{i,p}(t_2 - \tau_{il,ip})c_{i,l}(t_1)\} dt_1 \\
& + \frac{1}{T_c T_b} \sum_{p=1, p \neq l}^{K_i} \sum_{q=1, q \neq l}^{K_i} \sqrt{P_{i,p}(n_1)P_{i,q}(n_2)} \mathbf{a}_{i,p}(n_1) \mathbf{a}_{i,q}(n_2)^\dagger \\
& \int_{nT_b}^{(n+1)T_b} \int_{nT_b}^{(n+1)T_b} \mathbf{E}\{b_i(t_1 - pT_c - \tau_{il,ip})b_i(t_2 - qT_c - \tau_{il,iq})\} \\
& \mathbf{E}\{c_{i,p}(t_1 - \tau_{il,ip})c_{i,q}(t_2 - \tau_{il,iq})\} \mathbf{E}\{c_{i,l}(t_1)c_{i,l}(t_2)\} dt_1 dt_2 \\
& + \frac{1}{T_c T_b} \sum_{j=1, j \neq i}^N \sum_{p=1}^{K_j} \sum_{q=1}^{K_j} \sqrt{P_{j,p}(n_1)P_{j,q}(n_2)} \mathbf{a}_{j,p}(n_1) \mathbf{a}_{j,q}(n_2)^\dagger \\
& \int_{nT_b}^{(n+1)T_b} \int_{nT_b}^{(n+1)T_b} \mathbf{E}\{b_j(t_1 - pT_c - \tau_{il,jp})b_j(t_2 - qT_c - \tau_{il,jq})\} \mathbf{E}\{c_{i,l}(t_1)c_{i,l}(t_2)\} \\
& \mathbf{E}\{c_{j,p}(t_1 - \tau_{il,jp})c_{j,q}(t_2 - \tau_{il,jq})\} dt_1 dt_2 \\
& + \frac{1}{T_c T_b} \int_{nT_b}^{(n+1)T_b} \int_{nT_b}^{(n+1)T_b} \mathbf{E}\{c_{i,l}(t_1)c_{i,l}(t_2)\} \mathbf{E}\{\mathbf{n}(t_1)\mathbf{n}(t_2)\} dt_1 dt_2 \tag{B.9}
\end{aligned}$$

Similarly, using Equation (B.6) then gives

$$\begin{aligned}
& \mathbf{R}_{zz_i,l}(n_1, n_2) \\
& = \frac{T_b}{T_c} \mathbf{\Lambda}\left(\frac{n_1 - n_2}{T_b}\right) \sqrt{P_{i,l}(n_1)P_{i,l}(n_2)} \mathbf{a}_{i,l}(n_1) \mathbf{a}_{i,l}(n_2)^\dagger \\
& + \frac{1}{T_c} \sum_{p=1, p \neq l}^{K_i} \sqrt{P_{i,p}(n_1)P_{i,p}(n_2)} \mathbf{a}_{i,p}(n_1) \mathbf{a}_{i,p}(n_2)^\dagger \\
& \int_{nT_b}^{(n+1)T_b} \int_{nT_b}^{(n+1)T_b} \mathbf{\Lambda}\left(\frac{t_1 - t_2}{T_b}\right) \mathbf{\Lambda}\left(\frac{t_1 - t_2}{T_c}\right) \mathbf{\Lambda}\left(\frac{t_1 - t_2}{T_c}\right) dt_1 dt_2 \\
& + \frac{1}{T_c T_b} \sum_{j=1, j \neq i}^N \sum_{p=1}^{K_j} \sqrt{P_{j,p}(n_1)P_{j,p}(n_2)} \mathbf{a}_{i,p}(n_1) \mathbf{a}_{i,p}(n_2)^\dagger \\
& \int_{nT_b}^{(n+1)T_b} \int_{nT_b}^{(n+1)T_b} \mathbf{\Lambda}\left(\frac{t_1 - t_2}{T_b}\right) \mathbf{\Lambda}\left(\frac{t_1 - t_2}{T_c}\right) \mathbf{\Lambda}\left(\frac{t_1 - t_2}{T_c}\right) dt_1 dt_2 \\
& + \frac{1}{T_c T_b} \int_{nT_b}^{(n+1)T_b} \int_{nT_b}^{(n+1)T_b} \mathbf{\Lambda}\left(\frac{t_1 - t_2}{T_c}\right) \sigma^2 \delta(t_1 - t_2) \mathbf{I} dt_1 dt_2 \tag{B.10}
\end{aligned}$$

Using Equation (A.12) of Appendix A, the PN code post-correlation covariance matrix becomes

$$\mathbf{R}_{zz_i,l}(n_1, n_2)$$

$$\begin{aligned}
&= \frac{T_b}{T_c} \Lambda \left(\frac{n_1 - n_2}{T_b} \right) \sqrt{P_{i,l}(n_1)P_{i,l}(n_2)} \mathbf{a}_{i,l}(n_1) \mathbf{a}_{i,l}(n_2)^\dagger \\
&\quad + \frac{2}{3} \sum_{p=1, p \neq l}^{K_i} \sqrt{P_{i,p}(n_1)P_{i,p}(n_2)} \mathbf{a}_{i,p}(n_1) \mathbf{a}_{i,p}(n_2)^\dagger \\
&\quad + \frac{2}{3} \sum_{j=1, j \neq i}^N \sum_{p=1}^{K_j} \sqrt{P_{j,p}(n_1)P_{j,p}(n_2)} \mathbf{a}_{i,p}(n_1) \mathbf{a}_{i,p}(n_2)^\dagger \\
&\quad + \frac{1}{T_c} \sigma^2 \delta(t_1 - t_2) \mathbf{I}
\end{aligned} \tag{B.11}$$

Therefore, the variance of the PN code post-correlation matrix is

$$\begin{aligned}
\mathbf{R}_{zz_{i,l}}(0) &= \mathbf{R}_{zz_{i,l}}(n, n) \\
&= \frac{T_b}{T_c} P_{i,l}(n) \mathbf{a}_{i,l}(n) \mathbf{a}_{i,l}(n)^\dagger + \frac{2}{3} \sum_{p=1, p \neq l}^{K_i} P_{i,p}(n) \mathbf{a}_{i,p}(n) \mathbf{a}_{i,p}(n)^\dagger \\
&\quad + \frac{2}{3} \sum_{j=1, j \neq i}^N \sum_{p=1}^{K_j} P_{j,p}(n) \mathbf{a}_{i,p}(n) \mathbf{a}_{i,p}(n)^\dagger + \frac{1}{T_c} \sigma^2 \mathbf{I}
\end{aligned} \tag{B.12}$$

B.2 The weighted post-correlation signal SINR

From the variance of the PN code post-correlation matrix, the i^{th} mobile's l^{th} branch weighted post-correlation signal SINR is

$$\begin{aligned}
&SINR_{post_{i,l}} \\
&= \frac{P_{i,l}(n) \mathbf{w}_{i,l}(n)^\dagger \mathbf{a}_{i,l}(n) \mathbf{a}_{i,l}(n)^\dagger \mathbf{w}_{i,l}(n) / B}{MAI + \sigma^2 \|\mathbf{w}_{i,l}(n)\|^2}
\end{aligned} \tag{B.13}$$

where the self-interference (SI) and the multiple access interference (MAI) represents the self-interference and the interference from other mobiles, respectively.

$$SI = \frac{2}{3W_{ss}} \sum_{p=1, p \neq l}^{K_i} P_{i,p}(n) \|\mathbf{w}_{i,l}(n)^\dagger \mathbf{a}_{i,p}(n)\|^2 \tag{B.14}$$

and

$$MAI = \frac{2}{3W_{s,s}} \sum_{j=1, j \neq i}^N \sum_{p=1}^{K_j} P_{j,p}(n) \|\mathbf{w}_{i,l}(n)^\dagger \mathbf{a}_{i,p}(n)\|^2 \tag{B.15}$$

where $B = 1/T_b$ is the information bit bandwidth, $W_{ss} = 1/T_c$ is the PN chip channel bandwidth, and $\|(\cdot)\|^2$ is the magnitude squared of (\cdot) .

Appendix C

First and second order statistics for a binary square pulse stochastic process

C.1 Autocovariance of pulse

This appendix references [29] and [12].

A CDMA chip pulse train with period T_c of the i^{th} mobile can be expressed as

$$c_i(t) = \sum_{n=-\infty}^{\infty} c_{i,n} p(t - nT_c) \quad (C.1)$$

where $c_{i,n} \in \{1, -1\} \forall n$ and

$$p(t) = \begin{cases} 1, & \text{for } 0 < t < T_c \\ 0, & \text{otherwise} \end{cases} \quad (C.2)$$

And a CDMA information bit square pulse with period T_b of the i^{th} mobile can be expressed as

$$b_i(t) = \sum_{n=-\infty}^{\infty} b_{i,n} u(t - nT_b) \quad (C.3)$$

where $b_{i,n} \in \{1, -1\} \forall n$ and

$$u(t) = \begin{cases} 1, & \text{for } 0 < t < T_b \\ 0, & \text{otherwise} \end{cases} \quad (C.4)$$

Generally, we can express Equations (C.1) and (C.3) as

$$s_i(t) = \sum_{n=-\infty}^{\infty} s_{i,n} p_T(t - nT) \quad (\text{C.5})$$

where $s(nT)$ is of value 1 or -1 for all n and

$$p_T(t) = \begin{cases} 1, & \text{for } 0 < t < T \\ 0, & \text{otherwise} \end{cases} \quad (\text{C.6})$$

We have

$$\mathbf{E}_s \{s_{i,n} s_{i,m}\} = \begin{cases} 1, & \text{for } n = m \\ 0, & \text{for } n \neq m \end{cases} \quad (\text{C.7})$$

or equivalently

$$\mathbf{E}_s \{s_{i,n} s_{i,m}\} = \delta(n - m) \quad (\text{C.8})$$

where $\mathbf{E}_s \{\cdot\}$ denotes the expectation of the binary random variable $s_{i,n} \in \{1, -1\}$.

Consider the expected value of $s_i(t)$

$$\mathbf{E} \{s_i(t)\} = \mathbf{E} \{s_{i,n} p_T(t - nT)\} = \mathbf{E}_s \{s_{i,n}\} p_T(t - nT) = 0 \quad (\text{C.9})$$

and the autocorrelation of $s_i(t)$

$$\begin{aligned} \mathbf{R}_{s_i}(t_1, t_2) &= \mathbf{E} \{s_i(t_1) s_i(t_2)\} \\ &= \sum_{n=-\infty}^{\infty} \sum_{m=-\infty}^{\infty} \mathbf{E}_s \{s_{i,n} s_{i,m}\} p_T(t_1 - nT) p_T(t_2 - mT) \\ &= \sum_{n=-\infty}^{\infty} \sum_{m=-\infty}^{\infty} \delta(n - m) p_T(t_1 - nT) p_T(t_2 - mT) \\ &= \sum_{n=-\infty}^{\infty} p_T(t_1 - nT) p_T(t_2 - nT) \end{aligned} \quad (\text{C.10})$$

Equation (C.10) shows that $s_i(t)$ is not a wide sense stationary process; however, it is a cyclostationary process because the first and second order statistics of $s_i(t)$ satisfy the following relations

$$\mathbf{E} \{s_i(t + T)\} = \mathbf{E} \{s_i(t)\}$$

and

$$\mathbf{R}_{s_i}(t_1 + T, t_2 + T) = \mathbf{R}_{s_i}(t_1, t_2)$$

In practice, the observer of the process $s_i(t)$ may have no knowledge whatsoever of the time reference for the sampling instants [10] [12]. Therefore, the cyclostationary process can be modified to obtain a wide sense stationary process by allowing a random time delay φ (phase randomization), where φ is a uniformly distributed random variable over $0 \leq t < T$ independent of $s_{i,n}$, i.e. with a probability distribution of

$$f_\varphi(t) = \begin{cases} \frac{1}{T}, & \text{for } 0 \leq t < T \\ 0, & \text{elsewhere} \end{cases} \quad (\text{C.11})$$

Thus, the sampling instants are changed to $t = nT - \varphi$. So we now have

$$s_i(t) = \sum_{n=-\infty}^{\infty} s_{i,n} p_T(t - nT - \varphi)$$

The mean of $s_i(t)$ is now

$$\begin{aligned} \mathbf{E}\{s_i(t)\} &= \sum_{n=-\infty}^{\infty} \mathbf{E}_s\{s_{i,n}\} \mathbf{E}_\varphi\{p_T(t - nT - \varphi)\} \\ &= \sum_{n=-\infty}^{\infty} \mathbf{E}_s\{s_{i,n}\} \int_0^T p_T(t - nT - \varphi) \left(\frac{1}{T}\right) d\varphi \\ &= 0 \end{aligned} \quad (\text{C.12})$$

where $\mathbf{E}_\varphi\{\cdot\}$ denotes the expectation of the uniformly distributed random variable φ .

The autocorrelation of $s_i(t)$ with $t_1 = t$ and $t_2 = t + \tau$ is

$$\begin{aligned} \mathbf{R}_{s_i}(t_1, t_2) &= \mathbf{E}\{s_i(t_1)s_i(t_2)\} = \mathbf{R}_{s_i}(t, t + \tau) \\ &= \sum_{n=-\infty}^{\infty} \sum_{m=-\infty}^{\infty} \mathbf{E}_\varphi\{\mathbf{E}_s\{s_{i,n}s_{i,m}|\varphi = \varphi\}\} \mathbf{E}_\varphi\{p_T(t_2 - mT - \varphi)\} \\ &= \sum_{n=-\infty}^{\infty} \sum_{m=-\infty}^{\infty} \int_0^T \delta(n - m) \left(\frac{1}{T}\right) d\varphi \int_0^T p_T(t_1 - nT - \varphi) p_T(t_2 - mT - \varphi) \left(\frac{1}{T}\right) d\varphi \\ &= \sum_{n=-\infty}^{\infty} \int_0^T p_T(t - nT - \varphi) p_T(t + \tau - nT - \varphi) \left(\frac{1}{T}\right) d\varphi \\ &= \sum_{n=-\infty}^{\infty} \int_{t-(n+1)T}^{t-nT} p_T(\varphi) p_T(\tau + \varphi) \left(\frac{1}{T}\right) d\varphi \\ &= \left(\frac{1}{T}\right) \int_{-\infty}^{\infty} p_T(\varphi) p_T(\tau + \varphi) d\varphi \\ &= \left(\frac{1}{T}\right) p_T(\tau) * p_T(-\tau) \end{aligned} \quad (\text{C.13})$$

which is now a wide-sense-stationary (WSS) process representation.

Therefore, with $p_T(t)$ being a square pulse, Equation (C.13) equals

$$\begin{aligned} \mathbf{R}_{ss_i}(t_1, t_2) &= \mathbf{R}_{s_i s_i}(\tau) = \mathbf{R}_{ss_i}(t_1 - t_2) \\ &= \begin{cases} 1 - \frac{|t_1 - t_2|}{T}, & \text{for } |t_1 - t_2| \leq T \\ 0, & \text{elsewhere} \end{cases} \end{aligned} \quad (\text{C.14})$$

by defining

$$\Lambda\left(\frac{t_1 - t_2}{T}\right) = \begin{cases} 1 - \frac{|t_1 - t_2|}{T}, & \text{for } |t_1 - t_2| \leq T \\ 0, & \text{elsewhere} \end{cases} \quad (\text{C.15})$$

Equation (C.14) can be represented as

$$\mathbf{R}_{ss_i}(t_1, t_2) = \Lambda\left(\frac{t_1 - t_2}{T}\right) \quad (\text{C.16})$$

C.2 Mean and autocorrelation of the PN chip and the information bit sequences

Equations (C.14) and (C.16) imply that the expected value and the autocovariance of the chips are, respectively

$$\mathbf{E}\{c_i(t)\} = 0$$

and

$$\begin{aligned} \mathbf{E}\{c_i(t_1)c_i(t_2)\} &= \mathbf{R}_{cc_i}(t_1 - t_2) = \begin{cases} 1 - \frac{|t_1 - t_2|}{T_c}, & \text{for } |t_1 - t_2| \leq T_c \\ 0, & \text{elsewhere} \end{cases} \\ &= \Lambda\left(\frac{t_1 - t_2}{T_c}\right) \end{aligned} \quad (\text{C.17})$$

Similarly, the expected value and the autocovariance of the information bits are respectively

$$\mathbf{E}\{b_i(t)\} = 0$$

and

$$\begin{aligned}\mathbf{E}\{b_i(t_1)b_i(t_2)\} &= \mathbf{R}_{bb_i}(t_1 - t_2) = \begin{cases} 1 - \frac{|t_1 - t_2|}{T_b}, & \text{for } |t_1 - t_2| \leq T_b \\ 0, & \text{elsewhere} \end{cases} \\ &= \mathbf{\Lambda}\left(\frac{t_1 - t_2}{T_b}\right)\end{aligned}\tag{C.18}$$

Bibliography

- [1] D. G. Brennan. Linear Diversity Combining Techniques. In *Proceedings of the IRE*, 1958.
- [2] J. R. Bunch and Christopher P. Nielsen. Updating the Singular Value Decomposition. *Numerische Mathematik*, 31:111–129, 1978.
- [3] J. R. Bunch, Christopher P. Nielsen, and Danny C. Sorensen. Rank-One Modification of the Symmetric Eigenproblem. *Numer. Math.*, 31:31–48, 1978.
- [4] N. L. B. Chan. Multipath Propagation Effects on a CDMA Cellular System. *IEEE Transactions on Vehicular Technology*, 43:848–855, November 1994.
- [5] R. D. Degroat. Efficient, numerically stabilized rank-one eigenstructure updating. *IEEE Trans. ASSP*, 38(2):301–316, February 1990.
- [6] R. D. DeGroat. Noniterative subspace tracking. *IEEE Trans. Sig. Proc.*, 40(3):571–577, 1992.
- [7] A. M. Earnshaw. *An Investigation into Improving Performance of Cellular CDMA Communication Systems with Digital Beamforming*. PhD thesis, Dept. of Electrical & Computer Engineering, Queen’s University, 1995.
- [8] A. M. Earnshaw and S. D. Blostein. “A chip-level IS95-compliant cellular CDMA simulator: Design, implementation, and analysis”. Technical report, Dept. of Electrical & Computer Engineering, Queen’s University, 1996.

- [9] A. M. Earnshaw and S. D. Blostein. Investigating the effects of imperfect digital beamforming on cell capacity in a cellular CDMA communication system. In *ICUPC*, pages 458–462, 1996.
- [10] L. E. Franks. *Signal Theory*. Prentice-Hall, Inc., 1969.
- [11] O. L. Frost. An algorithm for linearly constrained adaptive array processing. *Proceedings of the IEEE*, 60(8):926–935, August 1972.
- [12] J. D. Gibson. *Principles of Digital and Analog Communications*. Macmillan Publishing Company, 1993.
- [13] G. H. Golub and Charles F. Van Loan. *Matrix Computations*. The Johns Hopkins University Press, 1989.
- [14] F. J. Harris. On the use of windows for harmonic analysis with the discrete Fourier transform. *Proceedings of the IEEE*, pages 51–83, January 1978.
- [15] J. D. Gibson (Editor in Chief). *The Mobile Communications Handbook*. Library of Congress Cataloging-in-Publication Data in conjunction with IEEE, 1996.
- [16] D. H. Johnson and Stuart R. DeGraaf. Improving the resolution of bearing in passive sonar arrays by eigenvalue analysis. *IEEE Transactions on Acoustics, Speech, and Signal Processing*, 30(4), August 1982.
- [17] D. H. Johnson and Dan E. Dudgeon. *Array Signal Processing: Concepts and Techniques*. P T R Prentice-Hall, 1993.
- [18] I. Karasalo. Estimating the Covariance Matrix by Signal Subspace Averaging. *IEEE Transactions on acoustics, speech, and signal processing*, 34:8–12, February 1986.
- [19] J. Karimi. Personal Hand-held Communications Via L-band CDMA-Based Geostationary Beamforming Satellites. Master’s thesis, Department of Electrical & Computer Engineering, Queen’s University, 1996.

- [20] B. H. Khalaj, A. Paulraj, and T. Kailath. 2D RAKE receivers for CDMA cellular systems. *IEEE International Conference on Communications*, pages 400–404, 1994.
- [21] W. C. Y. Lee. Effects on correlation between two mobile radio base-station antennas. *IEEE Transactions on Communications*, 21(11):1214–1224, November 1973.
- [22] W. C. Y. Lee. *Mobile Communications Engineering*. McGraw-Hill Book Company, 1982.
- [23] R. A. Monzingo and T. W. Miller. *Introduction to Adaptive Arrays*. A Wiley-Interscience Publication, 1980.
- [24] A. F. Naguib. *Adaptive Antennas for CDMA Wireless Networks*. PhD thesis, Dept. of Electrical Engineering, Stanford University, 1995.
- [25] A. F. Naguib and A. Paulraj. Recursive Adaptive Beamforming for Wireless CDMA. In *IEEE International Conference on Communications*, volume 3 of 3, pages 1515–1519, 1995.
- [26] A. F. Naguib and Arogyaswami Paulraj. Performance of CDMA Cellular Networks with Base-Station Antenna Arrays. In *International Zurich Seminar on Digital Communications*, 1994.
- [27] A. F. Naguib, Arogyaswami Paulraj, and Thomas Kailath. Capacity improvement with base-station antenna arrays in cellular CDMA. *IEEE Transactions on Vehicular Technology*, 43:691–698, August 1994.
- [28] A. Papoulis. *Probability, Random Variables, and Stochastic Processes*. McGraw-Hill, Inc., 1991.
- [29] J. G. Proakis. *Digital Communications*. McGraw-Hill, Inc., 1989.

- [30] Qualcomm Inc. Mobile station-base compatibility standard for dual-mode wide-band spread system, 1993.
- [31] D. J. Rabideau. Fast, Rank Adaptive Subspace Tracking and Applications. *IEEE Transactions on Signal Processing*, 44:2229–2244, September 1996.
- [32] T. S. Rappaport. *Wireless Communications Principles and Practice*. Prentice Hall PTR, 1996.
- [33] J. Salz and J. H. Winters. Effect of fading correlation on adaptive arrays in digital mobile radio. *IEEE Transactions on Vehicular Technology*, pages 1049–1057, November 1994.
- [34] R. Schreiber. Implementation of Adaptive Array Algorithms. *IEEE Transactions on Acoustics, Speech, and Signal Processing*, 34:1038–1045, October 1986.
- [35] M. Schwartz, William R. Bennett, and Seymour Stein. *Communication Systems and Techniques*. IEEE Communications Society, IEEE press, 1996.
- [36] W. Y. Shiu and S. D. Blostein. Adaptive Digital Beamforming in Cellular CDMA Systems Using Noniterative Signal Subspace Tracking. In *IEEE International Conference on Communications*, 1997.
- [37] H. Steyskal. Digital beamforming antennas: An introduction. *Microwave Journal*, pages 107–122, January 1987.
- [38] F. G. Stremmer. *Introduction to Communication Systems*. Addison-Wesley Publishing Company, 1990.
- [39] S. C. Swales, M. A. Beach, D. J. Edwards, and J. P. McGeehan. The performance enhancement of multibeam adaptive base-station antennas for cellular land mobile radio systems. *IEEE Transactions on Vehicular Technology*, 39(1):56–67, 1990.

- [40] G. L. Turin. Introduction to spread-spectrum antimultipath techniques and their application to urban digital radio. *Proc. IEEE*, 68(3):328–353, 1980.
- [41] G. L. Turin. The Effects of Multipath and Fading on the Performance of Direct-Sequence CDMA Systems. *IEEE JSAC*, SAC-2(4):597–603, July 1984.
- [42] B. D. Van Veen and K. M. Buckley. Beamforming: A versatile approach to spatial filtering. *IEEE ASSP*, pages 4–24, 1988.
- [43] W. X. Wang. Video Image Transmission Via Mobile Satellite Channels. Master’s thesis, Department of Electrical & Computer Engineering, Queen’s University, 1995.
- [44] B. Widrow, P. E. Mantey, L. J. Griffiths, and B. B. Goode. Adaptive antenna systems. *Proceedings of the IEEE*, 55(12), December 1967.
- [45] G. Wu, A. Jalali, and P. Mermelstein. On Channel Model Parameters for Micro-cellular CDMA Systems. *IEEE Transactions on Vehicular Technology*, 44:706–711, August 1995.
- [46] H. Ye, R. D. DeGroat, E. M. Dowling, and D. A. Linebarger. Spherical subspace tracking for efficient, high performance adaptive signal processing applications. *Signal Processing*, 50(2):101–121, April 1996.
- [47] W. Yung. Direct-Sequence Spread-Spectrum Code-Division-Multiple-Access Cellular Systems in Rayleigh Fading and Log-normal Shadowing Channel. In *IEEE International Conference on Communications*, volume 2 of 3, pages 871–877, 1991.